

Université Lille 1

École Doctorale de Sciences de la Matière, du
Rayonnement et de l'Environnement

Spécialité

Molécules et Matière Condensée

Thèse de Doctorat

Par

Chang LIU

ayant pour titre

Effect of Sulphur on Fischer-Tropsch Synthesis:
Promoted Molybdenum and Cobalt Catalysts

Soutenue le 27 Mars 2015 devant la commission d'examen composée de :

Rapporteurs : M^{me} Sylvette Brunet, Directrice de recherche, IC2MP, Université de Poitiers
M. Christophe Geantet, Directeur de recherche, IRCELyon

Examineurs : M. Pascal Fongarland, Professeur, Université Lyon 1
M. Eric Marceau, Maître de conférences, Université Paris 6
M. Ye Wang, Professeur, Université de Xiamen, coordinateur du projet
OLSYNCAT (Chine)
M^{me} Mirella Virginie Maître de conférences, ENSCL, coencadrante
M^{me} Anne Griboval-Constant, Maître de conférences, Univ. Lille 1, codirectrice
M. Andrei Khodakov, Directeur de recherche, UCCS, directeur de thèse

Remerciements

Je voudrais remercier premièrement le directeur de ma thèse, Dr. Andrei Khodakov, Directeur de Recherche CNRS, pour ses orientations. Il m'a fait partager ses expériences et ses connaissances sur la recherche scientifique. Il m'a aidé beaucoup professionnellement et personnellement. Ses précieux conseils m'ont été toujours très utiles durant la durée de ma thèse.

Je remercie le Dr Anne Griboval-Constant, Maître de conférences et le Dr Mirella Virginie, Maître de conférences, qui sont les co-encadrantes de ma thèse. Elles m'ont suivi tout au long de ma thèse pendant trois ans. Elles m'ont aidé lors de la mise en œuvre des techniques expérimentales et également lors la rédaction de ma thèse. Je les remercie profondément pour leur patience et leur gentillesse.

Je remercie aussi le Prof. Ye Wang, à Univ-Xiamen. J'ai l'honneur de travailler dans labo de Prof. Wang pendant ma thèse. Et je voudrais remercier tout le monde de labo de PCOSS, avec qui j'ai passé deux mois très sympathique.

Mes remerciements vont également à Madame Carole Lamonier, Madame Lancelot Christine, Madame Barbara Declerck-Boulanger, Monsieur Oliver Gardoll, Monsieur David Porier, Monsieur Gérard Cambien, Monsieur Johann Jezequel, Monsieur Jorge Beiramar, etc. Ils m'ont donné plusieurs d'aides sur des manipulations expérimentales. Je leurs remercie beaucoup. Je dois remercier l'ensemble du personnel à UCCS, ils sont toujours gentils. Je suis content de travailler ensemble avec eux.

Here I especially appreciate all my Chinese friends in France: Mengnan, Mengdie, Xiaofeng, Haiqin, Wenhao, Fangli, Kang, Wang, Tong, Zhiping, Yaqian, Yi, Nan, Hui, Kai, etc. They always support me and help me during six-year-live in Lille. Without them I cannot succeed in my study. I wish them happy and healthy, and I love them all.

Je remercie l'Agence Nationale de la Recherche (Projet OLSYNCAT) pour le financement de ma thèse. Finalement je voudrais remercier beaucoup mes parents et ma copine Rong pour m'accompagner toujours. L'expérience de thèse sera toujours le trésor très précieux de ma vie.

Content

Abstract	1
Chapter One Introduction and objectives	3
I General introduction	7
II History and current situation	9
II-1 Biomass	9
II-2 Biomass to synthesis gas via gasification	10
III Fischer-Tropsch synthesis	14
III-1 Iron based FT catalysts	15
III-2 Cobalt based FT catalysts	17
III-3 Mechanism of FT reaction	17
III-4 Kinetics of FT reaction	24
III-5 Thermodynamics of FT reaction	25
IV Fischer-Tropsch to light olefin process	26
IV-1 Light olefin synthesis	26
IV-2 Current development of FTO process	29
V Effect of sulphur on FT synthesis	34
V-1 Effect of sulphur on iron based catalysts	35
V-2 Effects of sulphur on cobalt based catalysts	37
V-3 Characterization of the catalyst exposed to sulphur	41
VI Sulphur resistant catalysts	43
VI-1 Sulphide catalysts	43
VI-2 Molybdenum disulphide catalysts for FT synthesis	44
VII Objectives	53
Chapter Two Experimental	59

<u>I Introduction</u>	<u>63</u>
<u>II Catalyst preparation</u>	<u>64</u>
II-1 Cobalt based catalysts	64
II-2 Molybdenum disulphide based catalysts	66
<u>III Characterizations</u>	<u>67</u>
III-1 Textural characteristics	68
III-2 X-ray diffraction	69
III-3 X-ray photoelectron spectroscopy	69
III-4 Laser Raman spectroscopy	70
III-5 H ₂ Temperature programmed reduction	70
III-6 CO ₂ -Temperature programmed desorption	71
III-7 Transmission electron microscope	71
<u>IV Catalytic measurements</u>	<u>72</u>
IV-1 Set-up for catalytic test	73
IV-2 Catalytic test procedure	77
IV-3 Catalysts test conditions	79
<u>V Conclusion</u>	<u>79</u>
<u>Chapter Three Catalytic behaviour of (Pt)Co/Al₂O₃ catalyst in presence of sulphur</u>	<u>83</u>
<u>I Introduction</u>	<u>87</u>
<u>II Characterization of Fresh Cobalt based catalysts</u>	<u>88</u>
II-1 Textural characteristics	88
II-2 XRD	89
II-3 H ₂ -TPR	91
II-4 XPS	94
<u>III Catalytic tests on Co based catalysts</u>	<u>95</u>
III-1 Effect on different Co content on supported catalysts	95
III-2 Effect of hydrogen disulphide in FT synthesis	96
<u>IV Characterization of spent catalysts</u>	<u>100</u>

IV-1 XRD on spent catalysts	100
IV-2 XPS on spent catalysts	101

V Discussion and Conclusion 103

V-1 Dispersion and reducibility of Co based catalysts	103
V-2 Effect of H ₂ S on Co/Al ₂ O ₃ and Pt-Co/Al ₂ O ₃	104
V-3 Conclusion	105

Chapter Four Structure and catalytic performance of carbon nanotube supported MoS₂ catalysts promoted with potassium 108

I Introduction 112

II Characterization on K₂MoS₇/CNT catalysts 113

II-1 Textural characteristics	113
II-2 XRD	114
II-3 XPS	117
II-4 H ₂ -TPR	122
II-5 CO ₂ -TPD	125

III FT catalytic performance on K₂MoS₇ catalysts supported on CNT 127

III-1 Results of catalytic tests	127
III-2 Catalyst stability	129

IV Discussion and conclusion 131

IV-1 Discussion	131
IV-2 Conclusion	134

Chapter Five Effect of potassium content on MoS₂/Al₂O₃ catalysts for FT synthesis 138

I Introduction 141

II Characterization of K Promoted MoS₂/Al₂O₃ catalysts 141

II-1 Characterization of calcined catalysts	141
II-2 Characterization on sulphided catalysts	147

III Catalytic tests on K₂MoS₇/Al₂O₃ catalysts 158

<u>IV Effect of reaction condition on K MoS₂/Al₂O₃ catalysts</u>	<u>161</u>
IV-1 Effect of GHSV	161
IV-2 Effect of pressure	163
IV-3 Effect of syngas ratio (H ₂ /CO)	165
<u>V Discussion and Conclusion</u>	<u>167</u>
<u>Chapter Six Effects of different alkali promoters and precursors on the structure and performance of MoS₂/Al₂O₃ catalysts</u>	<u>176</u>
<u>I Introduction</u>	<u>179</u>
<u>II Alumina supported molybdenum sulphide catalysts promoted with different alkali metals</u>	<u>180</u>
II-1 Characterization	180
II-2 Catalytic test	193
II-3 Discussion	196
<u>III Alumina supported molybdenum catalysts promoted with different potassium precursors</u>	<u>199</u>
III-1 Characterization	199
III-2 Catalytic test	209
III-3 Discussion	211
<u>IV Conclusion</u>	<u>213</u>
<u>General Conclusion</u>	<u>216</u>

Abstract

This thesis focuses on the study of promoted molybdenum catalysts supported on alumina or carbon nanotubes for the synthesis of olefins from synthesis gas obtained from biomass. The catalysts were studied at every stage of their preparation by different characterization techniques and tested in fixed bed reactor. The results showed that both types of sites are present on the K-MoS₂ catalysts: MoS₂, which leads to the production of methane and a mixed K-Mo-S phase which leads to the synthesis of olefins. The decrease in activity observed with catalysts supported on carbon nanotubes was attributed to the low rate of sulphidation. The basicity of the promoters and the size of the molybdenum sulphide crystallites are important parameters influencing the olefins synthesis. A moderate basicity as well as large size of molybdenum crystallites are favorable to the synthesis of light olefins.

Keywords: *Fischer-Tropsch synthesis; biosyngas; hydrogen disulphide; molybdenum sulphide; supported catalysts; alkali promoter; light olefins*

Résumé

Cette thèse porte sur l'étude de catalyseurs promus à base de sulfure de molybdène supporté sur alumine ou nanotubes de carbone pour la synthèse d'oléfines à partir du gaz de synthèse issu de la biomasse. Les catalyseurs ont été étudiés à chaque étape de leur préparation par différentes techniques physico-chimiques et spectroscopiques et testés dans un réacteur à lit fixe. Les résultats ont montré que deux types de sites sont présents sur les catalyseurs K-MoS₂ : MoS₂, qui conduit à la production de méthane et une phase mixte K-Mo-S qui conduit à la synthèse d'oléfines. La baisse d'activité observée avec les catalyseurs supportés sur nanotubes de carbone a été attribuée au plus faible taux de sulfuration. La basicité des promoteurs et la taille des cristallites sont des paramètres importants qui influencent la synthèse d'oléfines. Une basicité modérée ainsi qu'une taille plus grande des cristallites de molybdène sont favorables à la synthèse d'oléfines légères.

Mots clés: *Synthèse Fischer-Tropsch; biosyngas; H₂S; sulfure de molybdène; catalyseurs supportés; oléfines légères*

Chapter One
Introduction and Objectives

Summary

I General introduction	7
II History and current situation	9
II-1 Biomass	9
II-2 Biomass to Synthesis Gas via Gasification	10
II-2-1 Gasification procedure	11
II-2-2 Gasification Reactors	12
III Fischer-Tropsch synthesis	14
III-1 Iron based FT catalysts	15
III-2 Cobalt based FT catalysts	17
III-3 Mechanism of FT reaction	17
III-3-1 Initiation of FT reaction	18
III-3-2 Chain Growth and Termination of FT synthesis	20
III-3-3 Mechanism of FT synthesis on MoS ₂ based catalyst	23
III-4 Kinetics of FT reaction	24
III-5 Thermodynamics of FT reaction	25
IV Fischer-Tropsch to Light Olefin process	26
IV-1 Light olefin synthesis	26
IV-2 Current development of FTO process	29
IV-2-1 FTO on iron catalysts	29
IV-2-2 Effect of promoters on iron based catalysts for FTO	31
IV-2-3 Effect of support on iron based catalysts for FTO	33
IV-2-4 FTO on other metal catalysts	34
V Effect of Sulphur on FT synthesis	34
V-1 Effect of sulphur on iron based catalysts	35
V-2 Effects of sulphur on cobalt based catalysts	37
V-2-1 Effect on the catalytic activity	37
V-2-2 Effect of sulphur on product selectivity	39
V-3 Characterization of the catalyst exposed to sulphur	41
VI Sulphur resistant catalysts	43

VI-1 Sulphide catalysts	43
VI-2 Molybdenum Disulphide Catalysts for FT synthesis	44
<i>VI-2-1 MoS₂ catalysts for methanation</i>	44
<i>VI-2-2 Promoted MoS₂ catalysts for alcohol synthesis</i>	45
<i>VI-2-3 MoS₂ based catalysts for light olefin synthesis</i>	49
<i>VI-2-4 Catalyst preparation</i>	50
VII Objectives	53
Reference	55

I General introduction

Development of new renewable energy resources has attracted considerable attention from the government, companies and academic researchers. [1]. Within a future sustainable society, biomass is expected to become one of the major renewable resources for the production of food, animal feed, energy and chemicals. [2,3]. Biomass can be further processed to other forms of energy like methane or liquid transportation fuels like biodiesel [4], which could be used as substitutes for fossil fuels.

The biomass gasification is considered one of the most efficient ways to convert the energy embedded in biomass. It is also becoming one of the best alternatives for the recycling organic waste. The syngas produced via gasification of biomass, which also called bio-syngas, is a gaseous mixture of hydrogen, carbon monoxide, carbon dioxide, methane, water vapour, and some trace species. All of these gases especially H₂, CO, CH₄ are important intermediates for production of fuels and chemicals.

Olefins serve as an important feedstock for the chemical and petrochemical industry because they participate in a wide variety of reactions: hydroformylation, hydroamination, metathesis, epoxidation, Woodward cis-hydroxylation, cyclopropanation, hydroacylation, Diels-Alders, Prins, Pauson-Khand, Paterno-Büchi reactions, hydrogenation, halogen addition reaction, hydrohalogenation, Sharpless bishydroxylation, ozonolysis, hydroboration-oxidation, oxymercuration-reduction. Olefins are typically obtained by cracking of petroleum fractions. In these processes olefins are obtained as by-side products; the selectivity to specific olefins is rather low. A market study from USA shows that demand for light olefins in the Americas is expected to increase with a rate of 3.4% over the period 2010-2020 to reach around 68.4 million tons by 2020 [5]. Actually, these important feedstocks are mainly produced by steam cracking in the petrochemical industry. In this process, gaseous or light liquid hydrocarbons are heated to 750–950 °C, and then light olefins are separated from the resulting complex mixture.

Fischer-Tropsch (FT) synthesis, which allows efficient utilization of both fossil and

renewable resources to fuel and chemicals, has attracted much attention. In this process a combination of chemical reactions converts both carbon monoxide and hydrogen into hydrocarbons and oxygenates. With a suitable catalyst, the selectivity of light olefins could reach a level around 70% [6,7,8,9], FT synthesis can be realized at the temperature of 200 – 350 °C, much lower than that of steam cracking. The feedstocks (CO, H₂) used in this process can be supplied from gasification of biomass and coal, or from natural gas reforming.

This thesis focuses on the design of new catalysts for FT synthesis in order to synthesize highly valuable chemical feedstocks (light olefins or alcohols) from syngas produced from biomass. The biosyngas usually contains several impurities such as hydrogen disulphide, with a concentration of several ppm [10]. Numerous reports [11,12,13,14,15] showed that hydrogen disulphide could be harmful for the performance of conventional Fischer-Tropsch reaction. Conventional FT synthesis catalysts are very sensitive to sulphur, which could readily contaminate them. [11,12]. In this thesis small amounts of H₂S in syngas will be used in order to evaluate sulphur deactivation effect on conventional FT synthesis catalysts.

Design of sulphur resistant catalysts is a major challenge for FT synthesis. In previous publications various kinds of sulphur tolerant catalysts have been used for this reaction, for example noble metals (Rh [16], Pd [17]) and transition metal sulphides (MoS₂ [18], WS₂ [19]). The most studied S-resistance catalyst is molybdenum disulphide catalyst, because this catalyst presents a high activity on FT synthesis, and can attain to a good yield of alcohols [18,20,21,22]. However, the promoters should be always added to MoS₂ catalysts. On the pure MoS₂ catalyst, the methane selectivity is particularly high [23]. The most used promoters are alkali carbonates (potassium carbonates, cesium carbonates, sodium carbonates) as well as cobalt and nickel salts [24,25]. Very few information is available in the literature about use of molybdenum sulphide catalysts for olefin synthesis.

II History and current situation

II-1 Biomass

Generally speaking, biomass is organic matter that has stored energy through photosynthesis. This is the oldest source of renewable energy, which was used since the humans learned to use fire [26]. Many different processes have been developed to release and convert the energy stored from biomass. Much of the current effort focuses on lignino-cellulosic biomass. Some common examples are wood chips, switch grass, corn stover, unused seed corn, and yard waste.

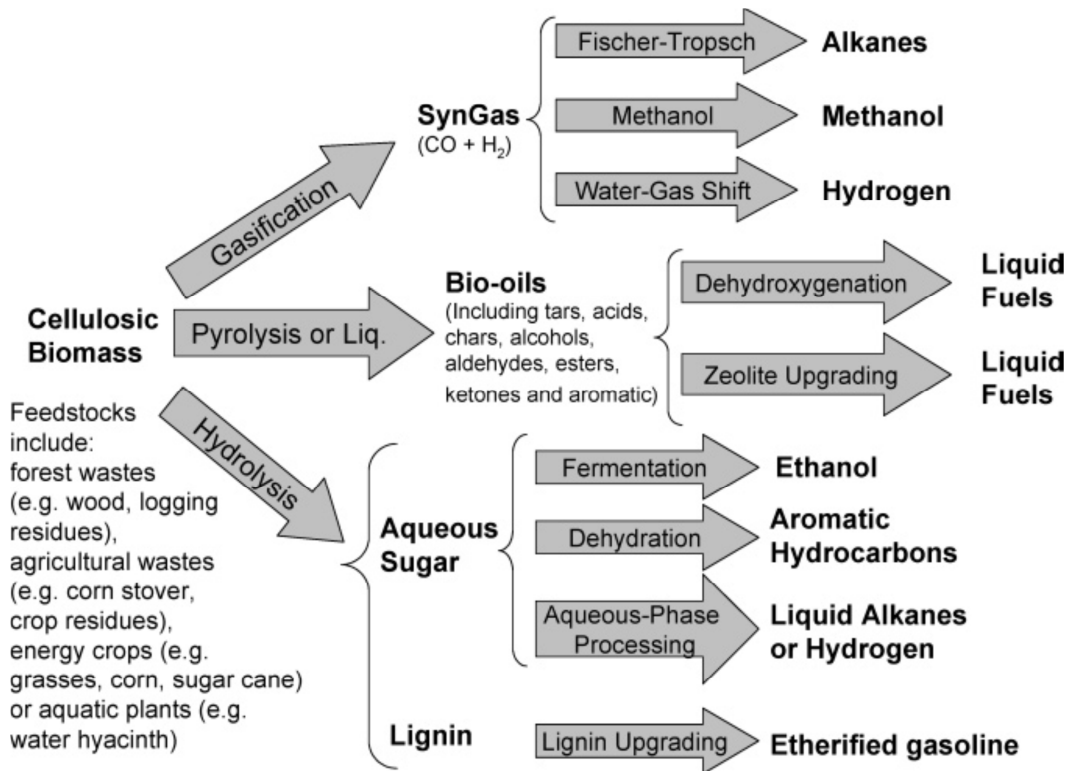


Figure 1-1: Applications of biomass through transformation [27]

Among many reasons for increased biomass utilization in those cases, environmental benefits are also very important. Perhaps the most significant environmental benefit of biomass is a potential reduction in carbon dioxide (CO₂) emissions. The production of second

generation fuels and chemicals from lignino-cellulosic biomass should result in over 70% reduction in GHG emissions into the atmosphere compared to fossil resources. Compared with coal, biomass feedstocks have lower levels of sulphur or sulphur compounds [28,29]. Therefore, substitution of biomass from coal in power plants has the effect of reducing sulphur dioxide (SO₂) emissions. Demonstration tests have shown that biomass co-firing with coal can also lead to lower nitrogen oxide (NO_x) emissions. The second generation lignino-cellulosic biomass can be converted using gasification to syngas, via pyrolysis to bio-oil or via hydrolysis to sugar and lignin.

II-2 Biomass to Synthesis Gas via Gasification

Gasification is a thermo-chemical process in which biomass reacts with air (or oxygen) and steams to produce synthesis gas, a mixture consisting primarily of CO, CO₂, H₂, and H₂O [27], as well as small quantities of gaseous impurities (e.g. H₂S, NH₃, CH₄, HCN, HCl), solid ash, and condensable compounds (e.g tars) (see Figure 1-2). The gas produced can be standardized in its quality and is easier and more versatile to use than the original biomass (e.g. it can be used to power gas engines and gas turbines or as a chemical feedstock for the production of liquid fuels) [4]. This mixture of syngas for gasification of biomass can be used to produce a range of products in following step, such as fuels via the Fischer–Tropsch process.

Gasification technology is the first step of biomass to liquid (BTL) process. BTL is a type of X to liquid (XTL) process (where X can be C (coal), G (natural gas) or B (biomass)). In XTL, different feed, coal, natural gas and biomass, are firstly transformed to the syngas intermediate, which contains principally hydrogen and carbon monoxide; secondly the syngas is turned to hydrocarbons or oxygenates; finally the products are separated, purified or processed for particular applications.

II-2-1 Gasification procedure

Biomass gasification is a rather complex process; there are four stages in the gasification:

(1) **Drying:** This stage, usually occurs at 100°C to 200°C, is a dehumidification step for following reactions. In biomass, the moisture content ranges from 5% to 35% [4], after drying stage, moisture contents less than 5% in biomass.

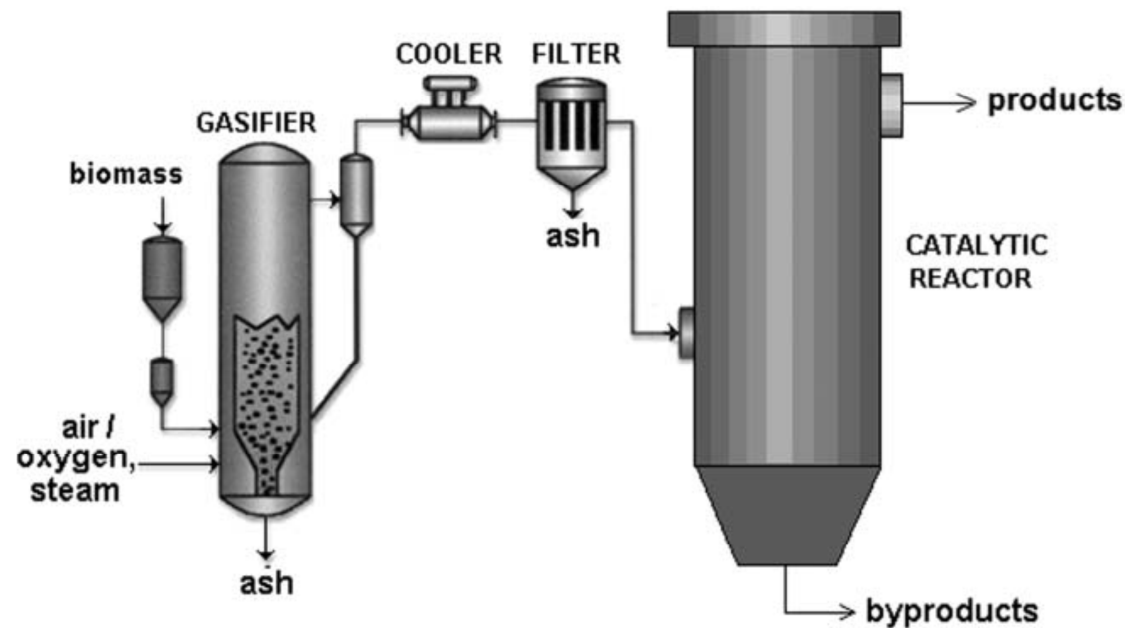


Figure 1-2: Mode for BTL procedure [30]

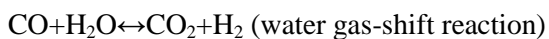
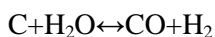
(2) **Pyrolysis:** Essentially, this stage is thermal decomposition of biomass in an atmosphere containing no oxygen. Pyrolysis produces gaseous, liquid and solid products:



(3) **Oxidation:** This is a reaction between solid charcoal and oxygen. Hydrogen present in the biomass is also oxidised to generate water. A large amount of heat is released with the oxidation of carbon and hydrogen. Depended on ratio of O_2 and carbon, the oxidation can result in CO (partial oxidation) as well as CO_2 (stoichiometric oxidation). Besides carbon, methane and even other hydrocarbons can be also reformed to CO and H_2 :



(4) Reduction: In the absence of oxygen, several reduction reactions occur in a higher temperature range (up to 800°C):



II-2-2 Gasification Reactors

Various kinds of gasification reactor have been designed and applied in industry. According to different gaseous flow routes, all these reactors can be divided to three principal types:

1. Updraft reactor (Figure 1-3A): where biomass enters from the top of the reactor and air/oxygen/steam enter from the bottom of the reactor, flow upward, and the product gas leaves from the top. The advantages of updraft reactors are that they represent a mature technology for heat production, can be used for small-scale applications, can handle feeds with a high moisture content, and there is no carbon in the ash. The disadvantages of updraft reactors are that they have a feed size limit, a high tar yield, and slagging potential.

2. Downdraft reactor (Figure 1-3 B): In this reactor the air or oxygen and the solid biomass enter at top of the reactor flow downward, and the product gas leaves at the bottom of the reactor. The product gas contains the lowest concentration of particulates and tars (approximately 1 g/Nm³) because most of the tars are combusted in this reactor. The flame temperature in this reactor is 1000-1400 °C, and the tars produced are almost exclusively tertiary tars. This reactor is ideal when clean gas is desired. Disadvantages of this type include

a lower overall thermal efficiency and difficulties in handling higher moisture and ash content.

3 Fluidized-bed reactor (Figure 1-3 C) where the biomass, which is previously reduced to a fine particle size, and air, steam, or oxygen enter at the bottom of the reactor. A high velocity of the gas steam forces the biomass upward through a bed of heated ceramic or silica particles. This reactor is good for large-scale applications, has a medium tar yield, and the exit gas has a high particle loading. The typical tar is of an intermediate level between the updraft and the downdraft reactor, and tars are a mixture of secondary and tertiary tars.

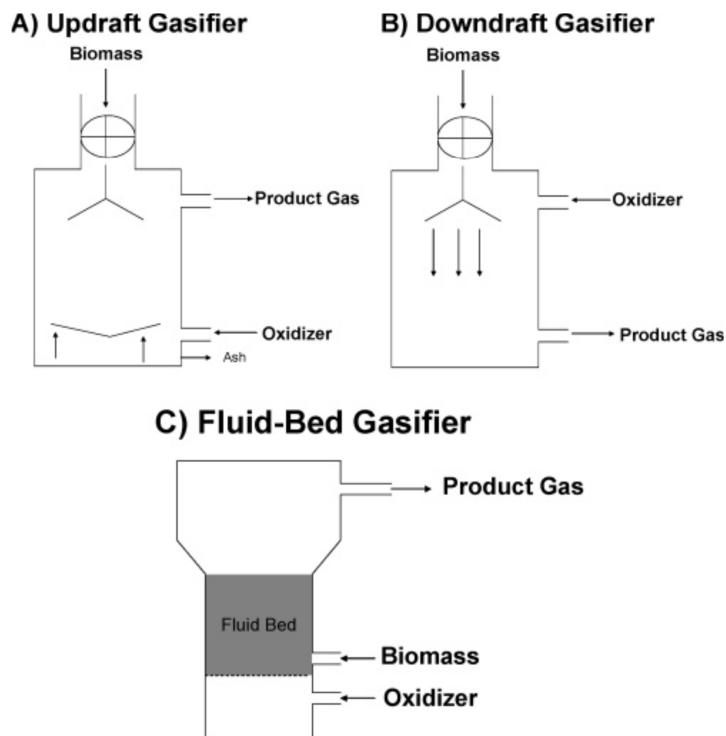


Figure 1-3: Reactors of biomass gasification [30]

II-3 Pretreatment of syngas before FT synthesis to avoid sulphur poisoning

In syngas produced by gasification of biomass, the concentration of H_2S could be up to 1 to 2 percent [27]. So in industrial application, the desulphurization procedure is necessary in

the gasification step [31]. Actually, there are two distinct routes of treatment: “wet” low temperature cleaning and “dry” high temperature cleaning.

The principal of “wet” cleaning is using cyclone separator and bag filter to separate gas physically and then using basic (usually NaOH) and acid (H₂SO₄) solution to absorb impurities [31], not only H₂S, but also COS, NH₃, HCl, HCN. With this method, 99% of these toxic impurities can be eliminated. Deeper purification is required however for FT synthesis which can be achieved by adsorption of sulphur using for example, zinc oxide.

“Dry” high temperature cleaning consists of several filters and separation units in which the high temperature of the syngas can (partly) be maintained, potentially resulting in efficiency benefits and lower operational costs.

III Fischer-Tropsch synthesis

Fischer-Tropsch synthesis is a catalytic reaction which converts syngas to hydrocarbons and alcohols. This reaction was uncovered by two German scientists, Franz Joseph Emil Fischer and Hans Tropsch, working at the Kaiser-Wilhelm-Institut for Chemistry. In 1925 they patented this technology in Germany and then in 1926 in the USA [32,33]. FT synthesis was firstly commercialized in Germany in 1936, and then it was widely used to produce synthetic fuels in Germany during the Second World War. After 1940s, FT synthesis had been desolated for a decade owing to cheap and available oil. The interest in this technology dramatically increased during the oil crisis of 1970s, because FT synthesis could supply hydrocarbons and alcohols from other fossil resources such as coal. Currently, the interest in FT synthesis is due both to the problem of rational valorisation of fossil and renewable resources and environmental concerns. In the last two decades a number of FT synthesis plants were commissioned in South Africa (Sasol, Moss gas), Malaysia (Shell) and Qatar (Sasol, Shell, Qatar Petroleum). A number of projects are currently being designed or under construction (Nigeria, Kazakhstan, China, ...). Iron, cobalt, ruthenium, nickel and copper are most common catalysts for syngas conversion. Ruthenium is a scarce and expensive metal,

whereas nickel only forms methane at reaction temperatures sufficiently high to suppress nickel carbonyl formation. Copper catalyst produce principally methanol. As a result, only cobalt and iron are the most used active metal for FT synthesis. In fact, when the FT synthesis was firstly discovered by Fischer and Tropsch, it was iron and cobalt that they took as catalysts and both the two metals are remaining as the only ones for industry

Despite that fact that FT synthesis process it has been used on the industrial scale, it still suffers from a number of challenges. The catalyst stability needs to be improved; selectivity enhancement would also be very advantageous. Economically, one would like to have the lowest possible CH₄ selectivity; CH₄ is an undesired product because of its low value.

III-1 Iron based FT catalysts

The FT reaction selectivity on iron catalysts depends on the reaction conditions. At a relatively high reactions temperature (around 615 K), Fe based catalysts show high olefin and oxygenate selectivity [23] (see Table 1-1), whereas at lower temperature, the Fischer-Tropsch process principally produces paraffin wax, then diesel as well as other light products can be obtained by hydrocracking [34]. Table 1-2 shows the comparison of selectivity at high/low temperature.

Table 1-1: Major Companies of industrial FT synthesis over the world [35]

Company	Country	Feedstock	Catalyst	Reactor	Producing capacity*
Sasol	North Africa	Initially coal, then nature gas	Fused K_Fe	HTFT fluidized bed	5000
			Precipitated K_Fe	LTFT fixed bed	
			Precipitated K_Fe	LTFT slurry phase	
		Mostly coal	Fused K_Fe	HTFT Fluidized bed	160000
				HTFT SAS reactor**	
Shell	Malaysia	Nature gas	Co/SiO ₂ ; Co/TiO ₂	LTFT fixed bed	14500
Petro SA	North Africa	Nature gas	Fused K_Fe	HTFT fluidized bed	22000
Sasol-QP	Qatar	Nature gas	Co/Al ₂ O ₃	LTFT slurry phase	34000
Shell	Qatar	Nature gas	Co/TiO ₂	LTFT fixed bed	140000
Chevron	Nigeria	Nature gas	Co/Al ₂ O ₃	LTFT slurry phase	34000

* Unit: barrels per day

**SAS reactor: Sasol Advanced Synthol reactor, fixed fluidized bed.

Iron based catalyst has high activity in the Water Gas Shift reaction (WGS) reaction ($\text{H}_2\text{O} + \text{CO} = \text{H}_2 + \text{CO}_2$) [36], so that it can operate with syngas produced via gasification of coal, which contains much more CO than H_2 . In late 1950s, Sasol commercialized a circulating fluidized bed reactor at their Sasolburg facilities where syngas from coal gasification is supplied. The iron catalyst is fluidized at high temperature to produce light ($\text{C}_2\text{-C}_5$) hydrocarbons as feedstock for industry. Subsequent to Sasol's successful commercialization of iron-catalysed FT synthesis, South Africa's national oil company (PetroSA) commercialized a GTL facility. Similar reactor (fluidized bed) and catalyst (Fe) was employed. In 2010, it still remains one of the world's largest GTL project, producing about 22000 barrels per day of high-quality FT synthesis-derived fuels. In USA Rentech has also developed iron-based FT synthesis. The Rentech Product Demonstration Unit (PDU) was then built in 2008. The PDU produced approximately ten barrels per day of ultra-clean diesel as well as naphtha, using syngas from both natural gas and biomass.

China has also seen fast growing FT technology. A high-temperature slurry-phase technology with associated iron-based catalyst is currently under development. The integrated technology significantly improves thermal reactor efficiency and enhances the catalytic activity. This technology has been demonstrated with a producing capacity of 4000 barrels per day in semi-commercial CTL facility in the province of Inner Mongolia. Meanwhile, another commercial CTL company is going to be set in the province of Shan Xi, with the promoted iron based catalysts.

Table 1-2: High temperature and low temperature of FT synthesis on Fe catalysts [37]

Product	High Temperature FT (HTFT)	Low Temperature FT (LTFT)
CH_4	8%	3%
C2-4 Paraffin	6%	4.5%
C2-4 Olefin	24%	4%
C5-C6	16%	7%
C7+	41%	77.5%
Alcohol	2.8%	3.8%
Ketone+ Acid	2.2%	0.2%
Aromatic	5%	0%

III-2 Cobalt based FT catalysts

Cobalt as a FT synthesis catalyst was first claimed by Fischer and Tropsch in their original patent of 1925 [38]. The commercialization of the FT synthesis by Germany and Japan in the period 1938–45 relied fully on cobalt catalysts. Since the oil crises of the 1970s the interest in cobalt-based FT synthesis catalysts reappeared. Many companies showed interest in cobalt FT synthesis, for example, BP, Conoco-Philips, Gulf, Exxon-Mobil, IFP, Johnson Matthey, Sasol, Shell, Statoil, and Syntroleum. Almost cobalt based FT synthesis processes focus on wax production, followed by hydrocracking to produce diesel. Thus, cobalt FT synthesis catalysts are exclusively utilized in low temperature FT synthesis, and are applied in fixed-bed, slurry-phase, and micro-channel FT synthesis reactors.

Generally, cobalt catalyst system consists of four components [39]: the active metal (cobalt content between 10% - 30%), a reduction promoter: usually noble metal, 0.05% - 1%, a structural promoter (ZrO_2 , La_2O_3 , 1% - 10%) and a support (refractory oxide or carbon materials).

The common preparation method for cobalt based catalyst is impregnation with cobalt nitrate solution $Co(NO_3)_2$. This salt can be decomposed to Co_3O_4 at a temperature over $310^\circ C$. Some inactive particles such as cobalt aluminate and cobalt silicate may be present a high fraction at higher calcination temperature [40]. The cobalt oxide crystallites are then reduced to metallic cobalt which represents the active phase for FT synthesis.

III-3 Mechanism of FT reaction

The mechanism of FT synthesis is currently under debate and a number of reaction schemes have been proposed for different catalysts. In this part, we will principally discuss the FT synthesis on cobalt based catalysts and molybdenum disulphide based catalysts that are used in our work. In all the proposed mechanisms FT reaction involves the following steps: (1) adsorption of syngas species, H_2 and CO (2) chain initiation (3) chain growth (4) chain

termination (5) desorption of products, hydrocarbon and/or oxygenate (6) readsorption of olefin and secondary reaction.

III-3-1 Initiation of FT reaction

A great number of surface species can be involved in the chain initiation and chain growth. It is generally accepted that the chain initiation is started from the adsorption of CO, following by dissociation or hydrogenation to form radicals such as CH, CH₂ and CH₃, which could be called the "structural blocks" for hydrocarbon.

III-3-1-1 CO adsorption

The CO molecules are adsorbed on the active sites of the catalysts. There are three representative modes of CO adsorption, as illustrated in Figure 1-4 [41,42,43].

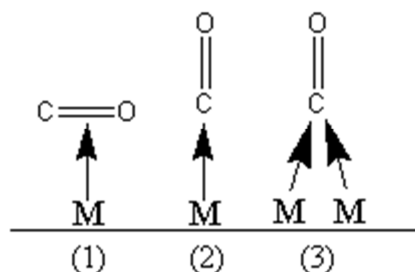


Figure 1-4: Three modes of CO adsorption to active metal (M)

Blyholder [44] proposed a model of carbon monoxide adsorption on FT active metal, this theory was the most commonly cited. In this model, CO is bonded with a form of its molecular axis as a C atom down position to the metallic surface (Figure 1-4 (2)). CO is considered as being typically a π acceptor. The less the metal is effectively positively charged, the weaker the C-O bond would be until it is broken [41]. The CO molecule could then be adsorbed in the dissociative or associative mode, which depends on the metal nature and the temperature, as shown in Figure 1-5.



(* is the active site on active phase of catalysts)

Table 1-5 shows different types of carbon monoxide adsorption on transition metals. At the temperatures of 200-300°C, which is the usual temperature for CO hydrogenation in industry, the borderline between associative and dissociative adsorption is shifted to the right in the periodic table and situated at the vicinity of Os, Rh and Ni.

On cobalt based catalysts, Ishihara et al. [45,46] indicated that crystal size of Co and nature of the support could have an important effect on CO adsorption. The electro-donative support favoured the dissociative of the CO molecules. The particle size of cobalt also plays a role in the CO adsorption [47].

Figure 1-5: Borderline between associatively and dissociatively adsorbed CO

← CO Dissociative			CO Associative →		
Cr	Mn	Fe	Co	Ni	Cu
Mo	Tc	Ru	Rh	Pd	Ag
W	Re	Os	Ir	Pt	Au
25°C			200-300 °C		

III-3-1-2 H₂ adsorption

The adsorption of hydrogen on the metal is generally dissociative ($\text{H}_2 + 2* \rightleftharpoons 2\text{H}^*$) [48]. Similar as CO adsorption, metal particle size is an important parameter, on smaller metallic particles; the metal-H bond is stronger. Besides, the effect of spillover could be observed, which is about the diffusion of hydrogen on the surface of catalysts, both particles of support and supports. This spillover effect could be controlled by the addition of promoters. Hydrogen adsorption on cobalt catalysts can be higher at higher temperatures; [42]. Moreover, at the ambient temperature, the fraction of reversibility of hydrogen is higher than that of CO.

The CO and H₂ molecules are adsorbed on the same metallic sites. The adsorption of CO was generally considered stronger and faster than that of hydrogen [45,45]. It is suggested that with increasing electro-negativity of the support ($\text{SiO}_2 > \text{TiO}_2 > \text{Al}_2\text{O}_3$), the donation of electron from metal to CO molecule decreases so the bond of metal-CO became weaker, while the adsorption of hydrogen was favourable [49].

The mechanistic studies for FT synthesis often assumed the formation of CH_2 and CH_3 species, while recent characterization and theoretical studies advocate formation of CH species [50].

III-3-2 Chain Growth and Termination of FT synthesis

Chain propagation and termination of FT reaction is quite a complex process. Most of mechanisms use CH_x structural block to “build” different hydrocarbon. Five different mechanisms have been proposed for the chain growth:

- 1) carbide mechanism [51], Figure 1-6;
- 2) alkyl mechanism [52], Figure 1-7;
- 3) alkenyl mechanism [53], Figure 1-8;
- 4) CO insertion mechanism [54], Figure 1-9;
- 5) oxygenate mechanism [55,56], Figure 1-10.

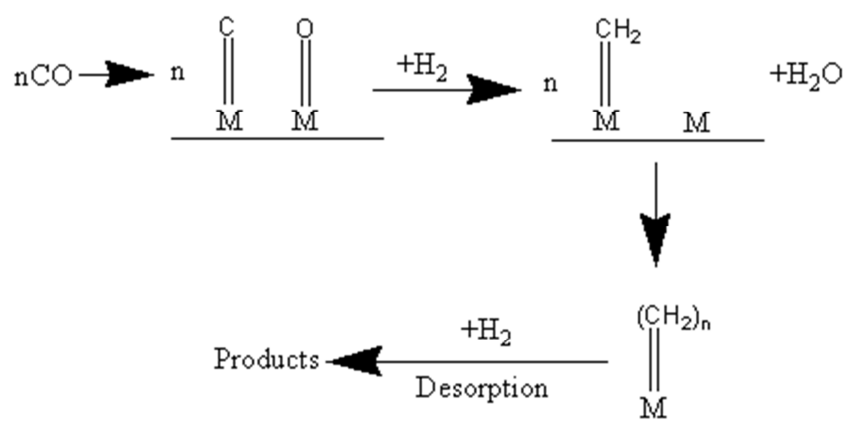


Figure 1-6: Carbide mechanism

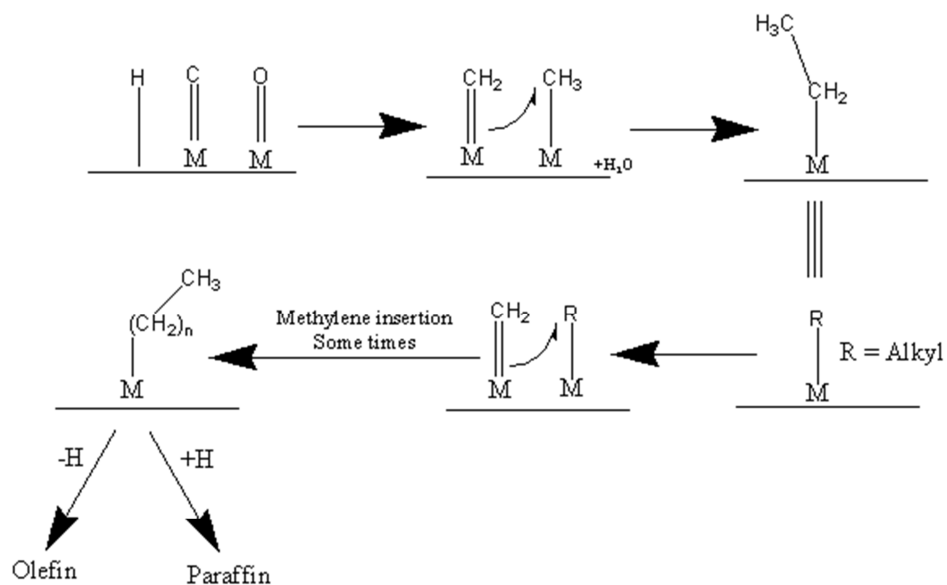


Figure 1-7: Alkyl mechanism

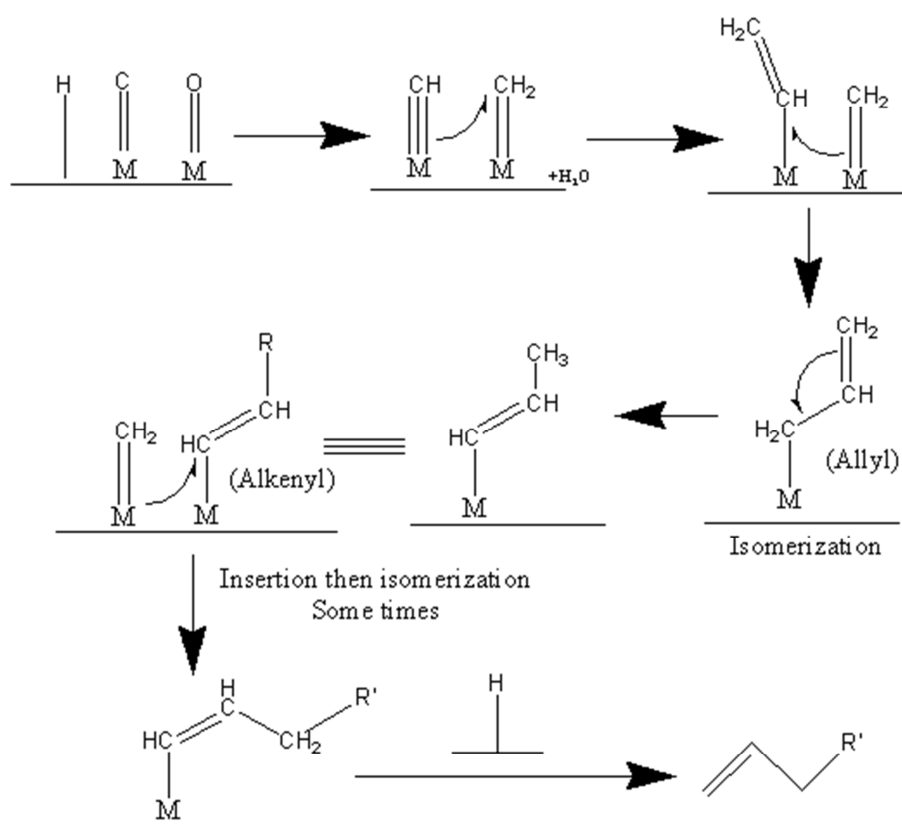


Figure 1-8: Alkenyl mechanism

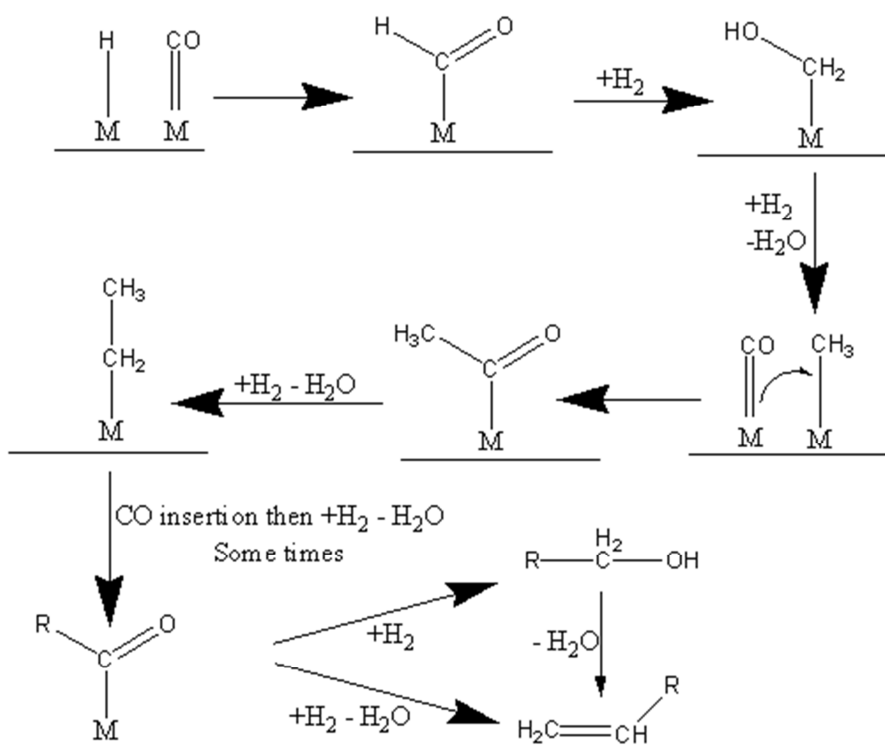


Figure 1-9: CO insertion mechanism

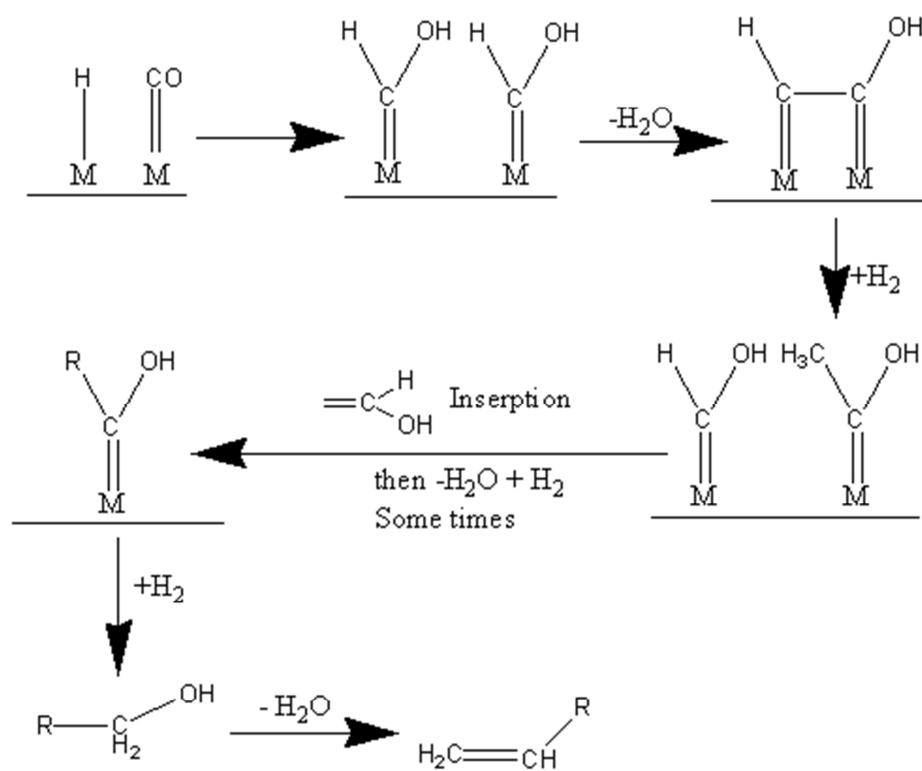
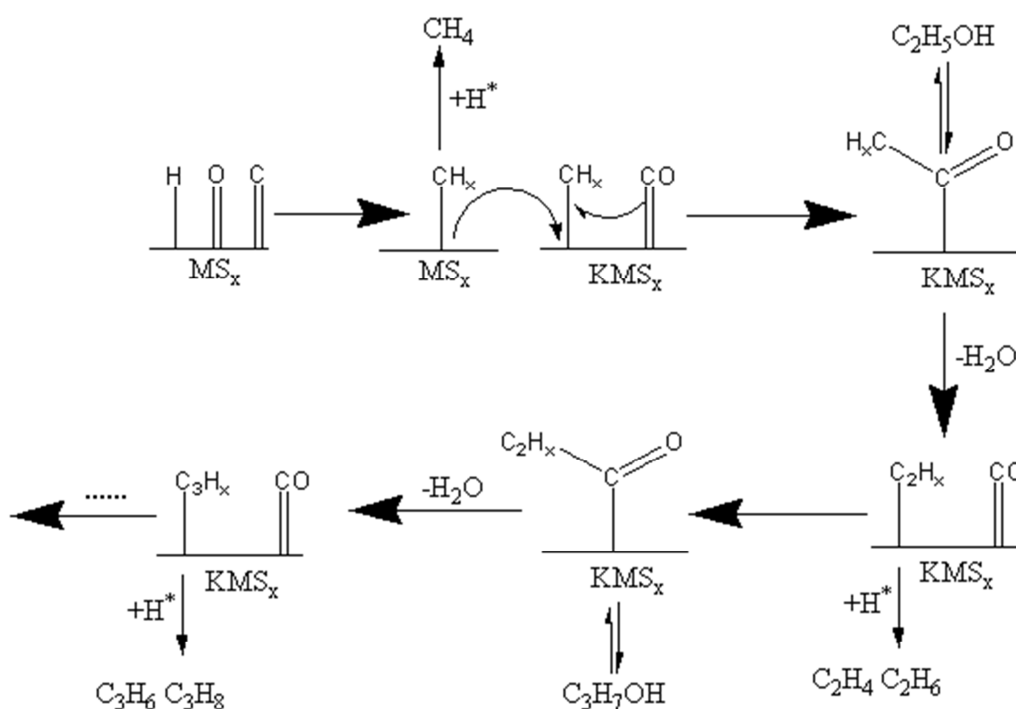


Figure 1-10: Oxygenate mechanism

III-3-3 Mechanism of FT synthesis on MoS₂ based catalyst

Bulk MoS₂ catalysts produce only methane and carbon dioxide [57,58]. The C₂₊ hydrocarbons and alcohols could not be formed unless the catalysts were promoted, by alkali or transition metals such as Co or Ni. Li et al [59] proposed a mechanism shown in Figure 1-11, where there were two kinds of active sites for the promoted MoS₂ catalysts. The first type of site is the metal sulphide, containing MoS₂, CoS_x, NiS_x as well as FeS_x. The dissociative adsorption of CO is much more rapid than non-dissociative adsorption on MoS₂, CoS_x, NiS_x, and FeS_x sites. Then the adsorbed C* species could combine with H* species to form methane or CH_x species as structural blocks. The KMS_x (M are the transfer metal as Mo, Co, Ni, Fe) phases present another type of sites. On this kind of active phases, the CO adsorbs molecularly, the adsorbed *CO species insert the CH_x species from MS_x sites, to form the oxygenate species such as *C₂H_xO. *C₂H_xO which can be hydrogenated to form ethanol and also can be dehydrated to alkene and alkane. The propagation of chain is caused by insertion of associatively adsorbed CO into the C_xH_y species [59,60].

Figure 1-11: FT reaction on K/MoS₂ based catalysts

This mechanism explains formation of alcohol, olefin and paraffin over promoted sulphide catalysts. This mechanism also explains why branched alcohols do not form on the promoted MoS₂ catalysts. Note that the adsorbed C_xH_y species could not be exactly defined as alkyl or alkenyl, and the mechanism of their hydrogenation to alkene and alkane is still unclear.

III-4 Kinetics of FT reaction

The kinetics of FT reaction has been addressed in numerous publications. The kinetics of FT synthesis often depends on the catalyst. Even for the same catalyst, the kinetics may be varied with the reaction conditions. Table 1-3 shows a few rate equations proposed for iron, cobalt and molybdenum sulphide catalysts.

Table 1-3: Rate Equation on different catalysts

No.	Founder	Rate Equation	Catalyst	Reference
1	Yates	$R = mP_{H_2}P_{CO} / (P_{CO} + nP_{H_2})$	Fe, Co	64, 65
2	B Sarup	$R = k(P_{CO}P_{H_2})^{0.5} / (1 + b(P_{CO})^{0.5})^2$	Co	64
3	Anderson	$R = aP_{H_2}^2P_{CO} / (1 + bP_{CO}P_{H_2}^2)^2$	Co	65
4	S.A Eliason	$R = k(P_{H_2})^x(P_{CO})y(a - a_\infty)^m$	Fe (deactivation mode)	61
5	Arakawa	$R = kP_{CO}(P_{H_2})^2 / (P_{CO}P_{H_2} + bPH_2O)$	Fe, Co	62
6	T.Y Parker	$R = k(P_{H_2})^3P_{CO} / (a(P_{H_2})^{0.5} + bP_{CO})$	KMoS ₂	63

Equation (1) was firstly proposed for commercial iron based catalyst [64], in the LTFT and HTFT reactor, then the same kinetic equation was also validated for cobalt based catalysts [65]. Both Equations (2) and (3) can be suitable for cobalt based catalyst. Equation (2) was tested at a constant temperature while in the case of equation (3) the temperature was variable [65,66]. In Equation (4), the kinetics of FT synthesis was combined with deactivation kinetics. Equation (5) could also be used on either Fe or Co based catalysts, this equation takes into account water pressure which is always present during FT synthesis. Equation (6) was

validated for MoS₂ based catalysts where the FT synthesis products consisted of paraffins and olefins, while alcohols were ignored. It is difficult to identify which one is a “best” equation. Probably the different equations are valid for a certain catalysts processing at the specific range of experimental conditions.

III-5 Thermodynamics of FT reaction

The thermodynamic parameters of major FT synthesis reactions are shown in Table 1-4.

Table 1-4: Parameters of FT reaction or by-reaction

Reaction	Equation	ΔH	ΔG	REF
Methanation	$\text{CO} + 3\text{H}_2 = \text{CH}_4 + \text{H}_2\text{O}$	-206.3(298K)	-94 (500K)	37
MeOH formation	$\text{CO} + 2\text{H}_2 = \text{CH}_3\text{OH}$		+21(500K)	37
MeOH formation	$\text{CO} + 2\text{H}_2 = \text{CH}_3\text{OH}$	-91 (298K)	-25.1(298K)	67
Ethane formation	$\text{CO} + 2\text{H}_2 = 1/3(\text{C}_2\text{H}_6) + \text{H}_2\text{O}$		-31(500K)	37
EtOH formation	$\text{CO} + 2\text{H}_2 = 1/2(\text{C}_2\text{H}_5\text{OH}) + 1/2\text{H}_2\text{O}$	-126.8(298K)	-105.5(298K)	67
EtOH formation	$\text{CO} + 2\text{H}_2 = 1/2(\text{C}_2\text{H}_5\text{OH}) + 1/2\text{H}_2\text{O}$		-27(500K)	37
Chain Propagation	$n\text{CO} + 2n\text{H}_2 = (\text{CH}_2)_n + n\text{H}_2\text{O}$	-165 (500K)		68
WGS	$\text{CO} + \text{H}_2\text{O} = \text{CO}_2 + \text{H}_2$	+41 (298K)		37
WGS	$\text{CO} + \text{H}_2\text{O} = \text{CO}_2 + \text{H}_2$	-39 (500K)	-28 (500K)	68
Carbon deposition	$\text{CO} + \text{H}_2 = \text{C} + \text{H}_2\text{O}$	-115 (500K)		68

* The unit for ΔH and ΔG is kJ/mol.

Most of FT reactions are favoured thermodynamically at lower temperatures and higher pressures. Most of them are exothermic. This suggests that temperature control can be challenging under some conditions and heat transfer could affect the catalytic performance. Note that for reactions of alcohol formation (here is methanol and ethanol), the ΔG decreased at a higher temperature. So a relative lower temperature could be favourable for synthesis of alcohol. Figure 1-12 illustrate this phenomena. The spontaneity for formation of different products follows the order: paraffin > olefin > alcohol.

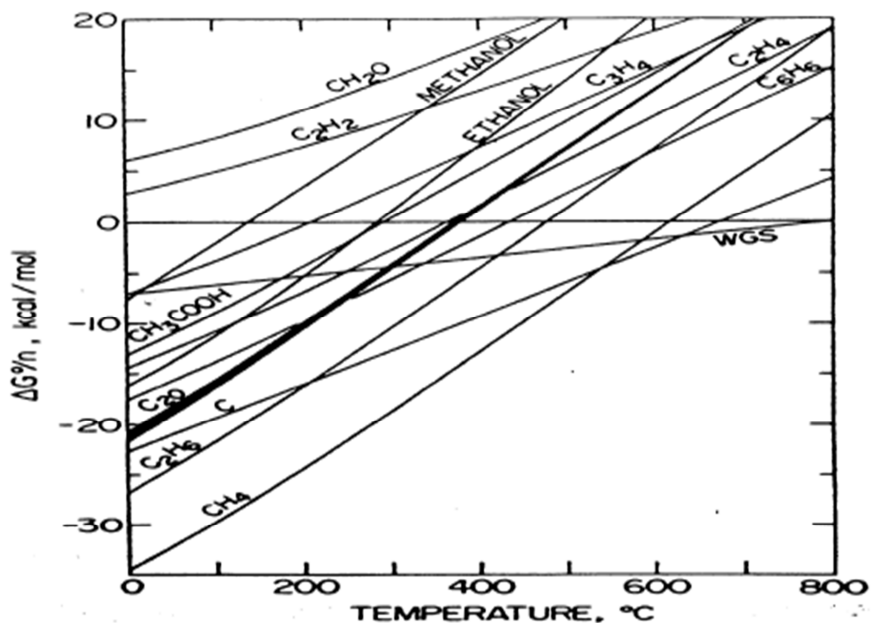


Figure 1-12: $\Delta G_{(298K)}$ of products via FT synthesis at different temperature.

IV Fischer-Tropsch to Light Olefin (FTO) process

IV-1 Light olefin synthesis

Lower olefins, containing ethylene, propylene and butylene are extensively used in the chemical industry as building blocks for synthesis of a wide range of products such as polymers, solvents, drugs, cosmetics, and detergents. Ethylene can be oxidized to ethylene oxide, a key raw material in the production of surfactants and detergents, as well as ethylene glycol that is widely used as automotive antifreeze as well as higher molecular weight glycols, glycol ethers and polyethylene terephthalate. Through polymerization, ethylene can be valorised into detergents, plasticisers, synthetic lubricants, additives, and also used as co-monomers in the production of polyethylenes. Ethylene is a fundamental building block for chemical industry and different applications of ethylene are shown in Figure 1-13. Propylene is the second most important starting product in the petrochemical industry after ethylene. Manufacturers of the plastic polypropylene account for nearly two thirds of all

demand of plastic, the worldwide sales of propylene reached a value of over 90 billion US dollars per years since 2008. Besides, propylene is also used to produce isopropanol (propan-2-ol), acrylonitrile, epoxypropane and epichlorohydrin. Butylene has four isomers: 1-butylene, isobutylene, cis-2-butylene and trans-2-butylene. 1-butylene is principally used for synthesizing butadiene. All butylenes can be polymerized to products various plasticisers. Isobutylene is also used for the production of methyl tert-butyl ether and isooctane, both of which are used as gasoline boosters.

Table 1-5: Feedstock for ethylene production

Year	1984	1995	2006
Ethane	22	27	32,4
Liquefied Petroleum Gas	15	14	6.7
Naphtha	54	48	43.1
Diesel	8	10	8.7
Others	1	1	9.1

Commercial ethylene production is mainly based on steam cracking of a broad range of hydrocarbon feedstocks. In Europe and Asia, ethylene is obtained mainly from cracking of naphtha, gas oil, and condensates, while in the U.S., Canada, and the Middle East ethylene is produced by cracking of ethane and propane. Table 1-5 shows different feedstock for ethylene production via steam cracking. Naphtha cracking is the major source of ethylene worldwide; however, ethane cracking has been gaining importance in recent years because of major surge in the production of shale gas.. Propylene is obtained mainly from naphtha steam crackers (globally about 65%) as a co-product with ethylene, and also from gasoline-making from fluid catalytic cracking units (FCCU) which supplies about 28% of propylene. In addition propylene can be produced via dehydrogenation of propane, but this procedure can only realized in the regions with abundant and cheap propane feedstock. Butylene is extracted by fractional distillation from the C₄ hydrocarbon mixture produced by catalytic cracking of long chain hydrocarbons left during refining of crude oil.

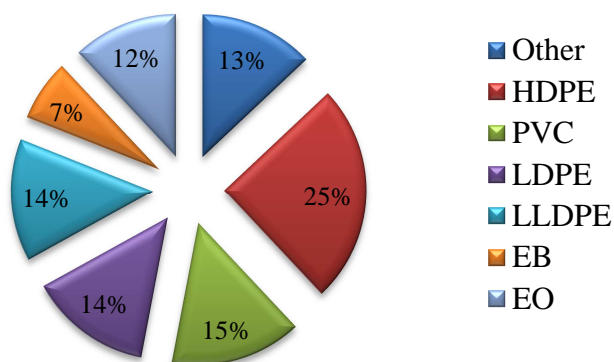


Figure 1-13: Ethylene consumption over different products in the world. HDPE: high-density polyethylene. PVC: Polyvinyl chloride. LDPE: low-density polyethylene. LLDPE: linear low-density polyethylene. EB: ethyl benzene. EO: ethylene oxide.

The demand of light olefin is always very important in petrochemical industry. Take ethylene as example, the consumption of ethylene in 2016 should attain over 160 million tons (Figure 1-14), 16% more than that in 2011. In 2008 and 2009, ethylene demand slightly decreased due to the global slowdown in the economic growth. Nevertheless, after that the demand continued to grow and should keep growing in the future. The analysts predict world-wide capacity for production of ethylene will be increasing fast in coming years in particular in the Mid-East and Asia regions (Table 1-6).

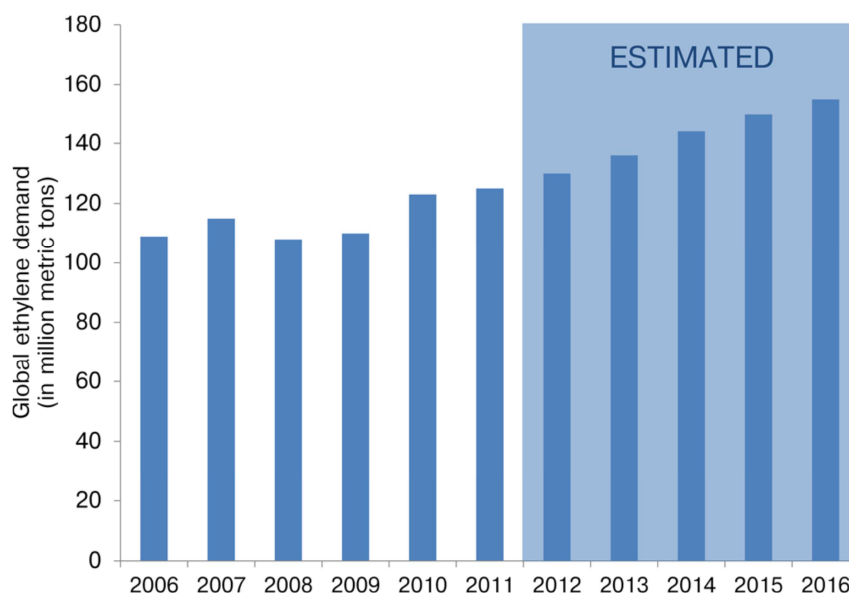


Figure 1-14: Ethylene demand in the period 2006–2011. Forecast for the period 2012–2016. Source: Chemical Market Associate

The conventional steam cracking method for olefin synthesis presents disadvantages relevant to high energy consumption, considerable CO₂ emission and low selectivity to the specific hydrocarbons. The Methanol-To-Olefins (MTO) technology involves a number of technological steps which reduce the overall conversion efficiency. In addition, the catalyst undergoes noticeable deactivation. As a result, the produced olefins get rather costly.

Table 1-6: Production of ethylene (thousands of tons)

Region	Year 2008	Year 2009	Year 2010
Asia	33362	39731	41088
Europe	24918	24918	19968
USA	28407	27554	23975
Middle East	19312	20602	N/A

IV-2 Current development of FTO process

High temperature Fischer-Tropsch (FT) synthesis represents a major interest for synthesis of light olefins. In FT synthesis, light olefins are produced directly using carbon monoxide hydrogenation without any intermediate steps (Figure 1-15). Recently many efforts have been dedicated to development of biomass as a renewable feedstock for the production of different compounds, including olefins. Fischer-Tropsch synthesis leading to olefins (FTO) is a direct route without any intermediates. The FTO process represents a strong alternative route for the sustainable production of lower olefins from biomass-derived synthesis gas.

IV-2-1 FTO on iron catalysts

Iron catalysts have shown so far the highest olefin productivity in direct FT synthesis; however they are sensitive to the presence of small amounts of sulphur in syngas [69]. The technology for olefin synthesis from syngas was firstly elaborated in South Africa. Since 1955 SASOL has produced chemicals and gasoline using the so called Synthol process [70].

The main aim of this process is to produce liquid fuels although lower olefins are also obtained depending on the operating conditions and the type of catalysts.

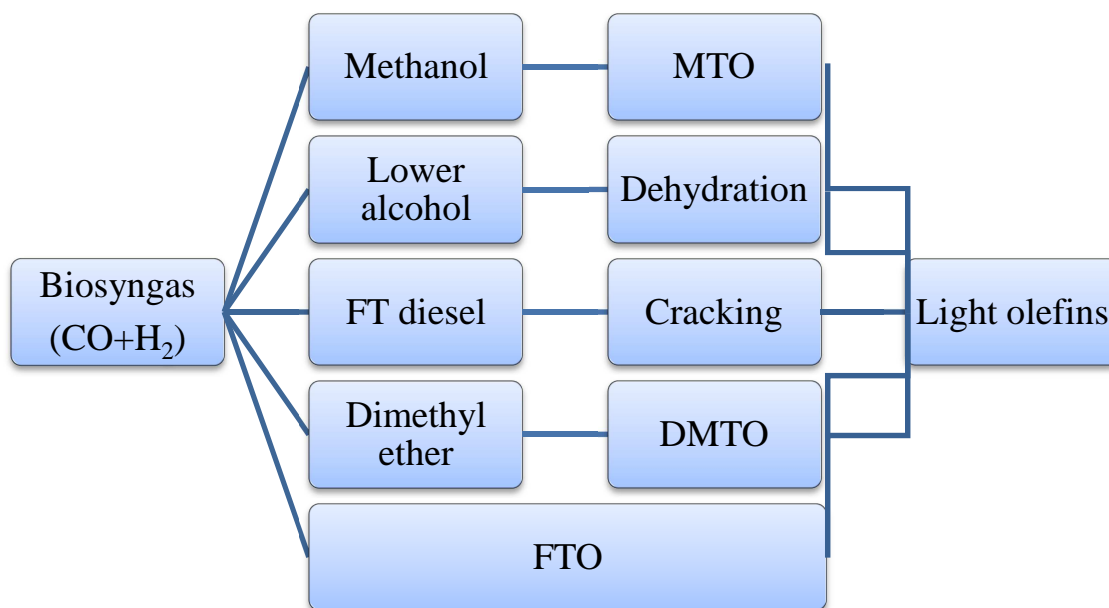


Figure 1-15: Biosyngas to light olefin procedure

Between the mid 1970s and mid 1980s iron based catalysts with oxides of other metals such as Ti, V, Mo, W, or Mn, were proposed for the HTFT process. Büssemeier et al reported [69, 71] that mixed oxide catalysts could produce light olefins with a selectivity of 70% and methane selectivity of 10% (280 °C, 10 bar, H₂/CO = 1). They also reported that a catalyst prepared by sintering of Fe, Ti, Zn, and K displayed high light olefins selectivity (75%) observed at high syngas conversion (87%) at 340°C [72]. Promotion of Fe-based bimetallic catalysts was widely used to improve the catalytic performance for the direct production of lower olefins from syngas. Co–Fe and Fe–Mn catalysts are the most studied systems. In the case of Co–Fe catalysts, attempts were made to improve catalytic stability and activity of the already olefin-selective Fe catalysts by alloying it with a more active cobalt Fischer–Tropsch catalyst. Fe–Co oxides prepared by co-precipitation of cobalt and iron nitrates were investigated by Mirzaei et al [73]. They reported that a potassium promoted (1.5 wt %) 40%Fe:60%Co (molar basis) catalyst modified with SiO₂ showed around 48% of ethylene and around 20% of propylene when tested at 450 °C, 1 bar, and a H₂/CO of 4 (CO conversion could reach 85%). Braganc et al [74] reported that both bimetallic catalysts supported by

HMS and SBA-15 were more active toward the C₂–C₄ hydrocarbon fraction, with an enhancement in the selectivity to branched light olefins. The HMS supported Co-Fe (25% total metal loading) catalyst showed higher activity than SBA-15 supported catalyst. The co-precipitated Ni–Fe catalysts modified with alumina were also tested for olefin synthesis from syngas. The report by Cooper et al. [75] showed that the addition of Ni to bulk Fe catalysts results in a low alkene/alkane ratio when the Ni content was below 60%. An extensive review dedicated to differed metallic catalysts for olefin synthesis from syngas was recently published by Torres Galvis and de Jong [76]. The best catalytic results relevant to olefin selectivity observed on promoted metallic catalysts are shown in Figure 1-16. Note however that syngas conversion on iron catalysts produces significant amounts of carbon dioxide. Carbon dioxide selectivity is usually not taken in consideration in most of the reports dedicated to olefin synthesis from syngas.

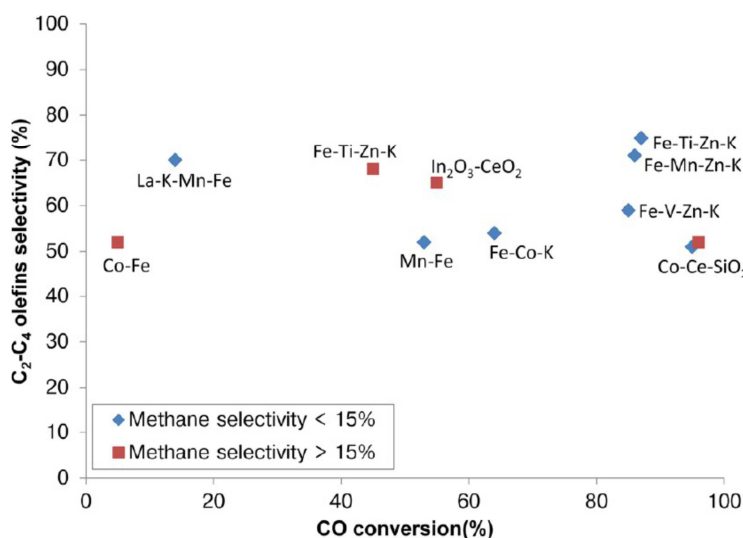


Figure 1-16: Light olefin selectivity VS CO conversion on different bimetallic catalysts [76]

IV-2-2 Effect of promoters on iron based catalysts for FTO

The most efficient promoters on iron catalysts which are used to increase olefin selectivity described in the literature are Mn, alkali-metals and sulphur. Mn decreases methane selectivity and increases C₂–C₄ olefin selectivity of Fe-based catalysts. Wang et al. [77] investigated Fe–Mn catalysts prepared by the sol–gel method or by co-precipitation. The

highest light olefin selectivity was obtained on co-precipitated catalysts with Mn:Fe = 15:85 (350 °C, 15 bar, H₂/CO = 2). At a very high CO conversion (90%), this catalyst showed high C₂–C₄ olefin selectivity (around 50%). Soled et al. [78] prepared Fe–Mn catalysts as solid solutions by mixing Mn₃O₄ and Fe₂O₃ and sintering the mixture at temperatures above 800 °C. When the catalysts were tested at 300 °C, 22 bar, and H₂/CO = 1, the catalytic test showed a high CO conversion (>94%), low methane production, and high light olefins selectivity.

Other most commonly used promoters are alkali metals. Potassium has been extensively studied as a promoter for iron catalysts, and it has been reported that it increases the chain growth probability and enhances olefin production. Furthermore, it has been claimed that potassium has an effect on structural properties of bulk catalysts such as surface area and pore size [79]. Product selectivity and catalytic activity are highly dependent on alkali promoters. Kang et al. investigated the influence of the synthesis method on the performance of Fe–Cu–Al–K catalysts [80]. The sample prepared with the sol–gel method exhibited the highest C₂–C₄ olefin selectivity of 11% and low methane selectivity (7%) at high CO conversion (96%). Torres Galvis et al [81] synthesized sodium promoted Fe/α-Al₂O₃ catalysts. The effect of Na was unclear at low reaction pressure (1 bar) but when the catalysts were tested at 20 bar, the methane selectivity became less important, but a significant increase in C₅₊ selectivity was observed, while the selectivity to C₂–C₄ olefins decreased. Sodium also had a negative effect on catalytic activity possibly caused by an enhanced extent of carbon deposition.

Sulphur has also been used as a chemical promoter to increase lower olefins selectivity. Several studies have shown that sulphur might act as a promoter for Fe catalysts, enhancing light olefin selectivity, reducing methane formation, and even increasing catalytic activity at low concentrations and under specific reaction conditions. Crous et al. [82] filed a patent for a Fe catalyst promoted with sodium and sulphur catalyst which showed high selectivity to light olefin (39%) and low methane formation (9%) at a syngas conversion of 41%. Promising results were also obtained with sulphur promoted catalysts where the promoter was not added during the preparation of the catalyst but it was incorporated in the catalytic system through exposure to H₂S [83].

IV-2-3 Effect of support on iron based catalysts for FTO

Iron can be used for FT synthesis in both bulk and supported catalysts. Bulk iron catalysts however could become mechanically instable under the conditions of catalyst activation [84] or high temperature FT synthesis [27]. The production of fine particles may lead to plugging the reactor equipment and thus could complicate the efficient use of fluidized bed technology for this highly exothermic reaction. Attempts made to improve the stability of these systems by precipitating the oxides in the presence of a structural promoter such as SiO₂ or Al₂O₃ [85].

Porous materials are used in the preparation of heterogeneous catalysts to maximize the surface area of the active phase. Catalysts containing highly dispersed iron nanoparticles can be easily prepared by impregnating method on those high surface area supports with iron salts, amount which nitrates are mostly used. The iron-containing nanoparticles of these catalysts have a relatively narrow size distribution and a homogeneous spatial distribution thus minimizing the formation of aggregates. Besides, iron has a strong interaction with most of the oxide supports, which results in the formation of mixed iron oxides that are not active for the FT reaction. It is known that iron aluminates [86] and iron silicates [87] are difficult to reduce, which inhibited the formation of the carbide (FeC_x) active phase.

Silica was used by several groups as a support for iron based catalysts. Commereuc et al. [88] prepared supported iron catalysts using iron carbonyl precursors and different oxide supports. High olefin selectivity (69%) was achieved when using a Fe/SiO₂ catalyst synthesized by impregnation of iron pentacarbonyl. The reaction conditions were 265 °C, 10 bar, H₂/CO of 1, and low CO conversion (5%). Stoop et al. [89] reported high olefin selectivity exhibited in FT reaction with a Ru_Fe/SiO₂ catalysts at 277°C, 1 bar, and H₂/CO of 2. At CO conversions below 3%, this bimetallic catalyst exhibited low methane selectivity and high olefin to paraffin ratios.. Zhang et al [90] found that a nickel could improve the reducibility of a precipitate K_Fe/SiO₂ catalyst which possessed high activity, high selectivity to olefin and light distillation cut oil and good stability.

Alumina is another useful support. Much higher catalytic conversion on alumina (96%) than silica (37%) supported K and Cu promoted iron catalysts was observed by Kang et al [91], while the catalysts did not show any difference in light olefin selectivity (around 20%), at $H_2/CO = 2$, $P = 10$ bar and $T = 300$ °C. The influence of different alumina supports on catalytic activity was investigated by Barrault et al. [92]. The catalysts were synthesized by precipitation of iron nitrate with ammonia in the presence of alumina. The FT reaction was performed at 15 bar and H_2/CO of 1. The highest selectivity to light olefins (43%) was observed for a γ -alumina supported catalyst (400 m²/g). A Na and S-promoted catalyst with a high selectivity to light olefins was designed by Torres Galvis et al. [72]. The catalysts were tested at 340 °C, 20 bar, and H_2/CO of 1. A high selectivity to light olefins (53%) was achieved by introducing Na and S as chemical promoters.

IV-2-4 FTO on other metal catalysts

Metals other than iron can also present activity in FTO process. Cobalt based catalysts with various composition were tested in the synthesis of light olefins from biosyngas. Mirzaei et al [93] reported that a Co–Ce catalyst modified with SiO₂ showed a C₂–C₄ olefins selectivity (50%) at 450 °C, 1 bar, $H_2 / CO = 2$ and at a CO conversion of 90%. Mirzaei et al [94] also reported that Mn-Co bimetallic catalysts presented a high selectivity to ethylene and propylene. Costa et al. [95] reported that a Th-Co catalyst prepared by sol-gel method produces the C₁–C₅ hydrocarbons with selectivity of 88%. at 240 °C and 1 bar with a H_2/CO ratio of 2. The olefin content was higher than 80%.

V Effect of Sulphur on FT synthesis

Good stability is primordial for FT catalysts which are supposed to operate for a few years. Unfortunately, traditional iron and cobalt catalysts could be deactivated during FT reaction. During FT reaction, the metallic active phases react with reactants or products, and then some change may happen on catalyst surface, so as to deactivate the active phases. These

changes could be: sintering [42], re-oxidation [96], attrition [97], reaction with support [98], carbon deposition [99] and poison (by N-contaminants [100] or by sulphur [101]). All these phenomena result in the loss of active sites.

The stability issue is particularly important for the catalysts operating with biomass derived syngas. The syngas obtained from gasification of biomass often contain a number of toxic impurities as ammonia and/or hydrogen disulphide, which could lead to fast catalyst deactivation (in less than 50 hours) even when they are present in very small quantities. This part of the literature review discusses influence of sulphur in syngas on the catalytic performance and stability of FT synthesis catalysts.

V-1 Effect of sulphur on iron based catalysts

The effect of sulphur on iron based catalysts has principally been evaluated using the indirect method such as addition S precursors in Fe bases catalysts. Bromfield and Coville [14] used Na_2S as precursor, to load sulphur on bulk iron catalysts and realized catalytic tests at $T = 523\text{K}$, $P = 8 \text{ bar}$ and $\text{H}_2 / \text{CO} = 2$. They found that the catalytic activity was enhanced by small amounts of sulphur then decreased when the S concentration attained to 20 000 ppmv. Higher sulphur loading on iron catalysts also led to a higher selectivity to C_1 to C_7 hydrocarbons. The relative stability of the catalysts was explained by sulphur oxidation by unreduced iron species. The sulphided catalysts on the other hand, are reduced to metallic iron rapidly by exposure to hydrogen and also exhibit a high surface concentration of sulphide. At low coverage each sulphide atom has previously been shown to poison 8–10 atoms of iron [102] and this may account for the poor F–T activity of the sulphide loaded catalysts. Sulphur poisoning also often leads to higher selectivity to methane and light hydrocarbons.

Duvenhage and Coville tested the stability of precipitated iron catalysts [103] with industrial syngas (containing some ppbv of H_2S), in a fixed bed reactor. They found that only on top of the reactor which is in direct contact with the syngas feed, H_2S could be detected in the spent catalyst bed. In the lower parts of reactor, H_2S was not detected. It was suggested that the upper portion of the reactor is acting as a ‘‘guard bed’’ to remove sulphur from the

feed. Kritzinger [83] et al recently reported that the catalytic activity of commercial iron catalysts (supplied by Sasol company) was not lost with syngas containing 32 ppmv of H₂S. Moreover, the ethylene selectivity even increased with addition of sulphur to syngas. A comparison of cobalt and iron catalysts conducted in that work was also indicative of better sulphur-resistance of iron catalyst compared to cobalt based counterparts. The presence of sulphur in the syngas often increases the selectivity to light hydrocarbon such as methane and C₂-C₄ olefins.

The effect of the carbide formation upon the sulphur resistance of the Fe catalyst has been investigated by Koizumi et al [104]. The H₂ or CO-pretreated catalyst was treated with 1000 ppm H₂S/He at 373K in situ. The H₂S treated catalysts were then subjected to the FT synthesis reaction in the absence of H₂S. Figure 1-17 shows CO conversions over variously treated catalysts as a function of the time on-stream. The catalyst treated with CO then H₂S shows a CO conversion comparable with that over the CO-pretreated one. On the other hand, the catalyst treated with H₂ then H₂S shows no activity at all. Thus the CO pretreated catalyst shows a superior sulphur resistance than the H₂-pretreated one. The reason of higher stability of carbided catalysts could be due to higher stability of iron carbide to sulphidisation compared to metallic iron species.

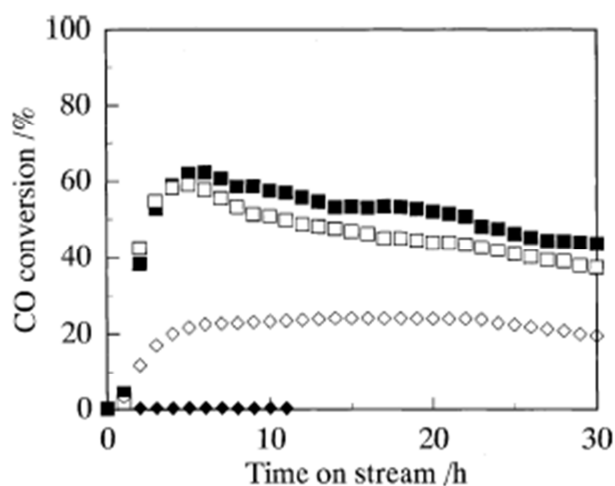


Figure 1-17: Catalytic properties of the Fe catalysts pretreated with various gases: (□) CO-pretreated sample, (■) CO then H₂S-treated sample, (◇) H₂-pretreated sample, (◆) H₂ then H₂S treated sample. Reaction conditions: 503 K, 1.6MPa.

Promotion of Fe based catalysts modified their resistance to sulphur. Koizumi et al [105] studied the S-resistance on Fe/MnO catalysts which showed enhanced olefin selectivity [106]. After the syngas containing H₂S was fed into reactor for FT synthesis, the rate of CO conversions over the Fe/MnO (ratio = 1/6) catalysts decreased gradually and were 80% of the initial value at the time on-stream of 10 h irrespective of the composition of the pretreatment gas (CO or syngas). It appears that for the Mn -promoted iron catalysts that CO pretreatment increases the FT reaction rate, while the CO pretreatment has little influence on the catalyst stability.

V-2 Effects of sulphur on cobalt based catalysts

V-2-1 Effect on the catalytic activity

Co catalysts can deactivate rapidly in the presence of small amounts of sulphur in syngas. Once the concentration of H₂S reaches 300 ppbv, the CO conversion on 15%Co_alumina catalyst started to decrease after a-few-hour on stream [101]. The decrease in the reaction rate of carbon monoxide was about 70% after 179 h time on stream. Sulphur had a significant impact on the performance of the FT catalyst at very low level of concentration. Pansare and Allison [101] tested 15%Co/Al₂O₃ catalyst using sulphur containing syngas. The concentration of H₂S varied from 0 to 1100 ppbv. Figure 1-18 shows that the CO conversion drops rapidly to zero, when the concentration of H₂S was about 600 ppbv, However, if concentration of H₂S was less than 50 ppbv, the catalysts would not be deactivated.

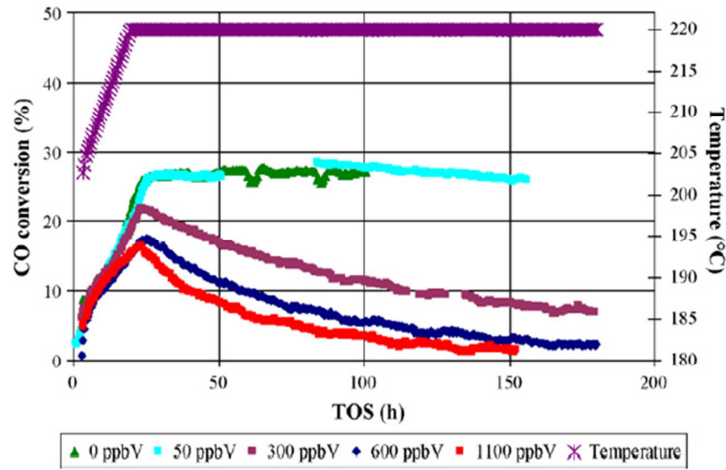


Figure 1-18: Effect of H₂S with different concentration in fed syngas to Co catalysts [101]

An attempt was to model the catalyst deactivation using the following equation:

$$a = a_0 \exp(-k_d t)$$

where k_d was the deactivation constant, a was the reaction rate of FT reaction while a_0 was the reaction rate without mixture of H₂S and t was the reaction time. A half-time-method was introduced to calculate k_d :

$$k_d = \frac{-\ln 0.5}{t_{1/2}}$$

where $t_{1/2}$ was the time when the CO conversion decreased to a half of CO conversion without sulphur. The values of deactivation constant as a function of inlet sulphur concentration are shown in Figure 1-19. The deactivation constant increases almost linearly with increase in sulphur concentration.

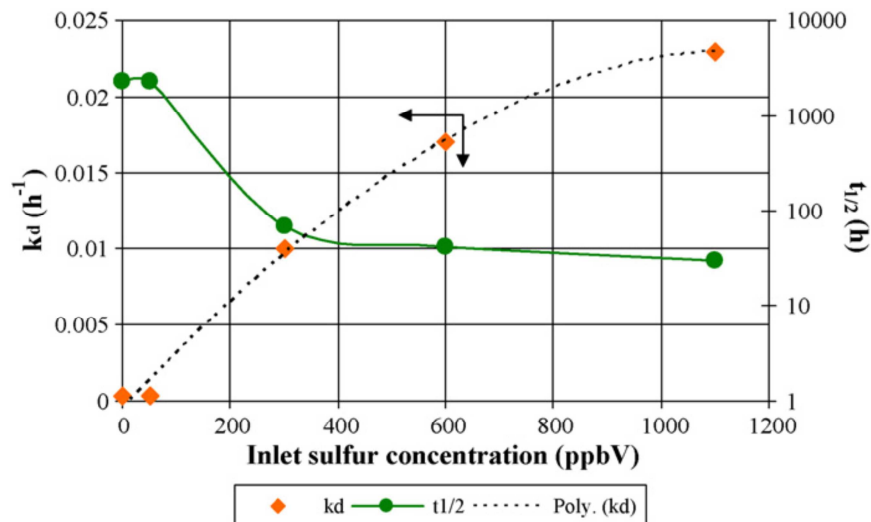


Figure 1-19: Deactivation factor as a function of H₂S concentration [101]

Bartholomew and Bowman [107] studied the effect of sulphur by introducing 0.5–8 ppmv H₂S in the reactor feed through Teflon lines. For the silica-supported cobalt catalyst a decline in catalyst activity was observed for the entire range of sulphur content in the feed. The activity decline appeared to be more intense for concentrations between 0.5 and 2 ppmv, and less sharp less for 5–6ppm of H₂S. A possible explanation of this trend could be that at higher sulphur concentrations, a surface sulphide of a different structure or multilayers of sulphide were created. Chaffee et al. also studied in situ sulphur poisoning using H₂S as the sulphur carrier in a fixed-bed reactor [108]. Commercial catalysts were used and the main focus of the study was to evaluate the effect of the H₂/CO ratio on the catalyst deactivation behaviour. For cobalt catalysts, H₂ rich feeds appeared to be more sensitive to sulphur poisoning than syngas with lower H₂/CO ratio.

V-2-2 Effect of sulphur on product selectivity

The presence of sulphur in syngas can also significantly affect the product distribution on cobalt based catalysts. Sulphur adding into syngas could present the effect of poisoning even at a lower concentration [101] on Co based catalysts. Addition of more than 300 ppbv of sulphur resulted in considerable changes in the performance of the catalyst. The CH₄ selectivity started increasing significantly after 50 h TOS and its value was more than twice compared to the run without sulphur at 100 h TOS. The production of C₅₊ hydrocarbons and wax decreased significantly which was evident from the considerable drop in the C₅₊ productivity and also from unchanged liquid level inside the reactor. The gaseous products formed during the reaction were composed mainly of CH₄ as is evident from selectivity values. Similar results were obtained with the addition of 600 and 1100 ppbv of sulphur. Methane selectivity also increased with increase in the sulphur concentration. The deactivation constants increased further while the half-life values decreased to a mere 30 h in the presence of 1100 ppbv of sulphur.

Li et al [109] reported the sulphur effect on the selectivity of TiO₂ supported Co catalyst at T = 523 K; P = 8 bar; H₂/CO molar ratio = 2; GHSV = 350 ml/h/g_{cat}. Table 1-7 shows the

results of catalytic tests. The selectivity of methane and C₂-C₄ hydrocarbon significantly increases, while C₅₊ hydrocarbon selectivity decreases. The C₁₂₊ products almost entirely disappeared on the catalyst containing 50 ppm of sulphur.

Table 1-7: Catalytic performance on 15%Co/TiO₂ catalysts with different S amounts [109]

S content	CO conversion	CH ₄ %	C2-C4%	C5-C11%	C12-C18%	C18+%
0 ppm	48.6%	21.5%	13.1%	47.0%	11.0%	7.4%
200 ppm	46.3%	21.0%	13.0%	48.0%	9,5%	8.4%
500 ppm	12%	47.0%	42.0%	10.5%	0.5%	0.0%

Visconti et al [15] also reported similar results. The addition of sulphur to the syngas feed favoured the selectivity of light products (C₁-C₄ hydrocarbon), while the C₅₊ hydrocarbon selectivity decreased (Table 1-8). The reaction conditions were T = 493K; P = 20 bar; H₂/CO molar ratio = 2.

Table 1-8: Catalytic performance on 15%Co/SiO₂ catalysts with different S amounts [15]

S content	CO conversion	CH ₄ %	C2-C5%	C5-C25%	C25+%	Olefin%
0 ppm	24.8%	8.9%	19.5%	51.4%	20.2%	21.3%
10 ppm	20.1%	10.9%	19.1%	50.0%	20.0%	22.6%
100 ppm	16,2%	10.4%	21.3%	51.6%	16.7%	24.1%
250 ppm	9.7%	18.7%	38.2%	39.5%	3.6%	37.8%
2000 ppm	3.7%	29.2%	45.9%	24.9%	0%	17.5%

Note however that the effect of sulphur on the reaction selectivity could be insignificant until the sulphur concentration reaches 250 ppm. An interesting phenomenon was that on the catalyst of 250 ppm sulphur, the olefin (light olefin as well as higher olefin) selectivity was higher than on cobalt catalysts which were unpoisoned with sulphur or sulphur was added in the amount less than 250 ppmv.

Differently to those results, the study of Bartholomew and Bowman [107] showed that sulphur addition can also increase the selectivity to heavier hydrocarbons of SiO₂ supported cobalt catalyst. A possible reason for the increased selectivity to higher molecular weight products could be the selective adsorption of the H₂S on sites which normally adsorb

hydrogen, resulting in a hydrogen deficient surface. Decreased water production, which is a result of the lower conversion, normally affects the product distribution in the opposite direction.

The deactivation is more observable on silica supported cobalt catalyst than alumina supported catalyst, with sulphur concentration of about 200-250 ppmv [101]. Curtis et al [110] analysed Co based catalysts supported by TiO₂ and SiO₂, and reported that the Co/SiO₂ catalysts were more sensible for H₂S poison.

It is worth noticing that industrial FT cobalt catalysts typically contain chemical or structural promoters such as Ru, Re or Pt [111]. H₂S effect on Re [15] and Pt [112] promoted Co/Al₂O₃ catalysts have been investigated and a similar effect (lower catalytic activity and C₅+ hydrocarbon selectivity) was presented as non-promoted Co catalysts.

V-3 Characterization of the catalysts exposed to sulphur

A number of reports have addressed the catalysts exposed to sulphur. After catalytic test with syngas with presence of H₂S, the spent catalyst samples were analysed with XRD and ICP to extract more information about the poisoning effects [101]. XRD analysis of all spent catalyst samples did not indicate bulk formation of cobalt sulphides or aluminium sulphide. This suggested that the adsorption of sulphur was only a surface phenomenon and the bulk of the catalyst was not affected. It is highly unlikely that elemental sulphur was formed leading to catalyst deactivation as majority of the research suggests formation of surface sulphides as the principal cause of catalyst deactivation [14,109]. Sulphur uptake by the catalyst was further confirmed by ICP as shown in Figure 1-20. Since the run lengths for all experiments were different, the sulphur uptake by the catalyst per unit time is plotted in Figure 1-20 as a function of inlet sulphur concentration. In Figure 1-20 it is observed that the sulphur uptake per unit time by the catalyst increased significantly with increase in the sulphur concentration in the inlet stream. The catalyst adsorbed about 3.2ppmw sulphur per hour when the inlet feed had 300 ppbV of sulphur. The sulphur uptake then increased linearly with increasing inlet sulphur and the highest value of 9.63 ppmw per hour was obtained when

the inlet stream had 1100 ppbV of sulphur. The data confirmed significant sulphur uptake by the catalyst during the reaction.

From a morphological point of view the added sulphur did not lead to appreciable variations in the catalyst characteristics [15]. On the contrary, sulphur can modify the catalyst reducibility: in particular, sulphided catalysts show, during the TPR analysis, a modest decrease of the peak of reduction, relative to metallic cobalt formation. Hydrogenation tests of propylene to propane also pointed out a decrease in the catalyst hydrogenating capability upon increasing the sulphur loading. In-situ XRD analysis showed that the intensity of metallic cobalt peak decreased with sulphur loading and on the 15Co/SiO₂ with 2000 ppmv S sample, there was no visible metallic Co peak. Li et al [109] also reported that on 15Co/TiO₂ with 500 ppmv S catalyst, the reducibility of cobalt was only one quarter of the catalyst without sulphur; the dispersion of cobalt was decreased as well. However, on 200 ppmv S loading sample, both reducibility and dispersion of cobalt did not show significant difference to unpoisoned catalyst.

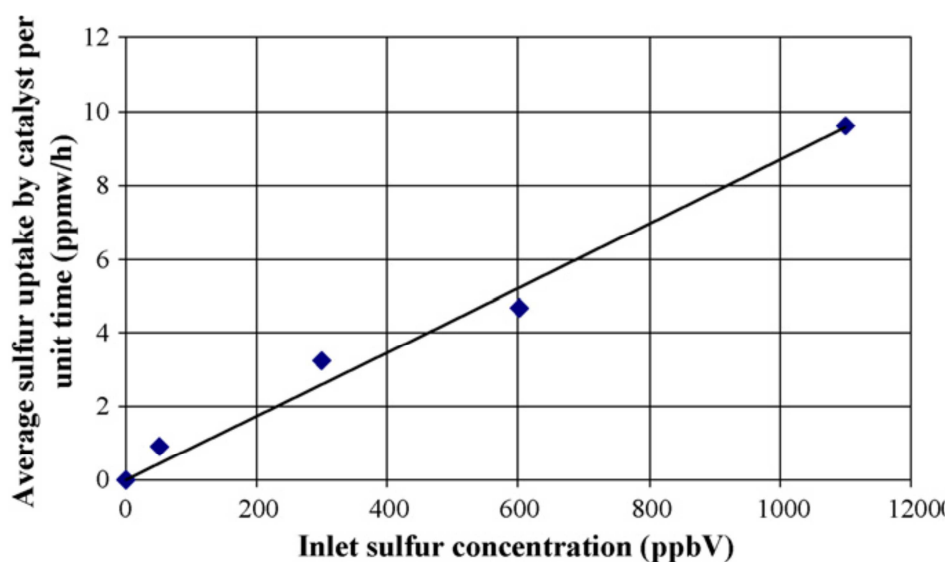


Figure 1-20: S uptake by catalysts, tested with ICP [109]

VI Sulphur resistant catalysts

The development of sulphur tolerant catalysts is expected to contribute for increasing a versatility of the FT process and its application for conversion of biomass and coal derived syngas. For example, the use of the sulphur tolerant catalyst can simplify the conventional, huge and complex process by omitting the desulphurization unit, which is quite advantageous for developing a novel on-site process that produces transportation fuels in the vicinity of small-scale and dispersed carbon resources. Various carbon resources such as remote gas fields, shale gas, biomass and waste materials as well as various process conditions for their reforming process, e.g. steam reforming, non-catalytic partial oxidation or gasification, can become available.

VI-1 Sulphide catalysts

Iron based catalysts are economic and of high activity but they presented low S tolerance, The sulphides of transition metals have been used in the petroleum industry in hydrodesulphurization, hydrodenitrogenation, and hydrogenation reactions for over 50 years. Molybdenum disulphide (MoS_2) when supported with an alkali can be used as a catalyst for the production of alcohols from syngas. The commercial Mo-based catalysts for conversion of synthesis gas to alcohols were first developed by Dow and Union Carbide companies. The functions of alkali are to reduce the hydrogenation ability of alkyl species to form alkanes and to increase the active sites for the formation of alcohols [113]. Alcohols could be synthesized on various kinds of active phase, such as iron, copper, molybdenum disulphide, palladium and so on. Alkali-modified molybdenum-based catalysts are more attractive due to their excellent resistance to sulphur poisoning. This saves the cost of ultra-desulphurization for feed gas [24]. The activity and selectivity to C_2+OH was found to be low due to chain growth possibility [114]. The effect of CO hydrogenation reaction towards the formation of higher alcohols depends on the catalyst, promoter and support.

Noble metals sulphides also present good S-resistance. The catalytic performance of Rh sulphide catalysts strongly depend on the catalytic support [104]. The rate of CO conversion over a sulphide Rh/TiO₂ is the highest whereas the products are exclusively hydrocarbon and CO₂. Similar product selectivity was obtained with a sulphided Rh/Al₂O₃. On the other hand, methanol is formed as a main product when SiO₂, MgO and/or active carbon are used as the support. It should be noted that the reduced Rh/SiO₂ is reported to yield the hydrocarbon exclusively whereas the sulphided Rh/SiO₂ mainly yields methanol [105]. It was suggested the cationic Rh sites could be stabilized by Rh–S bonds in Rh sulphide (Rh₁₇S₁₅) and active for the methanol formation. Nevertheless, the supported Rh sulphides show higher activities than the bulk Rh sulphide since the supported Rh sulphides may be in highly dispersed states. Pd sulphide is another active phase for methanol synthesis. The best productivity was found on silica supported Pd₁₆S₇ catalysts [115] and the most effective promoter for sulphide Pd was Ca [116].

VI-2 Molybdenum Disulphide Catalysts for FT synthesis

VI-2-1 MoS₂ catalysts for methanation

Molybdenum sulphide has noticeable carbon monoxide hydrogenation activity and can be used for synthesis of hydrocarbons and oxygenates. The non-promoted MoS₂ catalysts can be used for methanation. Liu et al [57] tested unsupported MoS₂ catalysts, at 550°C, 30 bar and H₂/CO = 1.5, the CO conversion attained to 85% and the selectivity of methane was around 58%. CO₂ was another product with selectivity of 40% and rather small amounts of ethane (<1%) were formed. The alumina supported MoS₂ catalysts were studied by Wang et al [117]. The fraction of MoS₂ loading on support varied from 5% to 35% and the highest CO conversion (about 47%) was found at 560°C, 30 bar and H₂/CO = 1. The BET surface decreased with higher MoS₂ loading but pore size and pore volume showed a minimum with

20%-25% loading MoS₂/alumina catalysts. A new compound, Al₂(MoO₄)₃ was detected in these catalysts which was due to the interaction between Mo and support.

VI-2-2 Promoted MoS₂ catalysts for alcohol synthesis

The promoted MoS₂ catalysts have shown interesting properties for alcohol synthesis from syngas. An alkaline metal (K, Rb and Cs) promoted non-supported MoS₂ was prepared using the aqueous alkaline metal carbonate solution instead of water [104]. Over Alkali/MoS₂, the produced alcohols were composed of methanol, ethanol, propanol and butanol. Figure 1-21 shows STY (space time yield) of C₂₊ alcohol and the chain growth probabilities of alcohol with Alkali/MoS₂ having various Alkali/Mo atomic ratios. The C₂₊ alcohol STY over M/MoS₂ strongly depends on the Alkali /Mo ratio and shows a maximum at the Alkali/Mo ratio of around 0.2 irrespective of the alkaline metal promoter. Among these catalysts Rb/MoS₂ having Rb/Mo ratio of 0.25 shows the highest C₂₊ alcohol STY. The chain growth probability of the alcohol with this catalyst is the highest as well.

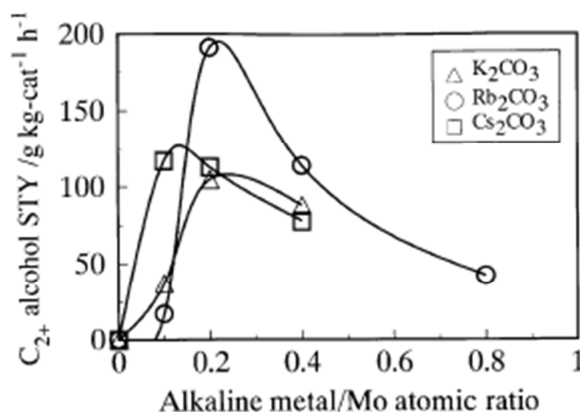


Figure 1-21: Alcohol productivity on different alkali promoted MoS₂ catalysts

Surisetty et al reported the catalytic performance of K promoted carbon nanotube (CNT) supported MoS₂ catalysts [24]. They investigated the effect of the quantity of K as well as Mo loading on catalysts. The catalysts were tested under different reaction conditions. There are several interesting results:

a) The fraction of K loading (3% to 9%, on 15% MoS₂/CNT) did not present significant effect on catalytic activity.

b) The hydrocarbon and CO₂ selectivity decreased when percentage of K became higher; the total alcohol selectivity increased with increasing of K fraction. What's more, the trend of MeOH selectivity was unusual: 3%K15%MoS₂/CNT < 9%K15%MoS₂/CNT < 6%K15%MoS₂/CNT.

c) Compared with 6%K15%Mo/CNT, 6%K20%Mo/CNT presented lower CO conversion and lower alcohol selectivity. The authors suggested that the effect was due to the larger crystal size of MoO₃ on 20%Mo/CNT.

d) On 9%K15%MoS₂/CNT catalyst, the CO₂ selectivity increased with temperature; hydrocarbon selectivity presented a minimum value at 330°C (290-340 °C); alcohol selectivity presented a maximum value at 320 °C (Figure 1-22).

e) On 9%K15%MoS₂/CNT catalyst, the hydrocarbon and CO₂ selectivity increased with pressure, while the alcohol selectivity decreased with pressure (Figure 1-23).

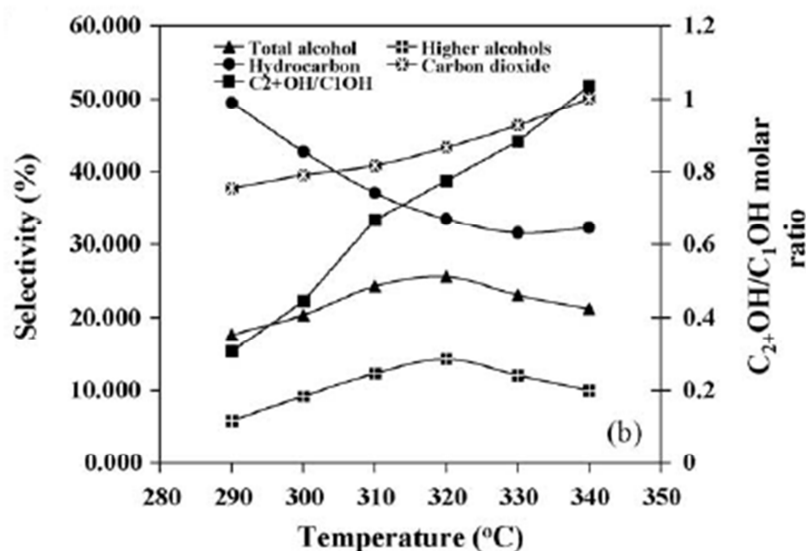


Figure 1-22: Selectivity and C₂₊OH/MeOH ratio with T (P = 70 bar, H₂/CO = 2) [24]

Li, Fu and Jiang [118] studied Rh/K/MoS₂/alumina catalyst. They uncovered that Rh could strongly interact with KMoS₂ system. The size of MoS₂ particles was affected by Rh. The presence of Ru makes the MoS₂ particle smaller and improves dispersion of MoS₂. The catalyst was tested at T = 600K, P = 40 bar and H₂/CO = 2. Rh promoter improved slightly the CO conversion and improved greatly the alcohol selectivity. Co also increases the alcohol yield and selectivity towards higher alcohols of MoS₂ catalysts [119-120]. The presence of C

in alkali-modified MoS₂ catalysts enhanced the C1→C2 homologation step that led to ethanol as the dominant product [121]. The addition of Ni to K/MoS₂ catalysts leads to methanation [119]. The Ni/K/MoS₂ catalysts can be further promoted with Mn. The Mn promotion leads to improved selectivity to higher alcohols [122]. The experiments were conducted at 250–350°C and 5–10 MPa [123].

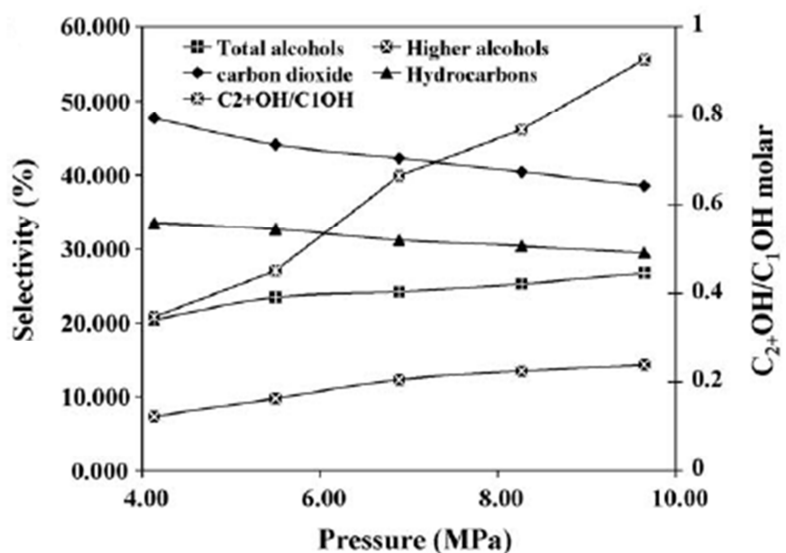


Figure 1-23: Selectivity and C₂+OH/MeOH ratio with P (T = 340 °C, H₂/CO = 2) [24]

Numerous publications have addressed Co(Ni) promoted K/MoS₂ catalysts, Table 1-9 presents some of the obtained results.

Table 1-9: Catalytic performance of Co(Ni)/K/MoS₂ catalysts

Nature of Catalysts	T(°C)	P (bar)	H ₂ /CO	CO%	CO ₂ %	Alcohol%	Ref
12.5%K 21.5% Clay Co : Mo = 0.5 (mol)	300	140	1.1	N/A	N/A	86%**	124
12.5%K 21.5% Clay Co : Mo = 1 (mol)	300	140	1.1	N/A	N/A	62%**	124
1.5%Rh9%K15%Mo/CNT	320	83	1	40.1%	34.6%	30.0%	125
6%Co1.5%Rh9%K15%Mo/ CNT	320	83	1	48.9%	18.9%	33.7%	125
4.1%Co3.1%K8.2%Mo/AC	330	50	2	14.3%	N/A	46.6%	126
2.7%Co9%K13.6%Mo/AC*	326	100	1	9%	N/A	62%**	127
Ni/K/Mo/AC	330	100	2	25%	N/A	74%**	122

*Catalytic test was fed with syngas mixing 220 ppmv of H₂S

** CO₂ free selectivity

Cobalt promoter can improve the catalytic activity and increase the alcohol selectivity. Note that the Co/Mo ratio is important for the catalytic performance. Various studies have shown that the activity for alcohol formation is optimized at a Co/Mo atomic ratio of 0.5 [124, 126,128,129]. The catalytic results can be explained by characterisation. Li et al [126] reported that in oxide state, molybdenum is partly present as K–Mo–O species and cobalt phases are mainly present as CoMoO₄ and CoMoO₃ with low Co loading, possibly due to the reducibility of active carbon at high preparation temperature, and CoMoO₄ with high Co loading. After sulphidation, molybdenum is mainly present as MoS₂ species, while cobalt in the form of “Co–S–Mo” phase at the low Co loading and as both “Co–S–Mo” species and Co₉S₈ crystallites at higher Co content. Co species operate as a synergistic system with molybdenum sulphide, rather than independently from the intercalated MoS₂ phase. Differently to cobalt, nickel promoter favours production of hydrocarbons [130], and activity on Ni promoted catalysts was lower than that of the Co promoted catalysts.

Christensen et al [127] conducted the catalytic test with molybdenum sulphides using H₂S containing syngas and obtained several important results. Irrespective of the presence of H₂S in the syngas feed, the sulphided catalyst requires an initiation period to achieve a steady state. With the H₂S concentrations from 0 to 57 ppmv, the fraction of higher alcohols gradually decreases with time on stream. With the H₂S concentrations at or above 103 ppmv the production of higher alcohols is always very significant. The analysis of the condensed alcohol product shows that the presence of sulphur in the syngas feed leads to the incorporation of sulphur species into the reaction products. This presence of sulphur in the produced alcohols was observed during substantial amount of time after the addition of H₂S to the feed has been discontinued.

The catalytic performance was affected by the nature of support. In the review of Surisetty et al [20], the catalytic performance of alkali-modified molybdenum-based catalysts supported on carbon based supports such as activated carbon (AC) and CNT [24, 125] were found better in terms of higher alcohols yield and selectivity compared to that of unsupported catalysts and catalysts supported on metallic oxide supports, such as SiO₂ and Al₂O₃. The surface acidity of metal oxides such as Al₂O₃ and ZrO₂ suppresses the formation of alcohols

and improves the hydrocarbon reaction rate. Activated carbon, as a neutral catalyst support, has many advantages for higher alcohols synthesis because of its large surface area, limited interaction between the support and the active material, resistance to acidic or basic media, and stability at high temperatures and pressures [131]. The hydrocarbon selectivity on activated carbon-supported molybdenum catalysts was found to be much less than that of SiO_2 , Al_2O_3 , and CeO_2 [132]. However, the microporous structure (pore size < 2 nm) of activated carbon limits the transportation of the reactants and products through the pores. In addition, narrow pores lead to the formation of coke which plugs the pores of the support and finally deactivates the catalyst [133]. Carbon in the form of multiwall carbon nanotubes (MWCNT) has been drawing attention as a new generation of catalyst support, due to their flexibility as support in tailoring the catalyst properties to specific needs [134]. MWCNTs as catalyst supports are increasingly used for reactions involving hydrogen as a reactant or product [135]. These materials have inert graphitic surfaces, are resistant to acidic or basic media, and possess unique properties such as meso/macroporous structures that mitigate transport limitations. They have uniform and straight pores that allow great metal dispersion. They exhibit high mechanical strength and thermal conductivity and can be highly purified [136].

VI-2-3 MoS₂ based catalysts for light olefin synthesis

Very few papers address olefin synthesis on MoS_2 based catalysts. The major goal of carbon monoxide hydrogenation on molybdenum sulphide catalysts is usually to obtain high selectivity to alcohols. Hydrocarbons are often presented as by-products of CO hydrogenation reaction. Different kinds of hydrocarbon were not analysed, or only paraffin was detected. H. Xiao et al [137] reported results of catalytic tests on non-supported K-MoS_2 catalysts. The total selectivity to hydrocarbons was 15%, but the selectivity of light olefins was not reported. Chiang et al [67] reported carbon monoxide hydrogenation on $\text{MoS}_2/\text{Al}_2\text{O}_3$ catalysts at $P = 50$ bar and $T = 200^\circ\text{C}$. The selectivity to C_{2+} hydrocarbon was 24%, but only paraffins were produced. Liakakou et al [138] used $\text{K-Ni-MoS}_2/\text{CNT}$ catalysts to synthesize C_{2+}

alcohols, while some hydrocarbons were also produced. The C₁-C₈ hydrocarbon selectivity was around 50%, at P = 60 bar, but only paraffins were detected. The hydrocarbon selectivity was higher at T = 280°C than 250°C. Ferrari et al [147] tested potassium promoted MoS₂/Al₂O₃ catalysts at T = 330°C and P = 60 bar, and found the C₂₊ hydrocarbon selectivity was quite low, smaller than 8%. However, they did not report the olefin and paraffin selectivity, but the olefin selectivity was not higher than 8%. Iranmahboob et al [124] found that the active carbon supported K-Co-MoS₂ catalysts produce only methane and ethane as hydrocarbons. Okatsu et al [139] used Mg-Al hydrotalcite supported K-MoS₂ catalysts to synthesize alcohols, and found the formation only of methane and ethane. Ethane was produced with selectivity of 6%.

A few papers report olefin production during CO hydrogenation on molybdenum catalysts but the olefin selectivity was often very low. Iranmahboob et al [140] synthesized K-Co-MoS₂ catalysts and found the C₁-C₄ hydrocarbon selectivity of 10% ~ 20% with methane as the principal product. They reported that C₂-C₄ olefins were also detected, while no information about olefin selectivity was available. Christensen et al [141] synthesized 9%K_2.7%Co_13.6%Mo carbon supported catalysts. The catalysts showed the CO₂ free ethylene selectivity of 1.1% at P = 100 bar, T = 326°C and H₂/CO = 1.

VI-2-4 Catalyst preparation

There are several different methods to prepare the MoS₂ species. The most used methods are directly decomposition method and impregnation method. This method involves thermodecomposition of a molecular precursor, ammonium tetrathiomolybdate, (NH₄)₂MoS₄. This method was firstly proposed by Bertzenius [142]. The transition metal promoter was co-precipitated with (NH₄)₂MoS₄, with the form of an organic salt, such as Ni(C₂H₄O)₂ or Co(CH₃O)₂. The alkali metal promoters are added after the decomposition. Woo et al [143] reported that on K promoted MoS₂ catalysts, the alcohol selectivity was as high as 71% (where CO₂ was not consisted) with a CO conversion of 13%, at T = 300°C, P = 50 bar, H₂/CO = 1.7. They also considered the different potassium promoters, K₂CO₃ and K₂S

promoters showed higher alcohol selectivity while with KCl and K₂SO₄ promoters the main products were hydrocarbon. Woo et al [143] also studied K₂CO₃/MoS₂ catalysts (molecular ratio of K/Mo = 2/3) and found that after putting the decomposed sample in open air for a week to let the catalyst oxidized, the catalyst became more active and more selective to C₁₋₃ hydrocarbon. The change of selectivity on oxidized K₂CO₃/MoS₂ was due to the enhanced dissociative adsorption of hydrogen [144].

Li et al [145] reported the performance of higher alcohol (C₂₊ alcohol) synthesis on K₂CO₃/MoS₂ (molecular ratio of K/Mo = 0.7) catalysts synthesized through thermodecomposition method, at T = 340°C, P = 100 bar H₂/CO = 2, the space-time yield of alcohol reached 0.3 g/(ml.h). However, adding some nickel to form a bi-promoted catalyst (molecular ratio of Ni/Mo = 1/3), the same space-time yield of alcohol could be attained at a lower temperature, T = 320°C, but the CO conversion increased on Ni/K/MoS₂ catalyst. Thermodecomposition method can only be used to synthesize unsupported catalysts.

The supported MoS₂ based catalysts are usually prepared using the impregnation method. This method starts from preparation of the solution of precursors that usually is the salt of active metals. For MoS₂ catalyst, the precursor is ammonium tetrahydroheptamolybdate (AMT, (NH₄)₆Mo₇O₂₄·4H₂O), which could be thermally decomposed to molybdenum oxide (MoO₃).



Then the solution is contacted with a dry porous support (alumina, silica, titania, carbon). After being contacted, the solution is aspirated by the capillary forces inside the pores of the support. The incipient wetness occurs when all pores of the support are filled with the liquid. But only initial impregnation is insufficient because internal force between support and precursor solution is intermolecular force and/or hydrogen bond [146], which are relatively weak interaction forces. Thereby drying and calcination is necessary to allow the distribution of the active phase over the support body.

As the thermodecomposition method, promoters could be introduced in MoS₂ catalysts with different ways. Transition metal promoters (cobalt, nickel and so on) are always

co-impregnated with molybdenum because the interaction between Mo and transition metal promoter is important for improving the catalytic performance [126]. The precursors are nitrate salts. Alkali metal promoter could be directly impregnated together with AMT solution (also called co-impregnation). Alternatively, the potassium promoters can also be added to catalyst with the form of carbonate powers after the drying of AMT impregnated catalysts (called physical mixing). Ferrari et al [147] found that the addition of potassium by physical mixing leads to better performance owing to more intimate interaction between potassium and MoS₂. This results in better catalyst stability. By using carbonate as the precursor of alkali metal, the CO conversion and alcohol selectivity were both higher than that on catalyst with K₂SO₄ as promoter, because sulphate salt of alkali is a neutral salt while their carbonate salt is basic [143,147].

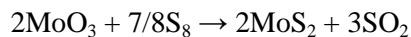
To transform molybdenum oxide to molybdenum sulphide, solid-gas sulphidation of the corresponding oxides is probably the most studied technique. A bunch of work has been done on it since the procedures of sulphidation of supported oxides by mixtures of hydrogen sulphide and hydrogen are routinely used to activate hydrotreatment catalysts. Afanasiev [148] et showed that formation of sulphide from the oxide requires reduction, since Mo⁶⁺ species should be transformed to the Mo⁴⁺ ones.



Note that molybdenum oxide species can be also sulphided by pure hydrogen sulphide or its mixtures with inert gas. In this case, hydrogen sulphide works at once as a sulphiding reducing agent, being necessarily decomposed to give some elementary sulphur:



Finally, even the vapour of elemental sulphur at sufficiently high temperature can transform the oxide to MoS₂.



Since the sulphidation with pure H₂S can form sulphur that may cover and deactivate the catalyst surface, diluted H₂S (often 10 vol.% H₂S) seems to be more suitable for the sulphidation.

VII Objectives

Development of novel routes for the efficient utilization of non-petroleum resources including biomass and coal to produce chemicals and ultraclean liquid fuels has attracted much attention because of environmental concerns and depletion of petroleum resources.

The present thesis focuses on the design of novel catalysts for the transformation of biomass- or coal-derived syngas into light olefins (C₂-C₄ olefins) which are an important feedstock for the chemical and petrochemical industry (Figure 1-24). Conventional Fischer-Tropsch catalysts are not stable in the presence of even small amounts of sulphur. Noble metal such as rhodium and palladium can be used as sulphur resistance catalysts, but their high price and rarity hinder their use on the industry. Hence, another kind of sulphur resistance catalyst, transition metal sulphides, especially molybdenum sulphides, can be considered as sulphur tolerance catalysts.

MoS₂ have demonstrated interesting catalytic properties for methane and alcohol synthesis through CO hydrogenation. Very few information about olefin synthesis on MoS₂ catalysts is available in the literature. The principal goal of this work was evaluate the potential of the promoted molybdenum sulphide catalyst to produce light olefins from sulphur containing syngas. The catalysts were supported on alumina and carbon materials. The specific goals of this thesis are summarized below:

1. To evaluate the deactivation of cobalt based catalysts caused by H₂S in syngas feed of a low concentration.

2. To study catalytic performance varied with the nature and fraction of alkali promoter as well as different supports on MoS₂ based catalysts.

3. To investigate the effect of reaction conditions (temperature, pressure and gas velocity) to the light olefin productivity on MoS₂ based catalysts.

This research work was performed in 2012-2015 at the “Unité de catalyse et de chimie du solide” (UCCS), University of Lille 1, France as a part the French-Chinese ANR-NSFC OLSYNCAT project in collaboration with University of Xiamen.

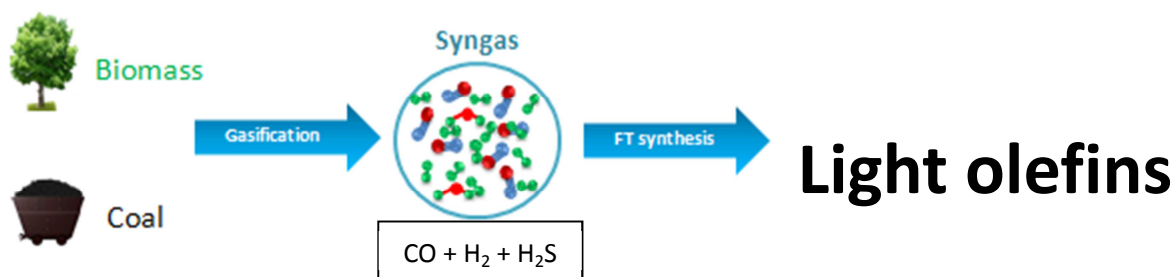


Figure 1-24: Transformation of biomass- or coal-derived syngas into light olefins

Reference

- [1] I.S. Nashawi, A. Malallah, M. Al-Bisharah. *Energy Fuel*. 24 (2010) 1788
- [2] Y. Lin, S. Tanaka, *Appl Microbiol Biotechnol*. 69 (2006) 62
- [3] Z. Deretsky, National Science Foundation, April 2010
- [4] M. Puig-Aenavat, J. Bruno, A. Coronas. *Renew. Sustain. Energy Rev*. 14 (2010) 2841
- [5] GBI Research, *Light Olefins Americas Market to 2020*, (2012)
- [6] F. Fazlollahi, M. Sarkari, A. Zare, A. Mirzaei, H. Atashi *J. Ind. Eng. Chem*. 18 (4) 1223
- [7] R. O'Brien, L. Xu, R. Spicer, S. Bao, D. Milburn, B. Davis. *Catal. Today*. 36 (1997) 325
- [8] M. Luo, R. O'Brien, S. Bao, B. Davis, *Appl. Catal. A: General*. 239 (2003) 111
- [9] P. Ajoy, H. Burton. *Catal. Today*. 36 (1997) 335
- [10] P. Mathieu, R. Dubuisson. *Energy Convers Manage*. 43 (2002) 1291
- [11] B. Wu, B. Liang, H. Xiang, Y. Li, Z. Zhang, B. Zhong, *Fuel* 83 (2004) 205
- [12] K. Naoto, M. Kazuhito, O. Toshihiko, Y. Muneyoshi. *Catal. Today*. 89 (2004) 465
- [13] S. Park, J. Bae, G. Jung, K. Ha, K. Jun, Y. Lee, H. Park, *Appl. Catal. A: General*. 413-414 (2012) 310
- [14] D. Duvenhage, N. Coville, *Appl. Catal. A: General*. 298 (2006) 211
- [15] C. Visconti, L. Lietti, P. Forzatti, R. Zennaro, *Appl. Catal. A: General*. 330 (2007) 49
- [16] M. Ichikawa. *Bull. Chem. Soc. Jpn*. 51 (1978) 2268
- [17] N. Koizumi, K. Murai, S. Tamayama, T. Ozaki, M. Yamada. *Energy & Fuels*. 17 (2003) 829
- [18] G. Quarderer, K. Cochran. European Patent 0119609B1 (1991)
- [19] J. Lee, S. Kim, K. Lee, I. Nam, J. Chung, Y. Kim, H. Woo, *Appl. Catal. A: Gen*. 110 (1994) 11–25.
- [20] K. Smith, R. Herman, K. Klier. *Chem. Eng. Sci*. 45 (1990) 2639
- [21] G. Mills. Summary of the Higher Alcohol Synthesis Workshop, B.R. Service Corporation, 1992
- [22] V. Surisetty, A. Dalai, J. Kozinski. *Appl. Catal. A: General* 404 (2011) 1
- [23] N. Koizumi, G. Bian, K. Murai, T. Ozaki, M. Yamada, *J. Mol. Catal. A: Chem*. 207 (2004) 173.
- [24] V. Surisetty, A. Tavasoli, A. Dalai. *Appl. Catal. A: General* 365 (2009) 243
- [25] K. Fang, D. Li, M. Lin, M. Xiang, W. Wei, Y. Sun. *Catal. Today*. 147 (2009) 133
- [26] M. Matthew, S. Whitney, A. Kimberly. *Energy & Fuel*. 23 (2009) 1874
- [27] G. Huber, S. Iborra, A. Corma. *Chem. Rev*. 106 (2006) 4044
- [28] M. Vannice. *Catal. Rev. Sci. Eng*. 14 (1976) 153
- [29] R. Perry, D. Green, *Perry's Chemical Engineer's Handbook*, 6th Edition, (New York, NY: McGraw-Hill Book Company, 1984), p. 9-5
- [30] M. Aznar, M. Gil, J. Martin, J. Frances, E. Corella. *J. Ind. Eng. Chem. Res*. 36 (1997) 5227
- [31] R. van Ree, A. Oudhuis, A. Faaij. Petten. The Netherlands: Netherlands Energy Research Foundation ECN, 1995
- [32] F. Fischer, H. Tropsch. *Chem*. 7 (1926) 97
- [33] H. Kölbl, H. Giehring. *Brennstoff-Chem*. 44 (1963) 343
- [34] J. van de Loosdrecht, F. Botes, I. Ciobica, A. Ferreira, P. Gibson, D. Moodley, A. Saib, J. Visagie, C. Weststrate, J. Niemantsverdiets). *Comprehensive Inorganic Chemistry II: From Elements to Applications*, 7 (2013) 525
- [35] R. O'Brien, L. Xu, R. Spicer, B. Davis. *Energy & Fuels*. 10 (1996) 921
- [36] U. Schwertmann, R. Cornell. Wiley-VCH: Weinheim. 2000
- [37] M. Peter, A. de Klerk. 2013 Wiley-VCH Verlag & Co. KGaA, Boschstr. 12, 69469 Weinheim, Germany
- [38] B. Davis. *Ind. Eng. Chem. Res*. 46 (2007) 938
- [39] A. Khodakov, W. Chu, P. Fongarland. *Chem. Rev*. 107 (2007) 1692

- [40] E. van Steen, G. Sewell, R. Makhothe, C. Micklethwaite, H. Manstein, M. de Lange, C. O'Connor. *J. Catal.* 162 (1996) 220
- [41] J. Hindermann, G. Hutchings, A. Kiennemann, *Catal. Rev. - Sci. Eng.* 35 (1993) 1
- [42] M. Heal, E. Leisegang, R. Torrington. *J. Catal.* 42 (1976) 10
- [43] M. Heal, E. Leisegang, R. Torrington. *J. Catal.* 51 (1978) 314
- [44] G. Blyholder. *J. Phys. Chem.* 68 (1964) 2772
- [45] T. Ishihara, K. Harada, K. Eguchi, H. Arai. *J. Catal.* 136 (1992) 161
- [46] T. Ishihara, N. Horiuchi, T. Inoue, K. Eguchi, Y. Takita, H. Arai, *J. Catal.* 136 (1992) 232
- [47] M. Zonneville, J. Geerlings, R. Vansanten, *J. Catal.* 148 (1994) 417
- [48] R. Brückner, *Mécanismes réactionnels en chimie organique* (ed. De Boeck). De Boeck Université, 1999
- [49] L. Fu, C. Bartholomew. *J. Catal.* 92 (1985) 376
- [50] Z. Liu, P. Hu. *J. Am. Chem. Soc.* 124 (2002) 11568
- [51] P. Emmett, Lecture No. 4, *Catalytic Processes Utilizing CO and H₂*. Oak Ridge National Laboratory, 1974
- [52] R. Brady III, R. Pettit. *J. Am. Chem. Soc.* 103 (1981) 1287
- [53] P. Maitlis, *Pure Appl. Chem.* 61 (1989) 1747
- [54] A.T. Bell. *Catal. Rev. - Sci. Eng.* 23 (1981) 203
- [55] H. Storch, N. Golumbic, R. Anderson, *The Fischer-Tropsch and Related Syntheses*. Wiley, New York, 1951
- [56] J. Kummer, P. Emmett. *J. Am. Chem. Soc.* 75 (1953) 5177
- [57] J. Liu, E. Wang, J. Lv, Z. Li, B. Wang, X. Ma, S. Qin, Q. Sun. *Fuel Proce. Technol.* 110 (2013) 249
- [58] J. Happel, M.A. Hnatow, L. Bajars, *Methods of making high activity transition metal catalysts*, In Google Patents: 1985
- [59] D. Li, C. Yang, W. Li, Y. Sun, B. Zhong, *Top. Catal.* 32 (2005) 233
- [60] S. Chuang, Y. Tian, J. Goodwin, I. Wender, *J. Catal.* 96 (1985) 388
- [61] S.A Eliason, C. Bartholomew. *Appl. Catal. A: General* 186 (1999) 229
- [62] H. Arakawa, A. Bell. *Ind. Eng. Proc. Des. Dev.* 22 (1983) 97
- [63] T. Park, I. Nam, Y. Kim. *Ind. Eng. Chem. Res.* 36 (1997) 5246
- [64] I. Yates, C. Satterfield, *Energy & Fuels* 5 (1991) 168
- [65] R. Anderso. *Catalysts for the Fischer-Tropsch synthesis - Vol. IV*. Reinhold, New York, 1956
- [66] B. Sarup, B. Wojciechowski. *Can. J. Chem. Eng.* 67 (1989) 62
- [67] S. Chiang, C. Chang, J. Shie, C. Chang, D. Ji, J. Tseng, C. Chang, Y. Chen. *Energies.* 5 (2012) 4147
- [68] R. Garcia, R. van Grieken, J. Iglesias, V. Morales, N. Villajos. *J. Catal.* 274 (2010) 121
- [69] M. Dry, H. Erasmus, de W. *Annu. Rev. Energy.* 12(1987)1
- [70] B. Bussemeier, C. Frohning, W. Kluy. *DE Patent* 2518964, 1976
- [71] B. Bussemeier, C. Frohning, G. Horn. *W. Kluy. US Patent* 4,564,642, 1986
- [72] T. Galvis, H. Bitter, J. Khare, C. Ruitenbeek, M. Dugulan, K. de Jong. *Science* 335 (2012) 835
- [73] F. Tihay, G. Pourroy, M. Richard-Plouet, A. Roger, A. Kiennemann. *Appl. Catal. A: General* 206 (2001) 29
- [74] L. Braganc, M. Ojeda, J. Fierro, M. Pais da Silva. *Appl. Catal. A: General* 423– 424 (2012) 146
- [75] H. Galvis, K. de Jong. *ACS Catal.* 3 (2013) 2130
- [76] M. Dry, G. Oosthuizen. *J. Catal.* 11 (1968) 18
- [77] T. Sano, H. Yanagisawa, K. Saito, K. Okabe, H. Okado, H. Takaya, K. Bando. *Appl. Catal.* 19 (1985) 247
- [78] M. Cooper, J. Frost. *Appl. Catal.* 57 (1990) L5
- [79] N. Lohitharn, J. Goodwin. *J. Catal.* 260 (2008) 7

- [80] S. Kang, J. Bae, P. Prasad, S. Park, K. Woo, K. Jun. *Catal. Lett.* 130 (2009) 630
- [81] H. Galvis, A. Koecken, J. Bitter, T. Davidian, M. Ruitenbeek, A. Dugulan, K. de Jong. *J. Catal.* 303 (2013) 22
- [82] R. Crous, T. Bromfield, S. Booyens. International Patent Application 2010. No. WO 2010066386.
- [83] J.Kritzinger. *Catal. Today* 2002, 71 (2002) 307
- [84] M. Shroff, D. Kalakkad, K. Coulter, S. Kohler, M. Harrington, N. Jackson, A. Sault, A. Datye. *J. Catal.* 156 (1995) 185
- [85] M. Sađlam. *Ind. Eng. Chem. Res.* 28 (1989) 150
- [86] J. Park, Y. Lee, P. Khanna, K. Jun, J. Bae, Y. Kim. *J. Mol. Catal. A* 323 (2010) 84
- [87] C. Zhang, H. Wan, Y. Yang, H. Xiang, Y. Li. *Catal. Commun.* 7 (2006) 733
- [88] D. Commereuc, Y. Chauvin. *Chem. Soc., Chem. Commun.* 4 (1980) 154
- [89] F. Stoop, K. van der Wiele. *Appl. Catal.* 23 (1986) 35
- [90] C. Zhang, Y. Yang, Z. Tao, H. Xiang, Y. Li. *J. Fuel Chem. Technol.* 34(6) (2006) 695
- [91] S. Kang, J. Bae, J. Cheon, Y. Lee, K. Ha, K. Jun, D. Lee, B. Kim. *Appl. Catal. B: Environmental* 103 (2011) 169
- [92] J. Barrault, C. Forquy, J. Menezo, R. Maurel. *React. Kinet. Catal. Lett.* 15 (1980) 153
- [93] N. Tsakoumis, M. Rønning, Ø. Borg, E. Rytter, A. Holmen. *Catal. Today.* 154 (2010) 162
- [94] A. Mirzaei, M. Faizi, R. Habibpour. *Appl. Catal., A.* 306 (2006) 98
- [95] J. Costa, A. Noels, A. Demonceau, A. Hubert. *J. Catal.* 105 (1987) 1
- [96] J. Li, X. Zhang, G. Jacobs, T. Das, B. H. Davis. *Appl. Catal. A: General.* 228 (2002) 203
- [97] R. Zhao, J. Goodwin Jr., R. Oukaci, *Appl. Catal. A: General.* 189 (1999) 99
- [98] W. Cho, M. Kakihana. *J. Alloy. Compd.* 298 (1999) 87
- [99] British Intelligence Objectives Sub-Committee, Interrogation of Dr Otto Roelen of Ruhrchemie A.G., B.I.O.S. Final Report No. 447; Item no 30 (1945). <http://www.fischer-tropsch.org>
- [100] S. LeViness, H. Robota, X. Zhan, J. Engman. *Proc. 79th ACS Symp. Colloid and Surface Science, Potsdam, NY, 12–15 June 2005*, pp 9-09
- [101] S. Pansare, J. Allison. *Appl. Catal. A: General.* 387 (2010) 224
- [102] M. Kiskinova. *Poisoning and Promotion in Catalysis based on Surface Science Concepts and Experiments*, Elsevier, Amsterdam, 1992
- [103] D. Duvenhage, N. Coville. *Appl. Catal. A: General.* 298 (2006) 211
- [104] N. Koizumi, K. Murai, T. Ozaki, M. Yamada. *Catal. Today.* 89 (2004) 465
- [105] N. Koizumi, Y. Kobayashi, M. Jiang, M. Yamada, *Prepr. Am. Chem. Soc., Div. Petro. Chem.* 45 (2000) 272
- [106] H. Kolbel, K. Tillmetz, (1979) *Hydrocarbons and oxygen-containing compounds and catalysts thereof*, US Patent 4,177,203
- [107] C. Bartholomew, R. Bowman. *Appl. Catal.* 15 (1985) 59
- [108] A. Chaffee, I. Campbell, N. Valentine, *Appl. Catal.* 47 (1989) 253
- [109] J. Li, N. Coville. *Applied Catalysis A: General.* 208 (2001) 177–184
- [110] V. Curtis, C. Nicolaides, N. Coville, D. Hildebrandt, D. Glasser. *Catal. Today* 49 (1999) 33
- [111] M. Dry. *Catal. Today.* 71 (2001) 227
- [112] D. Sparks, G. Jacobs, M. Gnanamani, V. Pendyala, W. Ma, J. Kang, W. Shafer, R. Keogh, U. Graham, P. Gao, B. Davis. *Catal. Today.* 215 (2013) 67
- [113] X. Li, L. Feng, L. Zhang, D. Dadyburjor, E. Kugler, *Molecules.* 8 (2003) 13
- [114] H. Woo, K. Park, Y. Kim, I. Namau, J. Chung, J. Lee, *Appl. Catal.* 75 (1991) 267
- [115] N. Koizumi, A. Miyazawa, T. Furukawa, M. Yamada. *Chem. Lett.* (2001) 1282
- [116] N. Koizumi, K. Murai, S. Tamayama, T. Ozaki, M. Yamada. *Energy & Fuels* 17 (2003) 829
- [117] B. Wang, G. Ding, Y. Shang, J. Lv, H. Wang, E. Wang, Z. Li, Xinbin M, S. Qin and Q. Sun. *Appl. Catal. A: General* 431–432 (2012) 14

- [118] Z. Li, Y. Fu, M. Jiang. *Appl. Catal. A: General* 187 (1999) 187
- [119] T. Tatsumi, A. Muramatsu, T. Fukunaga, H. Tominaga, in: M.J. Phillips, M. Ternan (Eds.), *Proc. 9th Intern. Congr. Catal.*, vol. 2, The Chemical Institute of Canada, Ottawa, 1988, p. 618
- [120] J. Iranmahboob, D. Hill, H. Toghiani. *Appl. Catal. A: Gen.* 231 (2003) 99
- [121] J. Santiesteban, C. Bogdan, R. Herman, K. Klier, in: M.J. Phillips, M. Ternan (Eds.), *Proc. 9th Intern. Congr. Catal.*, vol. 2, The Chemical Institute of Canada, Ottawa, 1988, p. 561
- [122] H. Qi, D. Li, C. Yang, Y. Ma, W. Li, Y. Sun, B. Zhong. *Catal. Comm.* 4 (2003) 339
- [123] X. Xiaoding, E. Doesburg, J. Scholten. *Catal. Today.* 2 (1987) 125
- [124] J. Iranmahboob, H. Toghiani, D. Hill. *Appl. Catal. A: General.* 247 (2003) 207
- [125] V. Surisetty, A. Dalai, J. Kozinski. *Ind. Eng. Chem. Res.* 49 (2010) 6956
- [126] Z. Li, Y. Fua, J. Bao, M. Jiang, T. Hu, T. Liu, Y. Xie. *Appl. Catal. A: Gen.* 220 (2001) 21
- [127] J. Christensen, P. Mortensen, R. Trane, P. Jensen, A. Jensen. *Appl. Catal. A: General* 366 (2009) 29
- [128] R. Stockmann, H. Zandbergen, A. van Langeveld, R. Moulijn, J. Mol. *Catal. A* 102 (1995) 147
- [129] S. Louwers, M. Craje, A. van der Kraan, C. Seanet, R. Prins. *J. Catal.* 144 (1993) 579
- [130] V. Surisetty, I. Eswaramoorthi, A. Dalai. *Fuel.* 96 (2012) 77
- [131] J. Duchet, E. van Oers, V. de Beer, R. Prins, *J. Catal.* 80 (1983) 386
- [132] B. Concha, G. Bartholomew, C. Bartholomew. *J. Catal.* 89 (1984) 536
- [133] M. Zaman, A. Khodadi, Y. Mortazavi. *Fuel Process. Technol.* 90 (2009) 1214
- [134] X. Pan, Z. Fan, W. Chen, Y. Ding, H. Luo, X. Bao. *Nat. Mater.* 6 (2007) 507
- [135] S. Sigurdson, V. Sundaramurthya, A. Dalai, J. Adjaye, *J. Mol. Catal. A: Chem.* 306 (2009) 23
- [136] M. Xiaoming, L. Guodong, Z. Hongbin, *Chin. J. Catal.* 27 (2006) 1019
- [137] H. Xiao, D. Lia, W. Li, Y. Sun. *Fuel Process. Technol.* 91 (2010) 383
- [138] E. Liakakou, E. Heracleous, K. Triantafyllidis, A. Lemonidou. *Appl. Catal. B: Environmental.* 165 (2015) 296
- [139] H. Okatsu, M. Morrill, H. Shou, D. Barton, D. Ferrari, R. Davis, P. Agrawal, C. Jones. *Catal. Lett.* 144 (2014) 825
- [140] J. Hensley, S. Pylypenko, D. Ruddy. *J. Catal.* 309 (2014) 199
- [141] J. Christensen, P. Jensen, A. Jensen. *Ind. Eng. Chem. Res.* 50 (2011) 7949
- [142] J. Bertzelius, *Traitement de Chimie*, Firman Didot Frères, Paris. 1830
- [143] H. Woo, I. Nam, J. Lee, J. Chung, Y. Kim. *J. Catal.* 142 (1993) 672
- [144] P. Hou, H. Wise. *J. Catal.* 93 (1985) 409
- [145] D. Li, C. Yang, N. Zhao, H. Qi, W. Li, Y. Sun, B. Zhong. *Fuel Process. Technol.* 88 (2007) 125
- [146] J. Schwarz. *Catal. Today* 15 (1992) 395
- [147] D. Ferrari, G. Budroni, L. Bisson, N. Rane, B. Dickie, J. Kang, S. Rozeveld. *Appl. Catal. A: General* 462–463 (2013) 302
- [148] P. Afanasiev. *C. R. Chimie* 11 (2008) 15982

Chapter Two
Experimental

Summary

I Introduction	63
II Catalyst preparation	64
II-1 Cobalt based catalysts	64
II-2 Molybdenum disulphide based catalysts	65
III Characterizations	67
III-1 Textural characteristics	68
III-2 X-ray diffraction	69
III-3 X-ray photoelectron spectroscopy	69
III-4 Laser Raman spectroscopy	69
III-5 H ₂ Temperature programmed reduction	70
III-6 CO ₂ -Temperature programmed desorption	71
III-7 Transmission Electron Microscope	71
IV Catalytic measurements	72
IV-1 Set-up for catalytic test	72
IV-2 Catalytic test procedure	75
IV-3 Catalysts test conditions	77
V Conclusion	78
Reference	79

I Introduction

This chapter addresses catalyst preparation, characterization techniques and catalytic tests for evaluation of catalysis behavior. The catalysts in this work were prepared either using an incipient wetness impregnation or mechanical mixing. Impregnation is the most often used method for supported catalysts [1]. Since this is simple method for experiment. The incipient impregnation method starts from preparation of the solution of precursors that usually is the salt of active metals. Then the solution is mixed to a dry porous support. After being contacted, the solution is aspired by the capillary forces inside the pores of the support. The incipient wetness occurs when all pores of the support are filled with the liquid. But only initial impregnation is insufficient because internal force between support and precursor solution is intermolecular force and/or hydrogen bond [2], which are relatively weak interaction forces. Thereby drying and calcination is necessary to allow the distribution of the active phase over the support. The calcination is also necessary to decompose precursors, decomposition mechanism for different catalysts are different, which will be presented in following paragraphs. Mechanical mixing was used in this thesis to promoted the catalysts with alkaline promoters

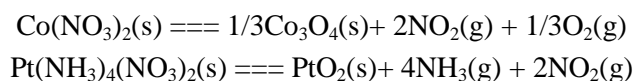
Catalyst characterization is important to provide qualitative as well as quantitative information about both physical and chemical properties of catalysts. The characterization of fresh prepared catalysts can show the structure and dispersion of catalysts; the characterization of activated catalysts will present the various species on catalysts and compared with results of catalytic tests, active site for FT synthesis may be identified; the characterization of spent catalysts can imply the behavior of active site in FT reaction with the comparison to fresh catalysts.

The catalytic tests were conducted under industrially relevant conditions under high pressure of syngas in the presence of small amounts of H₂S in the gas feed typical for syngas generated from biomass.

II Catalyst preparation

II-1 Cobalt based catalysts

Nitrates ($\text{Co}(\text{NO}_3)_2 \cdot 6\text{H}_2\text{O}$ and $\text{Pt}(\text{NH}_3)_4(\text{NO}_3)_2$, Sigma-Aldrich) were used as precursors for respectively cobalt and platinum/cobalt catalysts. The nitrates have an excellent dissolvability in water and can be thermally decomposed [3]. Aqueous solutions of precursors were prepared firstly, volume of the solution depends on the water-recovery volume on alumina support, which was decided through the visual method [4]. The alumina employed in this work, which was produced by Puralox (Puralox SCCA-5/17), the water-recovery volume is measured as $0.6 \text{ ml}_{\text{water}} \cdot \text{g}^{-1}_{\text{alumina}}$. The quantity of precursors depends on the content of active metal (cobalt) and/or promoter (platinum) in catalysts to be synthesized, for example to synthesize 10g of 25%Co/Al₂O₃ one needs 12.2g $\text{Co}(\text{NO}_3)_2 \cdot 6\text{H}_2\text{O}$. After preparation of the aqueous solution of precursor, the solution dripped very slowly on the support. Stirring was maintained during impregnation (Figure 2-1). Then impregnated support was dried in an oven at 60°C for 12 hours. Finally, the Co/Al₂O₃ catalysts and PtCo/Al₂O₃ catalysts were calcined at 450°C, a heating rate of 3°C/min, for six hours, and in a controlled air atmosphere (flow rate of 200 ml.min⁻¹). At this temperature the $\text{Co}(\text{NO}_3)_2$ can be thermally decomposed to cobalt oxide, Co₃O₄ and the $\text{Pt}(\text{NH}_3)_4(\text{NO}_3)_2$ precursor can be thermally decomposed to platinum dioxide, PtO₂.



High calcination temperature is helpful to decompose the precursor but it is unfavorable for the reducibility of cobalt based catalysts, because at higher temperature, the Co-aluminate which is inactive in FT synthesis can form [5]. Then these oxides were reduced to active metal in-situ in reactor by hydrogen. Four catalysts were prepared with different cobalt contents: 3%Co, 6%Co, 9%Co, and 25%. 25% of cobalt is considered to be the maximum of cobalt loading which allow obtaining highly dispersed cobalt species on the surface of

alumina support [5]. The quantity of platinum is quite low, only 0.1%, because platinum is an expensive noble metal [6]. The use of platinum, can improve cobalt reduction, presumably by hydrogen spillover from the promoter surface. Thus, addition of small amounts of noble metal shifts the reduction temperature of cobalt oxides and cobalt species interacting with the support to lower temperatures [7].

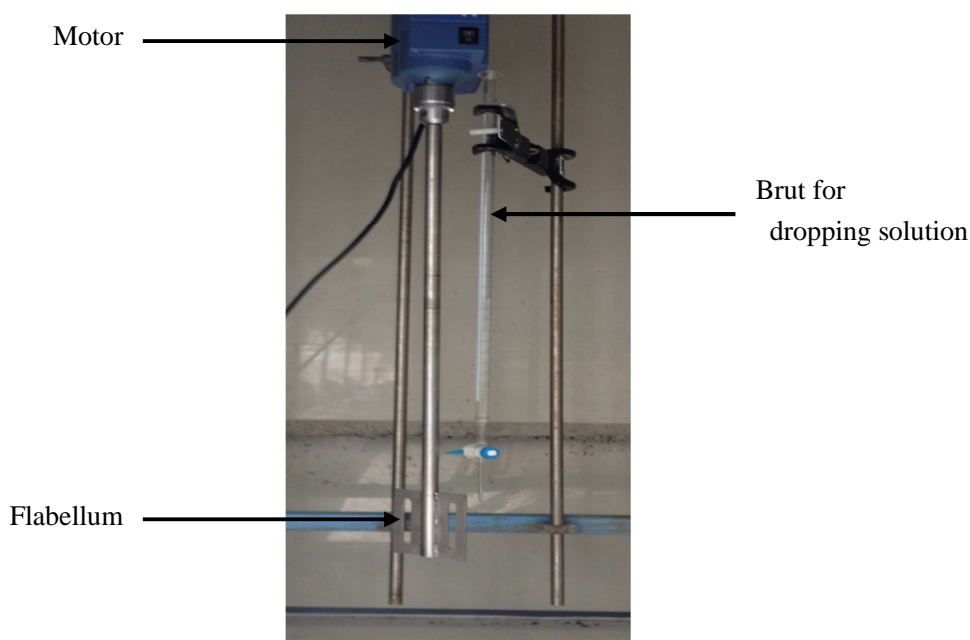


Figure 2-1 Stirring machine for catalyst synthesis

The 25%Co/alumina catalyst was prepared by two successive impregnations, and for every impregnation a half of total quantity of precursor is employed. When preparing 25%Co/alumina catalysts, we firstly prepared 12.5%Co/alumina, then another impregnation with same quantity of $\text{Co}(\text{NO}_3)_2$ precursor should be realized on that calcined 12.5%Co/alumina, then after another drying and calcination 25%Co/alumina was synthesized. In our work, 25%Co/ Al_2O_3 and 0.1%Pt25%Co/ Al_2O_3 were synthesized through this “double” impregnation method.

II-2 Molybdenum disulphide based catalysts

For MoS₂ based catalysts, the precursor was ammonium molybdate (AMT, (NH₄)₆Mo₇O₂₄·4H₂O, Sigma-Aldrich), which could be thermally decomposed to molybdenum oxide (MoO₃). The support is the Al₂O₃ previously used (in part II-1) with the water recovering volume of 0.6 ml_{water}·g⁻¹_{alumina}. The solvability of AMT is less than that of nitrate salts so that to prepare the catalyst containing more than 10%Mo, a two-times impregnation is necessary. Some alkali metals like sodium, potassium and cesium were also introduced in molybdenum disulphide catalysts as promoters, precursor of them were carbonates salt: Na₂CO₃ (Sigma-Aldrich), K₂CO₃ (Prolabo) and Cs₂CO₃ (Sigma-Aldrich). In order to investigate the effect of promoter precursors, for K-Mo catalysts, K₂SO₄ (Sigma-Aldrich) and KOH (Prolabo) were also used as the precursor of potassium promoter.

Potassium promoter has been directly impregnated together with AMT solution (called co-impregnation), and in another way, it can also be added into catalyst by milling with carbonate powers and dried AMT impregnated catalysts (called *mechanical mixing*). We have conducted catalyst synthesis through these two different methods in order to compare catalytic properties. As cobalt based catalysts, molybdenum sulphide based catalysts with more than 10%Mo were synthesized with the stirring machine on the impregnation step.

Finally, the MoS₂ based catalysts (promoter already added) were calcined at 550°C, a heating rate of 1°C/min, for two hours, and in air flow (flow rate of 100 ml·min⁻¹). 550°C is sufficient for the decomposition of precursor (NH₄)₆Mo₇O₂₄, and a relatively low heating rate can make the calcinations more efficient [8]. After calcination, Mo in the molybdenum based catalysts exists as molybdenum oxide MoO₃. The detail information for synthesis of molybdenum is showed in Table 2-1.



In order to modify the catalytic performance, different kinds of supports were employed, such as carbon nano-tube (CNT). CNT needs to be treated with 63% nitric acid before catalyst synthesis to eliminate impurities. Differently from alumina, CNT supported catalysts must be

calcined in inert atmosphere (N_2 flow rate of $100 \text{ ml}\cdot\text{min}^{-1}$), because CNT can be oxidized in air during calcination. However, the other details of the synthesis procedure were exactly the same as alumina supported catalysts.

Table 2-1 List of synthesized MoS_2 based catalysts

Catalysts (wight%)	Promoter : Mo (mol/mol)	Support	Symbol	Impregnation
2%K6%Mo	0.8	Alumina	2K6M	Hand stirring; Signal impregnation
6%K6%Mo(co-im)*	2.5		6K6M(co-im)	
6%K6%Mo(me-mi)*	2.5		6K6M(me-mi)	
15%Mo	0		15M	Machine stirring; double impregnation
3%K15%Mo	0.5		3K15M	
6K%15%Mo	1		6K15M	
12K%15%Mo	2		12K15M	
15K%15%Mo**	2.5		15K15M	
18K%15%Mo	3		18K15M	
24K%15%Mo	4		24K15M	
6%K20%Mo	0.7		6K20M	
9Na%15%Mo	2.5		9Na15M	
52%Cs15%Mo	2.5		52Cs15M	
15K%15%Mo(S)**	2.5		15K15M(S)	
15K%15%Mo(H)**	2.5		15K15M(H)	
15%Mo	0	Carbon nano-tube	15M_CNT	
1.5%K15%Mo	0.25		1.5K15M_CNT	
3%K15%Mo	0.5		3K15M_CNT	
6%K15%Mo	1		6K15M_CNT	
9%K15%Mo	1.5		9K15M_CNT	
15%K15%Mo	2.5		15K15M_CNT	

* Different synthesis methods (co-im: co-impregnation, me-mi: mechanical mixing)

** Different precursor: K_2CO_3 for 15K%15%Mo; K_2SO_4 for 15K%15%Mo(S); KOH for 15K%15%Mo(H)

III Characterizations

In this work various different characterization technologies were employed, in order to provide insights into the physical and chemical properties of catalysts. Characterization can help us to study fundamentally the influence of catalyst composition on the catalytic performance. Characterization of the fresh and spent catalysts may point out the active site of catalysts as well as possible catalyst deactivation. A wide range of characterization technologies were involved:

- Textural characteristics: to determine surface area and pore size of support material and catalysts.
- X-Ray Diffraction (XRD): to analyze crystallized compounds on catalysts, possibly to calculate the particle size of the particles.
- X-ray Photoelectron Spectroscopy (XPS): to quantitatively determine elements on catalyst surface, it is possible to analyze atoms of different oxidation state, moreover, atoms neighbored with different functional group may be also spared.
- Laser Raman spectroscopy (LRS): usually is a complement of XRD, this is a qualitative technique, not quantitative.
- H₂-Temperature programmed reduction (H₂-TPR): to study the reducibility of active phase on catalysts, and also to quantitatively analyst different phases through reduction temperature.
- CO₂-Temperature programmed desorption (CO₂-TPD): to characterize the basicity of catalysts
- Transmission Electron Microscope (TEM): to observe objects with the order of a few angstroms. TEM is used to observe the internal structure of catalysts, especially nanoparticles.

III-1 Textural characteristics

The BET surface area, pore volume, pore diameter and pore size distribution of the catalysts were determined by N₂ physisorption at 77 K using a Micromeritics ASAP 2010 apparatus. Prior to the experiments, the samples were outgassed at 423 K for 5 h. The total pore volume was calculated from the amount of vapor adsorbed at a relative pressure (P/P_0)

close to unity assuming that the pores are filled with the condensate in liquid state, where P and P_0 are the measured and equilibrium pressures, respectively. The pore size distribution curves were calculated from the desorption branches of the isotherms using BJH formula [9] that refers to capillary condensation in the mesopores.

III-2 X-ray diffraction

The ex situ X-Ray Diffraction patterns were recorded by a Siemens D5000 diffractometer using Cu $K\alpha$ radiation. The catalysts were scanned from 2θ of 5° to 70° with a scanning rate of $0.02^\circ \cdot s^{-1}$. In order to determine the average crystallite sizes of the catalysts, we use the half-width of the intense peak of the diffraction pattern and the Scherrer equation:

$$L = \frac{C\lambda}{\beta \cos\theta}$$

where C is a constant (here $c = 0.89$), λ is the X-ray wavelength (here λ is 0.154 nm), β is the full-width half-maximum (FWHM) of the intense peak of the diffraction pattern, θ is the Bragg angle, L is the volume-averaged size of the crystallites. Both β and θ must be taken on rad as unit in this formula. The results of XRD were analyzed with *JADE* software (version 5.0) and *Math* software (version 2.0). The FWHM was measured by *JADE* software, while the identification of peaks was realized by the both software.

III-3 X-ray photoelectron spectroscopy

XPS spectra were recorded with a VG ESCALAB 220 XL spectrometer equipped with a monochromatic Al $K\alpha$ ($E = 1486.6$ eV) X-ray source. The binding energies (BE) of Mo3d, Co2p, C1s, S2p, K2p, Na1s and Cs3d were determined by computer fitting of the measured spectra and referred to the Al2p peak of the support at 74.6 eV, using *Casa XPS* software. The binding energies were estimated to within ± 0.2 eV. Both fresh and spent catalysts have been

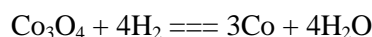
characterized by XPS, the spent catalysts and MoS₂ based catalysts after sulphidation have been passivated in a flux of 1% O₂ in argon at room temperature before XPS.

III-4 Laser Raman spectroscopy

The laser Raman spectrometry is constituted by a multi-channel Raman spectrometer (Dilor XY800) with a Krypton ion laser (Spectra Physics model Beamlok) which allows wavelength ranging from the ultraviolet to the near infrared fields. The powdered catalysts were put on a thin glass holder and pressed. The laser wavelength is 532 nm and a filter with diameter of 0.6 is employed. The spectrometer consists of three floors of 800 mm focal length equipped with a holographic grating plan 1800 lines / mm. The dispersed by the spectrometer radiation is received by the CCD (Charge Coupled Device) detector cooled with liquid nitrogen. The *LabSpec* software allows acquisition and data processing.

III-5 H₂ Temperature programmed reduction

The H₂-temperature-programmed reduction was carried out in AutoChem II 2920 (Micromeritics) with 5vol% H₂ diluted in argon stream. The total flow rate is 50 ml.min⁻¹. The temperature ramping rate was 10 K/min. The temperature was increased from room temperature to 1000°C. This method is used to decide the reducibility of cobalt based catalysts. The reduction of cobalt oxide occurs as this following reaction.



Through the quantity of consumed hydrogen we can calculate how much cobalt oxide was reduced during the TPR test, so the percentage of reducible active metal (Co in this case) among total active metal could be decided. Reduction degree of active phase means the percentage of reducible active metal (Metal^R%, g/g), it is calculated by the following equation:

$$\text{Metal}^{\text{R}}\% = \frac{x n_{\text{H}_2} M}{m_{\text{cata}} \text{Metal}\%}$$

Where x is the stoichiometric factor (cobalt $x = 0.75$), n_{H_2} is the molecular quantity of consumed hydrogen (mol), which is decided by interpretation of reduction peak in TPR profiles. M is the molecular mass of active metal (for cobalt $M = 58.9 \text{ g.mol}^{-1}$, for nickel $M = 58.7 \text{ g.mol}^{-1}$), m_{cata} is the total mass of catalyst that is used in TPR test (g), $\text{Metal}\%$ is the percentage of active metal in catalyst.

III-6 CO₂-Temperature programmed desorption

The Temperature Programmed Desorption of carbon dioxide was carried out in a quartz reactor connected with a mass spectrometer. The temperature programme was realized with AutoChem II 2920 Micromeritics. The samples were first pre-treated in a flow of helium ($40 \text{ cm}^3/\text{min}$) at 400°C for 1h, in order to dry the sample, and then the temperature was lowered to 30°C . CO_2 was adsorbed on the sulphided samples using a pulse technique (0.49 cm^3 of CO_2) at 30°C . The CO_2 desorption was measured during continuous temperature increase ($10^\circ\text{C}.\text{min}^{-1}$) up to 800°C .

However, it should be noticed that the catalysts were pre-treated at 400°C , the same as the sulphidation temperature. Hence desorbed CO_2 at over 400°C may be due to the adsorption before analyst. In this case the quantitative characterization of this zone (over 400°C) is not exact. So we just calculate the quantity of desorbed CO_2 between 30 and 400°C , with integration by *Origin* software.

III-7 Transmission Electron Microscope

Transmission electron microscopy operates on the same basic principles as the light microscope but uses an electron beam of very low wavelength (less than 1 angstrom) as source. It is possible for TEM to get an image with a resolution of 1000 times. The electron

beam travels through the sample that was put in the vacuum [10]. Some electrons should be scattered and disappear from the beam when the density of material is high. At the bottom of the microscope the non-scattered electron hit a fluorescent screen and a shadow image presents with different parts of the sample displayed in varied darkness [10]. The dense areas and areas containing heavy elements (elements of high molecular mass) appear dark due to more electrons that are scattered in sample. This is called the bright field image [10].

TEM measurements were performed using a TECNAI microscope (Figure 2-2) operating at a voltage of 200 kV. The sample powder was ultrasonically dispersed in ethanol and deposited on a copper grid prior to the measurements. In TEM measurement, each catalyst was imaged with different resolution to obtain not only the entire morphology of catalysts, but the image of particles of active phases as well. Images were taken at different parts in the observed field of microscopy.



Figure 2-2 TECNAI microscope

IV Catalytic measurements

IV-1 Set-up for catalytic test

A catalytic unit dedicated to Fisher-Tropsch synthesis in presence of H_2S was designed and built in this thesis (Figure 2-3).

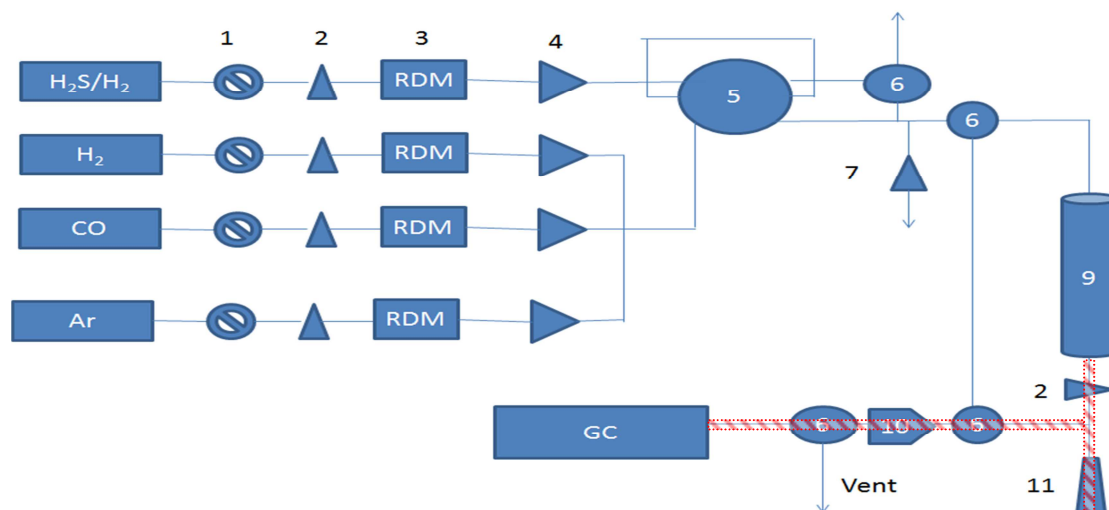


Figure 2-3 Design of unit for FT synthesis (1 Valve; 2 Filter; 3 Flow controller; 4 Check valve ; 5 Six-way valve; 6 Three way valves; 7 Proportional relief valve; 9 Milli-reactor (with oven, thermocouple) ; 10 Pressure regulator; 11 Condenser (red part is heating system for condenser))

The fixed bed tubular reactor with a small inner diameter (1.4 mm) was used. As Fischer-Tropsch synthesis is a highly exothermic reaction, the principal advantage of the millimeter fixed bed reactor is a strong radial heat transfer ability, because of its small reactor diameter and high surface to volume ratio, So the catalyst temperature can be better controlled [11]. As H_2S was used in our reaction, all tubes and most of the component parts in this unit were treated sulphunert by *RESTEK* company, so as to protect the system against sulphur corrosion and/or sulphur adsorption. The flow rates were controlled by electronic valve, and a thermocouple was installed inside the reactor and in contact with the catalyst allowing accurate control of the temperature (Figure 2-4), so that the reaction temperature could be controlled very exactly.

Before the catalysts are loaded in the reactor, they were sieved in the size range of $75\ \mu\text{m}$ to $100\ \mu\text{m}$. The weight of MoS_2 based catalysts loaded in the reactor is exactly 100mg, in this

case the catalyst always occupies the length of 2-3 cm in the fixed bed reactor.

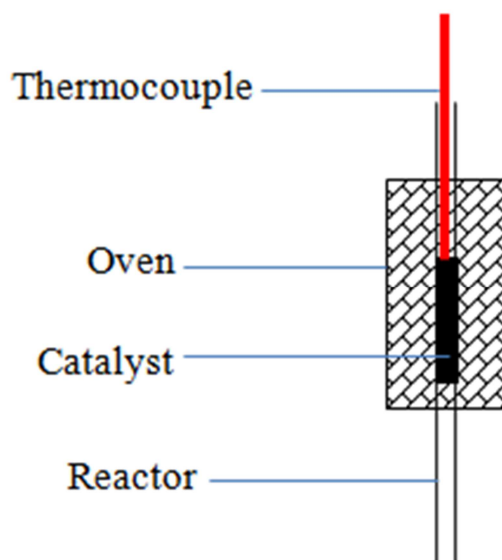


Figure 2-4 Structure of fixed bed reactor

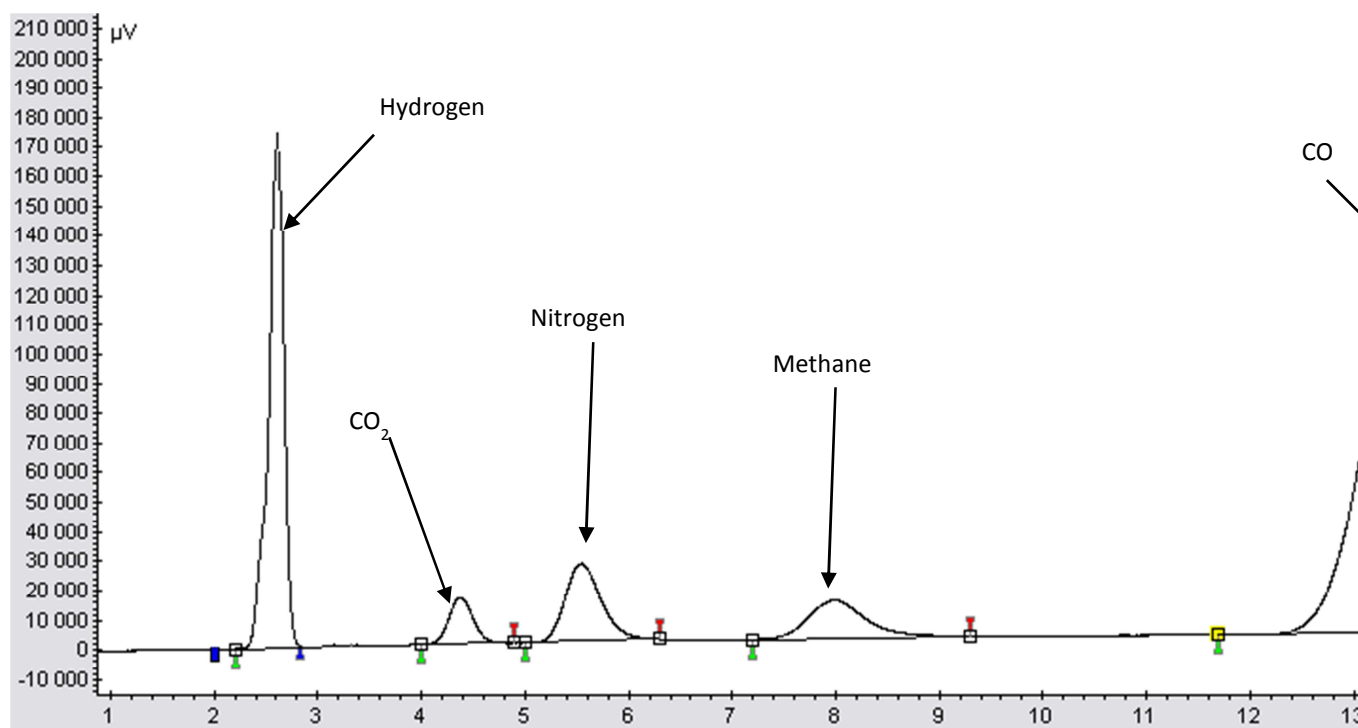
The reactor hydrodynamics depends on the bed length [12]. The bed length must fit to attain the plug flow regime inside reactor. A simplified relation is presented as formula:

$$L_b / d_p > 50 \text{ and } d_r / d_p > 10$$

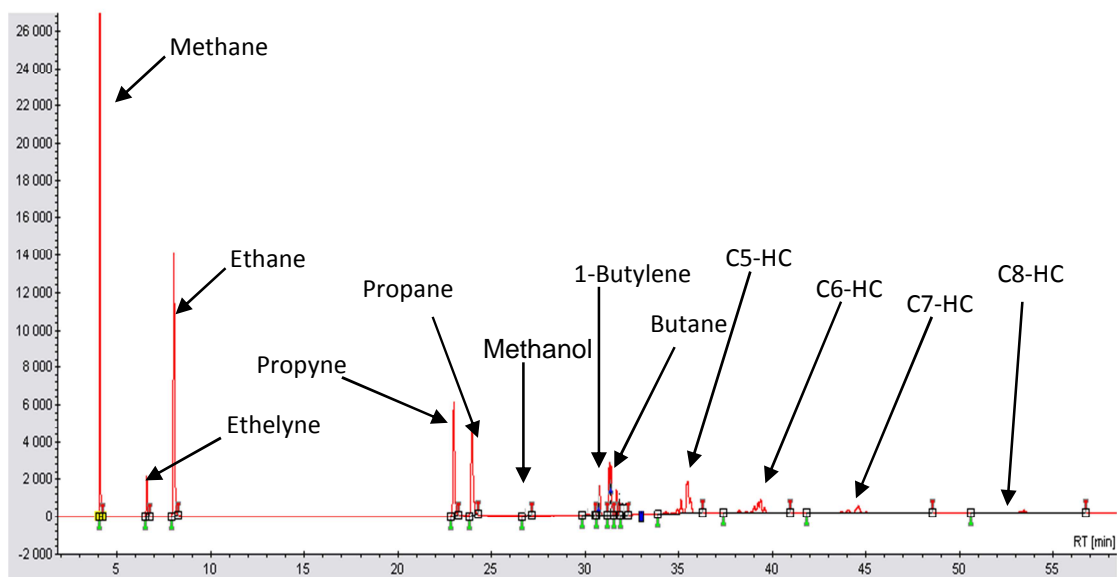
where L_b is the catalytic bed length, d_p is the particles size of catalyst and d_r is the diameter of milli form reactor. If ratio between bed length and particular size is more than 50 and ratio between reactor diameter and particular size is more than 10, the fixed bed could attain the plug flow regime. In our case, the catalytic bed length is between 2 cm to 6 cm, and diameter of reactor is 1.4 mm, and the particle size for catalysts we used is always between 50 – 150 μm , so L_b/d_p is always higher than 200 and $d_r/d_p > 9-10$.

For all tests, the nitrogen, methane and carbon monoxide gases were analyzed on-line by

gas chromatography (Bruck GC-456) with a TCD (thermal conductivity detector), see in Figure 2-5 (1). Other gaseous organic products (paraffins, olefins and alcohols) were detected by a flame ionic detector (FID) of the same gas chromatograph (Figure 2-5 (2)). Sulphide products (H_2S , carbon oxide sulphide (COS), methanethiol (CH_3SH), ethanethiol ($\text{C}_2\text{H}_5\text{SH}$), and dimethyl sulphide (CH_3SCH_3)) were analyzed on-line by another gas chromatography (Bruck GC-450) with a pulsed flame photometric detector (PFPD). The parameters of GC condition are listed in Table 2-2. For TCD detector, only carrier gas (helium or argon) is supplied as make-up gas and reference gas, but for flame detector, FID and PFPD, hydrogen and air are also needed for combustion.



(1)



(2)

Figure 2-5: Images for chromatograph (1) TCD, (2) FID

Table 2-2: GC Parameter

GC Type	GC-450	GC-456		
Detector	PFPD	TCD	FID	
Injection method	Split ratio=1:5	-	Split ratio=1:20	
Carrier gas	Helium	Helium	Helium	
Injection heating	100°C	120°C	120°C	
Column pressure	10 psi	10 psi	10 psi	
Column temperature	35°C	35°C	35°C to 200°C	
Regeneration	250°C	250°C	250°C	
Detector Temperature	250°C	200 °C	250°C	
Flow rate* (ml/min)	H ₂	13	-	30
	Air	17	-	300
	He/Ar/Air	10(Air)	20+30	28

*Here are the flow supplied for detectors, for TCD there are make-up gas (20 ml/min) and reference gas(30 ml/min)

The CO conversion is based from the molar flow rates of CO into and out of the reactor according to below equation:

$$\text{CO conversion} = \left(1 - \frac{F_{\text{CO}}^{\text{out}}}{F_{\text{CO}}^{\text{in}}}\right) \times 100\%$$

where $F_{\text{CO}}^{\text{in}}$ is the CO molar flow into the reactor and $F_{\text{CO}}^{\text{out}}$ is the CO molar flow in the reactor outlet. The selectivity of each product is based on the total number of carbon atoms in the product, CO_2 -free selectivity, and therefore is defining as the below equation:

$$\text{Product selectivity} = \frac{n \times F_{\text{product}}^{\text{out}}}{F_{\text{CO}}^{\text{in}} \times \text{CO conversion} - F_{\text{CO}_2}^{\text{out}}} \times 100\%$$

where $F_{\text{product}}^{\text{out}}$ is the product molar flow out the reactor, the product can be methane, alcohol or hydrocarbon, and n is the number of carbon atom in the molecular product. The carbon balance was always better than 90%

IV-2 Catalytic test procedure

Cobalt based catalysts were reduced in hydrogen flow (5 ml/min) at 350°C for 16 hours. Then, the reactor was cooled down at lower temperature (150°C),. After purging with Helium flow (5 ml/min) for 30 minutes, the syngas with a molar ratio of $\text{H}_2/\text{CO} = 2$ is introduced firstly in by-pass, then it is gradually introduced through the fixed bed reactor. The gas bottle of CO contains 5% of nitrogen that was used as an internal standard for calculating carbon monoxide conversion. The pressure was gradually raised to 20 bar with an electronic back pressure regulator supplied by Bronkhorst. Then, the temperature was increased to 220°C with a slow ramp (1°C/min). The procedure for testing cobalt catalysts is shown in Figure 2-6. The catalytic tests with the presence of hydrogen disulphide were also realized, for these tests, the reduction step and the cooling step are the same as the test without H_2S . A bottle of hydrogen which contains 20 ppmv H_2S was employed. So in syngas the concentration of H_2S is about 13.3 ppmv as the ratio of H_2 to CO is two.

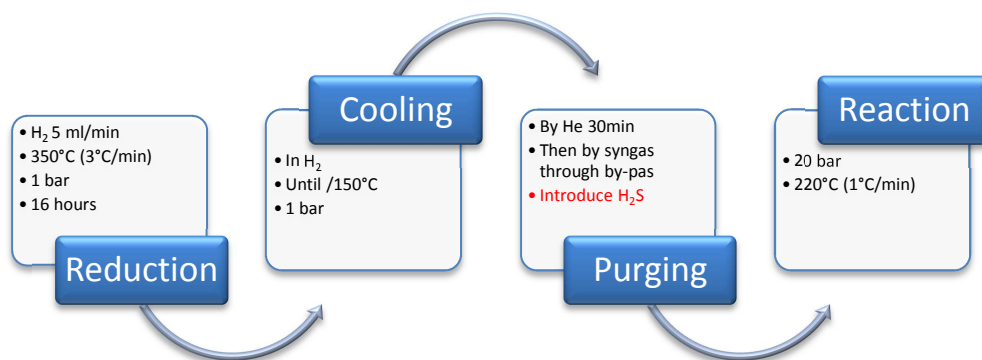
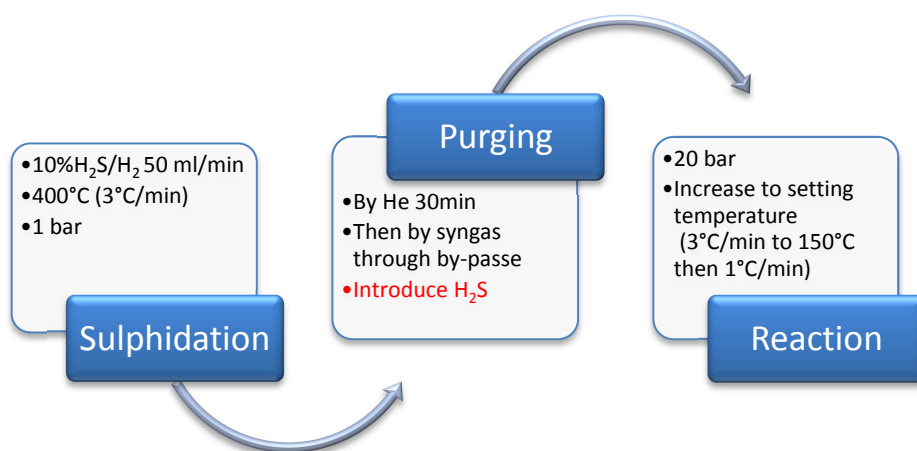


Figure 2-6 Procedure of catalyst testing for cobalt based catalysts

These molybdenum based catalysts need to be sulphided before test, in our work the sulphidation was conducted ex-situ. The calcined Mo based catalyst was introduced in a glass reactor, and then a total flow rate of 100 ml.min⁻¹ of hydrogen and hydrogen disulphide (10% of H₂S in H₂) was directed to the reactor. The sulphidation was realized at 400°C with a heating rate of 3°C.min⁻¹ to avoid MoS₂ sublimation which occurs at 450°C. After the sulphidation the catalysts were collected and kept in a sealed plastic ampoule. Molybdenum disulphide is stable in air at ambient temperature and the oxidation does not occur until 316°C, however, since temperature reaches 150°C, MoS₂ can be slowly oxidized in air [13]. After the sulphidation molybdenum based catalysts were introduced into the fixed bed reactor. The system is purged firstly through reactor by helium and then by syngas. The procedure of catalytic test is presented in Figure 2-7. Molybdenum disulphide catalysts have been tested at different temperatures. The reaction temperature was a least 300°C.

Figure 2-7 Procedure of catalyst testing for MoS₂ based catalysts

IV-3 Catalysts test conditions

GHSV (Gas hourly space velocity, $\text{L}\cdot\text{h}^{-1}\cdot\text{g}^{-1}$ or $\text{ml}\cdot\text{h}^{-1}\cdot\text{g}^{-1}$) is one of the most important key factors for catalysis reactions. It depends on total gaseous flow rate and total catalyst weight feed in the reactor [14].

$$\text{GHSV} = 60 \cdot F^T / m_{\text{cata}}$$

where F^T is total flow rate for FT synthesis ($\text{L}\cdot\text{min}^{-1}$ or $\text{ml}\cdot\text{min}^{-1}$), so the factor “60” was used for the conversion of unit, m_{cata} is the weight of used catalyst in catalytic test (g).

GHSV affects significantly CO conversion in catalytic tests. There is no doubt that CO conversion fall down with increasing of GHSV [15]. An appropriate GHSV is necessary. Through our research, for Co based catalysts GHSV should be $14 \text{ L}\cdot\text{h}^{-1}\cdot\text{g}^{-1}$, and for MoS_2 based catalysts GHSV should be $2.1 \text{ L}\cdot\text{h}^{-1}\cdot\text{g}^{-1}$. However, GHSV was varied in catalytic tests of MoS_2 based catalysts in order to determine the effect of GHSV on catalytic performance.

The temperature for Co catalysts is always 220°C [16]. For MoS_2 based catalysts we tried different temperatures and finally chose 360°C (detail discussion is presented in next chapters). The reaction pressure in our work is relatively low, because lower pressure is favorable for light olefin selectivity [17,18]. For all catalysts the 20 bar pressure was used, and for MoS_2 based catalysts even lower pressure was also involved to investigate the effect of pressure on catalytic performance.

V Conclusion

This chapter describes the method for preparation of Al_2O_3 supported Co based catalysts as well as supported MoS_2 based catalysts. To investigate the different catalytic performance of various catalysts, characterization should be realized on fresh, activated and spent catalysts. The characterization techniques and their experimental protocols are described in this chapter. The catalysts were tested in micro fixed bed reactor. Conventional FT catalysts (Co) and sulphur tolerance catalysts (MoS_2) are investigated respectively. In the next chapter, H_2S

effect on Co based catalysts will be evaluated.

Reference

- [1] S. Lee, Y. Aris. *Catal. ReV. Sci. Eng.* 27 (1985) 207
- [2] J. Schwarz. *Catal. Today.* 15 (1992) 395.
- [3] CAS (Chemical Abstracts Service) data, No. 10141-05-6
- [4] Thesis of Heline KARACA, Univ-lille1. July, 09, 2010
- [5] W. Chu, P. Chernavskii, L. Gengembre, G. Pankina, P. Fongarland, A. Khodakov, J. *Catal.* 252 (2007) 215
- [6] P. Chaumette, C. Verdon, Patent : UK 2 258 414, (1993) Institut Français du Pétrole.
- [7] G. Jacobs, P. Patterson, Y. Zhang, T. Das, J. Li, B. Davis. *Appl. Catal. A: General.* 233 (2002) 215
- [8] J. Zhang, J. Chen, J. Ren, Y. Li, Y. Sun. *Fuel.* 82 (2003) 581
- [9] E.P. Barrett, L.G. Joyner, P.P. Halenda. *J. Am. Chem. Soc.* 73(1951) 373
- [10] J.Niemansverdriet. *Spectroscopy in Catalysis*, 3rd version, Wiley-VCH (2007)
- [11] S. Chambrey, P. Fongarland, H. Karaca, S. Piché, A. Griboval-Constant, D. Schweich, F. Luck, S. Savin, A. Khodakov. *Catal. Today.* 171 (2011) 201
- [12] E. Nauman. *Chem. Eng. Commun.*, 8 (1981) 53
- [13] CAS (Chemical Abstracts Service) data, No. 1317-33-5
- [14] P. Danckwerts. *Chem. Eng. Sci.* 2 (1953) 1
- [15] H. Karaca, O. Safonova, S. Chambrey, P. Fongarland, P. Roussel, A. Griboval-Constant, M. Lacroix, A. Khodakov. *J. Catal.* 277 (2011) 14
- [16] A.Khodakov, W. Chu, P. Fongarland. *Chem. Rev.* 107 (2007) 1692
- [17] E. Colley, R. Copperthwaite, G. Hutchings, G. Foulds, N. Coville. *Appl. Catal. A: General* 84 (1992) 1
- [18] R. Madon, E. Iglesia. *J. Catal.* 139 (1993) 576

Chapter Three

Catalytic behaviour of (Pt)Co/Al₂O₃ catalyst in presence of sulphur

Summary

I Introduction	85
II Characterization of Fresh Cobalt based catalysts	86
II-1 Textural Characteristics	86
II-2 XRD	87
II-3 H ₂ -TPR	89
II-4 XPS	91
III Catalytic tests on Co based catalysts	92
III-1 Effect on different Co content on supported catalysts	92
III-2 Effect of Hydrogen Disulphide in FT synthesis	93
IV Characterization of Spent Catalysts	97
IV-1 XRD on spent catalysts	97
IV-2 XPS on spent catalysts	98
V Discussion and Conclusion	100
V-1 Dispersion and Reducibility of Co based catalysts	100
V-2 Effect of H ₂ S on Co/Al ₂ O ₃ and Pt-Co/Al ₂ O ₃	101
V-3 Conclusion	101
Reference	103

I Introduction

The syngas coming from gasification of biomass contains several impurities. One of the most important impurities is sulphur that could be a poison for the conventional FT catalysts [1]. In previous literatures, the presence of H₂S in syngas feed could inhibit the catalytic activity [2,3,4] and affect the product selectivity [4,5]. There is a general consensus in the literature that sulphur containing compounds should be removed from biosyngas for stable operation of Fischer-Tropsch synthesis [6]. However, the detailed effect of H₂S in syngas on FT synthesis catalysts and the mechanism of H₂S for poisoning active catalyst remains still a challenge.

The conventional alumina supported catalysts [7] were used in this thesis to investigate the H₂S effect in syngas on the catalyst structure and performance in FT synthesis. Co/Al₂O₃ catalysts with different Co content have been synthesized and tested for FT synthesis. Pt was used as a promoter to Co/Al₂O₃ catalysts to study the H₂S effect on noble metal promoted Co/Al₂O₃ catalysts. The list of the synthesized catalysts given in Table 3-1. The catalysts were characterized by BET, XRD, XPS and H₂-TPR. XRD and XPS were measured on both fresh prepared and spent Co based catalysts. The catalytic performance was evaluated in a fixed bed reactor with or without presence of hydrogen disulphide in syngas feeding. The reaction conditions for catalytic test were [8]: T=220°C, P=20 bar, H₂/CO = 2 and a high GHSV of 14000 ml.g⁻¹.h⁻¹. These are usual conditions of low temperature FT synthesis.

Table 3-1 list of Co/Al₂O₃ catalysts and their symbol

Metals loading (wt. %)	Symbol
3%Co	3Co
6%Co	6Co
9%Co	9Co
25%Co	25Co
0.1%Pt and 25%Co	Pt25Co

Our work in this chapter will focus on:

- Stability evaluation of conventional cobalt catalysts in the presence of H₂S in syngas.

- Sulphur effect on products selectivity of Co catalyst.
- Analysis of catalysts after catalytic tests, in order to investigate the interaction between sulphur and Co active site.

II Characterization of fresh cobalt based catalysts

II-1 Textural Characteristics

BET surface area, BJH pore volume and pore diameter of supported cobalt catalysts (after calcination) and γ -alumina support are listed in Table 3-2. These results show that the BET surface area, pore volume and diameter for all of catalysts were lower than that of the alumina support. The effect can be due to pore blocking of alumina support with cobalt oxide and effect of alumina “dilution” with cobalt. Indeed, the BET surface area is decreasing with increase in cobalt loading, the surface area of 25%Co/Al₂O₃ (111 m².g⁻¹) is much smaller than that of 3%Co/Al₂O₃ (170 m².g⁻¹). Meanwhile, pore volume and pore diameter for alumina support, Al₂O₃ supported cobalt catalysts show the similar trends, which also suggest the pore blockage should be caused by cobalt loading. These results agree with previous research [6,8].

Table 3-2: BET surface area and pore size on calcined cobalt/Al₂O₃ catalysts

Samples	BET surface area (m ² /g)	Pore volume (cm ³ /g)	Pore diameter (nm)
γ -Alumina	186	0.51	8,9
3Co	170	0.45	8.1
6Co	157	0.43	7.9
9Co	147	0.40	7.6
25Co	111	0.25	7.3
Pt25Co	112	0.23	7.3

Interestingly, Pt promoter seems to have no significant effect on the BET results. This result is different from previous literatures [9,10] where high Pt loading is used. Jermwongratanachai et al [9] observed a slight decrease in BET surface area after promotion with platinum. They explained that the increase of BET surface area could be due to the presence of Pt, Co oxides with a smaller size were formed, and these small particles blocked pores on surface of Al₂O₃ support to a lesser extent than larger crystallites. However, only 0.1 wt.% Pt was added as promoter in our Co/Al₂O₃ catalysts, so the effect of Pt on surface area as well as pore size appears to be rather insignificant.

II-2 XRD

Supported Co catalysts were characterized by XRD analysis. Figure 3-1 shows the XRD patterns of cobalt catalysts with different cobalt loading. After calcination, cobalt nitrate precursor is decomposed to Co₃O₄, the cobalt species were mainly Co₃O₄ phase (JCPDF 65-3103, $2\theta = 19.42^\circ, 31.21^\circ, 36.57^\circ, 59.36^\circ, 65.36^\circ$). The alumina diffraction peaks could be also seen (JCPDF 50-0741, $2\theta = 31.86^\circ, 37.53^\circ, 39.28^\circ, 45.67^\circ, 66.60^\circ$). For the catalysts 3%Co/Al₂O₃ and 6%Co/Al₂O₃, the peak of cobalt oxide at $31.21^\circ, 65.36^\circ$ and of alumina at $31.86^\circ, 66.60^\circ$ could not be well separated because of the low cobalt loading so cobalt oxide peak intensity is weak while the alumina peak intensity is relatively high.

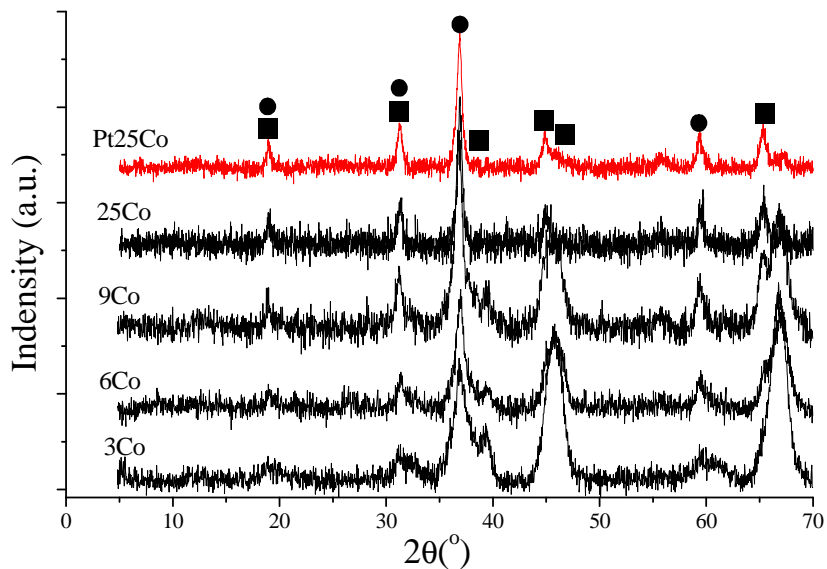


Figure 3-1: XRD pattern on Co/Al₂O₃ catalysts with different Co content and Pt promoted Co/Al₂O₃ catalyst (●Co₃O₄ ■Al₂O₃)

The Co₃O₄ crystallite diameter was calculated by the Scherrer equation (mentioned in chapter two). The peak chosen to calculate the crystallite diameter of cobalt oxide is the one at 36.57°, this peak does not coincide with any other peaks on supported cobalt based catalysts, so that measurement of FWHM (full-width half-maximum) can be reliable.

Dispersion can describe the distribution of active cobalt site on catalyst surface. It is known that for cobalt based catalysts, in FT procedure, a high dispersion is favourable for the catalytic activity [11,12]. Dispersion is strongly related to the crystal diameter of active particles [13]:

$$\text{Dispersion} = \frac{96}{D_{\text{Co}^0}} \%$$

where D_{Co^0} is the crystal diameter of Co⁰. Note that the ex-situ XRD of calcined catalysts gives only crystallite diameter of cobalt oxide. The formula which takes into account the molar volumes of Co₃O₄ and Co [14], was used to calculate the diameter of the metallic cobalt particles from the diameter of cobalt oxide crystallites

$$D_{\text{Co}^0} = 75\% D_{\text{Co}_3\text{O}_4}$$

The dispersion of metallic cobalt in cobalt based catalysts is shown in Table 3-3. The particle diameter evaluated from XRD patterns is also listed in the same table. Cobalt crystallite diameter increases with increase of cobalt content loaded on catalysts. Smaller particle diameter leads to better dispersion of cobalt species, but larger cobalt particles can more easier reduced that smaller ones. [15]. Thus both cobalt dispersion and reducibility contribute to the catalytic activity.

Table 3-3: Particle diameter and Co⁰ dispersion on cobalt based catalysts

Catalyst	D _{Co₃O₄}	D _{Co⁰}	Dispersion of Co ⁰
3Co	5.6 nm	4.2 nm	22.9%
6Co	8.0 nm	6.0 nm	16.0%
9Co	10.5 nm	7.9 nm	12.2%
25Co	12.5 nm	9.4 nm	10.2%
Pt25Co	12.4 nm	9.3 nm	10.3%

Table 3-3 also represents the cobalt dispersion on the platinum promoted catalyst. We can observe that the particle diameter of cobalt oxide is similar for non-promoted and promoted catalysts. This result is consisting with previous literature [9,16,17]. For example, Jermwongratanachai et al [9] reported on 25wt.%Co/Al₂O₃ catalyst with addition of 0.5wt.%Pt, the Co⁰ particle diameter (from XRD pattern at the peak of 37°) was the same as non-promoted 25wt.%Co/Al₂O₃ catalyst.

II-3 H₂-TPR

The H₂-TPR profiles for cobalt based alumina supported catalysts are shown in Figure 3-2. On 9% cobalt loading catalyst, a strong TPR peak is detected at 375°C. With high cobalt loading catalyst (25%Co) the profile presents a similar peak at 375°C but the intensity is much higher. Then the peak at 375°C is attributed to the reduction of Co₃O₄ in cobalt based catalysts. Heated with hydrogen, cobalt oxide (Co₃O₄) is reduced to cobalt monoxide (CoO) then is finally reduced to metallic cobalt (Co⁰) [18]. However, the two reduction steps of cobalt oxide may not always be observed as two well separated peaks in H₂-TPR [18].

Moreover, on 25Co catalysts, there is a small peak at 235°C. This peak is assigned to the reduction of residual nitrate species that have not been decomposed during calcination [19].

At higher temperature (between 450°C to 800°C) the reduction peak is attributed to the reduction of cobalt aluminate [20], which is due to the interaction of cobalt and alumina support that is more difficult to reduce than cobalt oxide [21]. Therefore, the formation of Co aluminate could inhibit the catalytic activity of cobalt based catalysts. To avoid the formation of Co-aluminate was also a key point for Co/Al₂O₃ catalyst, the use of different noble metal promoter was helpful to improve the reduction of cobalt based catalysts. After 800°C, no reduction peaks is observed, indicating no formation of hardly reducible aluminate species.

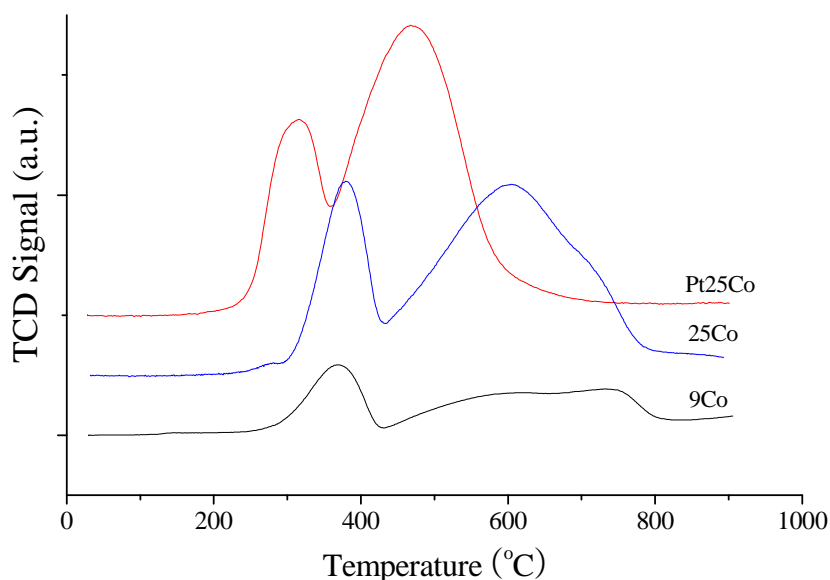


Figure 3-2: H₂-TPR of alumina supported Co catalysts

In Figure 3-2 H₂-TPR analysis of the Pt promoted Co/Al₂O₃ catalyst is also represented. Similar peaks are also observable on Pt promoted catalyst, and a shift of about 90°C to lower temperature is presented, for both reduction of cobalt oxide and cobalt aluminate, indicating that the Co based catalysts can be easier reduced with the presence of Pt. The noble metal such as platinum can catalyse reduction of cobalt by hydrogen, presumably by hydrogen spillover from the promoter surface [22]. It was believed that Pt was situated on the edge of

the cluster and that reduction occurred on Pt first, allowing hydrogen to spill over to cobalt oxide and nucleate cobalt metal sites [10]. Thus, addition of small amounts of noble metal shifts the reduction temperature of cobalt oxides and cobalt species interacting with the support to lower temperatures.

CoAl₂O₄ cobalt aluminate is more difficult to be reduced than cobalt oxide. [23,24,25]. The reducibility of cobalt catalysts can be calculated with the total H₂ consumption during H₂-TPR (showed in Figure 3-2), with following equation:

$$\text{Reducibility} = \frac{3/4 N_{\text{H}_2} M}{\text{Co}\%}$$

where N_{H₂} is the H₂ consumption during H₂-TPR characterization (unit: mol_{H₂}/g_{catalyst}), M is the molecular mass of cobalt (58.9 g.mol⁻¹), Co% means the percentage of Co loading on catalysts (9% or 25%) and 3/4 is from the stoichiometric of the cobalt oxide reduction:

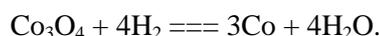


Table 3-4: Reducibility of supported cobalt based catalysts

Catalyst	H ₂ consumed for reduction (ml.g ⁻¹)	Reducibility
9Co	35.5	71.4%
25Co	112.2	81.4%
Pt25Co	128.1	92.9%

The reducibility of cobalt oxide is better with high Co loading catalyst (25Co) than that on low Co loading catalyst (9Co). This result agreed with the conclusion of Iglesia [15], who reported Co/Al₂O₃ catalysts with high content of Co showed a better reducibility, because the particle size was larger than low Co content catalysts. The extent of cobalt reduction was 81.4% with 25Co. Pt promotion results in even better cobalt reducibility (92.9%). Therefore, the role of Pt to favour the Co catalyst reducibility is not only lowering the reduction temperature, but also making a larger fraction of cobalt oxide reducible. This result is consistent with the study

of Jacobs et al [26] who found the same function of platinum promoter by comparing H₂-TPR of 25%Co/Al₂O₃ and 0.5%Pt25%Co/Al₂O₃ catalysts.

II-4 XPS

XPS was measured on fresh 25Co and Pt25Co catalyst. The results are shown in Table 3-5. On Pt promoted catalysts no Pt was detected due to the low Pt content (0.1%) in the Pt25Co catalyst. On the fresh catalysts the Co atomic ratio is low. This indicates the Co was not very well dispersed on catalyst surface. Cobalt XPS atomic ratio on fresh Pt25Co is higher than that on fresh 25Co, indicating that a better Co dispersion is observable in Pt25Co than in 25Co.

Table 3-5 XPS atomic ratio on calcined 25Co and Pt25Co catalysts

Catalyst	Al(%)	Pt(%)	O(%)	Co(%)
25Co	34.7	-	64.0	1.3
Pt25Co	36.1	0.0	60.8	3.1

Co_{2p} XPS spectra of 25Co and Pt25Co catalysts are presented in Figure 3-3. The observed XPS peaks at 780.9 eV and 796.6 eV are characteristics of Co 2p_{1/2} and 2p_{3/2} of the cobalt oxide (Co₃O₄) [27], while the peaks at 803.5 eV and 786.5 eV correspond to the cobalt(II), which may exist as CoO and cobalt aluminate [28]. On fresh catalysts, there is no significant difference in the Co_{2p} XPS between 25Co and Pt25Co catalysts.

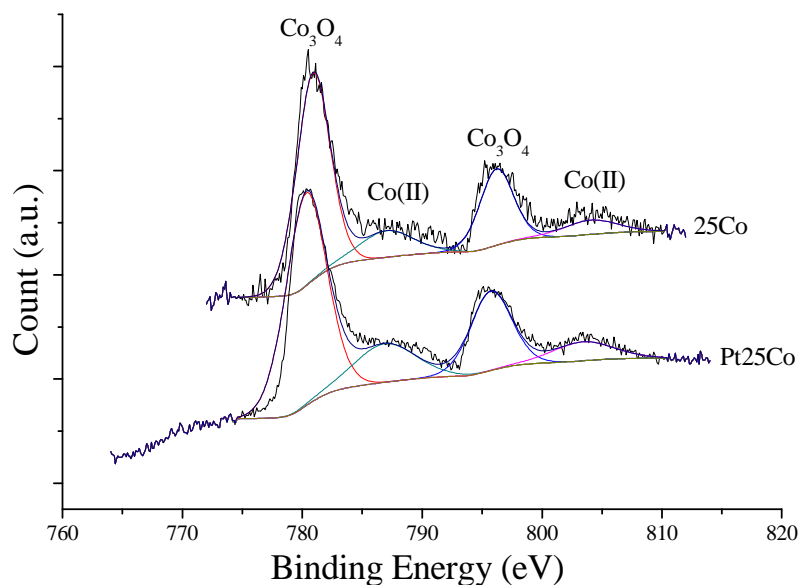


Figure 3-3: XPS of 25Co and Pt25Co

III Catalytic tests on Co based catalysts

III-1 Effect on different Co content on supported catalysts

The 9%Co/Al₂O₃, 25%Co/Al₂O₃ and Pt25%Co/Al₂O₃ catalysts were tested using the procedure presented in Figure 3. The CO conversion versus time is shown in Figure 3-4. These tests were realized at 220°C and 20 bar, and GHSV = 14000 ml.g_{catalyst}⁻¹.h⁻¹. Obviously, the more cobalt was loaded to alumina support, the higher CO conversion was observed. For 25Co catalyst the catalytic activity was relatively stable at around 24%. On the 9Co catalyst the CO conversion is lower than that on the 25Co catalyst, and remained stable within 40 hours on stream. Carbon monoxide conversion was less significant on 9Co. It was also stable with time on stream similarly to the cobalt catalysts containing higher cobalt content.

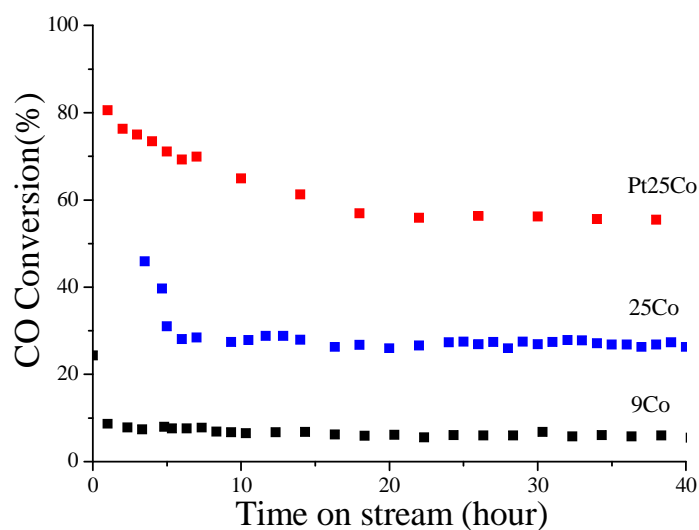


Figure 3-4: CO conversion for catalytic tests on different Co/Al₂O₃ catalysts

III-2 Effect of hydrogen disulphide in FT synthesis

The 25Co catalyst was tested in absence and presence of H₂S. The obtained results are compared in Figure 3-5. In the presence of H₂S, an obvious catalytic deactivation appeared after 4 hours on stream. The CO conversion decreased from 24% to 4% after 40 h. A continuous decrease in the catalytic activity indicates that the H₂S interacts with the Co active site all along the catalytic tests. The H₂S was introduced while the pressure was rising up to 20 bar and the temperature was rising up to 220°C. It meant that cobalt catalyst had already contacted with H₂S and been deactivated for 4 or 5 hours before the FT reaction. That is why the CO conversion was lower just at the beginning of the catalytic tests.

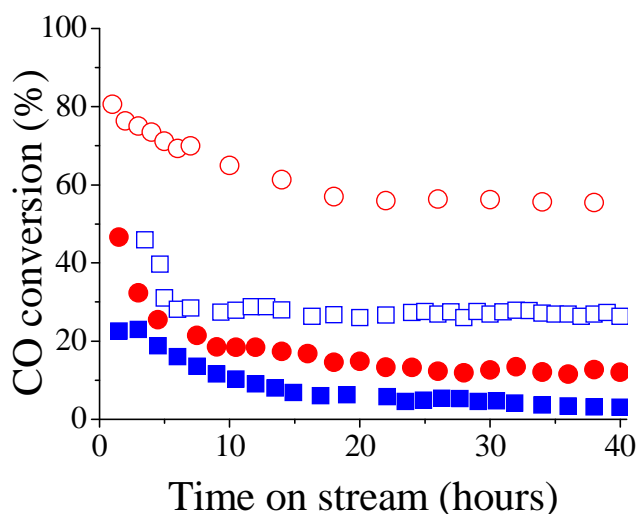


Figure 3-5: CO conversion on 25Co (Blue Square) and Pt25Co (Red Round) catalysts without (empty) and with (full) H₂S (13.3 ppmv) in syngas feed. T = 220°C, P = 20 bar, GHSV = 14000 cm³/(g.h), H₂/CO = 2. (□25Co/syngas, ■25Co/syngas+H₂S, ○Pt25Co/syngas, ●Pt25Co/syngas+H₂S)

The H₂S deactivation effect on Pt promoted catalyst is as important as on 25Co catalyst. The 25Co catalyst could maintain the activity during the last 20-hour reaction, and CO conversion was kept at around 9% in the end. Besides, on Pt25Co the trend of CO conversion as a function of time is akin to that on 25Co. The low CO conversion at first few hours is caused by the initial contact with H₂S and the continuous conversion decrease is due to the successive sulphur adsorption. However, the Pt25Co catalyst showed however higher activity than 25Co even in the presence of sulphur after 40 hours on stream.

Figure 3-6 showed the difference of FT products selectivity for the tests performed with or without H₂S on both 25Co and P25Co catalysts. The CH₄ and the C₂-C₄ hydrocarbon selectivity were higher when the feed contains 13.3 ppmv of H₂S. The ratio of light olefins to light paraffins also increased in presence of H₂S. Finally, the selectivity of C₅₊ hydrocarbon decreased in the presence of H₂S.

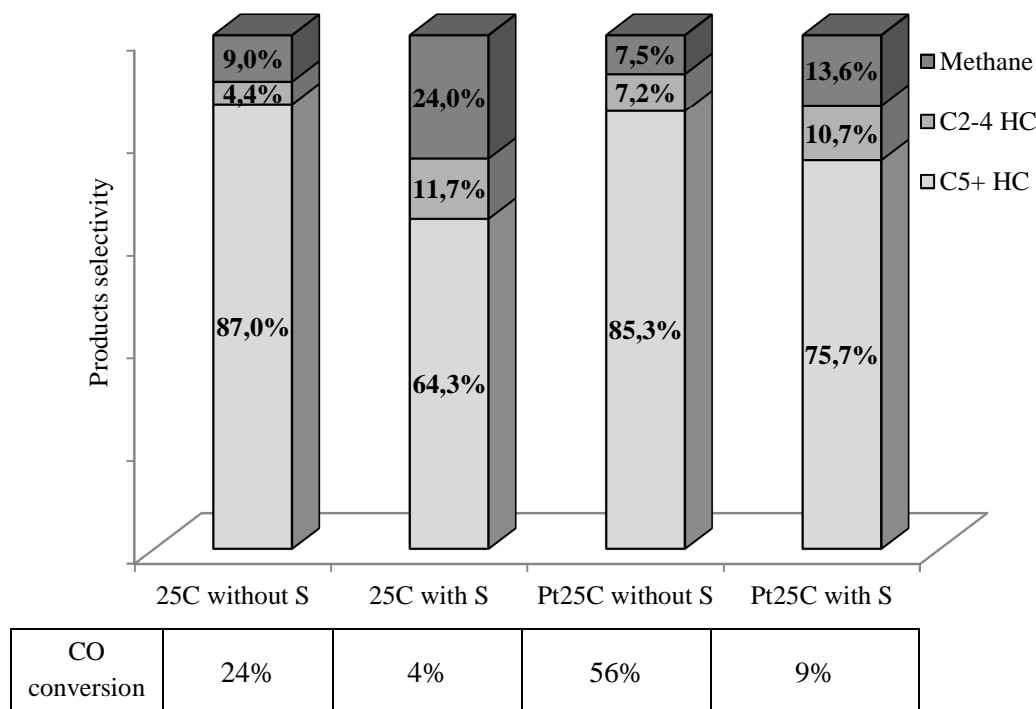


Figure 3-6: Products selectivity on 25Co and Pt25Co catalysts without and with sulphur (13.3 ppmv) in syngas feed. T = 220°C, P = 20 bar, GHSV = 14000 cm³/(g.h), H₂/CO = 2.

Pansare [4] suggests that the decrease in C₅₊ selectivity and the increase in C₁-C₄ selectivity with H₂S might indicate that the sulphur poisoning can affect the catalyst chain growth probability. The formation of heavier hydrocarbons needs high density of the active site on Co⁰ [29]. The adsorption of sulphur on Co could decrease active sites density and thus affected the hydrocarbon chain growth. It is notable that the effect of sulphur on selectivity was less significant in Pt promoted catalysts than in unprompted counterparts. Promotion effect of Pt also helps to maintain the catalytic activity even in the presence of sulphur.

The sulphur in the reactor outlet was measured by sulphur sensitive PFPD detector. Figure 3-7 showed the H₂S concentration at the reactor outlet and CO conversion as functions of time on stream.

The H₂S concentration was almost zero at the reactor outlet with the 25Co and Pt25Co catalysts. This suggests that sulphur was completely absorbed by Co catalysts. The CO conversion also decreased, indicating the loss in the catalytic activity, could be caused by adsorption of sulphur.

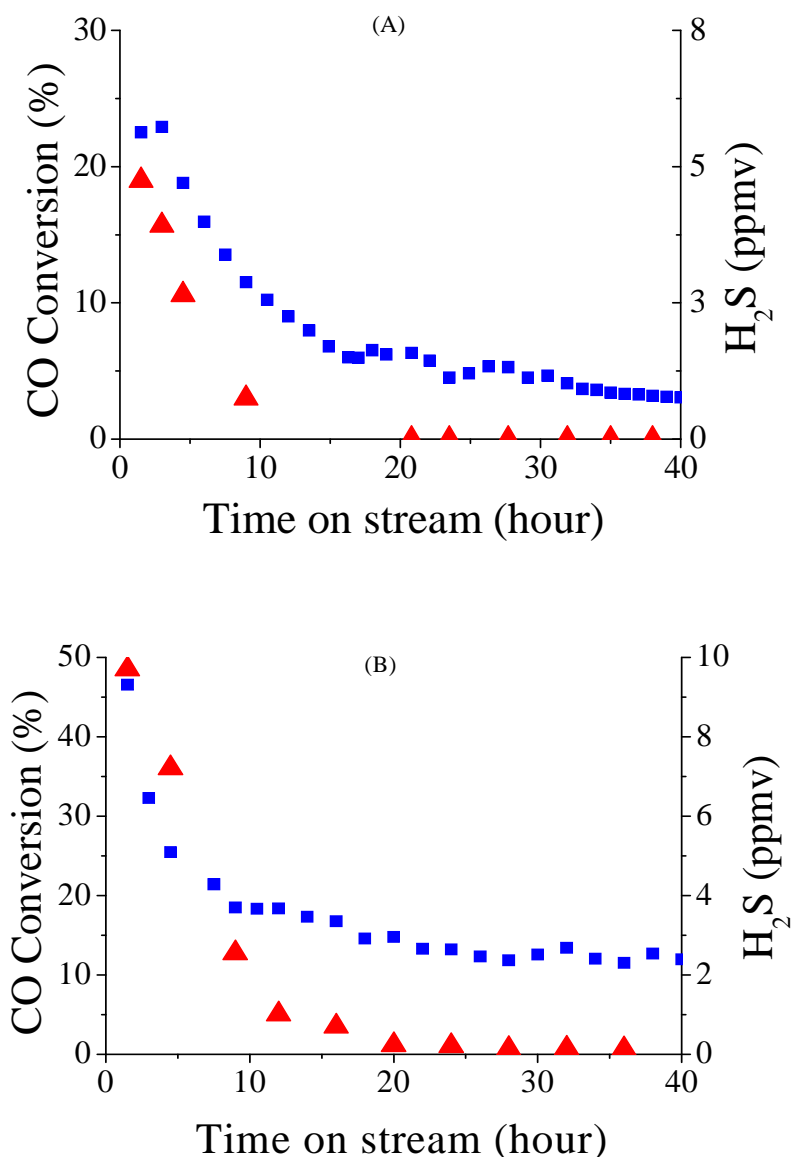


Figure 3-7: CO conversion (square) and H₂S concentration (triangular) in gas feed after passing reactor bed on (A) 25Co and (B) Pt25Co.

Interestingly, after ten hours on stream, the CO conversion was not decreasing as significantly as before, while the catalysts continue absorbing H₂S from the syngas. This suggests that after saturation of the active phase sulphur adsorb on the surface sites which might be not directly involved in the reaction.

IV Characterization of spent catalysts

IV-1 XRD on spent catalysts

The 25%Co/Al₂O₃ catalyst after catalytic tests in part III_2 was characterized by XRD. The result is presented in Figure 3-8. After the test the catalyst was exposed to air. This suggests that the active phase on catalyst surface may have been partially oxidized.

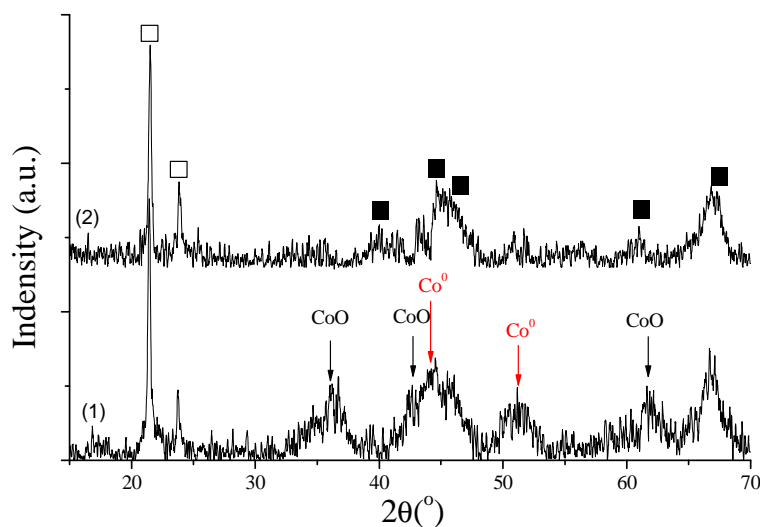


Figure 3-8: XRD pattern of spent 25Co catalysts: (1) with syngas (2) with syngas + H₂S. □SiO₂ (quartz wool) ■Al₂O₃

On both spent 25Co catalysts with and without H₂S, there are two XRD peaks at 20.5° and 23.8°, corresponding to SiO₂ (JCPDF 85-0021, 2θ = 21.5°, 23.7°). This is because of quartz wool that was used in reactors for holding catalysts. When catalysts were taken out, some quartz wool could be mixed with the catalysts. And quartz wool is made of silica that is inert for FT synthesis. The γ-alumina support is detected on XRD pattern for both spent catalysts, too.

For the spent catalysts after being tested without sulphur, cobalt monoxide (CoO) phase (JCPDF 88-2325, 2θ = 36.2°, 42.3°, 61.4°) and metallic cobalt phase (JCPDF 01-1259, 2θ = 44.0°, 51.2°) are observed. This metallic cobalt found on the spent 25Co catalyst is cubic cobalt (Co fcc). This is consistent with previous report [30]. Indeed, cobalt fcc phase is

usually detected after the catalysts reduction at relatively higher temperatures. No additional peaks attributed to cobalt sulphide were detected after catalysts exposure to H₂S containing syngas on both catalysts. This is probably due to very low concentration of H₂S in syngas feed and the fact that the formed Co sulphide was mostly amorphous. In this case, XRD cannot completely explain the effect of H₂S on the observed decrease in the catalytic performance.

IV-2 XPS on spent catalysts

Atomic ratio of different elements (Co, Al, O, C, Si and S) on fresh and spent catalysts is presented in Table 3-6 and Table 3-7.

Table 3-6: XPS atomic ratio on fresh and spent 25Co catalyst

Sample	Al(%)	C(%)	O(%)	Si(%)	Co(%)	S(%)	S/Co
Fresh	34.7	-	64.0	-	1.3	-	-
Spent without H ₂ S	1.4	94.5	3.4	0.4	0.3	-	-
Spent with H ₂ S	5.6	61.7	25.1	5.9	1.5	0.2	0.13

Table 3-7: XPS atomic ratio on fresh and spent Pt25Co catalyst (%)

Sample	Al(%)	C(%)	O(%)	Si(%)	Co(%)	S(%)	S/Co
Fresh	36.1	-	60.8	-	3.1	-	-
Spent without H ₂ S	2.2	86.5	9.5	1.4	0.4	-	-
Spent with H ₂ S	5.7	67.7	21.0	3.8	1.4	0.4	0.28

In spent catalysts a small quantity of Si was usually detected, because of the presence of quartz wool in the reactor for catalytic tests. The carbon concentration detected by XPS is very high on all these spent catalysts. The presence of carbon is probably due to the accumulation of the products of FT synthesis on the catalyst surface. It can be found that C atomic ratio on spent catalysts exposed to H₂S-containing syngas is much higher than for S-free syngas. This can be due to higher hydrocarbon productivity observed on alumina supported cobalt catalysts with sulphur free gas (see Figure 3-6).

The S/Co ratio on the spent catalysts exposed to H₂S is < 1. This suggests that not all cobalt atoms are combined with S atoms. On Pt25Co the S/Co ratio is two times more than on 25Co, which is probably due to higher fraction of active site present on this catalyst.

Co_{2p} and S_{2p} XPS spectra of 25Co and Pt25Co catalysts are presented in Figure 3-9 and Figure 3-10, respectively. The XPS peaks at 780.9 eV and 796.6 eV are characteristic of Co 2p_{1/2} and 2p_{3/2} of the cobalt oxide (Co₃O₄) [27] and those at 803.5 eV and 786.5 eV are characteristics of Co 2p_{1/2} and 2p_{3/2} in cobalt(II), which exists as CoO and cobalt aluminate [28]. In the spent catalysts exposed to H₂S, the XPS Co(II) signal can be also attributed to Co-S compounds.

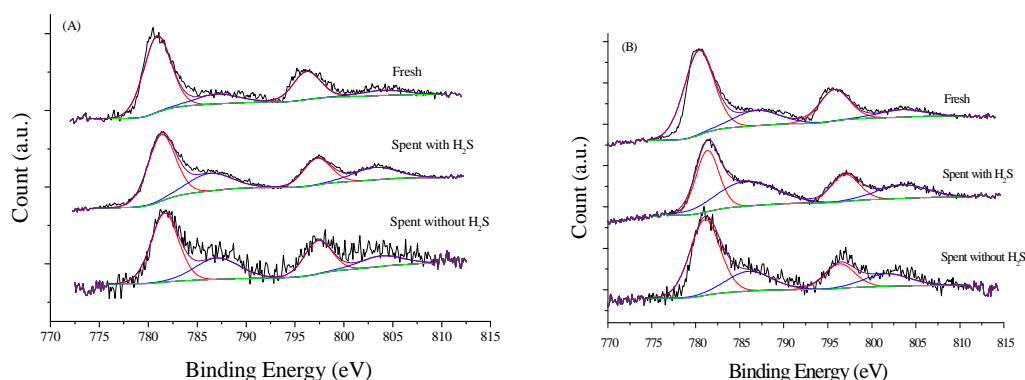


Figure 3-9: XPS Co_{2p} spectra of the fresh and spent catalysts (A) 25Co, (B)Pt25Co

The XPS bonding energy of S_{2p} in spent catalysts (with H₂S) was 168.8 eV (Figure 3-10), which was corresponding to CoSO₄ (BE = 168.6eV, [31]) and/or Al₂(SO₄)₃ (BE = 169.5 eV, [32]). Cobalt in CoSO₄ existed as Co²⁺, which agreed with the Co(II) of the XPS spectra of Co_{2p} on the spent catalysts with H₂S. It is possible that those two sulphates generate from the passivation step. In addition, cobalt sulphate can also form from cobalt sulphide via oxidation by water produced in FT synthesis. We can suggest that the observed catalyst deactivation can be due to formation of both cobalt sulphide and cobalt sulphate. In addition to sulphide, the presence of cobalt sulphate can also irreversibly deactivate cobalt catalysts [2,4,33,34].

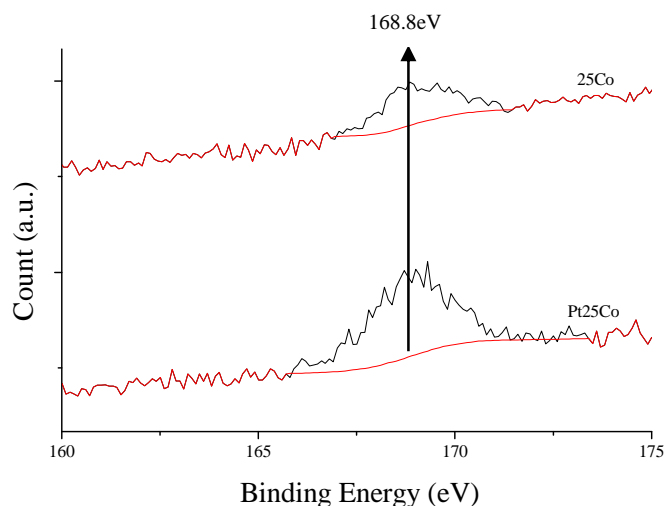


Figure 3-10: XPS S_{2p} spectra of 25Co and Pt25Co catalysts after the test with H₂S

V Discussion and conclusion

V-1 Dispersion and reducibility of Co based catalysts

Co/Al₂O₃ catalysts with different cobalt content and with platinum promoter were characterized and evaluated in FT process. According to the results of XRD and XPS, Co species on alumina supported catalysts after calcination exist as Co₃O₄ because of the decomposition of Co(NO₃)₂ precursor. The Co dispersion decreases with increase in Co content in alumina supported catalysts (see Table 3-3). Meanwhile, more Co loading on catalysts enhanced the cobalt reducibility (see Table 3-4). Previous study suggests that small cobalt particles could often lead an incomplete reduction of cobalt oxide [35]. This hypothesis was confirmed by the TPR and XRD results: on 9%, 10% and 25% Co loaded catalysts. Cobalt particles become larger with the increase in cobalt loading on catalysts, and the reducibility is also increased.

The Pt promotion significantly enhances the catalyst reducibility. On Pt25Co catalyst the reduction temperature of cobalt oxide was lowered and the quantity of reducible cobalt increased. The effect of Pt on cobalt dispersion in the Co/Al₂O₃ catalysts was moderate due to

the small quantity of Pt promoter. The higher reducibility on the Pt25Co catalyst made a better catalytic performance: higher catalytic activity and lower methane selectivity.

V-2 Effect of H₂S on Co/Al₂O₃ and Pt-Co/Al₂O₃

Our results suggest that addition of even small amounts of H₂S to syngas leads to significant catalyst deactivation and inhibits the CO conversion. After 40 hours reaction, on 25Co catalyst the CO conversion decreased from 26% to only 4% and on Pt25Co catalyst it decreased from 57% to 9%. For both Pt promoted and non-promoted catalysts, we found that with H₂S the catalytic activity was 85% lower than the catalytic activity with clean syngas. These results are consistent with previous work of Pansare [4]. Other papers [2,3] also reported similar results. In all, H₂S presented a serious poison effect to activity of Co based catalysts.

The product selectivity was also different between the catalytic tests with and without addition of H₂S. Partial catalysts contamination with sulphur results in lower C₅+ selectivity. This indicates that the sulphur inhibits carbon chain growth on Co catalysts [36].

The alumina supported cobalt catalyst promoted with platinum (Pt25Co) presented higher catalytic activity than 25Co. In addition, the effect of H₂S to hydrocarbon product selectivity is less significant on Pt25Co catalyst than that on 25Co.

The adsorption of sulphur on the catalysts was further confirmed by XPS. The Co-S mixed phases could be detected; indicating the interaction of Co site and H₂S really took place and caused the deactivation of Co based catalysts.

It is interesting to note that the H₂S concentration in syngas is rather low, only 13.3 ppmv. The catalysts were deactivated as soon as they contacted with sulphur, and within a dozen of hours, the catalytic activity had already become significantly low. This indicates that cobalt based catalysts were particularly sensitive to the presence of H₂S and could be easily deactivated.

V-3 Conclusion

The presence of small amounts of H₂S in syngas leads to obvious deactivation of alumina supported Co and PtCo catalysts. The catalytic activity on both catalysts decreased dramatically within 40 hours reaction. The C₅₊ hydrocarbon productivity was significantly reduced with addition of H₂S in syngas feed. The XPS results showed the presence of Co-S species (CoSO₄) in the catalysts exposed to sulphur containing syngas. H₂S could block the active site on cobalt based catalysts and cause the deactivation.

The obtained results indicate importance of development of sulphur resistant FT catalysts. In the following chapters, sulphur tolerant MoS₂ based catalysts will be designed for FT synthesis. We will try to improve its catalytic performance by modifying the support and promotion.

Reference

- [1] G. Huber, S. Iborra, and A. Corma. *Chem. Rev.* 106 (2006) 4044
- [2] C. Bartholomew, R. Bowman. *Appl. Catal.* 15 (1985) 59
- [3] A. Chaffee, I. Campbell, N. Valentine. *Appl. Catal.* 47 (1989) 253
- [4] S. Pansare, J. Allison. *Appl. Catal. A: General.* 387 (2010) 224
- [5] C. Visconti, L. Lietti, P. Forzatti, R. Zennaro. *Appl. Catal. A : General.* 330 (2007) 49
- [6] J. Geerlings, J. Wilson, G. Kramer, H. Kuipers, A. Hoek, H. Huisman. *Appl. Catal. A: General.* 186 (1999) 27
- [7] A. Khodakov, W. Chu, P. Fongarland. *Chem. Rev.* 107 (2007) 1692
- [8] B. Davis. *Ind. Eng. Chem. Res.* 46 (2007) 938
- [9] T. Jermwongratanachai, G. Jacobs, W. Ma, W. Shafer, M. Gnanamani, P. Gao, B. Kitiyanan, B. Davis, J. Klettlinger, C. Yen, D. Cronauer, A. Kropf, C. Marshall. *Appl. Catal. A : General.* 464–465 (2013) 165
- [10] G. Jacobs, J. Chaney, P. Patterson, T. Das, J. Maillot, B. Davis. *J. Synchrotron Rad.* 11 (2004) 414
- [11] R. van Hardeveld, E. Hartog. *Adv. Catal. Rel. Subj.* 22 (1972) 75.
- [12] S. Ho, M. Houalla, D. Hercules. *J. Phys. Chem.* 94 (1990) 6396.
- [13] D. Bukur, X. Lang, J. Rossin, W. Zimmerman, M. Rosynek, E. Yeh, C. Lil. *Ind. Eng. Chem. Res.* 28 (1989) 1130
- [14] D. Schanke, S. Vada, E. Blekkan, A. Hilmen, A. Hoff, A. Holmen, J. Catal. 156 (1995) 85
- [15] E. Iglesia. *Appl. Catal. A : General.* 161 (1997) 59
- [16] P. Van Berge, S. Barradas, J. Van De Loodsrecht, J. Visagie. *Erdoel Erdgas Kohle.* 117 (2001) 138
- [17] M. Ronning, D. Nicholson, A. Holmen. *Catal. Lett.* 72 (2001) 141
- [18] P. Arnoldy, J. Moulijn. *J. Catal.* 93 (1985) 38
- [19] H. Xiong, Y. Zhang, S. Wang, J. Li. *Catal. Comm.* 6 (2005) 507
- [20] G. Jacobs, T. Das, Y. Zhang, J. Li, G. Racoillet, B. Davis. *Appl. Catal. A : General.* 233 (2002) 263
- [21] W. Chu, M. Kakihana. *Alloys Compd.* 287 (1999) 87
- [22] H. Leibold, A. Hornung, H. Seifert. *Powder Technol.* 180 (2008) 265
- [23] N. Tsubaki. *J. Catal.* 199 (2001) 236
- [24] E. Lira, C. López, F. Oropeza, M. Bartolini, J. Alvarez, M. Goldwasser, F. Linares, J. Lamonier, M. Zurita, J. Mol. Catal. A: Chemical 281 (2008) 146
- [25] S. Sun, N. Tsubaki, K. Fujimoto. *Appl. Catal. A: General* 202 (2000) 121
- [26] G. Jacobs, T. Das, P. Patterson, J. Li, L. Sanchez, B. Davis. *Appl. Catal. A: General.* 247 (2003) 335
- [27] T. Chuang, C. Brundle, D. Rice. *Surf. Sci.* 59 (1976) 413
- [28] A. Khassin, T. Yurieva, V. Kaichev, V. Bukhtiyarov, A. Budneva, E. Paukshtis, V. Parmon. *J. Mol. Catal. A: Chemical.* 175 (2001) 189
- [29] J. Gaube, H. Klein. *J. Mol. Catal. A: Chemical* 283 (2008) 60
- [30] M. Gnanamani, G. Jacobs, W. Shafer, B. Davis. *Catal. Today.* 215 (2013) 13
- [31] T. Koranyi, I. Manninger, Z. Paal, O. Marks, J. Gunter. *J. Catal.* 116 (1989) 422
- [32] K. Arata, M. Hino. *Appl. Catalysis* 59 (1990) 197
- [33] N. Koizumi, K. Murai, T. Ozaki, M. Yamada. *Catal. Today.* 89 (2004) 465
- [34] M. Tijmensena, A. Faaija, C. Hamelinck, M. van Hardeveld. *Biomass Bioenergy.* 23 (2002) 129
- [35] S. Sun, K. Fujimoto, Y. Yoneyama, N. Tsubaki. *Fuel.* 81 (2002) 1583
- [36] R. Espinoza, A. Steynberg, B. Jager, A. Vosloo. *Appl. Catal. A: General.* 186 (1999) 13

Chapter Four

Structure and catalytic performance of carbon nanotube supported MoS₂ catalysts promoted with potassium

Summary

<u>I Introduction</u>	109
<u>II Characterization on K MoS₂/CNT catalysts</u>	110
II-1 Textural Characteristics	110
II-2 XRD	111
II-3 XPS	114
II-4 H ₂ -TPR	119
II-5 CO ₂ -TPD	122
<u>III FT catalytic performance on K MoS₂ catalysts supported on CNT</u>	124
III-1 Results of catalytic tests	124
III-2 Catalyst Stability	126
<u>IV Discussion and conclusion</u>	128
IV-1 Discussion	128
IV-2 Conclusion	131
<u>Reference</u>	132

I Introduction

In the previous chapter, we have found that the Co based catalysts can be easily deactivated with presence of low concentration of H₂S. Therefore, in this chapter, we focus on investigation of sulphur tolerant catalysts and our attention is turn toward molybdenum disulphide catalyst.

In the literature, different materials were employed as supports for MoS₂ catalysts. Kim et al [1] and Concha et al [2] have investigated silica and alumina supports in Fischer-Tropsch synthesis for alcohols production. They have found that CO conversion on MoS₂/SiO₂ catalysts was lower than on MoS₂/Al₂O₃ catalyst, however MoS₂/SiO₂ exhibited a better productivity in alcohols [3].

As was recently pointed out by Védrine [4], the structure and properties of the active sites in heterogeneous catalysts are strongly affected by electronic effects. Addition of different promoters may therefore lead to the modification of molybdenum sulphide structure, electronic properties and reactivity of active sites. The selectivity of molybdenum disulphide catalysts can be modified using promotion. Alkali metals are the most used promoters. Previous reports indicate higher selectivity of potassium-modified MoS₂-based catalysts to mixed alcohols at high pressures [5].

Morrill et al [6] have studied hydrotalcite support (HTC, mixed-metal oxide of MgO and Al₂O₃) for K promoted MoS₂ catalysts [7]. They have found that at high reaction pressure (over 100 bar) and reaction temperature of 310°C, the K-MoS₂/HTC catalysts exhibited a higher alcohol selectivity, with a K/Mo molecular ratio of 0.6. They have also reported that at low Mo loading (5%), the catalyst presented a higher C₂₊ alcohol selectivity than at high Mo loaded (15%). It could be due to the readsorption of alcohols and secondary reactions which consumed the alcohols.

Most of publications describe bulk molybdenum sulphide catalysts, while very few reports have addressed the supported systems. The supported catalysts represent several advantages compared to bulk catalyst such as more efficient use of active phase, better chemical, mechanical and thermal stability. In addition, the support can affect chemical and

electronic structures of the active sites and thus the catalytic performance of supported catalysts.

Carbon material is a support which is widely used. Murali et al [8], have found that carbon supported catalysts presented a high alcohols yield and selectivity compared to that of unsupported MoS₂ catalysts. According to the literatures [9,10,11,12], the carbon supports the most used are activated carbon (AC) and carbon nanotube (CNT). CNT supported catalysts generally presents a higher C₂₊ alcohol productivity than AC supported catalysts [5,6,13]. Moreover, CNT supported catalysts are more stable than AC supported catalysts.

This chapter focuses on the structure and performances of a molybdenum sulphide catalyst supported on carbon nanotube support followed by addition of potassium promoter in different amount. The molybdenum content in the catalysts has been fixed at 15 wt%. The potassium has been added with potassium carbonate by mechanical mixing. The catalysts have been synthesized in order to study different alkali/Mo atomic ratio. The catalytic tests were realized under the following conditions: temperature = 360°C, pressure = 20 bar and ratio H₂/CO = 2. The catalysts were characterized with N₂ adsorption (BET surface area), XRD, H₂-TPR, XPS and CO₂-TPD.

II Characterization on K_MoS₂/CNT catalysts

II-1 Textural characteristics

The textural characteristics of carbon nanotube and calcined K_Mo/CNT catalysts determined by BET/BJH method are shown in Table 4-1. The surface area and pore volume typically after addition of molybdenum: from 163.3 m²/g to 68.6 m²/g. and from 0.56 cm³/g to 0.32 cm³/g. The surface area still decreases with addition of K content.

The surface area slightly decreases with the increased in K content while the pore volume remains in the average of 0.22 cm³/g for the promoted catalysts. These results are in agreement with previous reports [14,15]. The decrease in surface area and pore volume is due

to pore plugging and CNT dilution particularly after addition of significant amounts of potassium carbonate.

Table 4-1: Textural proprieties of CNT, calcined Mo/CNT and potassium promoted Mo/CNT catalysts

Samples	BET surface area (m ² /g)	Pore volume (cm ³ /g)	Pore diameter (nm)
CNT	163.3	0.56	17.2
15M/CNT	68.6	0.32	16.2
1.5K_15M/CNT	49.4	0.20	17.6
3K_15M/CNT	45.9	0.21	15.3
6K_15M/CNT	43.5	0.18	15.7
9K_15M/CNT	42.7	0.26	17.6
15K_15M/CNT	40.7	0.24	18.4

II-2 XRD

The **CNT support and the calcined K₂MoS₄/CNT** catalysts were characterised by XRD. The patterns are shown in Figure 4-1. The crystallized CNT phase can be detected (JCPDF 075-0621, $2\theta = 26.23^\circ, 42.21^\circ, 44.36^\circ$) with a good crystallinity on all catalysts. However, the intensity of the CNT decreases with the increase in the K loading. This suggests that the basic carbonate promoter could attack the CNT structure.

The MoO₂ phase (JCPDF 032-0671, $2\theta = 26.03^\circ, 37.02^\circ, 37.93^\circ, 53.04^\circ, 53.51^\circ, 53.97^\circ, 60.20^\circ, 66.66^\circ$) was clearly observed in the XRD patterns of all catalysts. The formation of this phase is due to the AMT precursor decomposition to MoO₂ during calcination under N₂ atmosphere [16]. With the increase in K content, the MoO₂ XRD patterns become less intense

and larger. On the 15K15M catalyst the MoO₂ phase is hardly present, indicating a well MoO₂ dispersion.

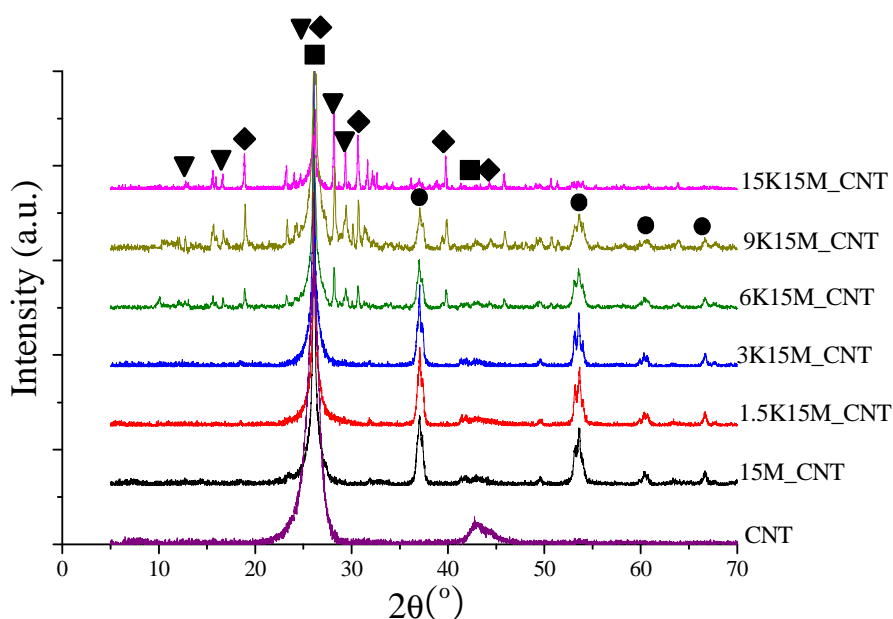


Figure 4-1: XRD patterns of CNT support and calcined CNT supported catalysts. ● MoO₂
 ■ CNT ▼ K₂Mo₄O₆ ◆ K₂MoO₄

The crystallized mixed Mo-K phases are detected at high K loaded (more than 3%): K₂MoO₄ (JCPDF 29-1011, $2\theta = 18.87^\circ, 26.27^\circ, 30.65^\circ, 39.42^\circ, 45.83^\circ$) and K₂Mo₄O₆ (JCPDF 87-0730, $2\theta = 13.08^\circ, 17.07^\circ, 25.49^\circ, 27.47^\circ, 30.15^\circ$).

The K₂CO₃ phase (JCPDF 87-0730, $2\theta = 12.98^\circ, 29.19^\circ, 37.54^\circ, 46.32^\circ$), due to the decomposition of the precursor during the calcination, is also visible on XRD pattern of the 6K_15M/CNT, 9K_15M/CNT and 15K_15M/CNT catalysts.

The XRD patterns of sulphided CNT supported MoS₂ based catalysts are presented in Figure 4-2. The CNT crystalline phase can be observed on all catalysts, but the intensity of the phase decreases with the increase in potassium, as seen previously for the calcined catalysts.

The MoS₂ phase (JCPDF 89-3040, $2\theta = 14.38^\circ, 32.68^\circ, 39.60^\circ, 49.79^\circ, 58.34^\circ, 60.15^\circ$) has been detected on all catalysts, with and without K promotion. The intensity of this phase is low and the peak is large, indicating a high dispersion of small MoS₂ particles size on the CNT.

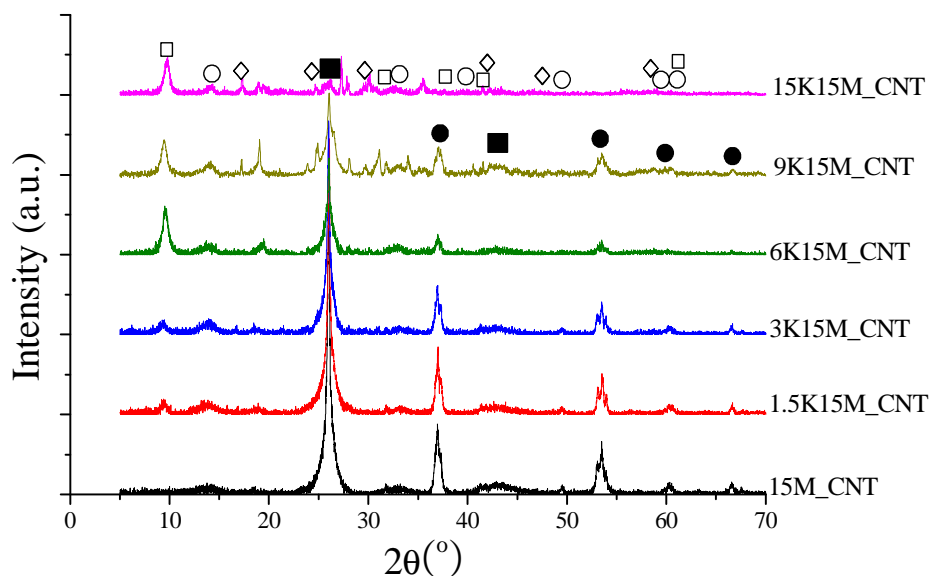


Figure 4-2: XRD patterns of sulphided CNT supported catalysts. ◯ MoS₂ ◻ KMoS₂ ◊ K₂MoS₄ ● MoO₂ ■ CNT

However, MoO₂ phase is still presents on main of the catalysts except for 15K_15M/CNT. The intensity of this phase continues decreasing with the increase in K content. This indicates that Mo oxide had not been completely sulphided and seems to be well stabilized on the CNT support. Moreover, the intensity of this phase decreases, the peak becomes larger as the K content increases, indicating a better dispersion of this MoO₂ phase along with K addition.

Mixed sulphided Mo-K species have been detected on all of the K promoted catalysts:

- KMoS₂ phase (JCPDF 18-1064, $2\theta = 9.66^\circ, 32.41^\circ, 36.13^\circ, 40.61^\circ, 60.46^\circ$);
- K₂MoS₄ (JCPDF 19-1001, $2\theta = 17.55^\circ, 24.23^\circ, 29.36^\circ, 41.19^\circ, 47.05^\circ, 58.40^\circ$) on the catalysts at higher K content: 9K_15M/CNT and 15K_15M/CNT.

Additionally, sulphided potassium phases have been observed on all catalysts:

- K₂S phase (JCPDF 65-3001, $2\theta = 34.21^\circ, 49.16^\circ, 61.26^\circ$);
- K₂S₃ (JCPDF 31-1095, $2\theta = 28.28^\circ, 30.02^\circ, 32.70^\circ$) and K₂S₅ (JCPDF 30-0993, $2\theta = 30.80^\circ, 31.56^\circ, 34.16^\circ$) on the catalysts at higher K content, 9K_15M/CNT and 15K_15M/CNT.

Those results indicate that the mixed oxide Mo-K phases can be sulphided as well as the potassium oxide phases.

The XRD pattern of both calcined and sulphided catalysts showed that with the increase in potassium content, the crystallinity of CNT decreases. The dispersion of molybdenum oxide also increases with higher potassium loading. The presence of MoO₂ on sulphided catalysts demonstrated the uncompleted sulphidation of CNT promoted catalysts. However, this phase is less important as the content of potassium increases. At higher potassium content, the fraction of the MoO₂ phase become less important, indicating the potassium could improve the sulphidation of Mo oxides. The presence of K-Mo mixed oxides and sulphides indicates chemical interaction between potassium and molybdenum.

At higher K content, the interactions between Mo and K are more important, leading to mixed phases which are easily sulphided.

II-3 XPS

The XPS surface element composition of the sulphided K₂MoS₄/CNT catalysts is given in Table 4-2. Different elements (C, O, S, K, Al, Mo) were observed on the catalyst surface, and their ratio varied as a function of the K precursor percentage.

For all catalysts, the carbon percentage is very high (presence of carbon nanotubes in the surface and subsurface layers) while the Mo percentage is quite low, indicating that Mo was not well dispersed on CNT surface.

On the 15M_CNT catalyst, the S/Mo ratio is 1.5, which is less than the stoichiometric ratio of MoS₂ phase. This result demonstrates that the sulphidation on Mo/CNT catalyst was not complete. This result is consistent with the XRD observations. However, for the K promoted Mo/CNT catalysts, this S/Mo ratio is higher than the stoichiometric ratio of MoS₂ phase. This could be due to the presence of sulphided potassium and mixed Mo-K sulphided phases on the catalyst surface (as seen in XRD). So, the percentage of sulphur on the surface is not only related to Mo, which influence and increase the S/Mo ratio. The ratio of S/(Mo+K) was also calculated (Table 4-2). This ratio for the K promoted catalysts is lower than for the

unpromoted catalyst. This indicates that compared with Mo, the sulphidation of K consumed less sulphur, and the extent of sulphidation of K and Mo on K-MoS₂/CNT catalysts could be independent on the potassium content.

For all promoted catalysts, the XPS K/Mo ratio is much lower than the atomic bulk ratio. This ratio remains relatively stable (2.15±0.25 %) although the increase in K content. However, it can be observed that the relative percentage of Mo and K increases on the CNT surface while the carbon percentage decreases. This suggests that the more basic carbonate promoter could attack the CNT support and the dispersion of K and Mo is better on 15K_15M/CNT catalyst. This is consistent with the XRD observations: the crystallinity of the CNT was particularly low for this catalyst and the presence of mixed Mo-K-S phases were easily observable.

Andersen et al [17] studied the interaction of potassium and molybdenum sulphides using Density Functional Theory and found high mobility of K on the MoS₂ catalyst. At a low content of potassium, the potassium injected most of its 4s electron charge into the MoS₂, and K is preferably present on catalyst surface. But with the increase in K content, potassium atoms tend to form an atoms chain over the interstitial of MoS₂ molecules. That could be a reason why on the 15K_15M/CNT catalyst, with high potassium content, the K/Mo ratio on catalyst surface becomes lower at higher potassium content.

Table 4-2: XPS surface atomic ratio in sulphided K_MoS₂/CNT catalysts

K%	XPS Atomic Ratio (%)					S/Mo ratio	K/Mo ratio	S/(Mo+K) ratio
	C	O	S	K	Mo			
0%	77.7	13.9	5.1	0	3.3	1.5	0	1.5
1.5%	80.8	10.9	4.2	2.7	1.4	3.0	1.9	1.0
3%	77.9	12.5	4.3	3.8	1.5	2.8	2.4	0.8
6%	80.8	10.3	4.1	3.4	1.4	2.9	2.4	0.8
15%	68.5	11.8	9.3	6.8	3.5	2.6	1.9	0.9

The Mo3d and S2p XPS spectra of the K_MoS₂/CNT catalysts are shown in Figure 4-3 A and B. In the catalysts, three-peak envelop of the Mo 3d signal is observed (Figure 4-3 A). It can be deconvoluted in three separate overlapping doublets. This suggests that molybdenum is in three different Mo oxidation states: Mo⁴⁺, Mo⁵⁺ and Mo⁶⁺. Binding energy at 228.9 eV

and 232.1 eV should correspond to Mo 3d_{5/2} and 3d_{3/2} of Mo⁴⁺ [18]. On XRD pattern (Figure 4-2), we have observed that both MoO₂ and MoS₂ phases existed on sulphided MoS₂_CNT catalysts. In these two phases, molybdenum is presented in the oxidation state of +4 (Mo⁴⁺). The binding energy of the MoS₂ phase is generally at 228.9 eV and 232.1 eV and the binding energy of the MoO₂ phase is generally at 229.3 eV and 232.4 eV [19]. Those two species are close in binding energy and are difficult to differentiate and deconvolute. In our case, we can observe that the XPS signal corresponds mainly to MoS₂ phase.

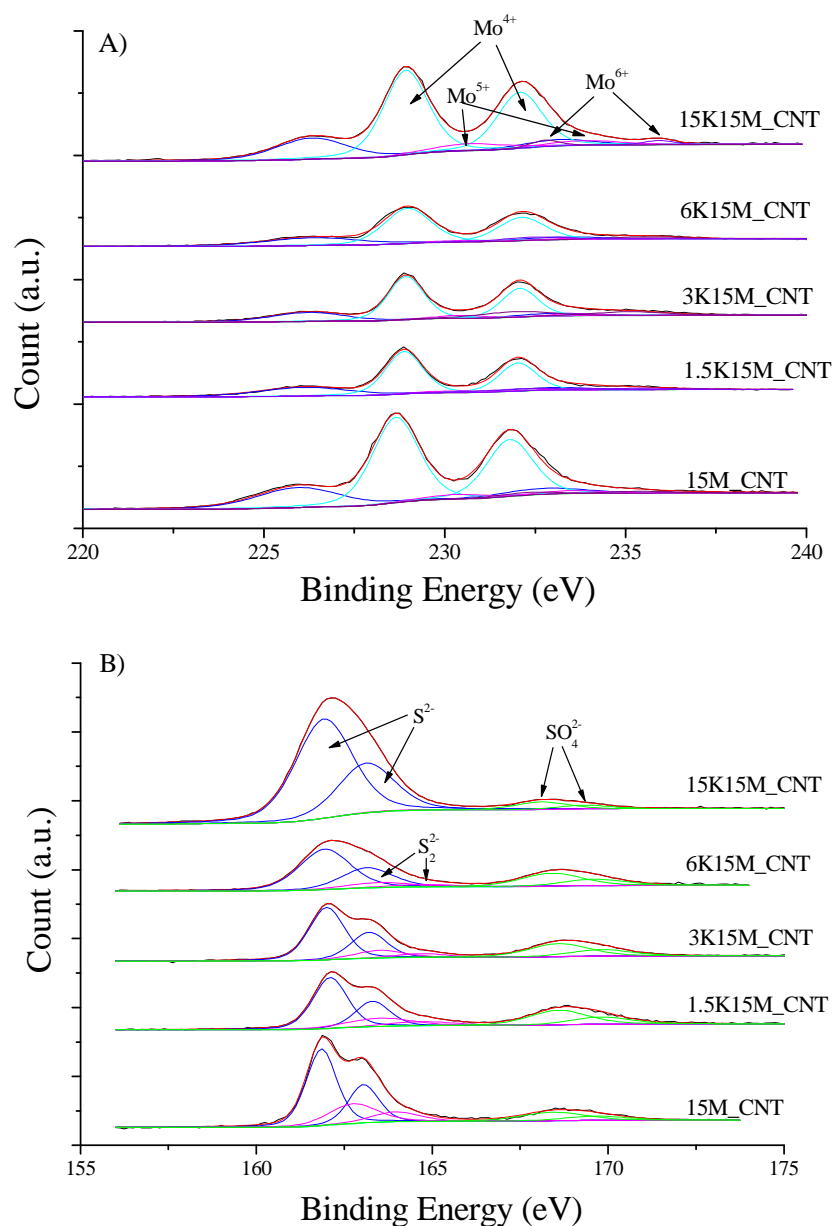


Figure 4-3: XPS spectra of peak decomposition of Mo3d (A) and S2p (B)

Binding energy at 230.6 eV and 233.7 eV should correspond to Mo⁵⁺ specie [20], while Mo⁶⁺ specie was detected with binding energy at 232.8 eV and 235.9 eV [21]. A previous study in the literature [20] specified that Mo⁵⁺ specie is due to the formation of Mo oxy-sulphides such as the MoO₂S₂ and MoOS₂ phase. The Mo⁶⁺ specie could be related to Mo oxides [15,16]. It was believed that Mo⁵⁺ and Mo⁶⁺ specie could come from:

- i) passivation step of catalysts after sulphidation;
- ii) uncompleted sulphidation of catalysts [22].

But in XRD pattern of sulphided catalysts (see Figure 4-2), we noticed the presence of K-Mo mixed sulphides phases such as K₂MoS₄, with Mo oxidation state of (+6). This indicates that Mo⁶⁺ species could be due to the formation of K-Mo mixed sulphides phases.

On the figure 4-3 A, the peak at binding energy of 226.2 eV, correspond to the contribution of S 2s spectra [23].

The peak decomposition of S2p XPS spectra is illustrated in Figure 4-3(B). Three different S species could be observed. The XPS peaks with the binding energies of 161.8 eV and 163.0 eV correspond to S2p_{3/2} and S2p_{1/2} of sulphide ions (S²⁻) [24], which might be present in potassium sulphides and/or Mo disulphide [25]. The binding energy around 163.5 eV and 164.7 eV could be possibly accounted by S2p_{3/2} and S2p_{1/2} of poly-sulphide ions (S₂²⁻), which are present in K sulphides such as K₂S₃ and K₂S₅. All those species have been detected by XRD. The S₂²⁻ phase can also be a contribution of atoms in sulphur rich Mo sulphides (MoS_{2+x}) that is believed to have the same proprieties as MoS₂ phase [26]. The S 2p XPS spectra also exhibit others broad peaks at 168.4 eV and 169.6 eV which are due to the presence of sulphates (SO₄²⁻) [27].

Moreover, it could be observed for both Mo 3d and S 2p XPS spectra, a slight shift in higher binding energy (0.3 eV) for the K promoted catalysts counterparts in comparison to the 15M/CNT catalyst. The promoted K_MoS₂/CNT catalysts however did show any noticeable difference in Mo and S binding energies. So the shift of binding energy for the catalysts with promotion should be due to the presence of K. In XPS, the binding energy of some element can be affected by neighboured atoms/groups. The presence of electrophile atoms/groups

results in the decrease in the electron density, in this case, the binding energy of analysed element also becomes higher. In K_MoS₂ catalysts, potassium exists as K⁺ ion. It is known the K⁺ is strong electrophile species, so binding energy of Mo and S could higher in the promoted catalysts.

The results of XPS peak decomposition showing the fractions of different Mo species or S species is presented are presented in Table 4-3.

Table 4-3: XPS Atomic percentage of different kinds of species for Mo and S, on K_Mo/CNT

Catalyst	Mo (%)			S (%)		
	Mo ⁴⁺	Mo ⁵⁺	Mo ⁶⁺	S ²⁻	S ₂ ²⁻	SO ₄ ²⁻
15M_CNT	90.0	6.4	3.6	60.7	24.9	14.3
1.5K15M_CNT	84.6	4.5	10.9	55.5	17.3	27.2
3K15M_CNT	73.9	6.9	19.2	61.5	12.2	26.3
6K15M_CNT	82.6	6.5	10.9	64.6	10.3	25.1
15K15M_CNT	85.2	11.3	3.5	92.9	0.7	6.4

The Mo⁴⁺ concentration is higher in 15M_CNT than in other promoted catalysts. Previous study [28] showed that addition of alkali metal could decrease the Mo⁴⁺ fraction, because of their inhibition effect on sulphidation with presence of potassium. Indeed, with addition of K, the Mo⁴⁺ ratio decreases and the Mo⁶⁺ fraction increased significantly in 1.5K_15M/CNT, 3K_15M/CNT and 6K_15M/CNT. Nevertheless, the 15K15M_CNT catalyst exhibits a drop in Mo⁶⁺ species for the benefit of a significant increase in Mo⁵⁺ species, higher than for the other catalysts.

For all catalysts, it is observed that the percentage of S²⁻ and S₂²⁻ is much important than the one of SO₄²⁻. It is noticeable that on the non-promoted MoS₂/CNT catalyst, the concentration of poly-sulphides (S₂²⁻) is higher than on K promoted MoS₂/CNT catalysts. With addition of K, the percentage decrease for 1.5K_15M/CNT, 3K_15M/CNT and 6K_15M/CNT catalysts. The S₂²⁻ phase should correspond to the Mo oxy-sulphides (MoO_xS_y) and poly-sulphides of alkali metal (such as K₂S₃). The sulphidation leads to more sulphide species on the surface than to polysulphide with the increase in K content. As explained previously, the SO₄²⁻ could come from the passivation step. On S²⁻ fraction becomes rather important and S₂²⁻ and SO₄²⁻ fractions rather low in the 15K_15M/CNT catalyst compared with

other CNT supported catalysts, and the percentage of S₂²⁻ and SO₄²⁻ are quite low. The oxidation is less important for this catalyst counterpart.

II-4 H₂-TPR

The H₂-TPR results for CNT supported MoS₂ catalysts with different potassium contents are shown in Figure 4-4. Three groups of peaks can be detected at different temperatures:

- Area 1 between 250 and 450°C;
- Area2 between 575°C and 750°C;
- Area3 between 750°C and 950°C.

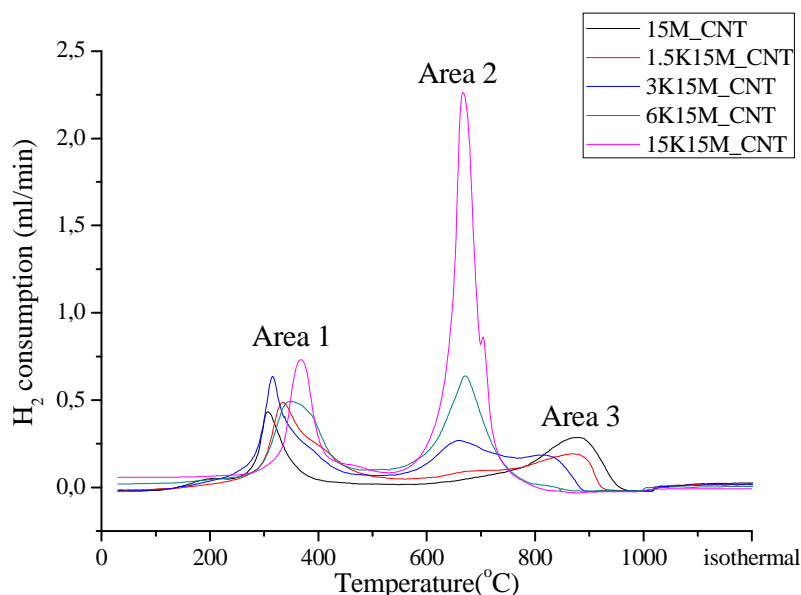


Figure 4-4: H₂-TPR on sulphided K_MoS₂/CNT catalysts

In agreement with Toulhouat et al [29], the low temperature H₂ reduction peaks in the range of 200°C – 430°C could be related to the hydrogenation of extra sulphur atoms (chemisorbed H₂S or SH groups) or sulphur atoms that are weakly bonded to the catalyst surface. Xiao et al [30] suggested that those species are adsorbed on low coordinated edge/corner sites of Mo sulphides. The edge/corner sites of Mo sulphides may contain active sites for CO hydrogenation. In the presence of hydrogen, those sulphur species could be

easily removed below 450°C. During catalytic tests at 360°C, the chemisorbed sulphur species could be partly removed with the release of these surface sites. Ramachandran et al [31] and Collins et al [32] also observed those low temperature peaks for Ni promoted MoS₂/Al₂O₃ catalysts. They assigned those species of hydrogen consumption at low temperature to species for the formation of hydrocarbons from syngas. They suggested however that these sites do not interfere into alcohol synthesis.

The medium temperature reduction peak (area 2) could be related to the hydrogenation of molybdenum/potassium mixed sulphides (K-Mo-S phases). Note that this peak is absent in the TPR profile of the non-promoted CNT supported molybdenum (15M_CNT) catalyst which does not contain potassium phases. Note that the area of this peak significantly increases with the increase in K loading. It can be suggested that peak 2 is strongly related with sulphided potassium phases. These species could be K-Mo-S and possibly potassium poly-sulphides ions, such as K₂S₃ and K₂S₅ which were detected in XRD pattern (see Figure 4-2). In addition, the sulphur atoms located at the edges or basal planes of molybdenum sulphide crystallites could also contribute to the hydrogen consumption in the temperature range of 575°C - 750°C, as reported by Toulhouat et al [29].

The third peak (750°C – 950°C) could be assigned to the reduction of MoO₂ phases to metallic Mo. The MoO₂ phase in the sulphided catalysts has been observed in the XRD patterns (Figure 4-2). Previously Brito et al [33] reported for unsupported MoO₃ catalysts, that MoO₃ can be reduced to MoO₂ at around 500°C and MoO₂ can be reduced to Mo at around 800°C. Lai et al [34] reported for active carbon supported catalysts that MoO₂ can be reduced to the metallic phase at 720-830°C.

Moreover, Mangnus et al [35] reported that the reduction of crystallized Mo sulphide requires the temperature higher than 1050°C. This suggested therefore that the H₂-TPR profiles do not show any peaks which might correspond to the reduction of MoS₂ to Mo metal.

The H₂ consumptions measured from the TPR profiles are given in Table 4-4. The results were calculated from TPR peaks decomposition and integration. For the 15M/CNT catalyst, Peak 1 showed rather low hydrogen consumption while no hydrogen was consumed in the

Area 2. Peaks 3 which were attributed to MoO₂ reduction showed the highest hydrogen consumption of all CNT supported catalysts. This indicates that a high amount of MoO₂ has not been sulphided for this unpromoted catalyst. This conclusion is consistent with the XRD and XPS observations.

Table 4-4: H₂ consumption in TPR experiments

Sample	H ₂ consumption (mmol _{Hydrogen} /g _{cata})		
	Peak 1	Peak 2	Peak 3
15M/CNT	1.24	<0.01	1.05
1.5K_15M/CNT	2.65	1.32	0.66
3K_15M/CNT	2.02	1.66	0.38
6K_15M/CNT	2.02	2.21	0.04
15K_15M/CNT	1.69	4.40	<0.01

For the potassium promoted MoS₂/CNT catalysts, the H₂ consumption indicates:

- A higher H₂-consumption in the area 1 (peak 1) than the non-promoted counterparts. Note however that the H₂-consumption is decreasing with the increase in K loading on the catalysts. Potassium addition can cover the MoS₂ surface and then block the adsorption of sulphur.
- A decrease in H₂ consumption for the area 2 (peaks 2) with the increase in K content. This is related to the sulphur reduction of K-S species. As said previously, those species are more present in the catalyst with the increase in potassium percentage.
- A decrease in the area 3 (peak 3) with increase of K content. H₂ consumption is zero for the 15K_15M/CNT catalyst. This indicates that no MoO₂ could be present in this catalyst. This is consistent with XRD results which show a decrease in the MoO₂ concentration with high potassium content.

To resume, the H₂-TPR indicated the presence of several species that could be reduced by hydrogen at different temperatures. The quantity of K-Mo mixed sulphides increases with

the increase in potassium content, while the MoO₂ phase becomes less important at higher potassium loadings. It can be suggested that potassium promotion leads to higher extent of the sulphidation of Mo/CNT catalysts

II-5 CO₂-TPD

The basicity of the catalysts was measured by CO₂-TPD. Figure 4-5 presents the CO₂ desorption curves measured between 30-800°C on catalysts after sulphidation.

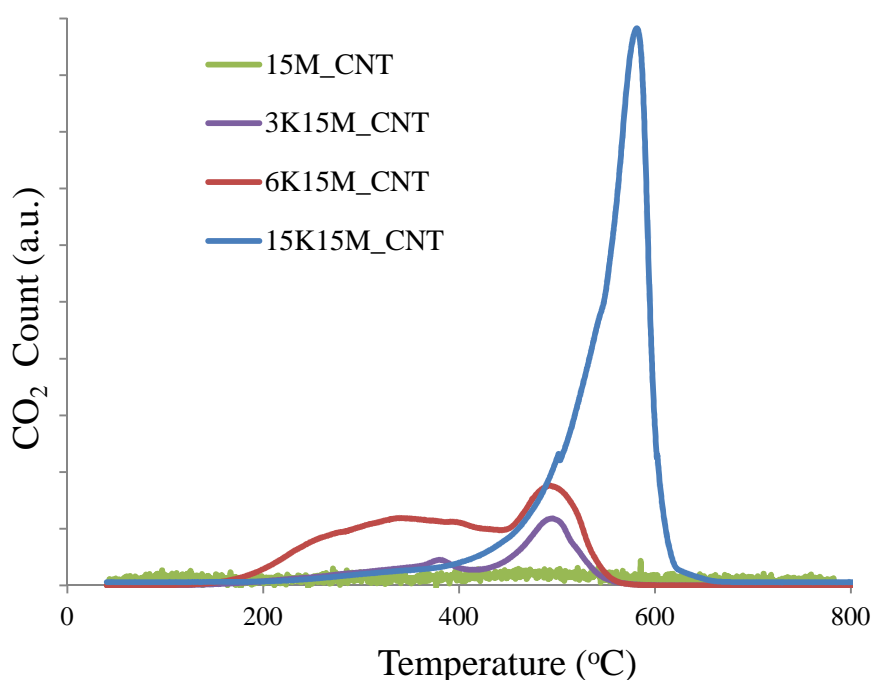


Figure 4-5: CO₂-TPD on sulphided K_MoS₂/CNT catalysts

It is clearly observed that the 15M/CNT catalysts did not show any CO₂ desorption from 30°C to 800°C. This indicates that the unpromoted MoS₂ catalyst does not contain measurable concentration of basic sites.

CO₂ desorption peaks can be detected, however in the presence of potassium. This suggests that potassium addition generates basic sites in the different K_MoS₂/CNT catalysts. The 3K_15M/CNT catalyst exhibits a small CO₂ desorption peak between 200°C and 410°C,

and another CO₂ peak between 420°C and 560°C. These two peaks can be attributed to weaker and stronger catalyst basic sites, respectively.

Similar peaks were also observed in the 6K_15M/CNT catalyst. However, the first CO₂ desorption peak was much broader, from 180°C to 450°C. The second CO₂ desorption peak is observed from 450°C to 560°C.

For the 15K_15M/CNT catalyst, no noticeable CO₂ desorption peak at lower temperature could be observed. However, the CO₂ desorption peak at higher temperature is more intense than for the other catalysts.

Table 4-5 displays the quantity of desorbed CO₂ at different temperature range. Our results suggest that the unpromoted MoS₂/CNT catalysts do not have basicity.

The quantity of desorbed CO₂ was slightly higher for the 6K_15M/CNT at low temperature than for the 3K_15M/CNT and 15K_15M/CNT catalysts. At high temperature, the quantity of desorbed CO₂ is much more important for 15K_15M/CNT catalyst than for the other catalysts.

Table 4-5: CO₂ desorption of CO₂-TPD on sulphided K-MoS₂/CNT catalyst

Catalyst	CO ₂ desorption (μmol/g _{catalyst})		
	Low temperature	High temperature	Total
15M/CNT	0.0	0.0	0.0
3K_15M/CNT	0.03	0.05	0.08
6K_15M/CNT	0.14	0.08	0.22
15K_15M/CNT	0.03	0.42	0.45

In summary, it was found that the basicity of CNT supported molybdenum sulphide catalysts depends on K content in the catalysts. Higher potassium loading results in higher concentration of basic sites. Higher potassium content also favours the appearance of strong and very strong basic sites.

III FT catalytic performance on K_MoS₂ catalysts supported on CNT

III-1 Results of catalytic tests

The catalysts were tested in a fixed bed tubular reactor. The sulphidation step was realized ex-situ before the catalytic tests. The reaction was conducted in the presence of 13.3 ppmv of H₂S in the syngas in order to keep the stability of MoS₂ based catalysts [36]. The reaction pressure was fixed at 20 bar in order to shift the reaction selectivity toward olefins [37]. Methane, olefins, paraffins, methanol, ethanol and carbon dioxide were the main products detected from the carbon monoxide hydrogenation on alumina supported molybdenum catalysts. The CO conversion and products selectivities at the steady state which were obtained at iso-GHSV for the non-promoted and potassium promoted CNT supported molybdenum sulphided catalysts are shown in Table 4-6.

Table 4-6: CO conversion and products selectivity on K_MoS₂/CNT catalysts (T = 360°C, P = 20 bar, GHSV = 1050 ml.g⁻¹.h⁻¹, H₂/CO = 2)

Catalyst	CO conversion (%)	Hydrocarbon selectivity (%)				Alcohol selectivity (%)		CO ₂ Selectivity (%)
		C1	C2-4 Olefin	C2-4 Paraffin	C5+	CH ₃ OH	C2+	
15M/CNT	37.4	24.7	0.1	27.3	0.0	0.0	0.0	47.9
1.5K_15M/CNT	19.1	22.9	2.5	26.7	1.6	7.0	1.6	38.1
3K_15M/CNT	17.7	20.7	9.6	11.9	6.3	10.1	3.7	37.5
6K_15M/CNT	16.3	17.4	5.4	8.4	10.8	11.9	5.6	40.2
9K_15M/CNT	16.8	20.4	3.7	12.2	18.2	7.6	6.7	31.3
15K_15M/CNT	9.3	17.1	2.9	1.8	34.0	14.3	8.6	21.4

For the unpromoted 15M/CNT catalyst, the carbon monoxide is hydrogenated to produce mainly methane, C₂-C₄ paraffins and carbon dioxide. The catalyst showed particularly a very high selectivity to methane and CO₂. Without K promotion, MoS₂ is not active for production of alcohols, olefins or heavy products (C₅₊ hydrocarbon). Liu et al [38] reported on

non-promoted MoS₂ catalysts, that the major products of carbon monoxide hydrogenation was methane and CO₂ with very low concentration of ethane (selectivity <1%). Wang et al [36] reported similar results. Note that the only active phase in the sulphided Mo catalysts was MoS₂.

In our work, note however that the selectivity to light paraffins can attain 27.3%. This can be possibly attributed to the presence of both MoS₂ and MoO₂ in the 15M/CNT catalyst (seen in XRD and H₂-TPR results). Tatumi et al [39] suggested that during CO hydrogenation, MoO₂ could be partly reduced to MoO_{2-x} phase, on which CO was non-dissociatively absorbed. MoO_{2-x} was considered to contain active sites for the C-C chemical bonds formation. This could be the reason why the selectivity to lighter paraffins was much higher on CNT supported catalysts compared to unsupported MoS₂.

The catalytic performance of the CNT supported catalysts is strongly affected by potassium promotion. At GHSV = 1050 ml.g_{cata}⁻¹.h⁻¹, the CO conversion decreases from 19.1 % to 9.3 % with the increase in K/Mo molar ratio from 0.2 to 2.5.

Addition of potassium leads to better selectivity to olefins and alcohols. For light olefins, the best yield was obtained on 3K_15M/CNT catalyst (K/Mo = 0.5), while the highest productivity of C₂₊ alcohol was measured on 9K_15M/CNT catalyst (K/Mo = 1.5).

The decrease in the CH₄ and CO₂ selectivities was also affected by the potassium addition, while the selectivity to long-chain hydrocarbons was significantly enhanced. This result is consistent to the previous work of Surisetty et al [9]. They reported that on K-MoS₂/CNT catalysts, for the same content of Mo, the increase in addition of potassium leads to a decrease in selectivity of CH₄ and CO₂.

The Table 4-6 resumes the evolution of the different products production rate in function of the different K/Mo atomic ratio. The C₂-C₄ olefin and alcohol productivities attain their maximum at intermediate potassium/molybdenum atomic ratio (between 0.5 and 1.5).

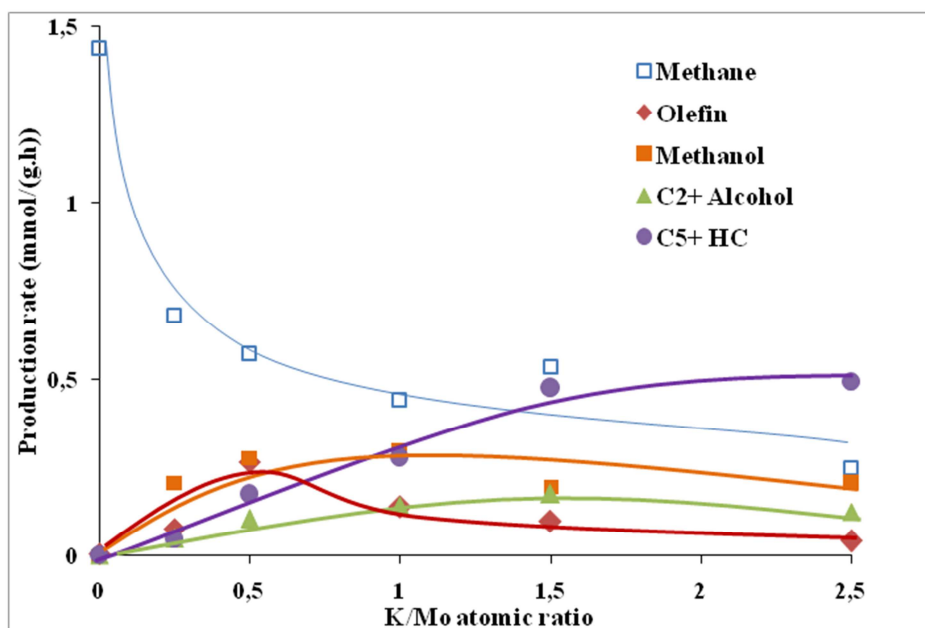


Figure 4-6: Reaction rate of the several products on CNT supported catalysts

Extremely high potassium contents (15K_15M/CNT) do not contribute to increase CO conversion and are not in the favour of olefin and alcohol yields. The only positive effect is the decrease of two undesirable products: methane and carbon dioxide.

III-2 Catalyst Stability

The catalytic performance of the K_MoS₂/CNT catalysts was tested as a function of time-on-stream in order to evaluate the catalyst stability. Figure 4-7 shows the CO conversion and selectivity of light olefin and methane at P = 20 bar, T = 360°C, GHSV = 1050 ml.g⁻¹h⁻¹.

The 15M/CNT catalyst exhibits a decrease in CO conversion within the first 20 h, then stabilization around 37.4%. The methane selectivity reaches a steady state earlier, within the first 10 h, and remains stable with time on stream. These results are consistent with previous work of Liu et al [38] who observed that on non-promoted catalysts the CO conversion is continuously decreasing in 100 h catalytic test but methane selectivity could keep stable. They suggested that the drop in the reaction rate could be due to the aggregation of MoS₂ active phase during FT synthesis. Slightly better stability was observed in our work on MoS₂/CNT

catalyst which is probably due to the use of a lower reaction temperature (360°C) compared to Liu et al who tested the catalysts at 550°C.

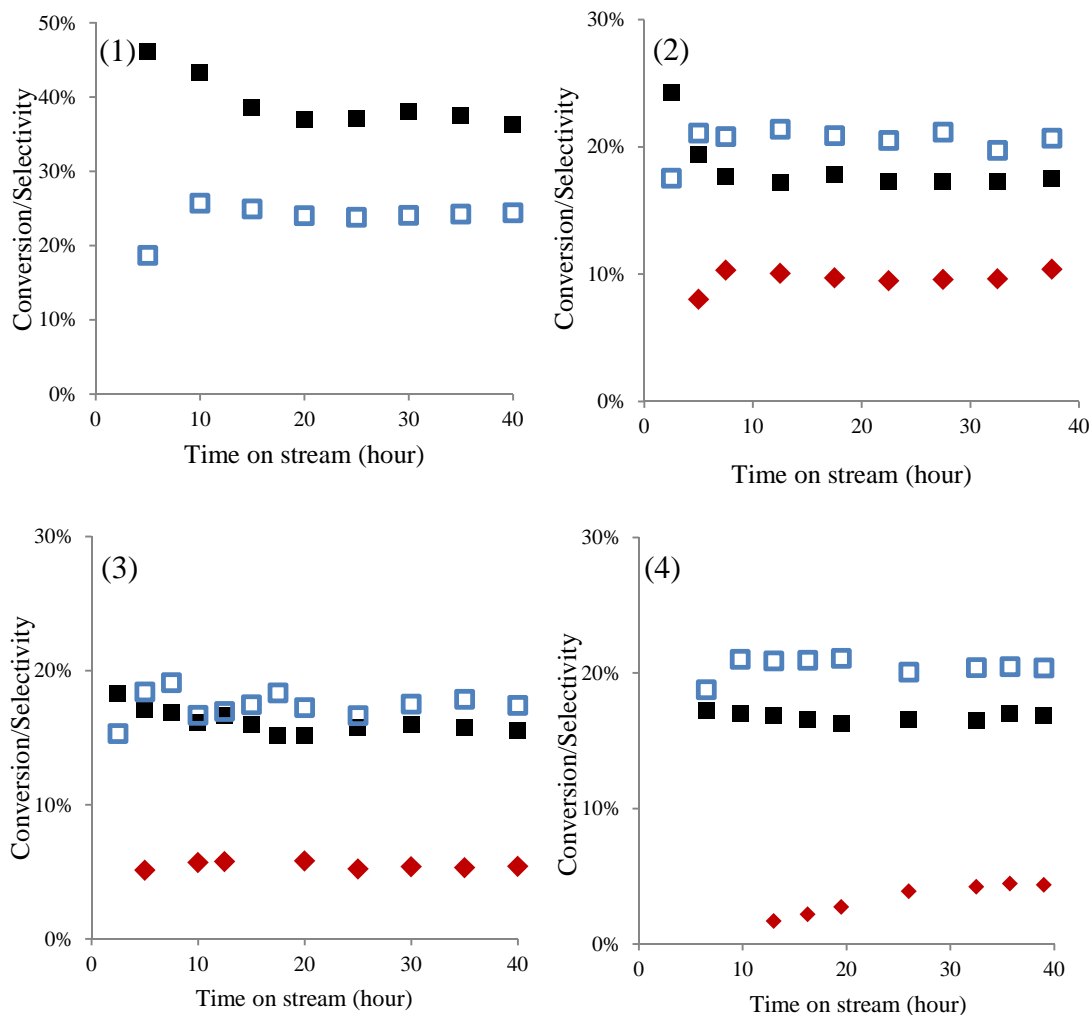


Figure 4-7: CO conversion (■) and selectivity of CH₄ (□) and C₂-C₄ olefin (◆) on (1)15M/CNT, (2) 3K_15M/CNT, (3) 6K_15M/CNT and (4) 9K_15M/CNT catalysts. Reaction condition: T = 360°C, P = 20 bar, GHSV = 1050 ml.g⁻¹.h⁻¹, H₂/CO = 2

The K promoted catalysts were relatively stable under the reaction conditions. The steady states were obtained within the first 5-10 h for CO conversion and CH₄ selectivity. It seems that the addition of promoters leads to a better catalyst stability, in comparison to the unpromoted counterpart.

IV Discussion and conclusion

IV-1 Discussion

In this chapter, carbon nanotube supported Mo disulphide catalysts were characterized with various techniques and tested in carbon monoxide hydrogenation. Our results show that addition of different amounts of K significantly influences the catalyst structure and catalytic performance in carbon monoxide hydrogenation.

The XRD patterns showed that the peak intensity of CNT decreased significantly with potassium content, indicating the CNT crystallinity decreased. The surface area of the catalysts also decreased significantly with potassium content.

In the sulphided K₂MoS₄/CNT catalysts, K-Mo mixed phases were detected in XRD patterns. With lower K loading (K% = 1.5%, 3%, 6%) only KMoS₂ phase was observed while both KMoS₂ and K₂MoS₄ phases could be detected in higher K loaded catalysts (K% = 9%, 15%). These phases could be reduced by hydrogen and exhibit peaks in the H₂-TPR profiles (Peak 2 in Figure 4-4).

The presence of these mixed K-Mo phase coincided with higher selectivity to heavy products (C₂₊ alcohol and C₅₊ hydrocarbon). The C₅₊ HC selectivity was significantly higher on 9K_15M/CNT and 15K_15M/CNT catalysts, compared to other catalysts. Several previous reports [28,40,41] suggest that K-Mo-S phases possess the active sites for higher alcohol synthesis. Li et al [42] found the CO was non-dissociatively adsorbed on K-Mo sulphides, and then C-C chemical bonds were formed. This indicates the K-Mo sulphides could be the active sites for long-carbon chain products, as higher alcohols and heavier hydrocarbons. This hypothesis is consistent with our work.

We can speculate that K₂MoS₄ phase which was observed only in 9K_15M/CNT and 15K_15M/CNT can be favorable for production of heavy products than KMoS₂ phase.

The K₂CO₃ precursors (before calcination) as well as potassium sulphides (after sulphidation) are also present in the catalysts with higher potassium content (6K_15M/CNT,

9K_15M/CNT and 15K_15M/CNT). Woo et al [22] reported the K₂CO₃ would be sulphided to K₂SO₄ during H₂S treatment. This potassium phase with no interaction with Mo is observed in the catalysts at high potassium content.

Mo⁵⁺ and Mo⁶⁺ species were detected in XPS Mo3d spectra of sulphided catalysts. This could be caused by:

- i) the passivation step,
- ii) the formation of Mo oxy-sulphides such as MoO₂S₂ and MoOS₂,
- iii) the formation of K-Mo mixed sulphides like K₂MoS₄.

XPS also showed the presence of Mo⁴⁺. The presence of these species could be due to both MoO₂ and MoS₂ phases. H₂-TPR results showed that the MoO₂ can be reduced at 750°C and 900°C (Peak 3 in Figure 4-4). The MoO₂ is an active phase for alcohol production and the MoS₂ is an active phase for methane production and hydrogenation reaction.

Different kinds Mo or S species detected and identified by XPS could be relevant to the catalytic performance. Woo et al [22] investigated the relation between the XPS atomic ratio and alcohol production. They reported that higher alcohol selectivity could be attributed to the Mo⁴⁺ species and lower fraction of the SO₄²⁻. Other papers [28,43] have reported similar conclusion. This is also consistent with our results. The ratio of sulphate phase decreases with increase in K content while the C₂₊ selectivity also increases (Figure 4-8).

The concentration of Mo⁴⁺ species was high in the 15K_15M/CNT catalyst while the C₂₊ selectivity also reached a maximum. On the other hand, lower fraction of the Mo⁴⁺ phase should improve the hydrocarbon selectivity. We observed that in the 3K_15M/CNT catalyst, the Mo⁴⁺ ratio was the lowest of all while the C₂-C₄ olefin selectivity was the highest. On the other catalysts, C₂-C₄ olefin production rate could be enhanced with a low ratio of Mo⁴⁺ phases (Figure 4-8). Less MoS₂ (Mo⁴⁺) means the hydrogenating ability should be less important. Colley and al [44] concluded that the catalyst with lower hydrogenating ability can improve the production of light olefin. This can explain why the C₂-C₄ olefin selectivity increased with low ratio of Mo⁴⁺ species.

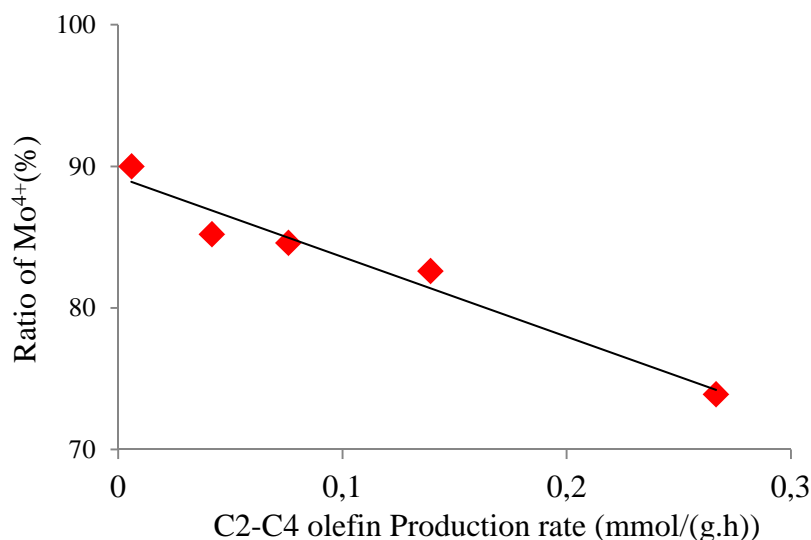


Figure 4-8: Light olefin production rate as a function of Mo⁴⁺ ratio

Potassium promotion also has a strong impact on the catalyst basicity. On K₂MoS₂/CNT catalysts, basicity was enhanced when K content increase. The maximum of light olefin selectivity was presented on the catalyst with moderate catalyst basicity. With increase in basicity the catalytic activity decreased. Hence, the catalyst basicity could be an important parameter which could affect the rate of secondary reactions such as readsorption of olefins or oxygenated products [45,46]. The catalysts with low basicity could inhibit the readsorption of light olefins and improve its selectivity.

For the catalyst with strong basicity, more heavy products were produced. On these catalysts, potassium sulphides (K₂S, K₂S₃, K₂S₅) were detected by XRD. With presence of those species, the strength of CO adsorption on active sites increases [47]. Thus, light olefin should easier react with these absorbed CO and the hydrocarbon with longer carbon chain could be more produced. That is why the potassium at higher content inhibited the C₂-C₄ olefin production.

In this chapter, the maximum of light olefins was obtained on 3K₂15M/CNT catalyst (K/Mo = 0.5) with a CO conversion of 17.7%. The CNT crystallinity decreased with potassium addition. The presence of MoO₂ in the sulphided catalysts suggests the incomplete sulphidation of CNT supported catalysts.

IV-2 Conclusion

The exposure of CNT supported MoS₂ based catalysts to H₂S does not lead to complete sulphidation. Lower extent of sulphidation can be possible one of the reasons responsible for their low activity. In the non-promoted MoS₂/CNT catalyst only methane and ethane were produced. Potassium promotion leads to the production of light olefins. The highest yield of light olefin was observed on the K-MoS₂/CNT catalyst when K/Mo atomic ratio was 0.5. With K/Mo > 0.5, the addition of potassium lowered the light olefin productivity.

The unpromoted catalyst contained MoS₂ molybdenum sulphide. Methane was produced on that phase. K-Mo mixed sulphides were detected in the K-promoted catalysts. These phases probably contain active sites for the synthesis of light olefins, alcohols and heavy hydrocarbons. Addition of potassium increases the basicity of the catalyst. A moderate basicity seems favourable for producing light olefins and alcohols. Potassium sulphides (K₂S₃, K₂S₅) were observed at higher potassium content. These phases lead to higher catalyst basicity which seems to be favourable for higher selectivity to C₅₊ hydrocarbons.

In the following chapter, we are going to study the effect of potassium content on the structure of catalysts and their performance in carbon monoxide hydrogenation on alumina.

Reference

- [1] M. Kim, S. Ha, D. Koh, C. Byun, E. Park. *Catal. Comm.* 35 (2013) 68
- [2] B. Concha, G. Bartholomew, C. Bartholomew. *J. Catal.* 89 (1984) 536
- [3] V. Surisetty, A. Dalai, J. Kozinski. *Appl. Catal. A: General* 404 (2011) 1
- [4] J.C. Védrine, *Appl. Catal. A* 474 (2014) 40-50.
- [5] G.J. Quarderer, K.A. Cochran, European Patent: 0119609B1, 1991
- [6] M. Morrill, N. Thao, H. Shou, R. Davis, D. Barton, D. Ferrari, P. Agrawal, C. Jones, *ACS Catal.* 3 (2013) 1665
- [7] V. Surisetty, A. Dalai, J. Kozinski. *Energy Fuels.* 25 (2011) 580
- [8] D. Murali, B. Concha, G. Bartholomew, C. Bartholomew. *J. Catal.* 89 (1984) 274
- [9] V. Surisetty, A. Tavasoli, A. Dalai. *Appl. Catal. A: General* 365 (2009) 243
- [10] J. Christensen, P. Mortensen, R. Trane, P. Jensen, A. Jensen. *Appl. Catal. A: General* 366 (2009) 29
- [11] Z. Li, Y. Fua, J. Bao, M. Jiang, T. Hu, T. Liu, Y. Xie. *Appl. Catal. A: General* 220 (2001) 21
- [12] V. Surisetty, A. Tavasoli, A. Dalai. *Appl. Catal. A: General* 365 (2009) 243
- [13] V. Surisetty, A. Dalai, J. Kozinski. *Ind. Eng. Chem. Res.* 49 (2010) 6956
- [14] A. Tavasoli, S. Karimi, M. Davari, N. Nasrollahi, T. Nematian. *J. Ind. Eng. Chem.* 20 (2014) 674
- [15] J. Wang, J. Xie, Y. Huang, B. Chen, G. Lin, H. Zhang. *Appl. Catal. A: General.* 468 (2013) 44
- [16] E. Liakakoua, E. Heracleousa, K. Triantafyllidisa, A. Lemonidou. *Appl. Catal. B: Environmental* 165 (2015) 296
- [17] A. Andersen, S. Kathmann, M. Lilga, K. Albrecht, R. Hallen, D. Mei. *J. Phys. Chem. C.* 115 (2011) 9025
- [18] T. Patterson, J. Carver, D. Leyden, D. Hercules. *J. Phys. Chem.* 80 (1976) 1700
- [19] A. Cimino, B. De Angelis. *J. Catal.* 36 (1975) 11
- [20] L. Benois, D. Gonbeau, G. Pfister-Guillouzo, E. Schmidt, G. Meunier, A. Levasseur. *Thin Solid Films.* 258 (1995) 110
- [21] S. Andersson, R. Howe. *J. Phys. Chem.* 93 (1989) 4913
- [22] H. Woo, I. Nam, J. Lee, J. Chung, K. Lee, Y. Kim. *J. Catal.* 138 (1992) 525
- [23] Th. Weber, J. Muijsers, J. van Wolput, C. Verhagen, J. Niemantsverdriet. *J. Phys. Chem.* 1996 (100) 14144
- [24] D. Zingg, L. Makovsky, R. Tischer, F. Brown, D. Hercules. *J. Phys. Chem.* 84 (1980) 2898
- [25] J. Hensley, S. Pylypenko, D. Ruddy. *J. Catal.* 309 (2014) 199
- [26] N. McIntyre, T. Chan, P. Spevack. *Appl. Catal.* 63 (1990) 391
- [27] X. Yu, F. Liu, Z. Wang, Y. Chen. *J. Electron Spectrosc. Relat. Phenom.* 50 (1990) 159
- [28] M. Jiang, G. Bian, Y. Fu, *J. Catal.* 146 (1994) 144
- [29] H. Toulhouat, S. Kasztelan, in: M.J. Phillips, M. Ternan (Eds.), *Proceedings, 9th International Congress on Catalysis, Calgary (vol.1: Chem.)* Institute of Canada, Ottawa, 1988, pp. 152-153
- [30] H. Xiao, D. Lia, W. Li, Y. Sun. *Fuel Proc. Technol.* 91 (2010) 383
- [31] R. Ramachandran, F. Massoth. *Canad. J. Chem. Eng.* 60 (1982) 17
- [32] R. Burch, A. Collins. *Appl. Catal.* 18 (1985) 373.
- [33] J.L. Brito, J. Laine. *J. Catal.* 139 (1993) 540
- [34] W. Lai, L. Pang, J. Zheng, J. Li, Z. Wu, X. Yi, W. Fang, L. Jia. *Fuel Processing Technology.* 110 (2013) 8
- [35] P. Mangnus, A. Riezebos, A. Vanlangeveld, J. Moulijn. *J. Catal.* 151 (1995) 178
- [36] B. Wang, G. Ding, Y. Shang, J. Lv, H. Wang, E. Wang, Z. Li, Xinbin M, S. Qin and Q. Sun. *Appl. Catal. A: General* 431–432 (2012) 144

- [37] H. Galvis, J. Bitter, C. Khare, M. Ruitenbeek, A. Dugulan, K. de Jong. *Science* 335 (2012) 835
- [38] J. Liu, E. Wang, J. Lv, Z. Li, B. Wang, X. Ma, S. Qin, Q. Sun. *Fuel Proce. Technol.* 110 (2013) 249
- [39] A. Muramatsu, T. Tatsumi, H. Tominaga. *J. Phys. Chem.* 96 (1992) 1334
- [40] N. Koizumi, G. Bian, K. Murai, T. Ozaki, M. Yamada. *J. Mol. Catal. A: Chem.* 207 (2004) 173
- [41] S. DeCanio, M. Cataloo, E. DeCanio, D. Storm. *J. Catal.* 119 (1989) 256
- [42] D. Li, C. Yang, W.H. Li, Y.H. Sun, B. Zhong, *Top. Catal.* 32 (2005) 233
- [43] Z. Li, Y. Fu, M. Jiang. *Appl. Catal. A: General* 187 (1999) 187
- [44] S. Colley, R. Copperthwaite, G. Hutchings, G. Foulds, N. Coville. *Appl. Catal. A: General.* 84 (1992) 1
- [45] E. Lowenthal, S. Schwarz, H. Foley. *Catal. Today.* 51 (1999) 187
- [46] G. Bian, Y. Fu, Y. Ma. *Appl. Catal. A: General.* 170 (1998) 255
- [47] H. Arakawa, A. Bell. *Ind. Eng. Chem. Process Des. Dev.* 22 (1983) 97

Chapter Five

Effect of potassium content on $\text{MoS}_2/\text{Al}_2\text{O}_3$ catalysts for FT synthesis

Summary

I Introduction	138
II Characterization of K Promoted MoS₂/Al₂O₃ catalysts	138
II-1 Characterization of calcined catalysts	138
<i>II-1-1 Textural Characteristics</i>	138
<i>II-1-2 XRD</i>	139
<i>II-1-3 LRS</i>	140
<i>II-1-4 TEM</i>	142
II-2 Characterization on sulphided catalysts	144
<i>II-2-1 XRD</i>	144
<i>II-2-2 LRS</i>	146
<i>II-2-3 XPS</i>	147
<i>II-2-4 H₂-TPR</i>	151
<i>II-2-5 CO₂-TPD</i>	152
<i>II-2-6 TEM</i>	154
III Catalytic tests on K_MoS₂/Al₂O₃ catalysts	155
IV Effect of reaction condition on K_MoS₂/Al₂O₃ catalysts	158
IV-1 Effect of GHSV	158
IV-2 Effect of pressure	160
IV-3 Effect of syngas ratio (H₂/CO)	162
V Discussion and Conclusion	164
Reference	170

I Introduction

In the previous chapter, we have studied K₂MoS₄/CNT catalysts. Different amounts of K significantly influence the catalyst structure and catalytic performance in carbon monoxide hydrogenation. We concluded that K₂MoS₄ phase can be more favorable for production of alcohols, olefins and long-chain hydrocarbons.

The present chapter addresses design of supported molybdenum sulphide catalysts for synthesis of olefins from syngas. Our work more particularly focuses on the effect of promotion with K and operating conditions on olefin selectivity over supported molybdenum sulphide catalysts. At different preparation stages, the catalysts were characterized by nitrogen adsorption, XRD, LRS, CO-IR, XPS, H₂-TPR, CO₂-TPD and TEM and tested in mill fixed bed reactor.

II Characterization of K Promoted MoS₂/Al₂O₃ catalysts

II-1 Characterization of calcined catalysts

II-1-1 Textural Characteristics

The textural characteristics of Al₂O₃ and calcined K₂MoO₃/Al₂O₃ catalysts determined using the BET/BJH method, are shown in Table 5-1. The Puralox alumina exhibited surface, pore volume and diameter in agreement with previous reports [1,2]. The surface area and pore volume decrease in the catalysts after addition of molybdenum and potassium. The decrease in surface area and pore volume is probably due to pore plugging and alumina dilution in particular after addition of significant amounts of potassium carbonate. No significant change in the pore diameter was observed.

Table 5-1: BET surface area and pore size of alumina, calcined $\text{Mo}/\text{Al}_2\text{O}_3$ and K promoted $\text{Mo}/\text{Al}_2\text{O}_3$ catalysts

Samples	BET surface area (m^2/g)	Pore volume (cm^3/g)	Pore diameter (nm)
Al_2O_3	186.4	0.51	8.9
15M	133.1	0.40	8.8
3K_15M	123.8	0.37	8.3
6K_15M	111.6	0.32	8.3
12K_15M	95.7	0.29	8.6
15K_15M	86.2	0.25	8.4
18K_15M	74.2	0.23	8.8
24K_15M	34.8	0.11	9.3

II-1-2 XRD

A series of $\text{K}_x\text{MoO}_3/\gamma\text{-Al}_2\text{O}_3$ catalysts were characterised by XRD (Figure 5-1).

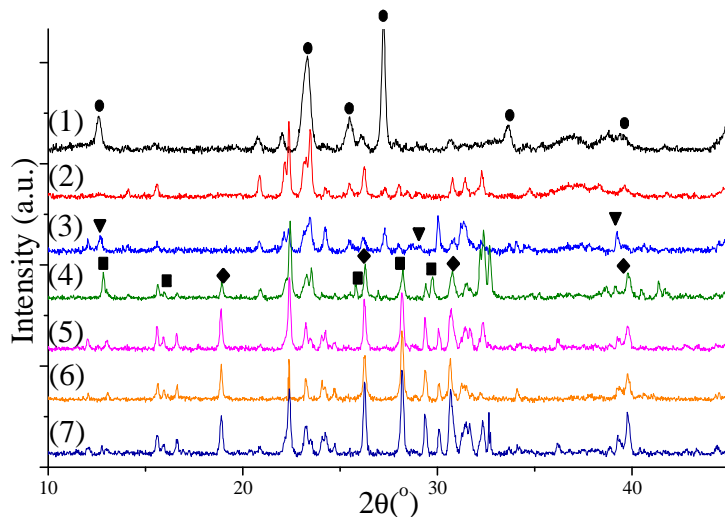


Figure 5-1: XRD patterns of calcined $\text{K}_x\text{Mo}/\text{Al}_2\text{O}_3$ catalysts (1) 15M, (2) 3K15M, (3) 6K15M, (4) 12K15M, (5) 15K15M, (6) 18K15M, (7) 24K15M. ● MoO_3 ▼ K_2CO_3 ■ $\text{K}_2\text{Mo}_4\text{O}_6$ ◆ K_2MoO_4

In addition to γ -alumina, the 15M catalyst exhibited higher intensities of MoO_3 XRD peaks which indicated higher fraction of the crystalline molybdenum oxide phase.

The XRD patterns of the calcined samples with 15 wt. % Mo and variable K content (from 0 to 24 wt. %) are also shown in Figure 5-1. An increase in potassium content resulted in a major drop in the intensity of MoO₃ peaks (JCPDF 05-0508, $2\theta = 25.70^\circ, 27.35^\circ, 33.73^\circ, 38.98^\circ$). This indicates stronger interaction between molybdenum, potassium and γ -Al₂O₃ at higher potassium contents.

The presence of K seems to favour mixed K-Mo phases. At K/Mo ratio higher than 0.5 (3K15M), MoO₃ phase was not detected anymore and all of the XRD patterns were assigned to mixed K-Mo-O oxides. The XRD patterns showed the presence of K₂MoO₄ (JCPDF 29-1011, $2\theta = 18.87^\circ, 26.27^\circ, 30.65^\circ, 39.42^\circ, 45.83^\circ$) and K₂Mo₄O₆ (JCPDF 87-0730, $2\theta = 13.08^\circ, 17.07^\circ, 25.49^\circ, 27.47^\circ, 30.15^\circ$) phases. The XRD intensity of those mixed phases increased with potassium content.

The K₂CO₃ phase (JCPDF 87-0730, $2\theta = 12.98^\circ, 29.19^\circ, 37.54^\circ, 46.32^\circ$) was also observed in the diffraction patterns. As expected, its intensity becomes also more important on the catalysts with high potassium contents [3].

Note that besides the two-component potassium molybdates, the catalysts also exhibited the presence of aluminium molybdate (Al₂(MoO₄)₃, (JCPDF 85-2286, $2\theta = 20.84^\circ, 22.15^\circ, 23.14^\circ, 30.79^\circ, 32.10^\circ$) and mixed potassium aluminium molybdates (KAl(MoO₄)₂, JCPDF 74-2008, $2\theta = 22.36^\circ, 31.40^\circ, 32.26^\circ, 51.97^\circ$). The Al₂(MoO₄)₃ phase was detected for all catalysts; its intensity slightly increases with addition of K. In agreement with Gutierrez et al. [4], the KAl(MoO₄)₂ phase was only detected in the catalysts with K/Mo molar ratio higher than 2.5 (15K15M and 24K15M catalysts).

II-1-3 LRS

The Raman spectra of the calcined K_xMoO₃/Al₂O₃ catalysts are shown in Figure 5-2. The spectra exhibit the presence of MoO₃, Al₂(MoO₄)₃ and polymeric surface molybdates. MoO₃ was identified in all the catalysts using Raman frequencies at 153, 288, 334, 662, 818 and 991 cm⁻¹ [5,6]. Promotion with K had a strong impact on absolute and relative intensities of the Raman bands. The intensity of the Raman MoO₃ bands decreased with an increase in

potassium content. In agreement with the XRD results, MoO_3 concentration became less significant with higher K loading, suggesting formation of K-Mo mixed oxides.

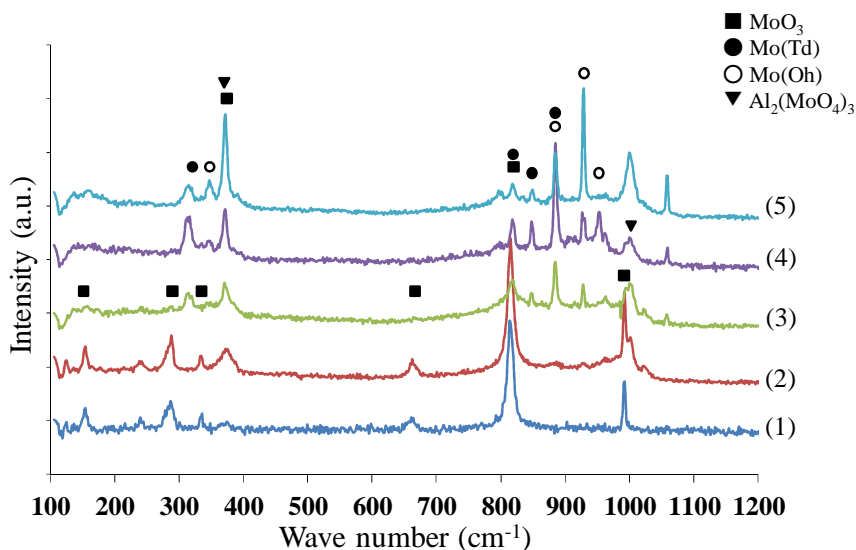


Figure 5-2: Raman spectra of calcined $\text{K}_x\text{Mo}/\gamma\text{-Al}_2\text{O}_3$ catalysts: (1)15M (2)3K15M (3)6K15M (4)15K15M (5)24K15M

In addition to MoO_3 , the Raman spectra also exhibit the bands at 372 and 1001 cm^{-1} corresponding to $\text{Al}_2(\text{MoO}_4)_3$ [7]. The intensity of the $\text{Al}_2(\text{MoO}_4)_3$ band increased with higher K loading. This suggests a strong interaction between molybdenum and alumina in the supported catalysts in the presence of potassium. This observation is also consistent with the XRD characterisation results.

The Raman bands at 314, 818, 848 and 896 cm^{-1} were attributed to the Mo–O–Mo asymmetric stretching modes of polymerized surface molybdenum oxide clusters in the tetrahedrally coordinated Mo^{6+} species such as MoO_4^{2-} and the Raman bands at 896, 929 and 954 cm^{-1} were attributed to the symmetric stretching of the Mo=O bond in octahedrally coordinated Mo^{6+} species such as $\text{Mo}_4\text{O}_6^{2-}$ and $\text{Mo}_7\text{O}_{24}^{2-}$ [5]. The latest two molybdenum species can be associated to the K-Mo mixed phases. Note that the mixed K-Mo phases (K_2MoO_4 and $\text{K}_2\text{Mo}_4\text{O}_6$) were also observed in XRD patterns (Figure 5-1).

The band at 929 cm^{-1} is also characteristic of well dispersed polymolybdate species [8]. The band at 372 cm^{-1} is probably due to the overlap of bands corresponding to $\text{Al}_2(\text{MoO}_4)_3$ and

polymolybdate species [7]. The intensities of the bands at 372, 929 and 1001 cm⁻¹ increased with higher K/Mo ratio.

In addition, the calcined K-promoted catalysts showed the presence of Raman bands at 961 cm⁻¹ and 1055 cm⁻¹. The peak at 961 cm⁻¹ can be assigned to the octahedrally coordinated Mo⁶⁺ species [5,7], while the assignment of the peak at 1055 cm⁻¹ cannot be exactly established. From our results, we inferred that these two bands might correspond to the KAl(MoO₄)₂ which was identified in the calcined catalysts using XRD.

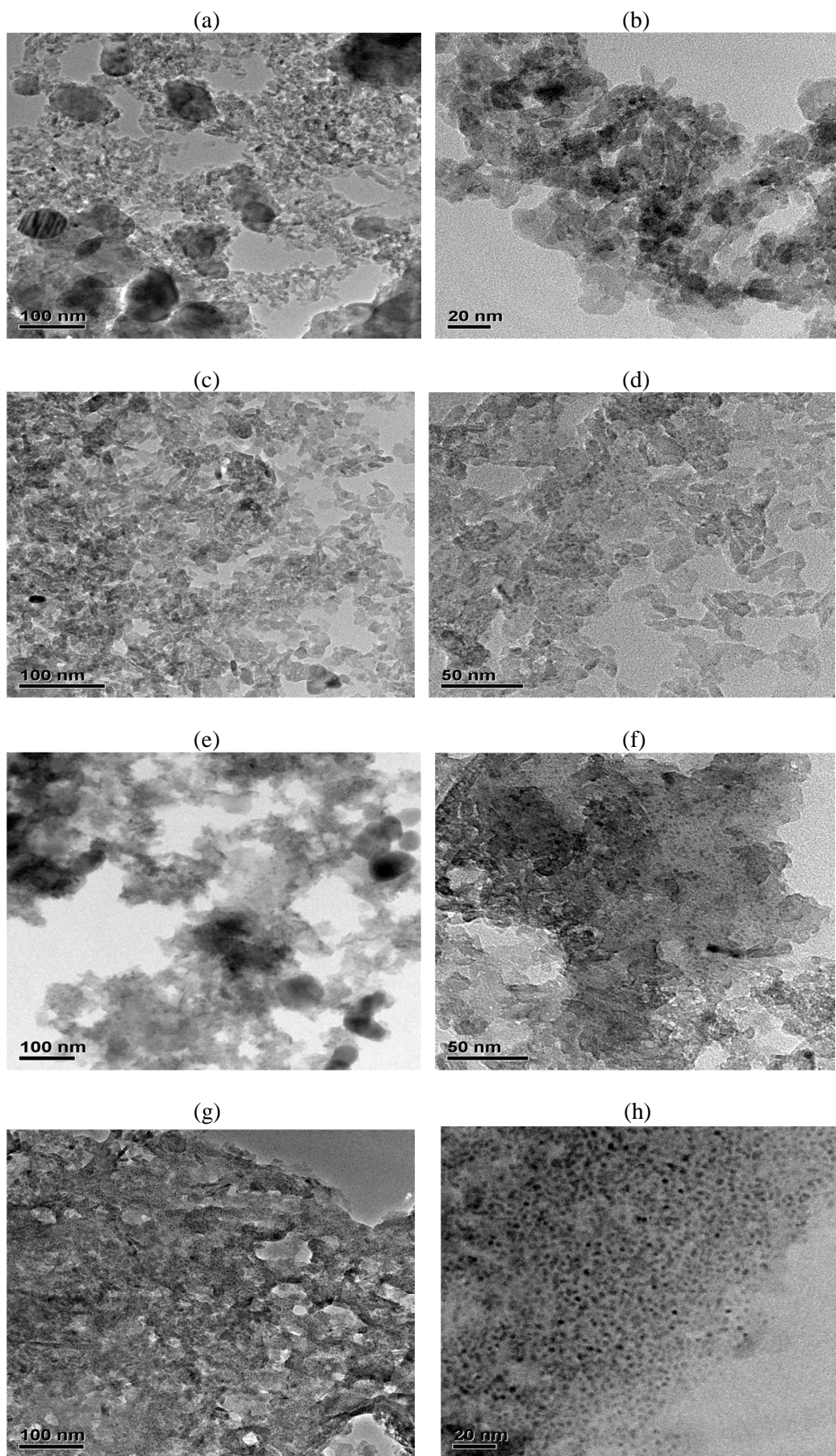
The Raman data suggest that on potassium promoted alumina supported MoS₂ catalysts, the mixed K-Mo, Mo-Al and K-Mo-Al oxides should be formed, as a result, stronger interaction between molybdenum, potassium and alumina can be detected.

II-1-4 TEM

Figure 5-3 displays the TEM images of the K_MoS₂/Al₂O₃ catalysts at different K ratio. The dark parts of the images correspond to the Mo species.

It can be observed that the potassium promoter affect the molybdenum dispersion. On the non-promoted catalyst (Figure 5-3 (a,b)), Mo are observed on the form of large particles. In presence of potassium, the Mo particle size became smaller. The Mo particles seem to be smaller and better dispersed in the 15K_15M catalyst. The particles size seems to be slightly bigger in 24K_15M catalyst, compared to 15K_15M.

On the other hand, for 15M and 3K_15M catalysts, the alumina crystals of the support can be distinguished. However, with the increase in K loading, the alumina crystals are hardly visible. This indicates that the crystallinity of Al₂O₃ decreases.



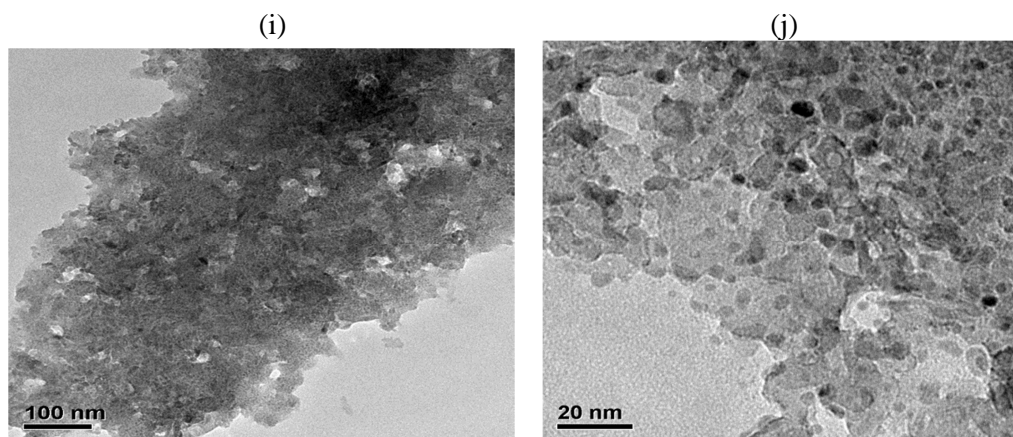


Figure 5-3: TEM images of calcined catalysts. (a, b)15M; (c, d)3K_15M; (e, f)6K_15M; (g, h)15K_15M; (i, j)24K_15M

Those results are in agreement with the XRD pattern of the calcined catalysts (Figure 5-1). The intensity of the alumina peak was decreasing as the K content was increasing. The inhibition of Al₂O₃ crystallinity is possibly due to:

- the interaction of potassium and/or molybdenum with the support (Al₂(MoO₄)₃ and KAl(MoO₄)₂ detected by XRD),
- the basic carbonate promoter could attack the alumina support.

II-2 Characterization on sulphided catalysts

II-2-1 XRD

Sulphided catalysts were obtained after sulphidation of calcined catalysts. The XRD patterns of sulphided K_MoS₂/γ-Al₂O₃ catalysts are shown in Figure 5-4. Interestingly, the diffraction peaks assigned to the molybdenum oxides, potassium molybdate and mixed oxide species almost completely disappeared after sulphidation.

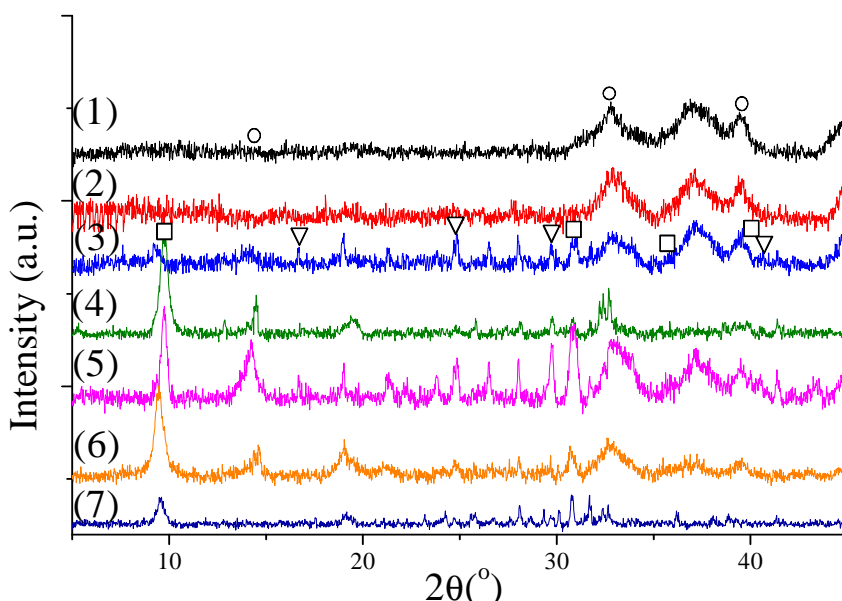


Figure 5-4: XRD patterns of sulphided $\text{K-MoS}_2/\text{Al}_2\text{O}_3$ catalysts: (1) 15M, (2) 3K_15M, (3) 6K_15M, (4) 12K_15M, (5) 15K_15M, (6) 18K_15M, (7) 24K_15M. ○ MoS_2 □ KMoS_2 ▽ K_2MoS_4

The XRD patterns indicate the presence of MoS_2 (JCPDF 89-3040, $2\theta = 14.38^\circ, 32.68^\circ, 39.60^\circ, 49.79^\circ, 58.34^\circ, 60.15^\circ$), K_2MoS_4 (JCPDF 19-1001, $2\theta = 17.55^\circ, 24.23^\circ, 29.36^\circ, 41.19^\circ, 47.05^\circ, 58.40^\circ$) or K-MoS_2 (JCPDF 18-1064, $2\theta = 9.66^\circ, 32.41^\circ, 36.13^\circ, 40.61^\circ, 60.46^\circ$). This suggests that the mixed K-Mo-O oxides were completely sulphided during the pre-treatment with H_2S [9]. Note that potassium carbonate was not detected in the sulphided catalysts.

When the potassium concentration is low, potassium sulphides cannot be meaningfully observed by XRD. At higher potassium content, XRD shows the presence of:

- potassium sulphide phases such as K_2S (JCPDF 65-3001, $2\theta = 34.21^\circ, 49.16^\circ, 61.26^\circ$), K_2S_3 (JCPDF 31-1095, $2\theta = 28.28^\circ, 30.02^\circ, 32.70^\circ$) and K_2S_5 (JCPDF 01-089-3999, $2\theta = 19.83^\circ, 30.78^\circ, 31.15^\circ$, not well observed until the $\text{K/Mo} = 2.5$);
- potassium sulphate phases such as K_2SO_4 (JCPDF 83-0681, $2\theta = 29.80^\circ, 30.79^\circ$) and $\text{K}_2\text{S}_3\text{O}_6$ (JCPDF 01-075-1479, $2\theta = 16.73^\circ, 18.10^\circ, 23.61^\circ, 24.90^\circ, 26.54^\circ, 28.08^\circ, 31.13^\circ$).

The intensity of XRD peaks attributed to $\text{Al}_2(\text{MoO}_4)_3$ and $\text{KAl}(\text{MoO}_4)_2$ was significantly reduced after sulphidation.

II-2-2 LRS

Raman spectroscopy was used for further characterisation of the sulphided $\text{K}_x\text{MoS}_2/\gamma\text{-Al}_2\text{O}_3$ catalysts. Major modifications of Raman spectra were observed after sulphidation (Figure 5-5).

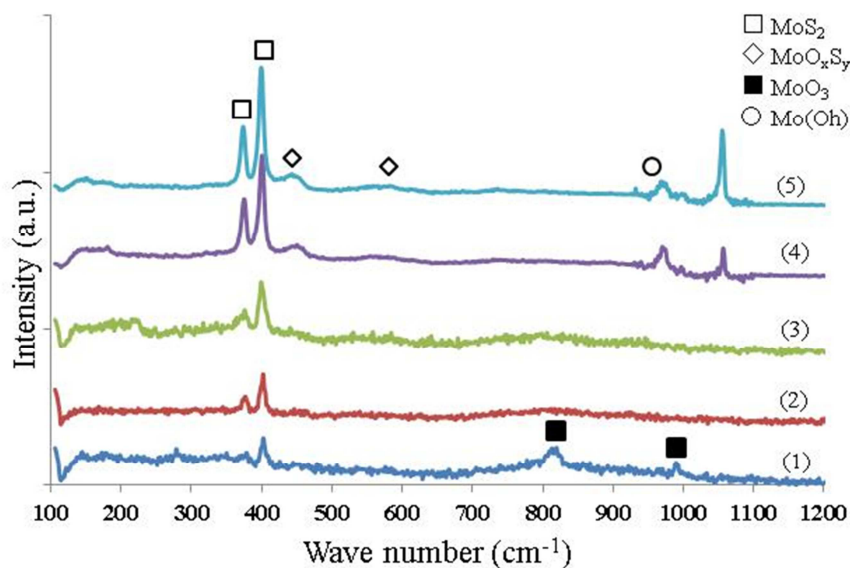


Figure 5-5: Raman spectra of sulphided $\text{K}_x\text{Mo}/\gamma\text{-Al}_2\text{O}_3$ catalysts: (1) 15M, (2) 3K_15M, (3) 6K_15M, (4) 15K_15M, (5) 24K_15M

The two intense bands at 378 cm^{-1} and 406 cm^{-1} , characteristic of MoS_2 , are observed in both non-promoted and potassium-promoted catalysts [3,5,10].

For the $\text{MoS}_2/\gamma\text{-Al}_2\text{O}_3$ catalyst, the bands at 818 cm^{-1} and 998 cm^{-1} corresponding to the MoO_3 were detected. This suggests that a part of the molybdenum remains as oxide after sulphidation of the non-promoted catalyst. The residual MoO_3 phase was not detected by Raman spectroscopy in sulphided K-promoted catalysts.

The catalysts with higher potassium content also present the bands at 450 cm^{-1} and $550\text{-}600\text{ cm}^{-1}$ which are characteristic of Mo oxysulphide [4,11]. This phase arises from the uncompleted sulphidation of MoO_3 oxide. The molybdenum oxidation state in this phase is +5 (further confirmed by XPS).

In the catalysts with K/Mo ratio ≥ 2.5 , the bands at 961 cm⁻¹ and 1055 cm⁻¹ were also detected which can be probably attributed to KAl(MoO₄)₂. Both of them were already present in the Raman spectra of the oxide catalysts (Figure 5-4).

II-2-3 XPS

The catalysts were also analysed by XPS. The surface composition for the sulphided samples calculated from XPS data is given in Table 5-2.

Table 5-2: XPS atomic ratio of different elements on MoS₂/Al₂O₃ based catalysts

Catalyst	K/Mo ratio on synthesized catalysts	XPS atomic ratio (%)						
		Al	O	K	S	Mo	C	K/Mo
15M	0	27.8	49.3	0	12.1	7.7	3.1	0
3K_15M	0.5	25.6	49.9	3.5	12.0	5.6	3.4	0.62
6K_15M	1.0	23.7	50.3	5.0	11.5	6.6	2.9	0.76
15K_15M	2.5	19.1	49.0	6.2	15.2	7.6	2.8	0.82
24K_15M	4.0	9.3	35.9	9.3	23.9	10.6	11	0.88

The surface atomic concentrations of aluminium, oxygen, potassium and sulphur varied as function of potassium promotion. It is noticeable that the surface concentration of aluminium and oxygen decreases in the samples with higher potassium content.

At the same time, the XPS data are also indicative of enrichment of catalyst surface with molybdenum. The surface K/Mo ratio measured from XPS is much lower than the bulk Mo/K ratio in the sulphided catalysts. Indeed, in the alumina supported molybdenum catalysts, a 8-times increase in the bulk K content (from 3% to 24%) results only in a very moderate increase (about 29%) in the surface K/Mo ratio. This suggests that molybdenum is highly dispersed on the catalyst outer surface, while potassium is mostly located in the catalyst bulk where it is undetectable by XPS.

The presence of carbon on catalyst surface is due to the CO₂ from air adsorbed on catalyst surface and the K₂CO₃ precursor left on catalysts. In this case, the high carbon

concentration on the 24K_15M catalyst should be caused by a high quantity of potassium added in catalysts, which can absorb more CO₂ and make more carbonate presented on catalyst surface.

The Mo 3d and S 2p XPS spectra of sulphided K_MoS₂/Al₂O₃ catalysts are shown in Figure 5-6 and Figure 5-7.

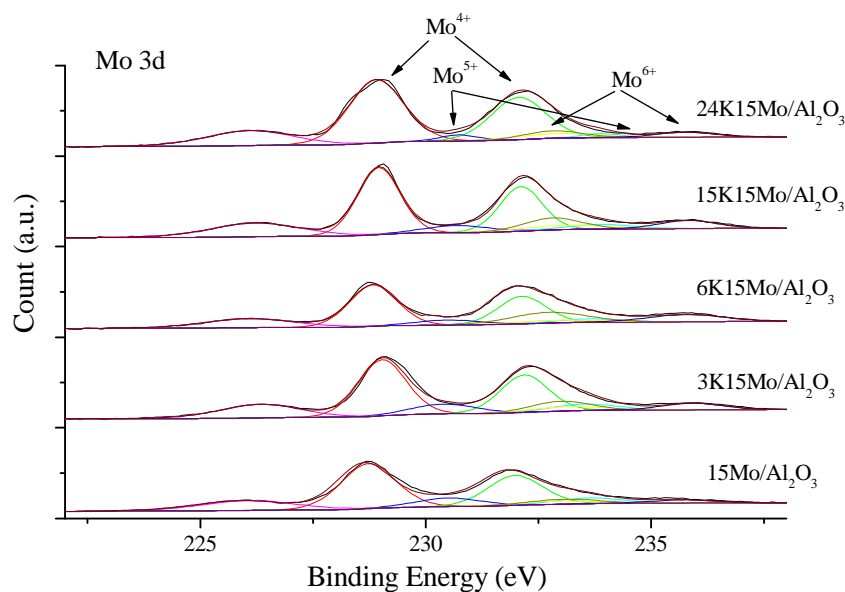


Figure 5-6: Mo 3d XPS spectra of the sulphided K-MoS₂/ γ -Al₂O₃ catalysts

In the Mo 3d XPS region, several peaks were observed. The broad envelop of the Mo 3d signal can be deconvoluted in three separate overlapping doublets. This suggests that molybdenum is present in three oxidation states: Mo⁴⁺, Mo⁵⁺ and Mo⁶⁺.

The more intense signals at 229.0 eV and 232.1 eV are characteristic of the Mo⁴⁺ species (3d_{3/2} and 3d_{5/2}) which are probably related to the MoS₂ phase [12]. In addition, the XPS shows the peaks with the binding energy of 232.8 eV and 235.9 eV characteristic of Mo⁶⁺ and 230.6 eV and 233.7 eV which can be assigned to Mo⁵⁺ species [13]. The values of the binding energy do not change with potassium addition. Only a very small shift of Mo 3d_{5/2} peak attributed to Mo⁴⁺ to lower binding energy species is observed. The shift of binding energy for the promoted catalysts could be due to the presence of potassium.

Note however the intensity of the peaks attributed to Mo^{6+} and Mo^{5+} species increases with higher K content [14]. This suggests higher concentration of oxidized molybdenum species in potassium promoted catalysts. The Mo^{6+} and Mo^{5+} present in the sulphided catalysts could be:

- (i) produced during the passivation,
- (ii) due to the formation of a K_2MoS_4 phase (also observed by XRD) where Mo exist as Mo^{6+} ,
- (iii) related to the formation of the oxy-sulphide species of the MoO_2S_2 and MoOS_2 type [15],
- (iv) due to the interaction of Mo and alumina resulting in $\text{Al}_2(\text{MoO}_4)_3$ which can be not sulphided under these conditions.

The S 2p XPS spectra are relatively complex for the sulphided K_Mo/ Al_2O_3 catalysts (Figure 5-7). The S 2p peaks showed a doublet which reveals the presence of two types of sulphur species. The XPS peaks with the binding energies of 161.6 eV and 162.8 eV correspond to sulphide ions (S^{2-}), which might be present in K_2S and/or MoS_2 . The binding energy around 162.6 eV and 163.8 eV could be possibly assigned to poly-sulphide ions (S_2^{2-}) in K-MoS_x and K_2S_x ($\text{K}_2\text{S}_3/\text{K}_2\text{S}_5$).

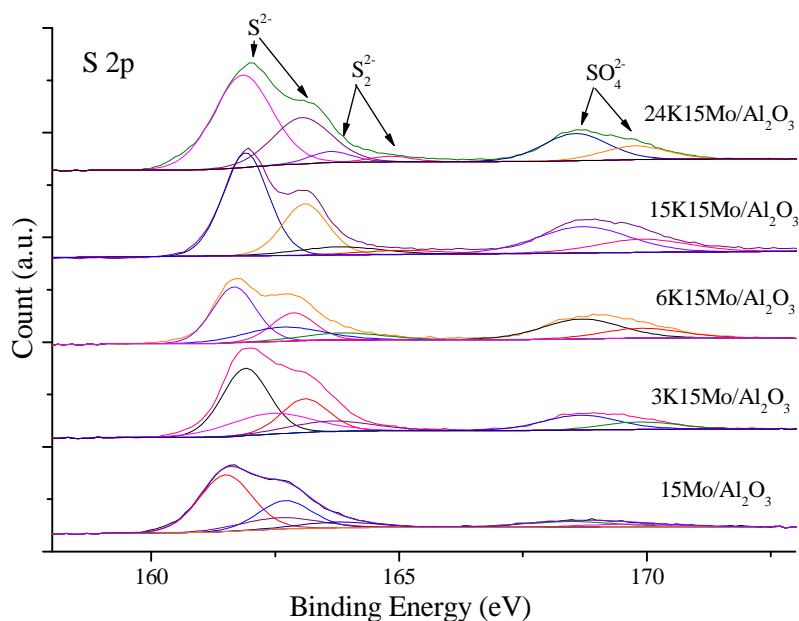


Figure 5-7: S 2p XPS spectra of the sulphided K-MoS₂/ γ -Al₂O₃ catalysts.

Addition of K also leads to a small shift of the S 2p XPS peaks to higher energies. The high energy shift of the sulphur XPS peaks in the 15K_15Mo/Al₂O₃ and 24K_15Mo/Al₂O₃ catalysts indicates that sulphur atoms may be neighbored by some high electronegativity atoms. These atoms might be for example K⁺ or Mo⁶⁺ ions [16].

The S 2p XPS spectra also exhibit other broad peaks at 168.9 eV and 170.1 eV which can be due to the presence of sulphates (SO₄²⁻). The intensity of these peaks increases with an increase in K/Mo ratio. The presence of sulphates on the catalyst surface might be mainly due to partial molybdenum oxidation during catalyst exposure to air during passivation.

The K 2p XPS spectra (not shown here) were also measured for these catalysts. The K 2p XPS peak was located at binding energies around 293.0 eV. The binding energy and peak shape were not affected by potassium content in the samples.

The decomposition of Mo 3d and S 2p XPS spectra suggests that Mo and S exist as different oxidation state. The ratio of these species is presented in Table 5-3. It is observable that Mo⁴⁺ is the major molybdenum species on the catalyst surface. The potassium promotion slightly affects the oxidation state of Mo.

Table 5-3: XPS Atomic percentage of different kinds of species for Mo and S

Catalyst	Mo (%)			S (%)		
	Mo ⁴⁺	Mo ⁵⁺	Mo ⁶⁺	S ²⁻	S ₂ ²⁻	SO ₄ ²⁻
15M	87.0	3.9	9.1	67.8	19.8	11.6
3K_15M	76.8	8.9	14.3	52.5	29.2	18.3
6K_15M	75.8	9.1	15.2	56.5	19.1	24.3
15K_15M	69.7	13.2	17.1	57.2	18.4	23.7
24K_15M	80.2	9.4	9.4	70.7	6.3	23.0

In the K-promoted catalysts, the contribution of Mo⁴⁺ species slightly decreases, while the fractions of Mo⁵⁺ and Mo⁶⁺ species are getting more significant. The presence of Mo⁵⁺ and Mo⁶⁺ could be associated with both formation of the MoO_xS_y oxy-sulphide, in which O atoms replaces the S atoms in the MoS₂ structure. The S²⁻ seems to be related to MoS₂ sulphides and K₂S sulphides, while S₂²⁻ could be principally present in unsaturated sulphide such as MoO_xS_y or K₂S_x [17]. Note that the MoO_xS_y or K₂S_x phases are also detected in sulphided catalysts by XRD and Raman spectroscopy.

II-2-4 H₂-TPR

The H₂-TPR profiles were measured for the sulphided K_MoS₂/Al₂O₃ catalysts. They are presented in Figure 5-8. Three types of TPR peaks are observed which correspond to various molybdenum and sulphur species [18]. The H₂ consumptions measured from the TPR profiles are given in Table 3.

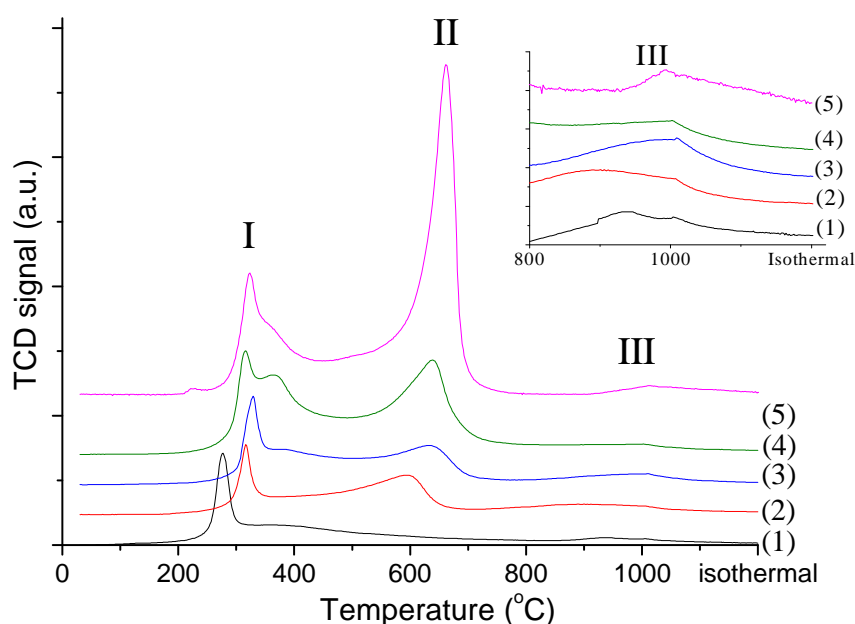


Figure 5-8: H₂-TPR of sulphided K_MoS₂/γ-Al₂O₃ catalysts (1)15M (2)3K15M (3)6K15M (4)15K15M (5)24K15M

Table 5-4: H₂ consumption in TPR experiments (mmolH₂/g_{catalyst})

Catalysts	Zone I	Zone II	Zone III
15M	1.34	0.00	0.53
3K_15M	1.12	0.71	0.50
6K_15M	1.47	1.11	0.46
15K_15M	2.42	2.24	0.42
24K_15M	1.82	4.24	0.25

In agreement with Toulhouat et al [19], the low temperature TPR peaks located between 230°C – 430°C could be related to the hydrogenation of extra sulphur atoms (chemisorbed H₂S or SH groups) or sulphur atoms that are weakly bond to the catalyst surface. Those easily

removable species are adsorbed on low coordinated edge/corner sites, which were believed to be responsible for the active sites of the molybdenum catalysts. A slight shift of these peaks towards higher temperature is observable with further addition of K. The presence of the alkali ion seems to stabilise the sulphur adsorption and leads to stronger interactions between S atoms and Mo atoms. The hydrogen consumption in the low temperature TPR peak is only slightly affected by the promotion with potassium (Table 5-4).

The TPR peaks between 530°C – 730°C could be related to the hydrogenation of molybdenum and potassium mixed sulphides and sulphates. Note that the peaks in this temperature range are absent in the TPR profiles of the unpromoted alumina supported molybdenum catalyst which does not contain potassium ions. The area of this peak significantly increases with the increase in K loading (Table 5-4). It can be suggested that the high temperature peaks could be assigned to the reduction of K-Mo-S species and possibly sulphate ions (such as the thiosulphate K₂S₃O₆). All these compounds have been observed in XRD patterns and their concentration also increases with potassium content. In addition, the sulphur atoms located at the edges or basal planes [29] of molybdenum sulphide crystallites could also contribute to these medium temperature TPR peaks.

Finally, the broad low intense high temperature TPR peaks at 950-1000°C seem to be related to the partial reduction of bulk MoS₂. It is known [18] that reduction of bulk MoS₂ occurs generally at the temperature between 700°C to 1050°C. The MoS₂ reduction temperature is usually related to the strength of the Mo-S bond, size of the particles, dispersion on the surface and interactions with the support. High reduction temperature in this case is indicative of relatively large molybdenum sulphide crystallites.

II-2-5 CO₂-TPD

The basicity of the sulphided catalysts was followed by CO₂-TPD (Figure 5-9). All the catalysts exhibited a broad CO₂ desorption peak, in the range 30–300 °C and several peaks at 600-800°C.

The high temperature peaks seem to be attributed to carbonate species. The carbonate composition seems to be affected by the presence of potassium. Taking into account very significant stability of carbonates which decompose only at very high temperature, these species are not likely to be involved in carbon monoxide hydrogenation.

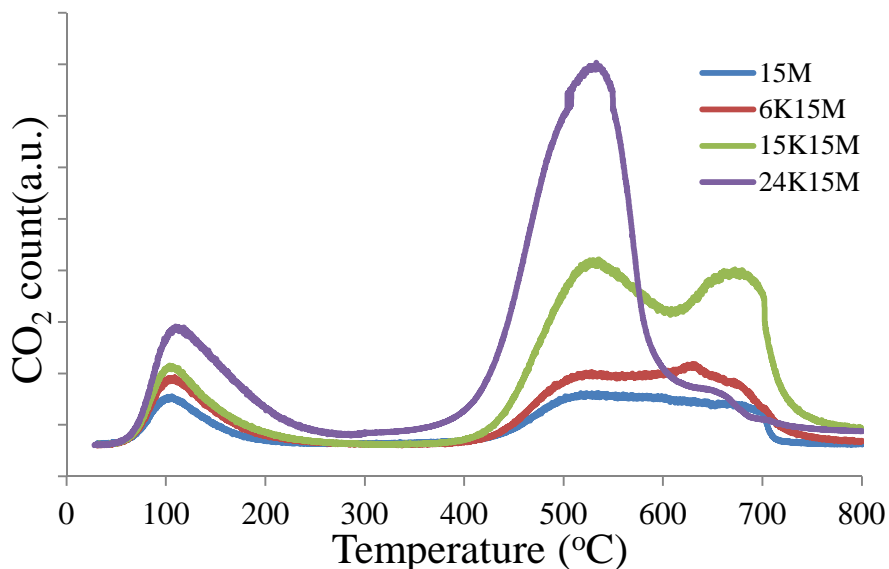


Figure 5-9: CO₂-TPD of sulphided K_Mo/Al₂O₃ catalysts

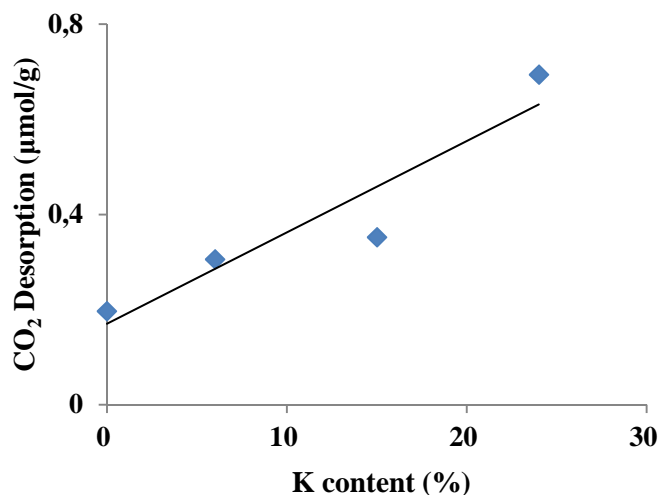


Figure 5-10: Area of low temperature CO₂ desorption peak as a function of potassium content in the sulphided promoted alumina supported molybdenum catalysts

Note that the total CO₂ adsorption measured from the CO₂-TPD low temperature peak increases significantly with the addition of potassium. This suggests that addition of

potassium leads to supplementary basic sites.

An almost linear slope was observed in the plot of CO₂ adsorption versus potassium content (Figure 5-10). The peak position was not affected by the presence of potassium.

For all the catalysts, the maximum of CO₂ desorption was between 104°C-109°C. This suggests that while the concentration of basic surface sites increases with increase in potassium content and the strength of the basic sites are not much influenced by the promotion with potassium compared with the alumina support.

II-2-6 TEM

In Figure 5-11, MoS₂ particle, which have the form of multilayer sheets, can be very well distinguished on all these three catalysts [20]. The MoS₂ particle size varied with K loading.

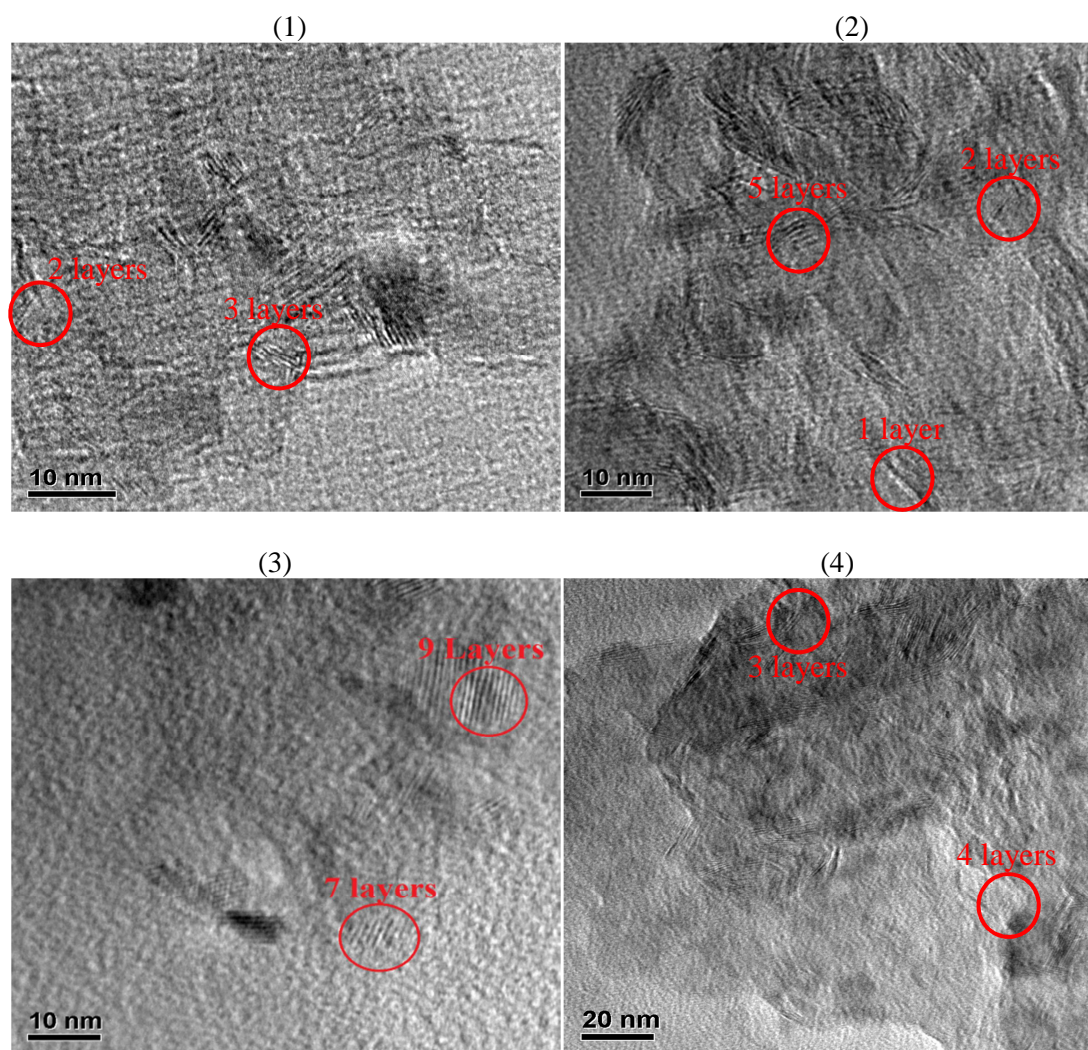


Figure 5-11: TEM images of sulphided catalysts. (1)15M (2)6K15M (3)15K15M (4)24K15M

For those MoS₂ based catalysts, it can be found that with addition of K, both number of layer stacking and slab length of MoS₂ particles increased. This indicates that for the 15M catalyst, the particle size is lower than on K promoted catalysts. As a result, the dispersion of MoS₂ is better for non-promoted catalyst (15M). This is different from what we observed for calcined catalysts concerning the dispersion of MoO₃ particles. Hence, the Mo dispersion on calcined and sulphided catalysts is different. This can demonstrate that the dispersion of Mo phases on Al₂O₃ support changed during the sulphidation step.

The layer stacking and slab length of MoS₂ particle size distribution were calculated from 20 TEM images for each sample and are represented in Table 5-5. It indicates that the non-promoted MoS₂ catalyst shows the smallest particle size. With different potassium content, the MoS₂ particle size contribution is different. The MoS₂ particle exhibits a more layer stacking and higher slab length in 15K_15M catalyst than in the other two promoted catalysts. On 24K_15M catalyst, the number of layer is similar as 15M, but its slab length remains quite high, similar to 15K_15M catalyst. Therefore, the MoS₂ particle size was improved with increase of K content, but when K percentage is too high, the MoS₂ particle size decreased.

Table 5-5: Layer stacking and slab length through statistics of TEM images

Catalyst	Number of layer	Slab length(nm)
15M	2.9	3.4
6K_15M	3.7	4.1
15K_15M	4.6	7.5
24K_15M	3.2	6.0

III Catalytic tests on K_MoS₂/Al₂O₃ catalysts

Methane, olefins, paraffins, methanol, ethanol and carbon dioxide were major reaction products detected in carbon monoxide hydrogenation on alumina supported molybdenum

catalysts (Table 5-6). The reaction was conducted at relatively low total pressure (20 bar) in order to shift the reaction selectivity from alcohols to olefins.

The catalysts were relatively stable under the reaction conditions. Carbon monoxide conversion and selectivities did not change during the first 60 h time on stream. The CO conversion and product selectivities at the steady state obtained at iso-GHSV for unpromoted and potassium promoted alumina supported molybdenum sulphide catalysts are shown in Table 5-6. Carbon dioxide was included in the total selectivity calculations.

Table 5-6: CO conversion and product selectivity on different K promoted catalysts at P = 20 bar, H₂/CO=2, T= 360°C, GHSV = 2100 cm³/(g_{cat}.h).

Catalyst	CO conversion (%)	Selectivity (%)						
		CH ₄	C ₂ -C ₄ Olefin	C ₂ -C ₄ Paraffin	C ₅₊ HC	MeOH	C ₂ + Alcohol	CO ₂
15M	48.9	51.4	0.05	0.2	0	0.05	0	48.3
3K15M	42.3	39.3	0.1	16.6	0	0.1	0	44.0
6K15M	41.0	35.2	0.2	15.5	0	7.5	1.6	40.1
12K15M	26.2	27.5	6.4	16.3	2.4	10.1	2.3	35.1
15K15M	21.3	18.9	10.7	15.9	6.3	13.2	1.9	33.2
18K15M	15.1	23.5	8.4	3.3	15.7	13.6	4.8	30.7
24K15M	11.2	21.7	4.8	2.3	24.4	14.0	1.8	31.0

The catalytic performance is strongly affected by promotion with potassium (Table 5-6, Figure 5-12). At GHSV=2100 ml.g_{cat}⁻¹.h⁻¹, the CO conversion decreases from 48.9 % to 11.2 % with the increase in K/Mo molar ratio from 0 to 4. Under these conditions, addition of potassium generally leads to better selectivity to olefins and alcohols [21]. The total olefin and alcohol selectivities increase respectively from 0.05 % to 10.5% and from 0.05% to 18.4 % whereas the total hydrocarbon selectivity fluctuates between 50% and 56%. Addition of potassium also results in lower selectivities to CH₄, while the selectivity to long-chain hydrocarbons (C₅₊ HC) has been significantly enhanced.

Figure 5-12 displays C₂-C₄ olefin, methanol and ethanol production rates as functions of potassium content in the catalysts. Minor light olefin and alcohol production rates were observed on the non-promoted molybdenum catalyst. Molybdenum was present in this catalyst as MoS₂ phase suggesting that this latter phase does not provide active sites for synthesis of higher hydrocarbons and alcohols.

The olefins and alcohol production rates passed through a maximum as a function of potassium content. The best results in terms of olefin and alcohol productivities were obtained at intermediate potassium contents. Note that extremely high potassium contents (>15wt.%) could be unfavourable for light olefin and alcohol synthesis.

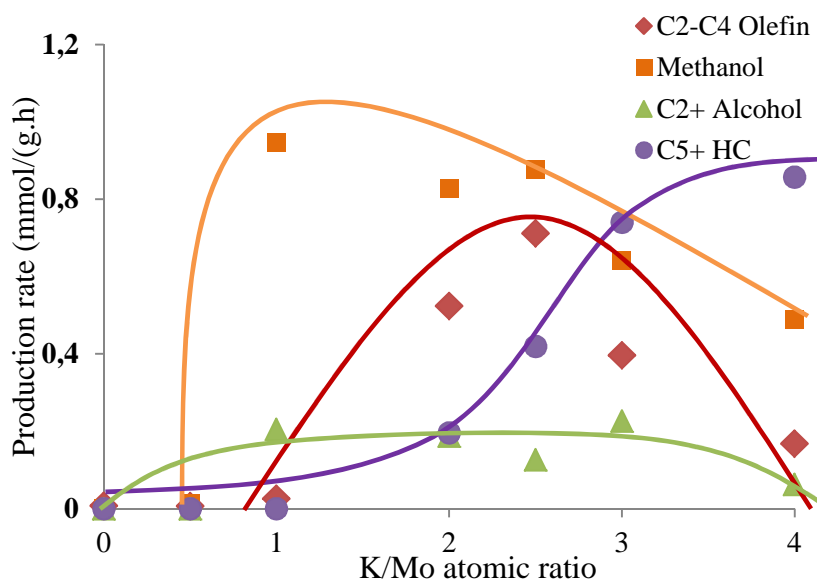


Figure 5-12: Light olefin, methanol, C_{2+} alcohol and C_{5+} hydrocarbon production rates on the K promoted alumina supported MoS_2 catalysts as a function of K/Mo atomic ratio

Carbon monoxide hydrogenation was conducted in the presence of 13.2 ppm_v of H_2S in syngas. Analysis of the reaction products using a selective PFPD detector showed the presence of trace amounts of several sulphur-containing compounds in the reactor outlet.

The distribution of sulphur containing products present in trace amounts is shown in Table 5-7. Their composition is also affected by potassium content in the catalysts. At low potassium content, mostly H_2S and COS were detected.

The PFPD detects total sulphur content of 14.5 ppm_v in the reactor outlet while the sulphur concentration in the feed is 13.3 ppm_v. It can be therefore suggested that the non-promoted alumina supported catalyst does not lose any noticeable amounts of sulphur during the reaction. This suggestion takes into account the decrease in the concentration of sulphur compounds which occurs during carbon monoxide hydrogenation. At higher potassium content, methanethiol, ethanethiol and dimethyl sulphide were also observed.

Interestingly, the production of mercaptans on potassium promoted catalysts coincides

with the noticeable selectivity of these catalysts to alcohols and light olefins. This may suggest some similarity in the mechanisms of the formation of mercaptans, olefins and alcohols on MoS₂ catalysts.

Table 5-7: Concentration of different sulphur compounds in the reactor outlet on different potassium promoted alumina supported molybdenum catalysts

Catalyst	Total S concentration (ppmv)	H ₂ S(%)	COS(%)	CH ₃ SH(%)	C ₂ H ₅ SH(%)	CH ₃ SCH ₃ (%)
15M	14.5	90.7	9.3	0.0	0.0	0.0
3K15M	14.4	88.5	11.5	0.0	0.0	0.0
6K15M	14.8	75.5	22.8	1.7	0.0	0.0
12K15M	24.7	60.4	28.1	7.2	1.9	2.4
15K15M	21.0	49.1	37.8	10.2	2.3	0.6
18K15M	20.3	61.6	25.6	9.9	1.5	1.4
24K15M	21.3	67.1	22.2	8.1	1.8	0.8

The total sulphur concentration in the outlet of the reactor (Table 5-7) is higher for potassium promoted catalysts (>20 ppm_v) than the sulphur content in feed (13.3 ppm_v). This suggests that sulphur is partially removed from the catalysts during the reaction. Sulphur loss could be more noticeable in the catalysts promoted with potassium relative to the unpromoted counterpart.

IV Effect of reaction condition on K_MoS₂/Al₂O₃ catalysts

IV-1 Effect of GHSV

On the non-promoted alumina supported molybdenum catalyst, methane and carbon dioxide were the major reaction products at a wide range of conversions, while the potassium-promoted catalysts exhibited higher selectivity to olefins, long-chain hydrocarbons and alcohols. The product selectivities on potassium-promoted catalysts were investigated as a function of gas velocity. The results are shown in Figure 5-13.

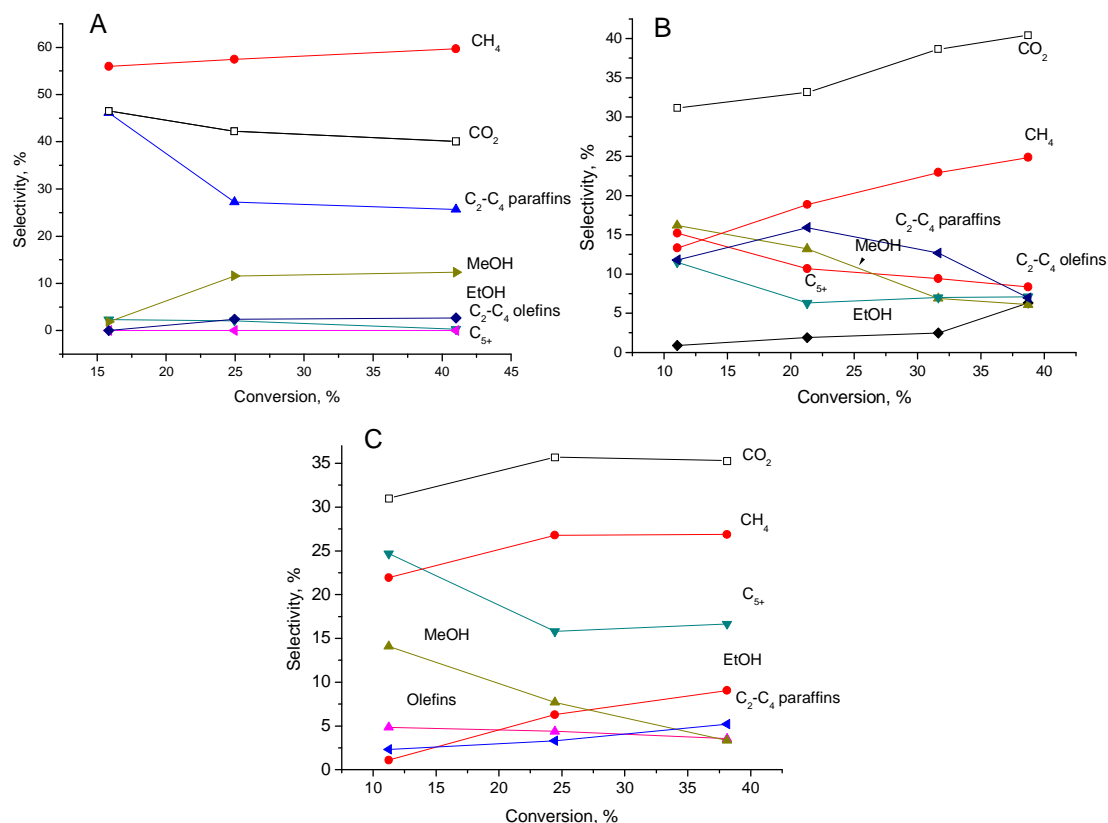


Figure 5-13: Selectivities as functions of carbon monoxide conversion for (A) 6K15M, (B) 15K15M and (C) 24K15M catalysts ($P = 20$ bar, $\text{H}_2/\text{CO}=2$, $T = 360^\circ\text{C}$)

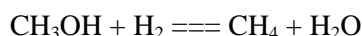
Carbon monoxide conversion at 360°C was adjusted in the range of 10% to 40% by varying GHSV. As expected, the increase in GHSV leads to lower CO conversion [22,23].

The selectivities to alcohols and hydrocarbons are also considerably affected by carbon monoxide conversion levels. Higher carbon monoxide conversion on all the catalysts leads to increase in methane selectivity, while selectivity to C_{5+} hydrocarbon drops at higher carbon monoxide conversion. Methane selectivity is particularly significant on the catalysts with low potassium content (Figure 5-13A), while the catalysts with higher potassium loading exhibit higher selectivity to C_{5+} hydrocarbons, methanol and higher alcohols (Figure 5-13B and C).

This type of behaviour suggests that methane may form via several reaction pathways. Noticeable methane selectivity at low carbon monoxide conversions suggests that methane could be possibly one of the primary reaction products. An increase in methane selectivity with higher conversion can be due to the methane production via hydrogenolysis of higher paraffins or methanol hydrogenation. Carbon dioxide selectivity is about 30-40% on all the catalysts. On 15K15Mo/ Al_2O_3 ($\text{K}/\text{Mo}=2.5$) and 24K15Mo/ Al_2O_3 ($\text{K}/\text{Mo}=4.0$), carbon dioxide

selectivity increases with higher carbon monoxide conversion which seems to be due to very significant water gas shift (WGS) reaction. Water is also produced when carbon monoxide is hydrogenated to hydrocarbons; the yield of water increases with CO conversion.

Interestingly, the methanol selectivity as a function of conversion varies differently on the catalysts with different potassium contents. The methanol selectivity increases with conversion on 12K15Mo/Al₂O₃ catalyst (K/Mo=2, Figure 5-13A), while methanol selectivity decreases with conversion on the catalysts with high potassium content (15K15M and 24K15M, Figure 5-13B and C). This might suggest different mechanisms of methanol formation as a function of potassium content. The drop in methanol selectivity coincides with increase in methane selectivity and selectivity to higher alcohols. Thus, the decrease in methanol selectivity with the increase in conversion on the catalysts with higher potassium contents can be attributed to the secondary reactions such as for example, methanol hydrogenation to methane:



Noticeable selectivity to olefins is observed as K/Mo molar ratio gets higher than 1.5. The best olefin selectivity is obtained for the 15K15M catalyst. On the catalysts with higher potassium content, the olefin and alcohol selectivities decrease with conversion.

IV-2 Effect of pressure

The different selectivity obtained at 10 bar and 20 bar on the 15K15M catalyst is shown in Figure 5-14.

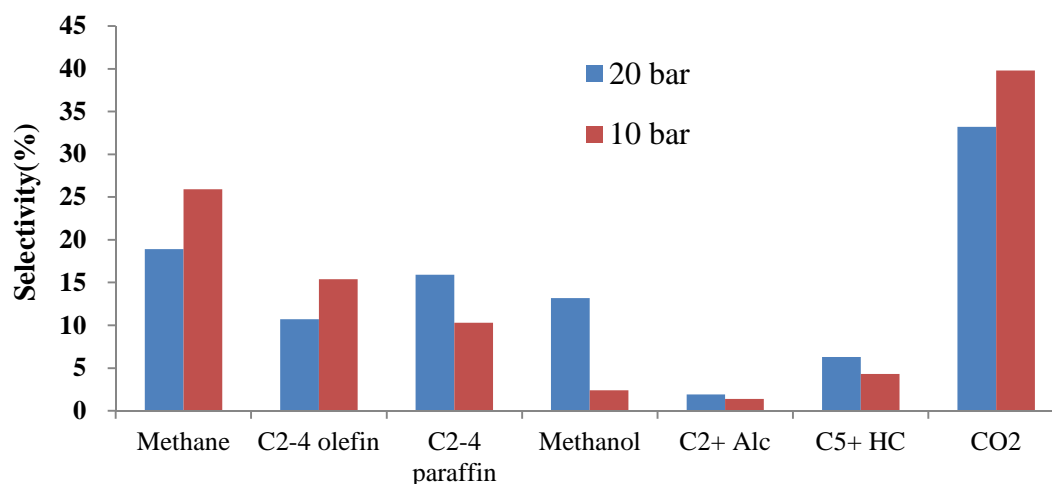


Figure 5-14: Selectivity on 15K15M catalyst. ($T = 360^{\circ}\text{C}$, CO conversion was kept around 20% by varying GHSV)

To compare the product selectivity, the CO conversion needs to remain constant. Hence, the GHSV varied in order to keep the CO conversion at around 20%.

At $P = 20$ bar, as presented before, the CO conversion was 21.3% with $\text{GHSV} = 2100 \text{ h}^{-1}$. At $P = 10$ bar, the CO conversion was 20.6% with $\text{GHSV} = 467 \text{ h}^{-1}$. When the reaction was realized at lower pressure, the methane selectivity increased while the longer carbon chain product (C_{5+} HC and C_{2+} alcohol) selectivity decreased. This is possibly due to the easier desorption of adsorbed species at low reaction pressure [24]. Olefin readsorption is often considered as an important step in FT synthesis which could result either in olefin hydrogenation or reinitiation of the polymerization chain [24]. Consequently lower selectivity to light chain paraffin which might result from olefin hydrogenation and lower selectivity to long chain hydrocarbons are observed at low reaction pressures. These results are consistent with previous report of Surisetty et al [21] who showed that lower pressure reaction pressure reduces alcohol selectivity and shift products distribution low molecular weight olefins. Similar study was realized by Quarderer et al [25] and Iranmahboob et al [26]. Both groups have reported that higher reaction pressure was favorable for alcohol selectivity and unfavorable for hydrocarbon selectivity.

The CO conversion and product selectivity on the 15K_15M catalyst at lower reaction pressure (10 bar) are presented in Figure 5-15.

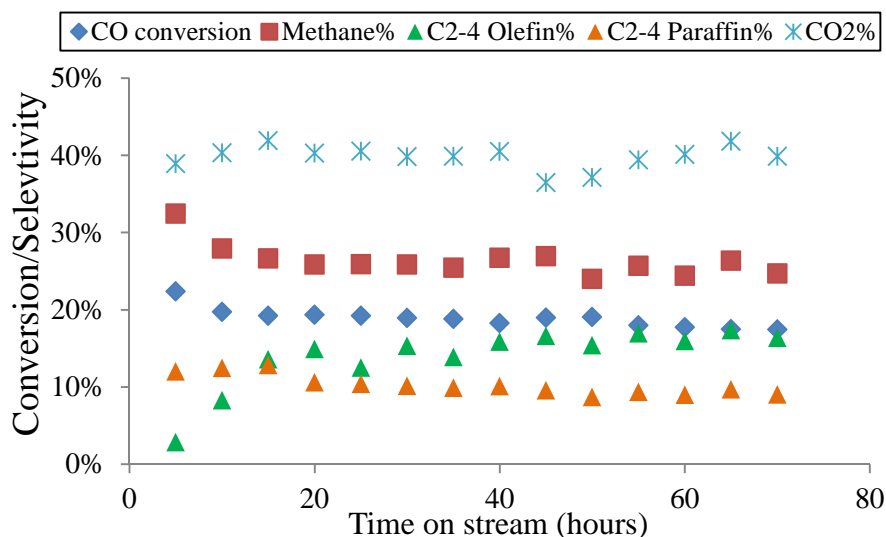


Figure 5-15: Catalytic performance of 15K15M catalyst, at $P = 10$ bar, $T = 360^\circ\text{C}$, $\text{GHSV} = 467 \text{ h}^{-1}$

The CO conversion was kept at around 20%, but in order to achieve this value, the GHSV should be reduced at $467 \text{ ml.g}_{\text{catalyst}}^{-1}.\text{h}^{-1}$. The CO conversion, as well as products selectivity are stable during the 70 hours time on stream when reaction pressure is set at 10 bar. In agreement with previous study [25,26], the reaction pressure did not affect the catalyst stability.

IV-3 Effect of syngas ratio (H_2/CO)

The results of selectivity on 15K15M catalyst are showed in Figure 5-16, with $\text{H}_2/\text{CO} = 1$ and 2. Note that the CO conversion was 21.3% at H_2/CO ratio of 2. It can be concluded that the H_2/CO ratio showed little effect on the carbon monoxide conversion. At the same time, H_2/CO ratio affects significantly the product selectivity.

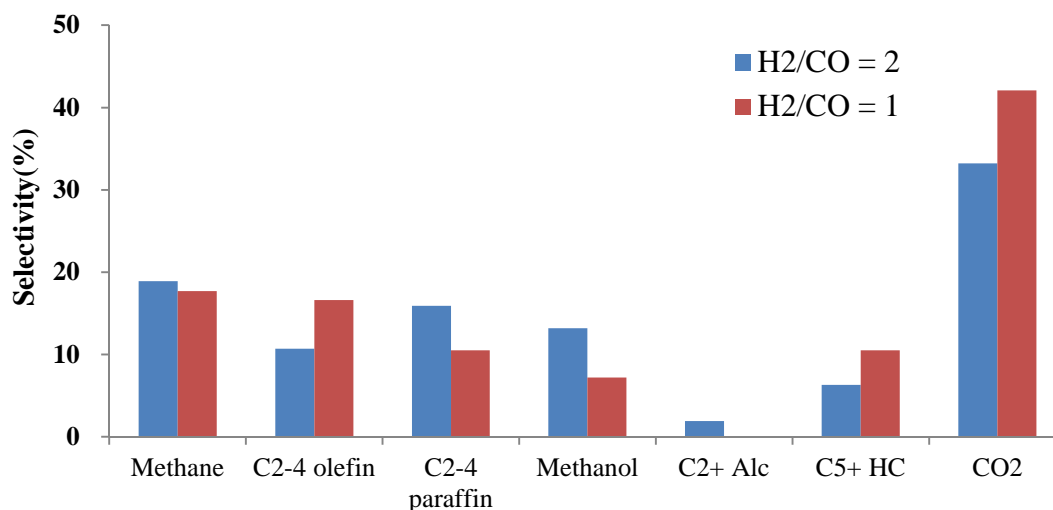
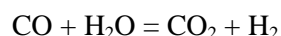


Figure 5-16: Effect of H_2/CO ratio on 15K15M catalyst ($P = 20$ bar, $T = 360^\circ\text{C}$, $\text{GHSV} = 2100$ h^{-1})

The CO_2 selectivity is higher at H_2/CO ratio of 1 because higher CO fraction in syngas could improve the water-gas-shift reaction [27,28]:



The alcohol selectivity becomes less important at $\text{H}_2/\text{CO} = 1$ than at $\text{H}_2/\text{CO} = 2$. This is concordance to previous work. Chiang et al [29] realized that the CO hydrogenation on MoS_2 catalysts at 30 bar, showed the highest $\text{C}_1\text{-C}_4$ alcohol selectivity at $\text{H}_2/\text{CO} = 2$, compared to alcohols selectivity obtained at $\text{H}_2/\text{CO} = 1$ or 3. Surisetty et al [30] reported that on K-Co- MoS_2 based catalysts, a high ratio of H_2/CO (equal to 2) improved catalytic activity and alcohol selectivity.

It is also observed that light olefin and C_{5+} hydrocarbon selectivities increased while light paraffin selectivity decreased with the decrease in H_2/CO ratio. This is consistent with previous results on cobalt based catalysts [31] and also on K-Co-Mo- Al_2O_3 catalysts [32], where the light olefin selectivity (CO_2 free selectivity) increased from 1.1% to 3.1% when H_2/CO ratio decreased from 1 to 0.1. Higher hydrogen fraction in the feed gas leads to higher CO hydrogenation [29].

The CO conversion and product selectivity in the catalytic test with H_2/CO ratio = 1 are plotted as a function of time on stream in Figure 5-17. The CO conversion is maintained at

about 20%. Methane, light paraffin and C₂-C₄ olefin selectivities attain their steady state after 17 h time on stream. Carbon dioxide selectivity remains stable with time on stream. These results demonstrate that at a ratio H₂/CO = 1, the catalytic performance could keep stable within 60 h time on stream.

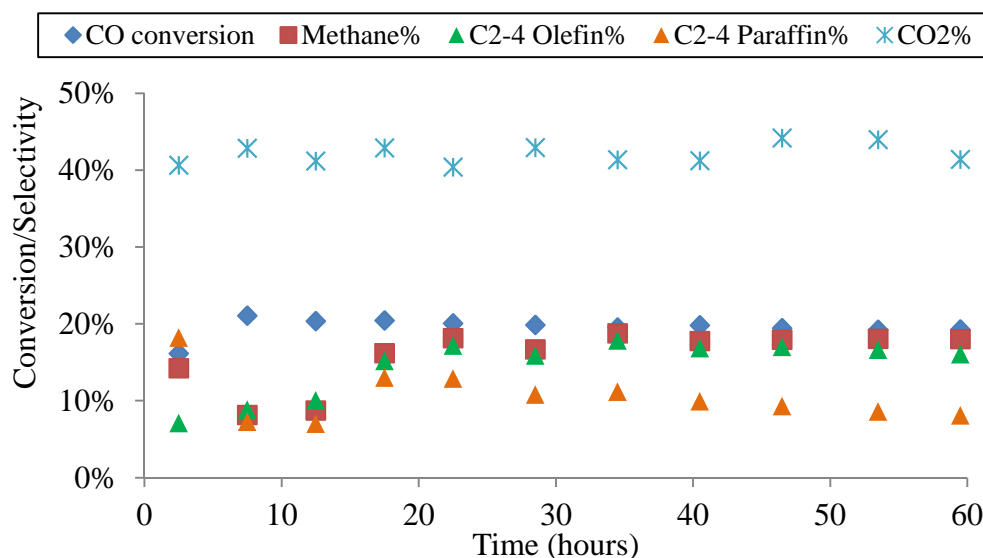


Figure 5-17: Catalytic performance on 15K15M catalyst, at P = 20 bar, T = 360°C, H₂/CO ratio = 1, GHSV = 2100 h⁻¹

V Discussion and conclusion

The obtained results have revealed a strong influence of potassium content in alumina supported catalysts on the structure of molybdenum phases and their performance in carbon monoxide hydrogenation.

At low potassium content, mainly molybdenum oxide and sulphides are observed, while at high potassium content, mixed phases of K-Mo, Mo-Al and K-Mo-Al are clearly identified (by XRD, LRS and XPS). Those phases are summarized in Table 5-8 for Mo/Al₂O₃ and some K promoted catalysts.

Table 5-8: Species on catalysts calcined and sulphide $\text{Mo}/\text{Al}_2\text{O}_3$ catalysts and K promoted catalysts (according to XRD and XPS results)

Catalysts	After calcination			After sulphidation			
	Mo oxide	Alkali-Mo Oxides	Alkali-Mo-Al mixed phases	Mo sulphide *	Alkali-Mo sulphides	Mo oxide **	Mo oxy-sulphides ***
15M	MoO_3	-	$\text{Al}_2(\text{MoO}_4)_3$	MoS_2 (87.0%)	-	9.1%	Low (3.9%)
3K_15M	MoO_3	-	$\text{Al}_2(\text{MoO}_4)_3$	MoS_2 (76.8%)	-	14.3%	High (8.9%)
15K_15M	MoO_3	K_2MoO_4 $\text{K}_2\text{Mo}_4\text{O}_6$	$\text{Al}_2(\text{MoO}_4)_3$ $\text{KAl}(\text{MoO}_4)_2$	MoS_2 (69.7 %)	K_2MoS_4 KMoS_2	17.1%	High (13.2%)
24K_15M	MoO_3	K_2MoO_4 $\text{K}_2\text{Mo}_4\text{O}_6$	$\text{Al}_2(\text{MoO}_4)_3$ $\text{KAl}(\text{MoO}_4)_2$	MoS_2 (80.2 %)	K_2MoS_4 KMoS_2	9.4%	High (9.4%)

*: The quantity of MoS_2 was determined by XPS. This phase could be presented by Mo^{4+} specie.

** : The quantity of Mo oxide was determined by XPS. This phase could be presented by Mo^{6+} specie

***: The quantity of Mo oxysulphides was determined by XPS. This phase could be presented by Mo^{5+} specie.

The XPS results shows a relatively high fraction of Mo^{4+} species (>0.75) probably associated to MoS_2 species. The catalytic data suggest that non-promoted molybdenum sulphide does not produce any noticeable concentration of alcohols and olefins. Indeed, the selectivity to long-chain hydrocarbons and alcohols was very low on the unpromoted alumina supported molybdenum catalyst [33]. In agreement with previous reports [3,34,35], it can be concluded that the active sites associated with molybdenum sulphide are not active for olefin and alcohol synthesis.

The increase in potassium content results in a higher fraction of Mo^{5+} and Mo^{6+} species associated to mixed K-Mo sulphide and molybdenum oxysulphides (MoO_xS_y). Woo et al [36] indicated that the oxidized $\text{K}_2\text{CO}_3/\text{MoS}_2$ catalyst i.e. with a significant amount of Mo^{6+} , produces mostly hydrocarbons while the catalyst containing mostly Mo^{4+} produces mainly alcohols. Those results are not consistent with our results. Indeed, the hydrocarbons and alcohols are not mainly produced with the catalyst which exhibits highest fractions of Mo^{6+} or Mo^{5+} species. Figure 5-12 shows that olefins and alcohol production rates decrease at high

potassium contents. These species are not favourable for carbon monoxide hydrogenation.

According to TEM images, the MoS_2 dispersion was lower on the K promoted catalysts compared to the unpromoted catalyst. Jiang et al [37] reported that MoS_2 particles with longer slab should be assigned to the well-crystallized MoS_2 which should be less active than smaller MoS_2 particle size. Yoosuk et al [38] and Ferrari et al [39] suggested that if promoters were very well incorporated within MoS_2 at higher potassium content, the particle size would become smaller. Those results are in agreement with our results. The 15K_15M catalyst with larger particle size is the more active catalyst for olefins and alcohols production. When potassium is added in a high content (24K_15M catalyst), we observed a decreased in the particle size and consequently, a decrease in the olefin selectivity.

Figure 5-18 shows the relation between selectivity to $\text{C}_2\text{-C}_4$ olefins and MoS_2 particle size contribution. With large MoS_2 particle, especially with higher slab length, the light olefin selectivity is higher. The smaller MoS_2 particles were believed to participate more in hydrogenation reaction because they exhibited more corner site that was the active site for hydrogenation [40,41]. This is not convenient for olefin synthesis because with a high hydrogenating ability, the olefin could be easier hydrogenated to paraffin.

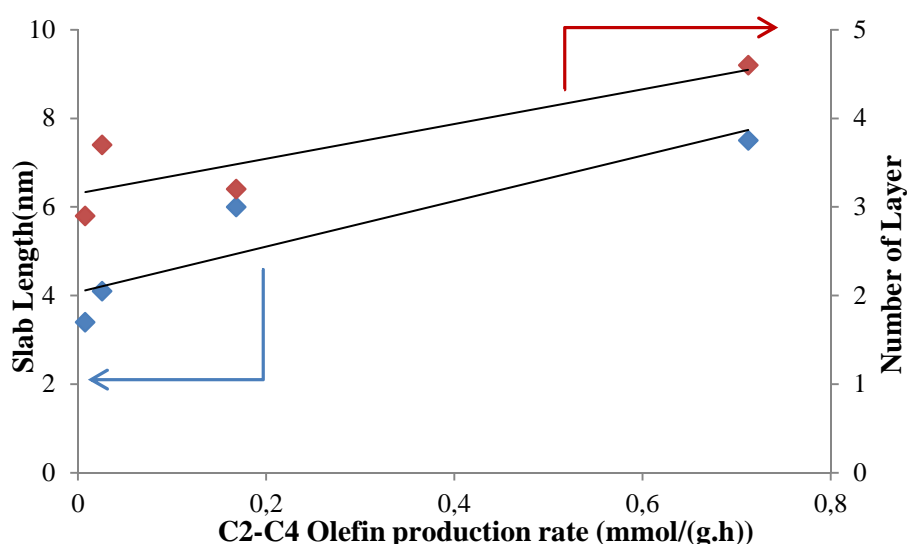


Figure 5-18: Light olefin productivity with the function of MoS_2 particle size contribution (number of layer and slab length)

Potassium promotion also has a strong impact on the catalyst basicity. Bian et al. [42]

demonstrated that when the sample possesses a strong acidity, the selectivity to mixed alcohols was low, while with a weak acidity, the selectivity to mixed alcohols became high.

The catalyst basicity could be an important parameter which would affect the rate of secondary reactions such as re-adsorption and hydration of olefins or oxygenated products [43]. In our catalysts, the mixed phases K-Mo-S seem to provide active sites for olefin and alcohol synthesis, however when the catalyst basicity is too high, a change in selectivity can be observed: less light olefins and paraffins are produced for the benefit of C₅₊ hydrocarbons.

Interestingly, higher GHSV, lower reaction pressure and lower H₂/CO ratio in syngas feed could be favorable for light olefin synthesis. Our data also showed that production of olefins and oxygenates coincided with appearance of methanethiol, ethanethiol and dimethyl sulphide on the catalysts with high potassium content (Table 5-6, Table 5-7). This indicates that similar active species are involved in both alcohol and thiol synthesis on promoted MoS₂ catalysts.

Interestingly, the data show a correlation between formation of the mixed species in the calcined and sulphided catalysts. Indeed, strong interaction between molybdenum and potassium already occurs at the stage of catalyst calcination and leads to mixed K-Mo oxides [44]. This interaction further governs the catalyst phase composition and catalytic performance [34]. XRD patterns did not show any detectable concentration of MoO₃ in the calcined K-promoted catalysts. MoO₃ readily converts into mixed K-Mo oxides after addition of relatively small amounts of potassium, when K content became high (K/Mo molar ratio > 2.5), MoO₃ cannot be detected any longer. The presence of potassium results also in formation of Mo-Al and K-Al-Mo mixed phases. The mixed Mo-K oxides are then converted in the presence of H₂S into mixed sulphide species. XRD shows that even mixed Mo-Al and K-Mo-Al oxides can be partially converted into molybdenum sulphides in the presence of H₂S.

Potassium addition affected the size of molybdenum species. In our work, on calcined catalysts Mo/Al₂O₃ catalysts with high potassium content were more favorable for alcohol selectivity, while the MoO₃ particle size decreased with addition of K promoter. This result agreed with the publication of A. Tavasoli et al. [45] who reported that on K-MoS₂ based

catalysts, a large particle size of MoO₃ was favorable for hydrocarbon selectivity while a small size was favorable for alcohol selectivity.

Comparison of the catalyst data with characterisation indicates a major role of mixed K-Mo sulphides in synthesis of olefins and alcohols on the K-promoted molybdenum catalysts.

The methanol selectivity increases with conversion on the catalysts with low molybdenum content, while it drops on the 15K15Mo/Al₂O₃ and 24K15Mo/Al₂O₃ catalysts. This suggest that methanol can be involved in secondary reaction on the catalyst with higher molybdenum content such as hydrogenation to methane or synthesis of olefins and C₂₊ alcohols. While promotion with potassium has a beneficial effect on the olefin and alcohol synthesis, the olefin and methanol production rates drop however at higher potassium contents.

Figure 5-12 shows simultaneous evolution of methanol, C₂-C₄ olefins and ethanol selectivity as function of the potassium content in the catalysts reaches 6 wt. %. At the same time, the methane selectivity has been significantly reduced at higher potassium loadings. The appearance of olefin and alcohols coincides with detection of mixed K-Mo-S species.

Comparison between alumina and CNT supported promoted MoS₂ catalysts

It is interesting to compare the performance of alumina supported and CNT supported K-promoted molybdenum sulphide catalysts. CNT supported catalyst were found to be less active than alumina supported counterparts (see in Figure 5-19). Lower activity of CNT catalyst can be attributed to the lower extent of sulphidation. MoO₂ could be detected by XRD and H₂-TPR after the sulphidation in the CNT supported catalysts. MoO₂ seems to be more difficult to be sulphided than MoO₃. Lower extent of sulphidation seems to be the major reason of lower activity of MoS₂/CNT catalysts. Note that this MoO₂ phase has not been detected in the catalyst synthesized on alumina support. The activity of both catalysts decreases with increase in potassium content. This can be due to the increase in molybdenum sulphide particle; with higher K content and the effects of potassium on the MoS₂ electronic structure.

The methane was produced on the MoS₂ phase; light olefin, alcohol and heavy hydrocarbon were produced on K-Mo sulphides. The variation of light olefin productivity with different K/Mo atomic ratio is shown in Figure 5-20.

The catalysts supported on both supports show a wave crest for the dependence of olefin productivity as function of potassium content. The optimal K/Mo ratio for production of C₂-C₄ olefins was found to be at 2.5 on alumina support, whereas this optimal ratio was 1.5 on CNT support. For catalysts supported on alumina or CNT, addition of potassium leads to the increase in the catalyst basicity. Potassium could interact with Al₂O₃ and form K-Mo-Al mixed phases. This suggests that on Al₂O₃ supported catalysts, a part of added potassium reacts with the support compared to CNT supported catalysts, and these K promoters did not take part in the FTS. Hence, more potassium needed to obtain an optimum in light olefin productivity. With an excess of potassium addition, a high fraction of potassium sulphides forms during the sulphidation step. Also, with alumina support, potassium could interact and form K-Mo-Al mixed phases. These phases lead to extra basicity and this is harmful for light olefin synthesis.

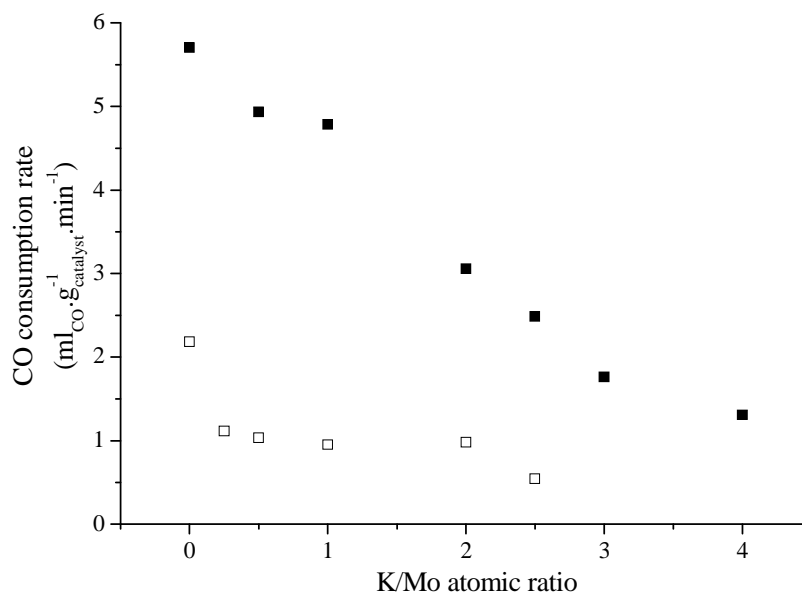


Figure 5-19: Reaction rate on $\text{MoS}_2/\text{Al}_2\text{O}_3$ and MoS_2/CNT catalysts with different K/Mo ratio (■ Al_2O_3 supported catalysts □ CNT supported catalysts)

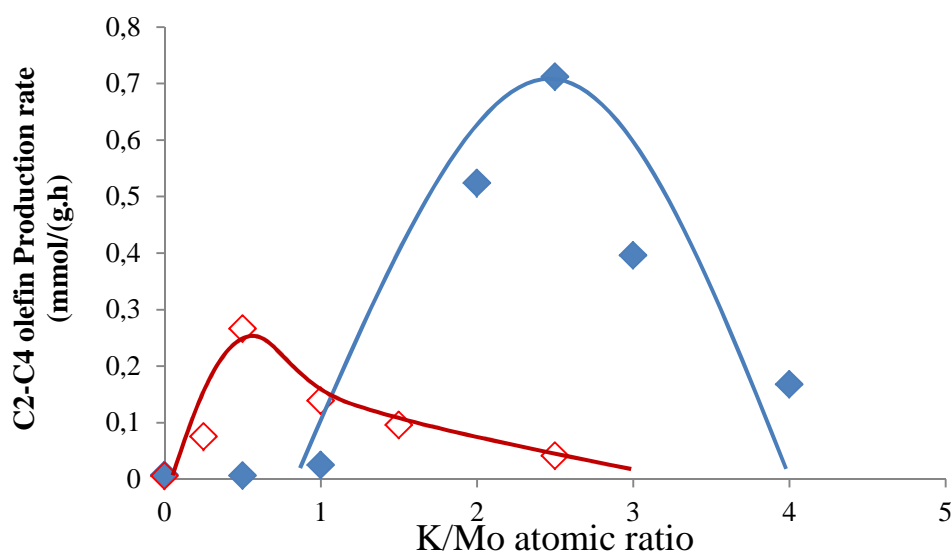


Figure 5-20: Formation rate of light olefin on $\text{MoS}_2/\text{Al}_2\text{O}_3$ and MoS_2/CNT catalysts with different K/Mo ratio (◆ Al_2O_3 supported catalysts ◇ CNT supported catalysts)

The catalyst basicity and acidity can be also modified by using different potassium precursors (potassium chloride, sulphate...). The following chapter focus on the effects of different alkali promoters and precursors on the structure and performance of $\text{MoS}_2/\text{Al}_2\text{O}_3$ catalysts.

Reference

- [1] J. Wang, P.A. Chernavskii, A.Y. Khodakov, Y. Wang, *J. Catal.* 286 (2012) 51
- [2] A. Jean-Marie, A. Griboval-Constant, A.Y. Khodakov, F. Diehl, *CR Chimie* 12 (2009) 660
- [3] M. Jiang, G. Bian, Y. Fu, *J. Catal.* 146 (1994) 144
- [4] O. Gutierrez, C. Kaufmann, J. Lercher, *ChemCatChem*, 3 (2011) 1480
- [5] Z. Li, Y. Fu, M. Jiang, *Appl. Catal. A: General*. 187 (1999) 187
- [6] G. Bian, L. Fan, Y. Fu, K. Fujimoto, *Appl. Catal. A: General*. 170 (1998) 255
- [7] A. Tavasoli, S. Karimi, M. Davari, N. Nasrollahi, T. Nematian, *J. Ind. Eng. Chem.* 20 (2014) 674
- [8] Z. Li, Y. Fu, J. Bao, M. Jiang, T. Hu, T. Liu, Y. Xie, *Appl. Catal. A: General*. 220 (2001) 21
- [9] N. Rueda, R. Bacaud, M. Virnat, *J. Catal.* 169 (1997) 404
- [10] L. Liang and V. Meunier, *Nanoscale*. 6 (2014) 5394
- [11] J. Liu, E. Wang, J. Lv, Z. Li, B. Wang, X. Ma, S. Qin, Q. Sun, *Fuel Process. Technol.* 110 (2013) 249
- [12] Th. Weber, J. Muijsers, J. van Wolput, C. Verhagen, J. Niemantsverdriet, *J. Phys. Chem.* 100 (1996) 14144
- [13] J. Hensley, S. Pylypenko, D. Ruddy, *J. Catal.* 309 (2014) 199
- [14] A. Chen, Q. Wang, Q. Li, Y. Hao, Y. Yang, *J. Mol. Catal. A: Chem.* 283 (2008) 69
- [15] L. Benoist, D. Gonbeau, G. Pfister-Guillouzo, E. Schmidt, G. Meunier, A. Levasseur, *Thin Solid Films* 258 (1995) 110
- [16] J. Iranmahboo, D. Hill, H. Toghiani, *Appl. Surface Sci.* 185 (2001) 72
- [17] G. Schrader, C. Cheng, *J. Catal.* 80 (1983) 369
- [18] J. Zhang, Y. Wang, C. Liu, *Appl. Catal. A: General*. 126 (1995) 219
- [19] H. Toulhouat, S. Kasztelan, in: M.J. Phillips, M. Ternan (Eds.), *Proceedings, 9th International Congress on Catalysis, Calgary (vol.1: Chem.)* Institute of Canada, Ottawa, 1988, pp. 152-153
- [20] H. Matte, A. Gomathi, A. Manna, D. Late, R. Datta, S. Pati, C. Rao, *Angew. Chem. Int. Ed.* 49 (2010) 4059
- [21] V. Surisetty, A. Tavasoli, A. Dalai, *Appl. Catal. A: General* 365 (2009) 243
- [22] J. Yang, G. Jacobs, T. Jermwongratanachai, V. Pendyala, W. Ma, D. Chen, A. Holmen, B. Davis, *Catal. Lett.* 144 (2014) 123
- [23] M. Feyzil, A. Mirzaei, *J. Fuel Chem. Technol.* 40 (2012) 1435
- [24] Rostam J Madon and E Iglesia, *J. Catal.* 139 (1993) 576-590
- [25] G. Quarderer, G. Cochran, *Eur. Patent No.* 0119609 (1984).
- [26] J. Iranmahboob, D.O. Hill, *Catal. Lett.* 78 (2002) 1
- [27] J. van de Loosdrecht, *Comprehensive Inorganic Chemistry II: From Elements to Applications*. Oxford: Elsevier; (2013) p528
- [28] T. Park, I. Nam, Y. Kim, *Ind. Eng. Chem. Res.* 36 (1997) 5246
- [29] S. Chiang, C. Chang, J. Shie, C. Chang, D. Ji, J. Tseng, C. Chang, Y. Chen, *Energies*. 5 (2012) 4147
- [30] V. Surisetty, A. Dalai, J. Kozinski, *Energy Fuel*. 24 (2010) 4130
- [31] H. Beuther, C. Kibby, T. Kobylinski, R. Pannell, *U.S. Patent*, 4,399,234 (1983).
- [32] C. Jakob, J. Peter, J. Anker, *Ind. Eng. Chem. Res.* 50 (2011) 7949-7963
- [33] B. Wang, Y. Yao, M. Jiang, Z. Li, X. Ma, S. Qin, Q. Sun, *J. Energy Chem.* 23 (2014) 35
- [34] M. Jiang, G. Bian, Y. Fu, *J. Catal.* 146 (1994) 144
- [35] N. Koizumi, G. Bian, K. Murai, T. Ozaki and M. Yamada, *J. Mol. Catal. A: Chem.* 207 (2004) 173
- [36] H. Woo, Y. Kim, I. Nam, J. Chung, J. Lee, *Catal. Lett.* 20 (1993) 221-229
- [37] M. Jiang, B. Wang, J. Lv, H. Wang, Z. Li, X. Ma, S. Qin, Q. Sun, *Appl. Catal. A: General* 466 (2013) 224
- [38] B. Yoosuk, J. Kim, C. Song, C. Ngamcharussrivichai, P. Prasassarakich, *Catal. Today*.

130 (2008) 14

[39] D. Ferrari, G. Budroni, L. Bisson, N. Rane, B. Dickie, J. Kang, S. Rozeveld. *Appl. Catal. A: General.* 462-463 (2013) 302

[40] E. Hensen, P. Kooyman, Y. van der Meer, A. van der Kraan, V. de Beer, J. van Veen, R. van Santen. *J. Catal.* 199 (2001) 224

[41] Y. Sakashita, Y. Araki, H. Shimada. *Appl. Catal. A: General.* 215 (2001) 101

[42] G. Bian, Y. Fu, Y. Ma, *Appl. Catal. A: General* 170 (1998) 255

[43] E. Lowenthal, S. Schwarz, H. Foley. *Catal. Today.* 51 (1999) 187

[44] H. Woo, J. Kim, I. Nam, J. Lee, J. Chung, Y. Kim. *Appl. Catal. A* 104 (1993) 199-

[45] A. Tavasoli, S. Karimi, M. Davari, N. Nasrollahi, T. Nematian. *Journal of Industrial and Engineering Chemistry.* 20 (2014) 674

Chapter Six

Effects of different alkali promoters and precursors on the structure and performance of $\text{MoS}_2/\text{Al}_2\text{O}_3$ catalysts

Summary

<u>I Introduction</u>	176
<u>II Alumina supported molybdenum sulphide catalysts promoted with different alkali metals</u>	177
II-1 Characterization	177
<i>II-1-1 XRD</i>	177
<i>II-1-2 XPS</i>	181
<i>II-1-3 H₂-TPR</i>	185
<i>II-1-4 CO₂-TPD</i>	188
<i>II-1-5 TEM</i>	187
II-2 Catalytic test	190
<i>II-2-1 Catalytic performance for CO hydrogenation</i>	190
<i>II-2-2 Concentration of sulphur compounds in catalytic tests</i>	191
II-3 Discussion	193
<u>III Alumina supported molybdenum catalysts promoted with different potassium precursors</u>	196
III-1 Characterization	196
<i>III-1-1 XRD</i>	196
<i>III-1-2 XPS</i>	198
<i>III-1-4 CO₂-TPD</i>	202
<i>III-1-5 TEM</i>	203
III-2 Catalytic test	206
<i>III-2-1 Catalytic performance for CO hydrogenation</i>	206
<i>III-2-2 Distribution of sulphur containing products</i>	207
III-3 Discussion	208
<u>IV Conclusion</u>	210
<u>Reference</u>	211

I Introduction

In previous chapters we have studied the effect of potassium promotion added from potassium carbonate on the structure and performance of MoS₂/Al₂O₃ catalysts. Note however that other alkali ions can be also used for promotion of MoS₂ based catalysts. It has been shown that different alkali metal promoters led to different alcohol productivity [1,2,3]. Koizumi [4] has compared the yield of C₂₊ alcohol on K or Cs promoted MoS₂ catalysts and has reported that when the atomic ratio of K (or Cs) to Mo was less than 0.2, higher C₂₊ alcohol productivity was observed more on Cs promoted MoS₂ catalysts. Zhang et al [5] has studied Na and K promoted MoS₂ catalysts for methanol synthesis and found that sodium could improve more significantly the yield of methanol than potassium promoter. Woo et al [6] reported selectivity of alcohol on MoS₂ based catalysts followed the order: K > Rb > Cs > Na > Li.

Besides the type of alkali metals, the nature of promoter precursors also affected the catalytic propriety. For potassium promoted MoS₂ catalysts, various kinds of salts were used: KCl [7], K₂SO₄ [8], K₂CO₃ [9,10], KOH [8,11] and CH₃COOK [12] to improve the catalyst alcohols selectivity, while light olefin production has not been reported on these catalysts. It was suggested that the potassium precursor could affect the catalytic behaviour in FT synthesis principally due to the different acidity [7,8]. It has been reported that with K₂CO₃ and CH₃COOK promoter, the catalytic performance (selectivity and catalytic activity) did not present notable difference because the acidity of these two salts is similar [12]. KCl could however inhibit the catalytic activity [7], because of active sites blocking on the catalysts by chlorine ions [13].

This chapter focuses on the structure and performance of the catalysts prepared by molybdenum impregnation on alumina followed by addition of the different alkali promoters. In addition to potassium, cesium and sodium were used as promoters. Precursors of Na and Cs promoters were carbonates (Na₂CO₃, Cs₂CO₃). The catalysts have been synthesized in order to maintain similar atomic ratio alkali/Mo for all the catalysts. The second part of this Chapter 6 addresses use of different potassium precursors for promotion of supported

molybdenum sulphide catalysts. The K_Mo catalysts have been promoted using potassium carbonate, sulphate or hydroxide (K₂CO₃, K₂SO₄, KOH).

The molybdenum content in the catalysts was kept at 15 wt.%. In the Chapter 5, we suggest that the light olefin productivity could be obtained with atomic ratio of K/Mo = 2.5. Hence, for MoS₂/Al₂O₃ catalysts with different promoters/precursors, the same atomic ratio was employed. The weight content depends however on the promoter molar weight. For sodium promoted catalysts, the Na content was 9 wt.% (9%Na15%Mo, labeled as 9Na15M), and for cesium promoted catalysts the Cs loading was 52 wt.% (52%Cs15%Mo, labeled as 52Cs15M). The potassium content was always 15 wt.% in all catalysts studied in this Chapter. The MoS₂/Al₂O₃ catalysts promoted with K₂CO₃, K₂SO₄ and KOH are labeled as 15K15M, 15K15M(S) and 15K15M(H). The catalytic tests were realized in milli-fixed bed reactor under the following conditions: temperature = 360°C, pressure = 20 bar, GHSV = 2100 h⁻¹ and ratio H₂/CO = 2. The catalysts were characterized by XRD, XPS, H₂-TPR, CO₂-TPD and TEM.

II Alumina supported molybdenum sulphide catalysts promoted with different alkali metals

II-1 Characterization

II-1-1 XRD

Calcined catalyst: The XRD pattern of 9Na15M, 15K15M and 52Cs15M catalysts are displayed in Figure 6-1. The calcined catalyst showed the presence of molybdenum oxide and mixed K-Mo oxide species. The MoO₃ phase was detected in the 15K15M catalyst using the following peaks: $2\theta = 11.97^\circ, 25.70^\circ, 27.35^\circ, 33.73^\circ, 38.98^\circ$ (JCPDF 05-0508). In this catalyst, K-Mo mixed phases are also observed as K₂MoO₄ (JCPDF 29-1011, $2\theta = 18.87^\circ, 26.27^\circ, 30.65^\circ, 39.42^\circ, 45.83^\circ$) and K₂Mo₄O₆ (JCPDF 87-0730, $2\theta = 13.08^\circ, 17.07^\circ, 25.49^\circ, 27.47^\circ$,

30.15°). The catalysts also showed the presence of the phases arising from interaction of Mo/K with the alumina support: Al₂(MoO₄)₃ (JCPDF 85-2286, 2θ = 20.84°, 22.15°, 23.14°, 30.79°, 32.10°) and KAl(MoO₄)₂ (JCPDF 74-2008, 2θ = 22.36°, 31.40°, 32.26°, 51.97°). Despite of the presence of all those different phases, some diffraction peaks were attributed to K₂CO₃ (JCPDF 87-0730, 2θ = 12.98°, 29.19°, 37.54°, 46.32°). This indicates that the precursor has not been completely decomposed in the catalyst.

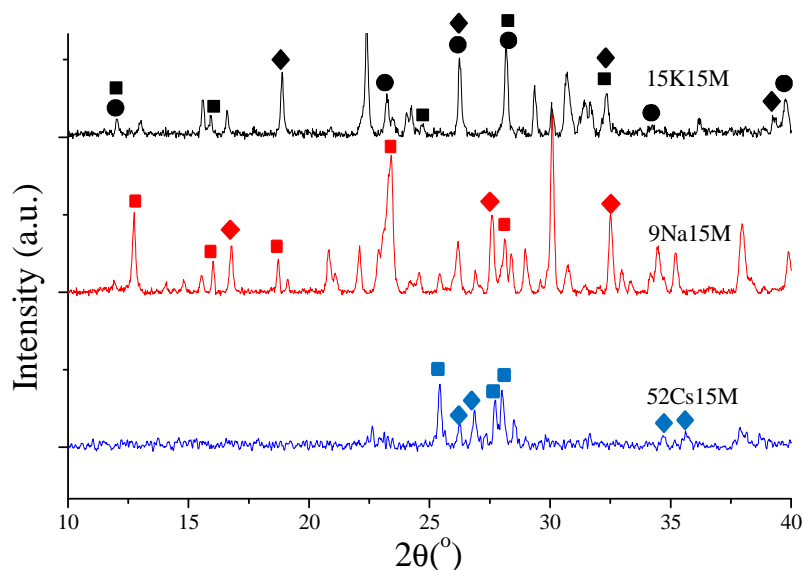


Figure 6-1: XRD pattern of calcined MoS₂/Al₂O₃ catalysts promoted by different alkali metals. ● MoO₃ ■ K₂Mo₄O₆ ◆ K₂MoO₄ ■ Na₂Mo₂O₇ ◆ Na₂MoO₄ ■ Cs₂Mo₅O₁₆ ◆ Cs₂MoO₄

The 9Na15M catalyst also exhibits the presence of the MoO₃ phase and mixed phases. The Na-Mo mixed oxide phases were detected such as Na₂MoO₄ (JCPDF 12-0773, 2θ = 16.84°, 27.68°, 32.58°, 48.96°, 57.14°) and Na₂Mo₂O₇ (JCPDF 73-1797, 2θ = 12.02°, 16.13°, 18.83°, 23.54°, 28.33°, 29.12°). Na-Mo-Al₂O₃ mixed phases on 9Na15M catalyst can be detected, such as Al₂(MoO₄)₃ and NaAl(MoO₄)₂ (JCPDF 54-0243, 2θ = 22.90°, 23.36°, 32.56°, 33.00°, 45.74°). The XRD patterns also showed the presence of residual Na₂CO₃ (JCPDF 19-1130, 2θ = 26.03°, 27.59°, 30.15°, 33.02°, 34.20°, 35.24°, 38.02°, 39.97°, 41.50°, 48.27°, 46.54°).

Interestingly, MoO₃ phase was not observed by XRD in the 52Cs15M catalyst. High molybdenum dispersion could be one of the reasons of low intensity of MoO₃ phase on the XRD patterns. The following Cs-Mo mixed phases such as Cs₂MoO₄ (JCPDF 24-0276, 2θ =

26.03°, 26.75°, 35.45°, 37.97°) and Cs₂Mo₅O₁₆ (JCPDF 70-0861, 2θ = 25.11°, 26.91°, 28.39°, 46.52°) were however detected. The catalyst also showed the presence of Mo-Al and Cs-Al mixed oxides such as Al₂(MoO₄)₃ and Cs₈Al₂O₆ (JCPDF 80-1522, 2θ = 23.11°, 23.64°, 24.59°, 26.21°, 31.68°, 38.36°). The calcined catalyst also showed the presence of diffraction peaks related to Cs₂CO₃ (JCPDF 87-0730, 2θ = 12.98°, 29.19°, 37.54°, 46.32°), indicating that the precursor has not been completely decomposed in the catalyst.

Sulphided catalysts: The XRD patterns of the sulphided 15wt.% Mo catalysts promoted K₂CO₃, Na₂CO₃ and Cs₂CO₃ are present in Figure 6-2.

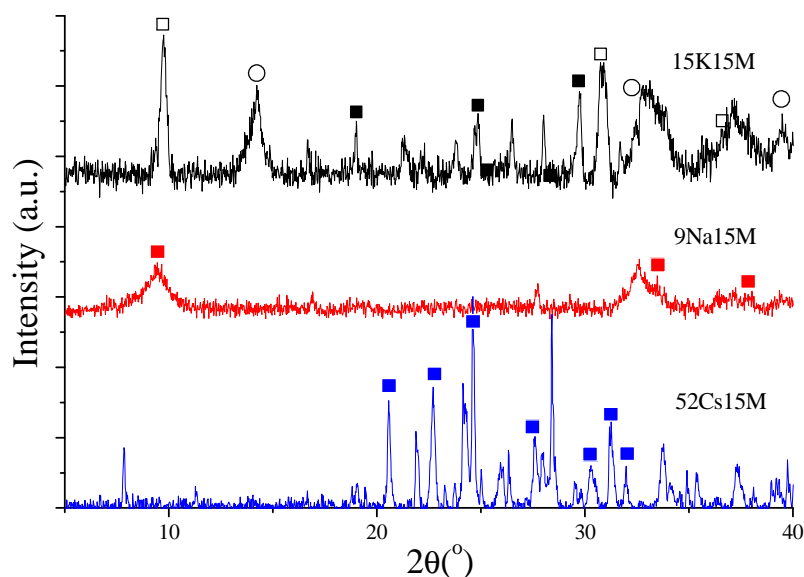


Figure 6-2: XRD pattern of sulphided MoS₂/Al₂O₃ catalysts promoted by different alkali metals. ○MoS₂ □KMoS₂ ■K₂MoS₄ ■NaMoS₂ ■Cs₂MoS₄

The MoS₂ XRD patterns were detected on the 15K15M catalyst, while the 9Na15Mo or 52Cs15M catalysts do not show any XRD peaks attributed to MoS₂. This result can signify that MoS₂ is highly dispersed on sodium and cesium promoted catalysts.

Different alkali and mixed alkali-sulphide phases have been detected in the three catalysts:

- mixed K₂MoS₄ and KMoS₂ as well as potassium sulphides (K₂S and K₂S₃) and potassium sulphate (K₂SO₄ and K₂S₃O₆) were detected in the XRD pattern of 15K15M catalyst,

- the NaMoS₂ (JCPDF 18-1257, 2θ = 9.76°, 33.80°, 38.61°, 43.25°, 56.14°) mixed sulphide phase were present in the XRD pattern of 9Na15M catalyst. Also, sodium sulphide such as Na₂S phase (JCPDF 47-0178, 2θ = 7.83°, 29.02°, 34.69°, 36.81°, 37.74°) and sodium sulphate Na₂SO₄ (JCPDF 83-1570, 2θ = 22.63°, 23.60°, 31.82°) were observed in the XRD patterns.

- The XRD pattern of 52Cs15M catalyst showed the presence of two mixed cesium-molybdenum sulphides: Cs₃MoS₃ (JCPDF 75-1287, 2θ = 11.01°, 29.41°) and Cs₂MoS₄ (JCPDF 85-0179, 2θ = 20.51°, 22.61°, 24.21°, 24.55°, 27.51°, 27.90°, 30.19°, 31.20°, 33.64°). Various Cs sulphide phases were also found: Cs₂S₅ (JCPDF 84-0286, 2θ = 13.90°, 18.65°, 20.44°, 28.62°, 30.06°), Cs₂S (JCPDF 31-0375, 2θ = 26.00°, 27.94°), Cs₂SO₄ (JCPDF 44-0065, 2θ = 24.12°, 27.10°, 28.28°, 28.48°) and Cs₂S₂O₆ (JCPDF 15-023, 2θ = 22.26°, 28.05°, 42.26°).

The Cs or Na promoted catalysts also showed XRD peaks corresponding to residual Mo oxides while on K promoted catalysts those phases are not observable. On sodium promoted MoS₂ catalyst (Na_xMoS₂/Al₂O₃), the Na₂MoO₄ (JCPDF 12-0773, 2θ = 16.84°, 27.68°, 32.58°, 52.12°, 57.14°) oxide phase was detected. The Cs_xMoS₂/Al₂O₃ catalyst exhibited various oxides phases: MoO₂ (JCPDF 032-0671, 2θ = 26.03°, 37.02°, 37.93°, 53.04°, 53.51°, 53.97°, 60.20°, 66.66°), Mo₉O₂₅ (JCPDF 81-1263, 2θ = 22.72°, 24.61°, 31.85°, 33.80°) and Mo₉O₂₆ (JCPDF 65-1292, 2θ = 22.04°, 25.80°, 25.94°).

According to Weber et al [14], the MoO₃ sulphidation proceeds via reduction of Mo⁶⁺ to Mo⁴⁺. Molybdenum in the oxidation state (+4) is then sulphided to MoS₂. In this case MoO₂, Mo₉O₂₅ and Mo₉O₂₆ can be considered as intermediates of MoO₃ sulphidation. These results seem to demonstrate that with promotion of potassium and sodium, calcined MoO₃/Al₂O₃

catalysts can be well sulphided, but on the 52Cs15M catalyst the sulphidation could be difficult.

II-1-2 XPS

The surface composition of the sulphide molybdenum catalysts promoted by Na, Cs and K is given in Table 6-1. Different elements are detected on the catalyst surface, and their ratio varies as a function of alkali promoters.

Table 6-1: XPS surface atomic ratio in sulphided MoS₂/Al₂O₃ with alkali metal promoters

Catalysts	XPS Atomic Ratio (%)					S/Mo ratio	Alkali/Mo ratio	S/(Mo+Alkali) ratio
	C	S	Al	Alkali	Mo			
9Na15M	3.8	11.1	39.1	4.8	5.9	1.73	0.82	1.04
15K15M	2.8	15.2	19.1	6.2	7.6	2.00	0.82	1.10
52Cs15M	17.7	17.3	16.5	16.7	10.0	1.71	1.66	0.65

On the Na promoted catalyst, the Al atomic concentration is higher than the other elements. This suggests that a significant fraction of alumina surface is not covered by the active phase. Hence, Mo, Na and S are not well dispersed in this catalyst. The ratio of S/Mo is 1.73, which is smaller than the stoichiometric S/Mo ratio in MoS₂ phase. This is probably due to the fact that Mo oxide phase is not easy to convert to sulphide in 9Na15M (as seen in XDR: Na₂MoO₄).

With K promoter, the atomic percentage of Al is smaller than 9Na15M, while Mo and K percentage are higher. This can indicate better dispersion of K and Mo on the catalyst surface. The S/Mo ratio is close to the stoichiometric ratio of MoS₂. It seems that molybdenum is well sulphided in the 15K15M catalysts. The XPS alkali/Mo ratio on 15K15M and 9Na15M catalysts is much smaller than 2.5 which could be expected from the bulk composition. The lower relative concentration of alkali ions detected by XPS can be explained by the formation of bulk mixed phases of alkali metal with the Al₂O₃ support, such as KAl(MoO₄)₂ and NaAl(MoO₄)₂ (both detected by XRD). The alkali ions in these bulk phases might be undetectable by XPS.

In the 52Cs15M catalyst, the XPS atomic concentrations of the alkali metals and Mo are higher compared to 9Na15M and 15K15M catalysts. This indicates that Cs and Mo are better dispersed on the catalyst surface. The S/Mo ratio on 52Cs15M is lower than the stoichiometric ratio. This suggests that molybdenum sulphidation is not complete for this catalyst. Indeed, residual Mo oxide was detected by XRD. The ratio of Cs/Mo was two times higher than Na/Mo and K/Mo, but still smaller than the ratio of the bulk catalyst (2.5). This could be explained by the formation of bulk Cs₆Al₂O₆, detected in XRD patterns. The 52Cs15M catalyst showed also significant surface carbon content, more important than 15K15M and 9Na15M. High carbon ratio on Cs promoted MoS₂ catalyst may be from:

- i) uncompleted carbonate precursor (Cs₂CO₃),
- ii) CO₂ absorbed on 52Cs15M catalysts. Higher CO₂ adsorption can be due to higher catalyst basicity. The basicity of catalysts will be tested using CO₂-TPD, in paragraph II-1-4.

The ratio of S/(Mo+alkali) is presented in Table 6-1. The ratio for 9Na15M and 15K15M catalysts is similar, and always higher than the ratio on the 52Cs15M catalyst.

The Mo3d and S2p XPS spectra of the 9Na15M, 15K15M and 52Cs15M catalysts are shown in Figure 6-3A and Figure 6-3B. On 9Na15M and 15K15M, three-peak envelop of the Mo 3d signal is observed. It can be deconvoluted in three separate overlapping doublets. This suggests that molybdenum is present in three oxidation states: Mo⁴⁺, Mo⁵⁺ and Mo⁶⁺. Interestingly, XPS did not detect Mo⁶⁺ oxidation state for the 52Cs15M catalyst.

The intense binding energy signals at 228.9 eV and 232.1 eV are characteristic of Mo 3d_{3/2} and 3d_{5/2} of the Mo⁴⁺ species [15,16] which are probably associated with MoS₂. The binding energies at 226.2 eV and 233.0 eV are characteristic of S 2s (particularly S²⁻ specie) [14,17]. Some contribution of the Mo 3d XPS spectra could come from Cs. Indeed, an overlapping can be observed because the Cs 4s has a binding energy of 230.0 eV [3].

The binding energies at 232.8 eV and 235.9 eV suggest the presence of Mo⁶⁺ species [15,18], while Mo⁵⁺ is detected from and the binding energy at 230.6 eV and 233.7 eV [19,20]. It is believed that the Mo⁶⁺ and Mo⁵⁺ species could be generated:

- (i) from the passivation step, where molybdenum can be reoxidized by air;

(ii) due to the formation of K₂MoS₄ and Na₂MoS₄ observed by XRD where Mo is present as Mo⁶⁺;

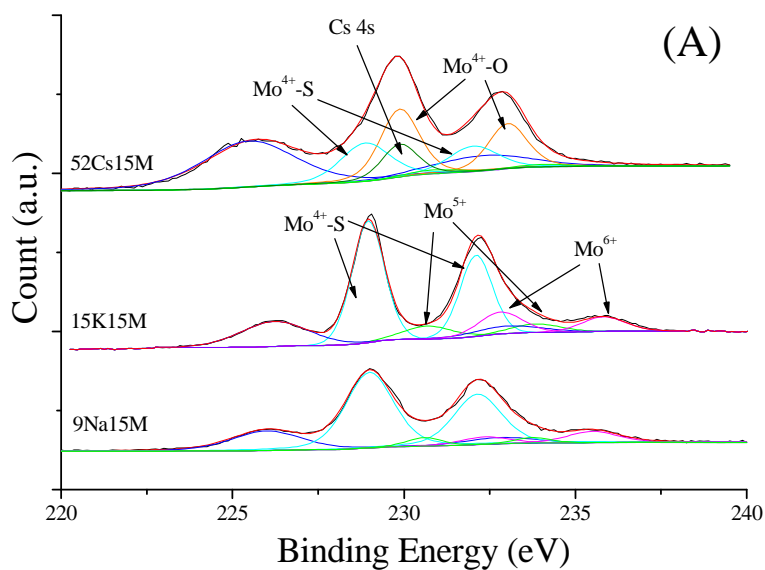
(iii) due to the formation of Mo oxide and Mo oxy-sulphide species of the MoO₂S₂ and MoOS₂ type [19],

(iv) due to the interaction of Mo and alumina leading to Al₂(MoO₄)₃. This compound can be difficult to sulphide.

The Mo⁴⁺ could be present in two kinds of species:

- MoS₂ phase, labeled as Mo⁴⁺-S, found on Na and K promoted MoS₂/Al₂O₃ catalysts (at 228.9eV and 232.1eV);

- MoO₂ phase, labeled as Mo⁴⁺-O at binding energy of 229.9 eV and 233.0 eV, according to the literature [15,21,22]. Note that this phase was also detected by XRD, especially in the 52Cs15M catalyst.



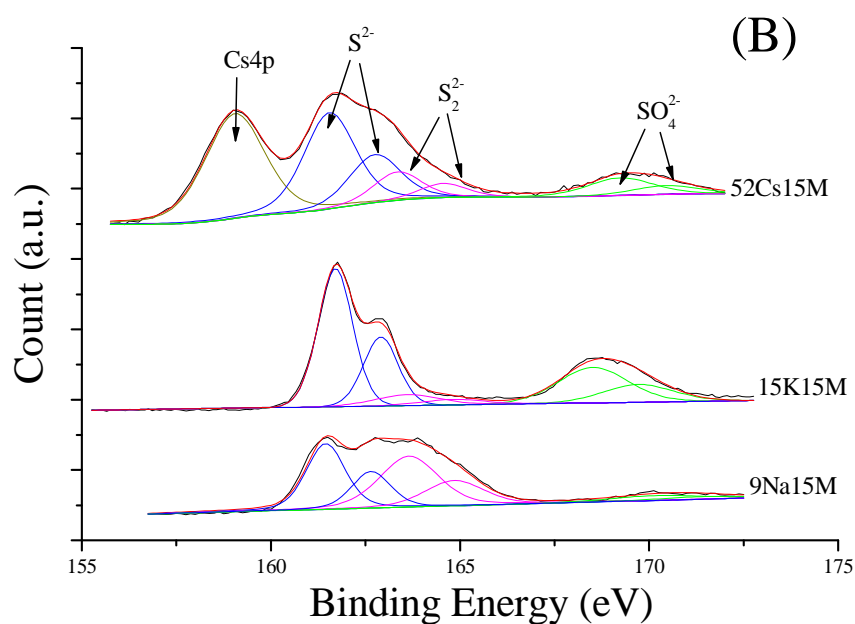


Figure 6-3: XPS spectra of peak decomposition of Mo3d(A) and S2p(B)

The S2p XPS spectra are presented in Figure 6-3B. The spectra show the presence of three different sulphur species in the promoted MoS₂/Al₂O₃ catalysts. The XPS peaks with binding energies of 161.6 eV and 162.8 eV correspond to sulphide ions (S²⁻), which might be present in alkali metal sulphides and/or Mo disulphide (MoS₂, K₂S, Na₂S, Cs₂S). The binding energy around 163.8 eV and 165.0 eV could be assigned to the contribution of poly-sulphide ions (S₂²⁻) in unsaturated Mo sulphide (MoO_xS_y), as well as species such as K₂S₃ and Cs₂S₅ [23], which can be detected by XRD. Additionally, the S 2p XPS spectra exhibit other broad peaks at 168.4 eV and 169.6 eV which can be due to the presence of sulphates (SO₄²⁻). Moreover, on the 52Cs15M catalyst, the peak at 159.1 eV corresponds to Cs 4p binding energy [24].

The concentration of different Mo species or S species is presented in

Table 6-2. The Mo⁴⁺ percentage for the 9Na15Mo catalyst is higher than for the two other promoted catalysts. However, after the distinction between the Mo⁴⁺ binding energies, the percentage of MoO₂ is more important than the one of MoS₂ for the 52Cs15M catalyst. This demonstrates that the sulphidation to MoS₂ on 52Cs15M catalysts is rather incomplete.

Table 6-2: Atomic percentage of different kinds of species for Mo and S

Catalyst	Mo (%)				S (%)		
	Mo ⁴⁺		Mo ⁵⁺	Mo ⁶⁺	S ²⁻	S ₂ ²⁻	SO ₄ ²⁻
	Mo ⁴⁺ -S	Mo ⁴⁺ -O					
9Na15M	80.5	-	6.8	12.7	43.5	48.9	7.6
15K15M	69.7	-	13.2	17.1	57.9	23.7	18.4
52Cs15M	40.1	55.8	4.1	-	66.2	18.3	15.5

For all promoted catalysts, it is observed that the percentage of S²⁻ and S₂²⁻ is much important than the one of SO₄²⁻. The S₂²⁻ phase should correspond to the Mo oxy-sulphides (MoO_xS_y) and poly-sulphides of alkali metal (such as K₂S₃ and Cs₂S₅). The Mo oxy-sulphides can also be associated with the Mo⁵⁺ phase. On 9Na15M and 52Cs15M catalysts, the low percentage of Mo⁵⁺ phase indicates a slow content of MoO_xS_y. The S₂²⁻ species on these two catalysts should be principally constituted by poly-sulphides. The sulphidation however leads to more sulphide species than to polysulphide with the K and Cs promoted catalyst. As explained previously, the SO₄²⁻ could arise from the passivation step. The oxidation is less important when the catalyst is promoted with Na.

II-1-3 H₂-TPR

The results of H₂-TPR for different alkali metal promoted MoS₂ catalysts are presented in Figure 6-4. The H₂ consumptions measured from the TPR profiles are given in Table 6-3. As we have discussed in chapter 4 and chapter 5, the TPR profiles show three H₂ consumption zones for K-MoS₂ catalysts that are respectively attributed to:

- (I) desorption of sulphur on catalysts surface and reduction of amorphous Mo sulphides;
- (II) reduction of K-Mo sulphides and/or K sulphides;
- (III) reduction of crystallized MoS₂.

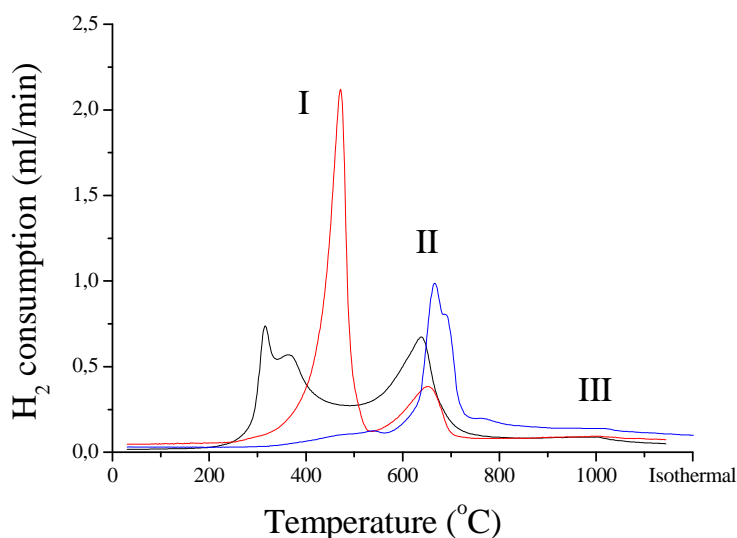


Figure 6-4: H₂-TPR on Alkali/MoS₂ catalysts (black: 15K15M, red: 9Na15M, blue: 52Cs15M)

The TPR profiles in zone I (200-500°C) shows rather different shape on those three catalysts (K, Na and Cs promoted). More hydrogen is consumed in zone I on Na-MoS₂ catalyst (Table 6-3) and the TPR peak shifts to higher temperature (Figure 6-4), compared with the 15K15M catalyst. This is consistent with the paper of Zhang et al [5], who reported that in the K promoted catalyst sulphur desorption on catalysts was smaller than on the Na promoted catalyst. The Cs-MoS₂ catalyst shows a very small reduction peak in this zone I. Toulhouat et al [25] suggested that the low temperature TPR peaks could be related to the hydrogenation of extra sulphur atoms (chemisorbed H₂S or SH groups) or sulphur atoms that are weakly bonded to the catalyst surface. Those easily removable species are adsorbed on low coordinated edge/corner sites, which were believed to be the active sites of the molybdenum catalysts. For the Na-MoS₂ catalyst, the peak attributed to these species shifts to higher temperatures. This suggests a more difficult hydrogenation of the easily removable sulphur atoms, indicating that a part of the active sites might be blocked by sulphur. This should result to a lower catalytic activity with Na promotion.

The K and Na promoted MoS₂ catalysts have a hydrogen consumption peak at similar temperature in zone II (500-800°C). With 52Cs15M catalyst, the hydrogen consumption peak shifts to higher temperature. According to the literature [5,25], the H₂ consumption at

600-800°C in zone II should be due to the mixed phase of alkali sulphides and/or alkali-Mo mixed sulphides. The phases KMoS₂, K₂MoS₄, NaMoS₂, Cs₃MoS₃ and Cs₂MoS₄ have been clearly identified in XRD patterns. These results are also in agreement with the conclusion of Chapters 4 and 5.

Moreover, the 52Cs15M catalyst shows a slight TPR peak between 750°C-800°C. It is possibly due to the presence of Mo oxide species in Cs-MoS₂ catalyst. These species have been identified from the XRD pattern, such as MoO₂. The reduction of MoO₂ usually takes place at 720-790°C [26]. The reduction of Cs-Mo sulphide phases occurs also at similar temperature region.

Zone III at 1000°C is related to the partial reduction of bulk MoS₂ crystals [25]. The reduction of bulk sulphur occurs generally at the temperatures between 700°C to 1050°C [27]. The maximum temperature for TPR analysis was 1000°C, the reduction of MoS₂ to metallic Mo (0) could be incomplete.

Table 6-3 shows the hydrogen consumption of each zone for all catalyst. The hydrogen consumption in Zone I is the highest on 9Na15M catalyst, while it is the lower on 52Cs15M. The quantity of consumed hydrogen is the contrary for the zone II, where the highest value is obtained for the 52Cs15M catalyst and the lower value is obtained for the 9Na15M. This indicates that the interaction between alkali metals and molybdenum should depend on the nature of alkali metals. The interaction increased with the order of 52Cs15M > 15K15M > 9Na15M.

Table 6-3: H₂ consumption in TPR experiments (mmolH₂/g_{catalyst})

Catalyst	H ₂ consumption in TPR profile		
	Zone I	Zone II	Zone III
9Na15M	3.44	1.24	0.31
15K15M	2.42	2.24	0.42
52Cs15M	0.34	3.07	0.16

II-1-4 CO₂-TPD

Figure 6-5 shows the CO₂-TPD spectra on the different alkali metal promoted MoS₂ catalysts. It is possible to observe two main CO₂ desorption areas:

- at lower temperature (30-300°C) related to weak basic sites of catalysts,
- at higher temperature (400-800°C) related to strong basic sites of the catalysts.

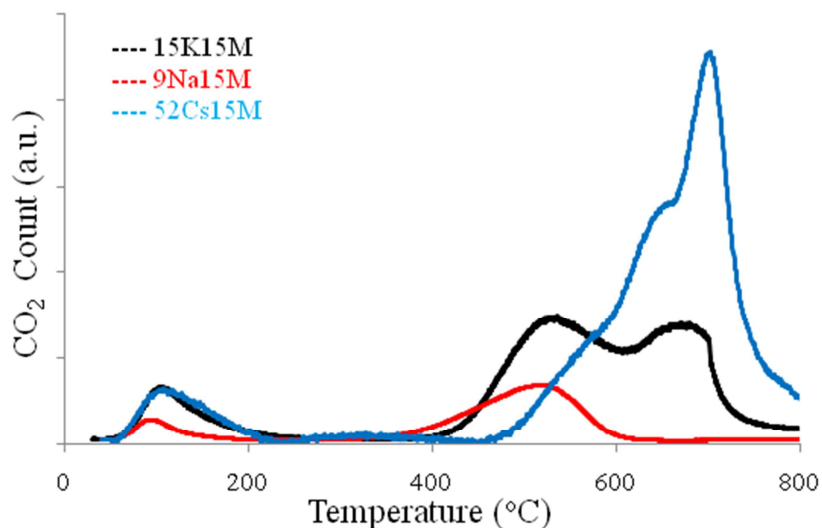


Figure 6-5: CO₂-TPD of sulphided MoS₂ catalysts with Na, K and Cs promoters

For the weak basic sites, the CO₂ desorption is less important in the 9Na15M catalyst than in 15K15M or 52Cs15M. The K and Cs promoted catalysts show rather similar CO₂ desorption profiles. For the strong basic sites, the quantity of CO₂ desorption followed the order: 52Cs15M > 15K15M > 9Na15M. This is also the order for the total basicity of the catalysts. Therefore, the total basicity depends on the basicity of each alkali metal promoter. The more basic is the promoter, the higher basicity exhibits the molybdenum sulphide catalyst.

II-1-5 TEM

Figure 6-6 displays TEM images of MoS₂/Al₂O₃ catalysts promoted by the different promoters. The 9Na15M and 15K15M catalysts show the dark parts in TEM images which can be considered as Mo species. Compared with other elements (K, Na, Al) in catalysts, the

Mo has the highest atomic weight and absorbs more electrons in the TEM. MoS₂ particles which have the form of multilayer sheets can be clearly observed [28].

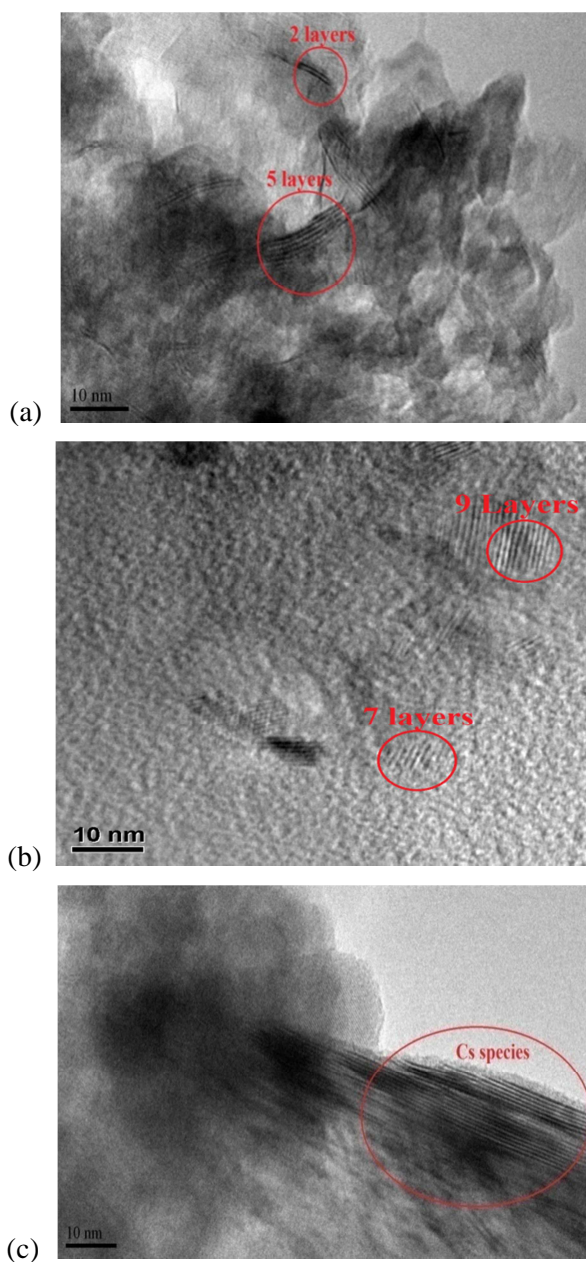


Figure 6-6: TEM images of (a) 9Na15M, (b) 15K15M, (c) 52Cs15M(H)

Note however, that the atomic weight of Cs is even higher than Mo. This makes a clear identification of molybdenum species in the Cs_xMo/Al₂O₃ catalysts. The TEM images of the MoS₂/Al₂O₃ catalysts promoted by Na and K show different MoS₂ particle sizes.

The layer stacking and slab length of MoS₂ particle size distribution were calculated from 20 TEM images for each sample and the results are presented in Figure 6-7.

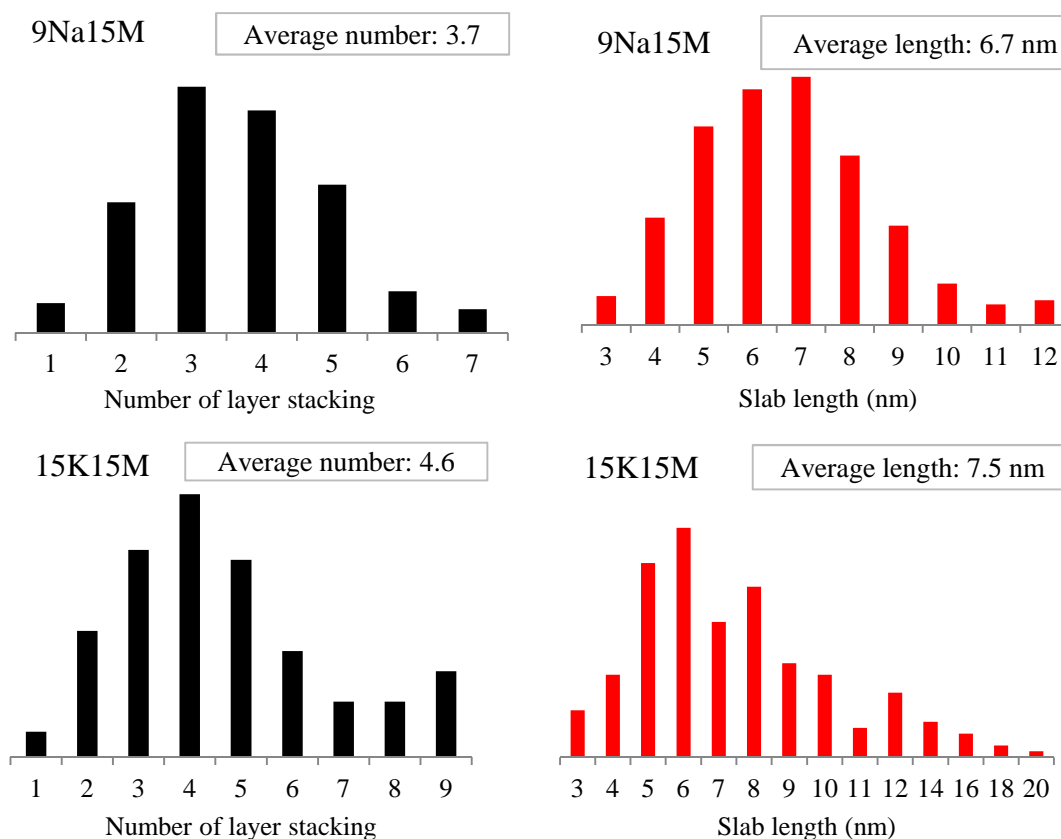


Figure 6-7: MoS₂ particle size distribution of TEM images

The MoS₂ particles are larger in the potassium promoted catalyst than in the sodium promoted catalysts. The MoS₂ particle exhibits a more layer stacking and higher slab length in the 15K15M catalyst. Moreover, there are several extremely large MoS₂ particles (layer number > 8, slab length > 12 nm) detected only in 15K15M catalyst but not in 9Na15M counterpart.

II-2 Catalytic test

II-2-1 Catalytic performance for CO hydrogenation

The results of catalytic test are presented in Table 6-4. The catalytic performance is strongly affected by the used promoter. The most important difference concerns the selectivity

to methane, light olefins, light paraffins and C₅₊ hydrocarbons. The CO₂ and alcohol selectivities remain more or less constant for the different promoted catalysts.

Table 6-4: Catalytic performance of Alkali_MoS₂/Al₂O₃ catalysts

Promoter	CO conversion	CH ₄ %	C ₂₋₄ Olefin%	C ₂₋₄ Paraffin%	MeOH%	C ₂₊ Alcohol%	C ₅₊ HC%	CO ₂ %
Na	17.9%	14.9%	5.7%	21.7%	17.2%	0.4%	1.6%	38.3%
K	21.3%	18.9%	10.7%	15.9%	13.2%	1.9%	6.3%	33.2%
Cs	20.0%	33.0%	0.4%	2.9%	11.7%	0.8%	20.2%	31.0%

The catalytic activity with Na promoted catalyst was less significant than that of Cs or K promoted catalysts which exhibited almost the same activity. The C₂-C₄ paraffins and methanol were more produced and the CO₂ selectivity was also slightly higher, leading to a lower C₅₊ selectivity.

The highest C₂-C₄ olefin selectivity was observed on the 15K15M catalyst. It is notable that for C₂₊ alcohol, the selectivity is also higher on potassium promoted catalysts, than on Na or Cs promoted catalysts.

On the cesium promoted catalyst, both methane and C₅₊ hydrocarbons are the main products formed during the catalytic test. Relatively, selectivity of both olefin and paraffin of C₂-C₄ was much lower on Cs_Mo/Al₂O₃ catalysts. Concerning the alcohol selectivity, mainly methanol was produced, even if the selectivity was lower than with the Na and K promoted catalysts. The light olefin selectivity followed the order K > Na > Cs.

II-2-2 Concentration of sulphur compounds in catalytic tests

During FT catalytic tests, the H₂S present in the gas feed could be also involved in the reaction and produce a number of products [29,30]. The sulphur products detected during the catalytic tests were presented in Figure 6-8. As reported in previous publications [29], hydrogen disulphide could contract with carbon monoxide or methanol to form several sulphur compounds: COS, methanethiol, ethanethiol and dimethyl sulphide. Obviously, the

quantity of these sulphur compounds was different on different alkali metal promoted catalysts.

On the sodium promoted catalyst, COS was the principal sulphur containing product with a small amount of methanethiol and ethanethiol produced.

On the potassium promoted catalyst, the conversion of H₂S was more significant. The concentration of both methanethiol and ethanethiol became higher.

On the 52Cs15M catalyst, the concentration of COS, methanethiol and ethanethiol was similar than on the 15K15M catalyst, but higher concentrations of unreacted H₂S were detected. Hence, the conversion of hydrogen disulphide was not very significant on the cesium promoted catalysts.

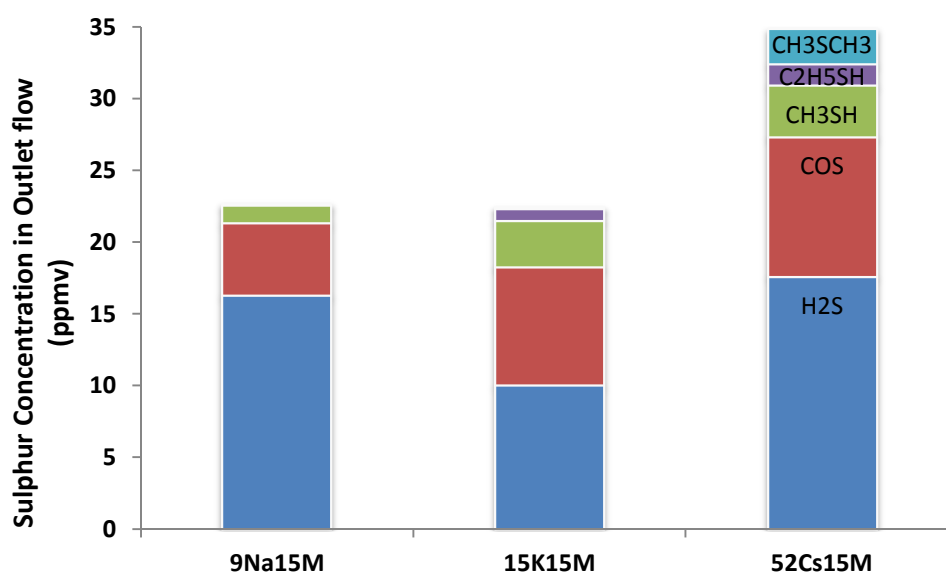


Figure 6-8: Concentration of different sulphur compounds in the reactor outlet on different alkali metal promoted 15 wt.% Mo/Al₂O₃ catalysts.

As reported on potassium promoted MoS₂ catalysts in chapter 5, the production of CH₃SH and C₂H₅SH could occur on the same active site as light olefin/alcohol production. A correlation could be possibly expected between mercaptans and production of long-chain hydrocarbons or oxygenates.

II-3 Discussion

Characterization and catalytic tests suggest that the nature of alkali metal promoter strongly affects the structure and performance of MoS₂ based alumina supported catalysts in CO hydrogenation.

Depending of the alkali promoter, different phases have been observed on the catalyst. Those phases are summarized in Table 6-5.

Table 6-5: Species on catalysts calcined and sulphide Mo/Al₂O₃ catalysts with different alkali metal promoters (according to XRD and XPS results)

Catalysts	After calcination			After sulphidation			
	Mo oxide	Alkali-Mo Oxides	Alkali-Mo-Al mixed phases	Mo sulphide **	Alkali-Mo sulphides	Mo oxide	Mo oxy-sulphides ***
9Na15M	MoO ₃	Na ₂ MoO ₄ Na ₂ Mo ₂ O ₇	Al ₂ (MoO ₄) ₃ NaAl(MoO ₄) ₂	MoS ₂ (80.5%)	NaMoS ₂	-	Low (6.8%)
15K15M	MoO ₃	K ₂ MoO ₄ K ₂ Mo ₄ O ₆	Al ₂ (MoO ₄) ₃ KAl(MoO ₄) ₂	MoS ₂ (69.7%)	K ₂ MoS ₄ KMoS ₂	-	High (13.2%)
52Cs15M	*	Cs ₂ MoO ₄ Cs ₂ Mo ₅ O ₁₆	Al ₂ (MoO ₄) ₃ Cs ₆ Al ₂ O ₆	MoS ₂ (40.1%)	Cs ₃ MoS ₃ Cs ₂ MoS ₄	MoO ₂ (55.8%)	Low (4.1%)

*: MoO₃ could not be detected by XRD possibly because MoO₃ was very well dispersed on the catalyst surface.

** : The quantity of MoS₂ was determined by XPS. This phase could be presented by Mo⁴⁺ specie.

***: The quantity of Mo oxysulphides was determined by XPS. This phase could be presented by Mo⁵⁺ specie.

The XRD patterns of calcined Na and K promoted catalysts (Figure 6-1) exhibited very intense peaks attributed to Al₂O₃, while the Al₂O₃ phase could be hardly detected on the 52Cs15M catalyst. This result is consistent with lower Al XPS atomic concentrations (Table 6-1), measured 52Cs15M. After sulphidation, molybdenum and sulphur have been found in different oxidation states: Mo⁴⁺, Mo⁵⁺ and Mo⁶⁺ for Mo and S²⁻, S₂²⁻ and SO₄²⁻ for S. These species could be detected and identified by XPS (Figure 6-3, Table 6-1). As suggested in Chapters 4 and 5, the presence of significant fractions of Mo⁵⁺ and Mo⁶⁺ in the K promoted MoS₂ catalysts leads to higher hydrocarbon production rates, while the catalyst with a

significant amount of Mo⁴⁺ produces mainly alcohols. Higher concentration of Mo⁴⁺ in 9Na15M than in 15K15M also results a higher alcohol selectivity. Lower alcohol selectivity observed on 52Cs15M could be also attributed to a lower fraction of Mo⁴⁺-S phase. Muramatsu et al [31] reported that MoO₂ phase (Mo⁴⁺-O) could be also active sites for alcohol production. Our catalytic results do not agree with that previous work. Indeed, the 52Cs15M catalyst containing higher fraction of Mo⁴⁺-O phase detected by XPS was less active in alcohol production. High percentage of Mo⁴⁺-O does not seem to increase alcohol selectivity.

In addition to Mo species, the fraction of different S species varies on different catalysts. Woo et al [6] reported that on K-MoS₂/Al₂O₃ catalysts, the fraction of sulphate phase had an effect on the products selectivity: lower SO₄²⁻ ratio could lead to a better alcohol selectivity. Therefore, high alcohol selectivity observed on 9Na15M catalyst could be due to low SO₄²⁻ concentration. The 15K15M and 52Cs15M catalysts contain similar fraction of sulphate ions. The alcohol selectivity was also similar.

The selectivity to C₅₊ hydrocarbons and C₂₊ alcohols varies a function of alkali metal promoter. According to previous studies [9,13, 32, 33], active sites associated with molybdenum sulphide are probably not involved in chain growth. The production of long-chain hydrocarbon and alcohols could be possibly attributed to alkali metal related phases [34]. The amount of alkali-Mo mixed phases can be measured by H₂-TPR, where the reduction peak between 500-800°C should be due to the reduction of alkali metal and Mo mixed sulphides (see part II-1-3). Table 6-3 suggests that more alkali-metal related Mo phases is present in the K promoted catalyst than Na promoted counterpart (through comparison of peak surface). Consequently, the heavy product selectivity was higher with K promoter. However, the 52Cs15M catalysts showed a very highly intense peak in the TPR profiles (zone II). In agreement with this hypothesis, the C₅₊ hydrocarbon selectivity was much more important with Cs promoter than with K or Na promoter.

Alkali metal promotion also has a strong impact on the catalyst basicity, which seems to principally affect the reaction selectivity. As discussed before, the catalyst basicity could be an important parameter which would affect the rate of secondary reactions such as

re-adsorption of olefins or oxygenated products [35,36]. The 9Na15M showed very low concentrations of weak and strong basic sites. The C₅₊ hydrocarbon selectivity increased with the increase of basicity on Na, K and Cs promoted MoS₂/Al₂O₃ catalysts. This indicates the C₅₊ hydrocarbon should be more easily produced with a high basicity. This conclusion is similar to that obtained in Chapter 4 and 5.

Sulphided MoS₂/Al₂O₃ catalysts with different alkali metal promoter were also investigated by TEM. It was found that alkali promoter can affect the size contribution of MoS₂ particle. The potassium increases the MoS₂ particle size, compared to sodium. Higher reaction rate was observed on the 15K15M catalyst. Jiang et al [37] reported that MoS₂ particles with longer slab should be assigned to the well-crystallized MoS₂ that shows very low catalytic activity. This previous work did not take into account the presence of the promoter. Our results suggest that, in addition to molybdenum dispersion, the presence of promoter could also affect the catalytic performance. Therefore, the low catalytic activity of 9Na15M should be due to the nature of sodium promoter. This result is consistent to the work of Woo et al [6] who reported that K promoted catalysts exhibited a higher CO conversion than Na promoted catalysts.

In Chapter 5, we have discussed the relation between light olefin productivity and MoS₂ particle size in TEM images. It was suggested that larger MoS₂ size could favor light olefin production. The results of this chapter also indicated the similar conclusion. On sodium promoted catalysts with smaller MoS₂ particles (less layer number and shorter slab length) the C₂-C₄ olefin productivity was lower, compared with potassium promoted MoS₂/Al₂O₃ catalyst. The hydrogenation activity of molybdenum sulphide nanoparticles is often attributed to corner sites. The smaller molybdenum sulphide nanoparticles might be more active in hydrogenation than larger ones because of more significant fraction of corner sites [38]. In this case, the olefins could be much easier hydrogenated to paraffin.

III Alumina supported molybdenum catalysts promoted with different potassium precursors

III-1 Characterization

The MoS₂/Al₂O₃ catalysts are promoted with the K₂CO₃, K₂SO₄ and KOH precursors and the catalysts are labelled as 15K15M, 15K15M(S) and 15K15M(H), respectively.

III-1-1 XRD

The **calcined catalysts** promoted with potassium hydroxide, potassium carbonate and potassium sulphate were characterized by XRD and the results are shown in Figure 6-9. After calcination, several kinds of oxide phases were observed.

MoO₃ (JCPDF 05-0508, $2\theta = 11.97^\circ, 25.70^\circ, 27.35^\circ, 33.73^\circ, 38.98^\circ$) was detected in the catalyst promoted with potassium carbonate (15K15M catalyst). K₂MoO₄ was the dominant K-Mo mixed phase (JCPDF 29-1011, $2\theta = 18.87^\circ, 26.27^\circ, 30.65^\circ, 39.42^\circ, 45.83^\circ$). In addition to K-Mo mixed oxides, Mo and K also reacted with alumina support during the calcination and lead to Al₂(MoO₄)₃ (JCPDF 85-2286, $2\theta = 20.84^\circ, 22.15^\circ, 23.14^\circ, 30.79^\circ, 32.10^\circ$) and KAl(MoO₄)₂ (JCPDF 74-2008, $2\theta = 22.36^\circ, 31.40^\circ, 32.26^\circ, 51.97^\circ$). The K₂CO₃ (JCPDF 87-0730, $2\theta = 12.98^\circ, 29.19^\circ, 37.54^\circ, 46.32^\circ$) was also present on XRD pattern of the 15K15M catalyst.

In 15K15M(S) catalyst, XRD pattern also showed the presence of MoO₃. K₂MoO₄ could not be detected, however, another K-Mo mixed phase, K₂Mo₄O₆ (JCPDF 87-0730, $2\theta = 13.08^\circ, 17.07^\circ, 25.49^\circ, 27.47^\circ, 30.15^\circ$), was observed. Mixed phases such as Al₂(MoO₄)₃ and KAl(MoO₄)₂ can be detected, as well as K₂SO₄ (JCPDF 83-0681, $2\theta = 29.80^\circ, 30.79^\circ$), from the precursor.

For the 15K15M(H) catalyst prepared using KOH, similar phases than for the 15K15M catalyst were observed: MoO₃, K₂MoO₄, Al₂(MoO₄)₃, KAl(MoO₄)₂.

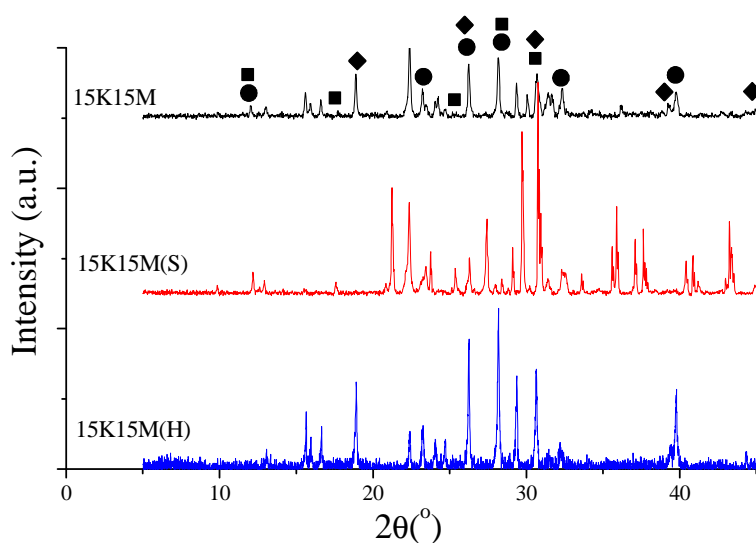


Figure 6-9: XRD pattern of calcined K-MoS₂/Al₂O₃ catalysts with different K precursors. ●MoO₃ ■K₂Mo₄O₆ ◆K₂MoO₄

The width of MoO₃ XRD peaks in the calcined samples and molybdenum dispersion is also affected by the potassium precursor. The MoO₃ phase on 15K15M(S) exhibits rather narrow XRD peaks than the other two catalysts, and the width of the MoO₃ peaks is similar on the 15K15M and 15K15M(H) catalysts. This is indicative of higher molybdenum dispersion in the catalysts promoted with potassium carbonate and hydroxide compared to potassium sulphate.

Sulphided catalysts: The XRD patterns of catalysts after sulphidation are shown in Figure 6-10. The catalyst phase composition strongly depends on the potassium precursor.

The MoS₂ phase in 15K15M was identified using the following position peaks: $2\theta = 14.38^\circ, 32.68^\circ, 39.60^\circ, 49.79^\circ, 58.34^\circ, 60.15^\circ$ (JCPDF 89-3040). In addition to MoS₂, K-Mo mixed sulphides phases can be also detected: K₂MoS₄ (JCPDF 19-1001, $2\theta = 17.55^\circ, 24.23^\circ, 29.36^\circ, 41.19^\circ, 47.05^\circ, 58.40^\circ$) or K-MoS₂ (JCPDF 18-1064, $2\theta = 9.66^\circ, 32.41^\circ, 36.13^\circ, 40.61^\circ, 60.46^\circ$). Potassium sulphides and sulphate were also present in 15K15M catalyst: K₂S (JCPDF 65-3001, $2\theta = 34.21^\circ, 49.16^\circ, 61.26^\circ$), K₂S₃ (JCPDF 31-1095, $2\theta = 28.28^\circ, 30.02^\circ, 32.70^\circ$), K₂S₅ (JCPDF 01-089-3999, $2\theta = 19.83^\circ, 30.78^\circ, 31.15^\circ$), K₂SO₄ (JCPDF 83-0681, 2θ

= 29.80°, 30.79°) and K₂S₃O₆ (JCPDF 01-075-1479, 2θ = 16.73°, 18.10°, 23.61°, 24.90°, 26.54°, 28.08°, 31.13°).

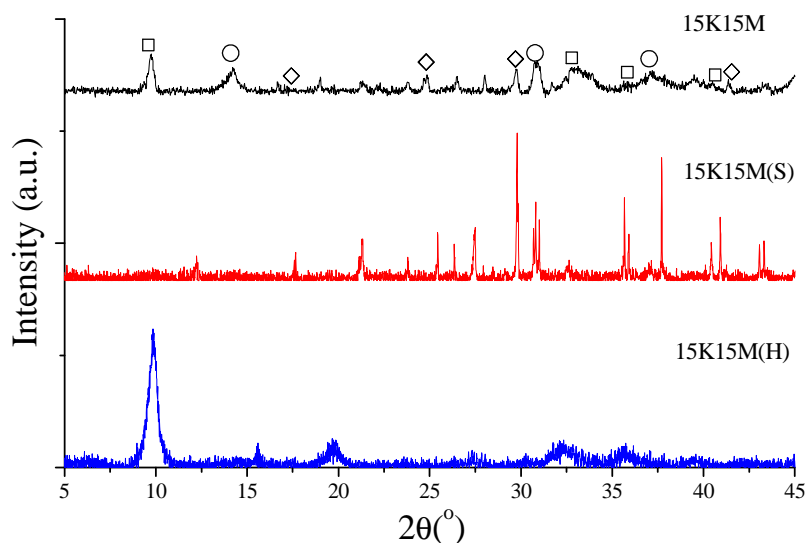


Figure 6-10: XRD pattern of sulphided K-MoS₂/Al₂O₃ catalysts with different K precursors. ○MoS₂ □KMoS₂ ◇K₂MoS₄

Interestingly, MoS₂ phase and K-Mo mixed sulphide phases were not detected in 15K15M(S) catalyst. This catalyst showed the presence of K₂SO₄ and K₂S₃O₆ phases.

For the 15K15M(H) catalyst, K₂MoS₄ and K-MoS₂ were identified from the XRD patterns. In addition, potassium sulphides such as K₂S₃ and K₂S₅ were detected. The catalyst however did show the presence of potassium sulphate phase K₂SO₄.

Note that XRD uncovered the presence of MoS₂ crystalline phase in 15K15M, while the intensity of MoS₂ patterns was rather low on the other two catalysts. This could be due to a higher MoS₂ dispersion in the 15K15M(S) and 15K15M(H) compared to 15K15M.

III-1-2 XPS

The XPS surface element composition of the sulphided catalysts promoted by different K precursors is given in Table 6-6. Different elements (C, O, S, Al, K, Mo) were observed on catalyst surface, and their ratio varied as function of the used precursor.

On 15K15M(S) catalyst, the Al and O concentrations were very high indicating the catalyst surface is not much covered by molybdenum and potassium species. Carbon atoms were also detected. The presence of C on catalyst surface is probably due to the CO₂ adsorption from the atmosphere. The XPS K/Mo ratio is much lower than the atomic bulk ratio (2.5) in 15K15M and 15K15M(S). This indicates that some potassium atoms can be not available for XPS analysis in these catalysts, indicating that potassium is mainly in the catalyst bulk. Lower Al XPS concentration was observed in 15K15M compared to 15K15M(S). This suggests that the basic carbonate promoter could attack Al₂O₃ support. The S/Mo and K/Mo ratios were similar in the 15K15M on 15K15M(S) catalysts. This indicates the similar extent of sulphidation on these two catalysts,

Table 6-6: XPS surface atomic ratio in sulphided K-MoS₂/Al₂O₃ with different precursor

Catalysts	XPS Atomic Ratio (%)						S/Mo ratio	K/Mo ratio	S/(K+Mo) ratio
	C	O	S	Al	K	Mo			
15K15M(S)	1.9	40.9	16.4	26.2	6.4	8.2	2.01	0.79	1.12
15K15M	2.8	49.0	15.2	19.1	6.2	7.6	2.00	0.82	1.10
15K15M(H)	29.0	29.5	15.7	4.2	14.2	7.4	2.14	1.93	0.73

Note that the 15K15M(H) catalyst showed rather different XPS concentrations compared to the sulphate and carbonate precursors. An extremely high carbon concentration could be caused by the strong basicity of KOH, which is favorable for CO₂ adsorption. High potassium XPS concentration indicates higher potassium dispersion on alumina surface. This results in higher K/Mo ratio and lower S/(K+Mo) ratio. Interestingly, the S/Mo ratio is higher than 2 in 15K15M(H). This ratio is more significant than the stoichiometric ratio for MoS₂. This suggests the presence of SH groups which are not necessarily linked to molybdenum. The XPS K/Mo ratio is also lower than the atomic bulk ratio (2.5) although more potassium atoms are on the catalyst surface compared to the two other catalysts.

Figure 6-11 represents the XPS Mo3d spectra. After the peak decomposition, three-peak envelop of the Mo 3d signal can be well deconvoluted in three separate overlapping doublets. This suggests that molybdenum is present in three oxidation states: Mo⁴⁺, Mo⁵⁺ and Mo⁶⁺. The position of these peaks is quite similar as XPS spectra in Figure 6-3(A).

The intense binding energy signals at 228.9 eV and 232.1 eV are characteristic of Mo 3d_{3/2} and 3d_{5/2} of the Mo⁴⁺ species that is contributed by MoS₂, and the binding energy at 226.2 eV and 233.0 eV are characteristic of 2s of S²⁻.

The binding energy for Mo⁵⁺ (at 230.6 eV and 233.7 eV) was detected on XPS spectra, and is assigned to Mo oxy-sulphides as MoO₂S₂ and MoOS₂ [19].

The Mo⁶⁺ phase was detected at binding energy of 232.8 eV and 235.9 eV. It is believed that Mo⁶⁺ phase corresponded to oxidation states of molybdenum [39].

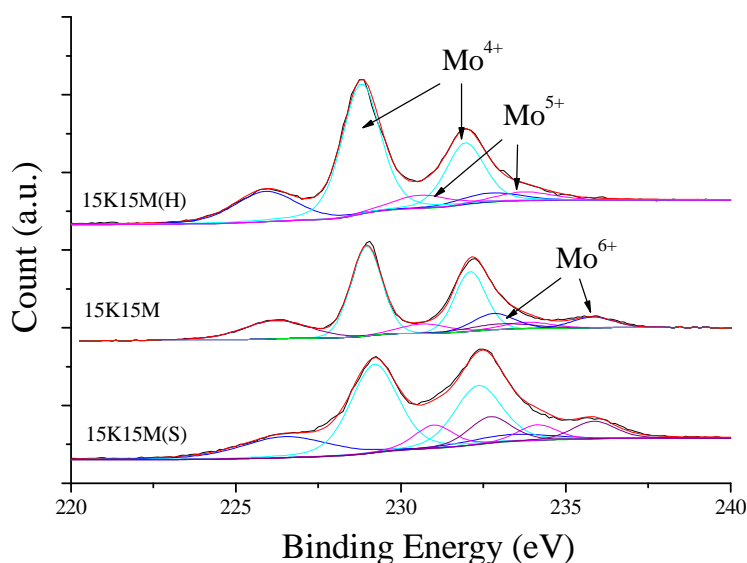


Figure 6-11: XPS spectra of peak decomposition of Mo3d on K-MoS₂ catalysts with different precursors

In XPS spectra, the Mo⁴⁺ and Mo⁵⁺ species were detected on all three catalysts, but Mo⁶⁺ is only present on the catalysts promoted with potassium sulphate and carbonate. The concentration of Mo⁶⁺ species on the catalyst promoted with the hydroxide precursor was very low.

The S 2p XPS spectra are shown in Figure 6-12. In the 15K15M(S), 15K15M and 15K15M(H) catalysts, three different S species were identified using the peak decomposition. The XPS peaks with the binding energies of 161.6 eV and 162.8 eV correspond to sulphide ions (S²⁻), which might be present in K sulphides and/or Mo disulphide. The binding energy around 163.8 eV and 165.0 eV could be possibly attributed to poly-sulphide ions (S₂²⁻) in

K-Mo mixed sulphides as well as to K₂S₃ and K₂S₅ species which were also identified by XRD.

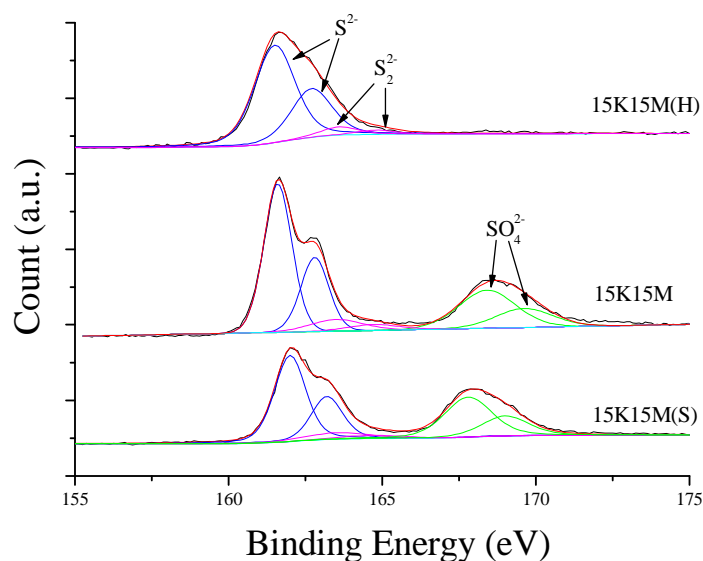


Figure 6-12: XPS spectra of peak decomposition of S2p on K-MoS₂ catalysts with different precursors

In 15K15M and 15K15M(S), the S 2p XPS spectra exhibit other broad peaks between 167.7 - 168.4 eV and 168.9 - 169.6 eV which can be due to the presence of sulphates (SO₄²⁻) [6, 20,40]. The S²⁻ was the principal sulphur species for all three catalysts and the S₂²⁻ phase seems to be less important. The SO₄²⁻ species however, were not present in the 15K15M(H) catalyst.

The atomic concentrations of different Mo and sulphur species are shown in Table 6-7. The 15K15M(H) catalyst presents the higher fraction of Mo⁴⁺ and Mo⁵⁺, while Mo⁶⁺ species were not observed.

Table 6-7: XPS Atomic percentage of different kinds of species for Mo and S

Catalyst	Mo (%)			S (%)		
	Mo ⁴⁺	Mo ⁵⁺	Mo ⁶⁺	S ²⁻	S ₂ ²⁻	SO ₄ ²⁻
15K15M(H)	78.6	21.4	0.0	92.7	7.3	0.0
15K15M	69.7	13.2	17.1	57.2	23.7	18.4
15K15M(S)	73.8	8.2	18.0	53.9	8.3	37.8

The Mo⁴⁺ fraction is the lowest for the 15K15M catalyst and the Mo⁵⁺ fraction is the lowest for the 15K15M(S) catalyst. Those two catalysts exhibit similar Mo⁶⁺ percentage.

In the 15K15M(H) catalyst, S²⁻ is the major species and the SO₄²⁻ concentration is zero. This is consistent with the XRD results where no K sulphate was detected for the 15K15M(H) catalyst. In the carbonate promoted MoS₂ catalyst, the S²⁻ species is less important than in the 15K15M(H). The sample also showed the presence of SO₄²⁻ and S₂²⁻. In the 15K15M(S) catalyst, the fraction of S²⁻ species is lower in comparison to the two other catalysts. The S₂²⁻ fraction is similar than the one of 15K15M(H) catalyst. But the fraction of SO₄²⁻ specie was the highest of all three catalysts. This can be due to the precursor used for catalyst preparation which brought a great deal of SO₄²⁻. A large fraction of these species remains intact after sulphidation.

III-1-4 CO₂-TPD

CO₂-TPD was realized on those three catalysts in order to determine their basicity. Figure 6-13 shows the CO₂ desorption profiles between 30-800°C.

As we have discussed earlier in this chapter, both weak and strong basic sites can be present in the catalysts: weak basic sites, for which CO₂ desorbs between 30-300°C, and strong basic sites, for which CO₂ desorbs between 400-800°C.

The CO₂ desorption profiles show only a single desorption peak at the temperatures of lower than 300°C for 15K15M(S). This indicates presence of only weak basic sites in this catalyst. In 15K15M, both weak and strong basic sites are present.

In the 15K15M(H) catalyst, besides usual weak basic and strong basic sites, there is a small CO₂ desorption peak at 300-400 °C, this could be attributed to medium-strength basic sites.

The quantity of adsorbed CO₂ depends on the promoter precursor and decreases in the following order: KOH > K₂CO₃ > K₂SO₄, just as the basicity of the precursors themselves.

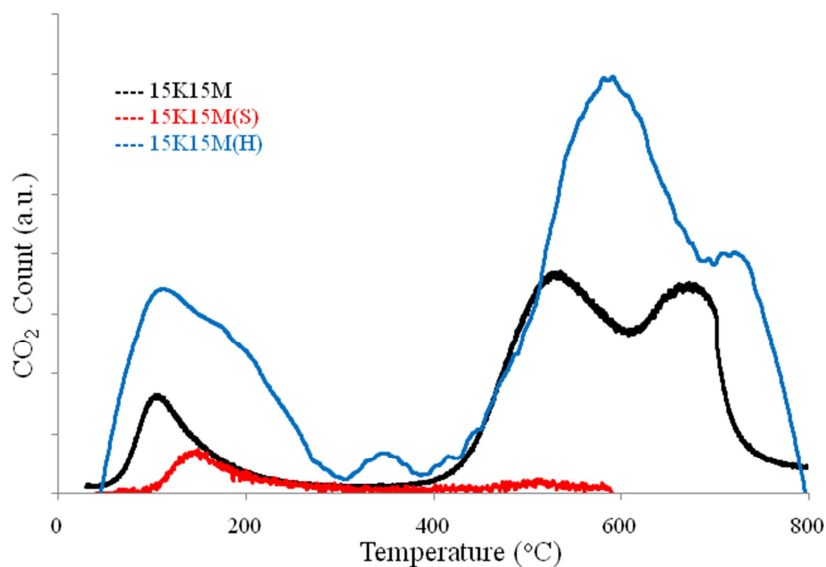


Figure 6-13: CO₂-TPD on K-MoS₂ catalysts promoted with different precursors

III-1-5 TEM

Figure 6-14 displays the images of K₂MoS₂/Al₂O₃ catalysts with different K precursors. The Mo species are better dispersed in 15K15M(S) (Figure 6-14 (c)) and 15K15M(H) (Figure 6-14(e)) catalysts than in the 15K15M catalyst. The highest molybdenum dispersion is observed in the 15K15M(S) catalyst (Figure 6-14 (a, b)). The 15K15M(H) and 15K15M catalysts show some molybdenum sintering, which seems to be more significant in 15K15M(H).

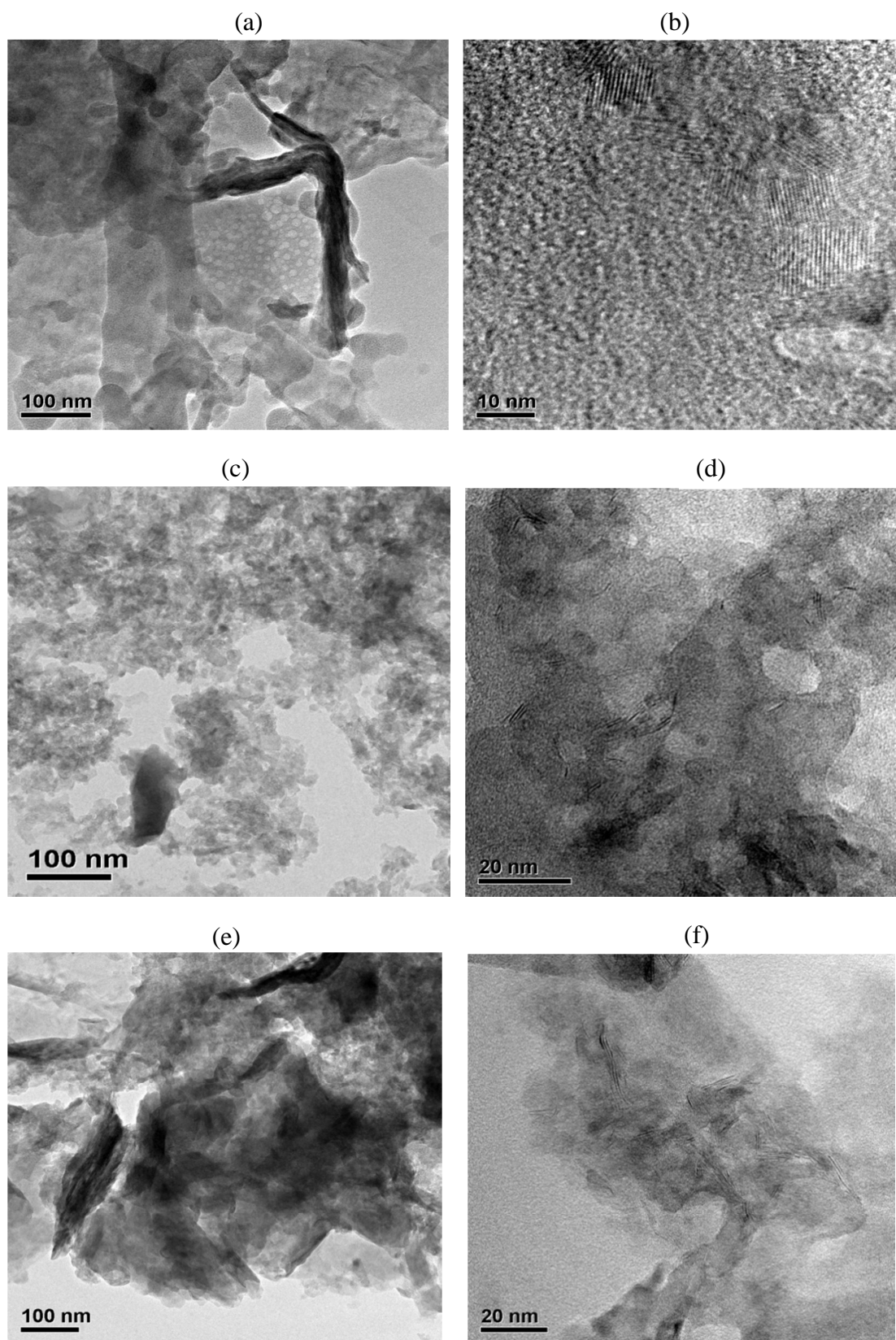
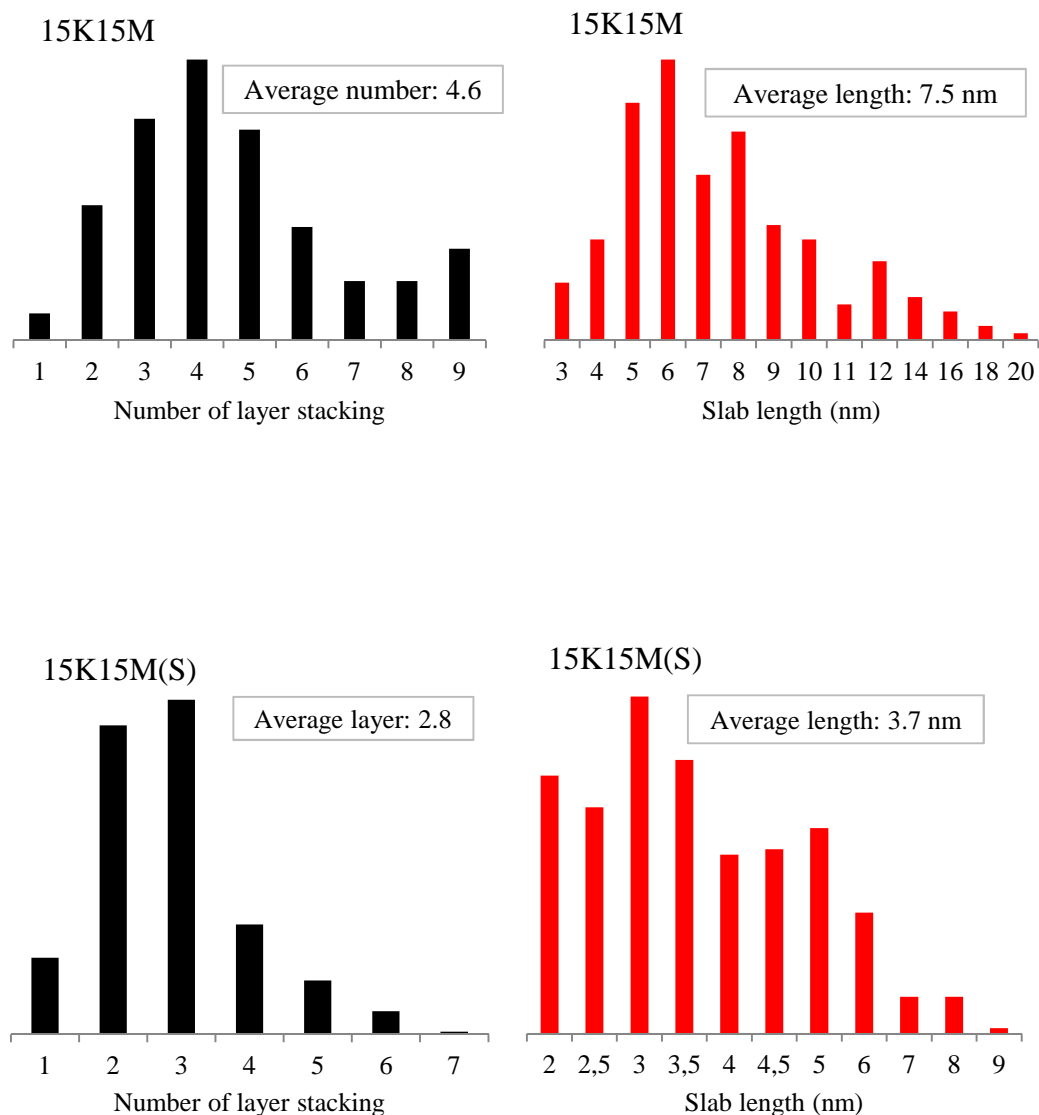


Figure 6-14: TEM images of 15K15M (a and b), 15K15M(S) (c and d), 15K15M(H) (e and f)

MoS₂ particles represent multilayer sheets in all these three catalysts ((b), (d) and (f)) [28]. The MoS₂ particle size varies with different K promoters. The MoS₂ particle size distribution (layer stacking and slab length) calculated from 20 TEM images for each sample is presented in Figure 6-15.

Compared to the K₂SO₄ and KOH promoted catalysts, the number of MoS₂ layers was the highest in K₂CO₃ promoted MoS₂/Al₂O₃ catalyst. Furthermore, 15K15M catalyst shows the largest MoS₂ slab length.



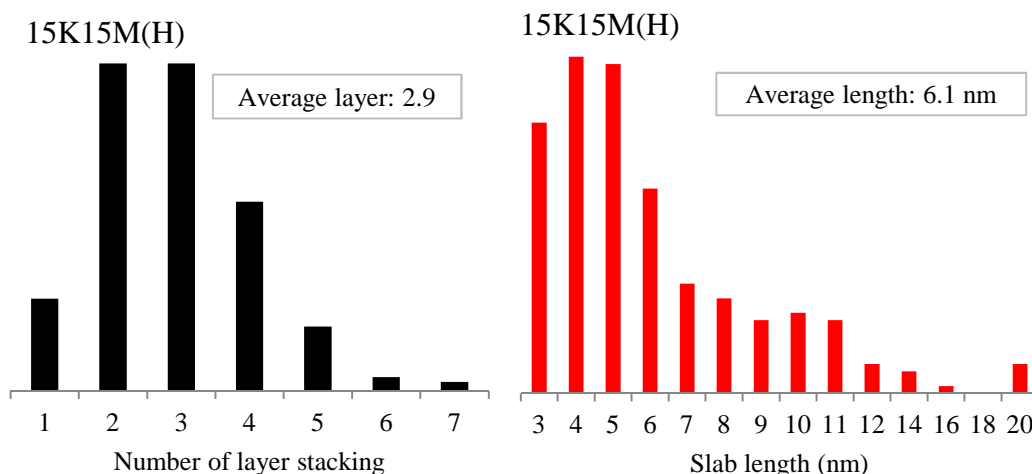


Figure 6-15: MoS₂ particle size distribution from TEM images

On 15K15M(S), the average layer number is 2.8, and the average slab length is rather low. On 15K15M(H), the average layer number is similar to that in 15K15M(S), but the average slab length of MoS₂ particles is larger than that in 15K15M(S). These results demonstrate that the MoS₂ particle size was larger in the 15K15M catalyst than in the other two. This observation is consistent with the above mentioned XRD results.

III-2 Catalytic test

III-2-1 Catalytic performance for CO hydrogenation

The catalytic performance data obtained for the supported K-MoS₂ catalysts with different K precursors are presented in Table 6-8. The 15K15M(S) showed the more significant carbon monoxide conversion, this catalyst produces more light (CH₄ and CO₂) and less heavy products (C₅₊ hydrocarbons and C₂₊ alcohols). The CO conversion is lower on 15K15M than on 15K15M(S), but the 15K15M catalyst shows the highest C₂₋₄ olefin selectivity. Methane and CO₂ selectivity were lower on 15K15M than the catalyst promoted by sulphate while C₅₊ HC selectivity was slightly higher. The promotion of MoS₂/Al₂O₃ catalyst with KOH leads to very low CO monoxide conversion. This catalysts also showed

low C₂-C₄ olefin selectivity, while the C₅₊ hydrocarbon and methanol selectivities significantly increased compared with 15K15M(S) and 15K15M.

Table 6-8: Catalytic performance of K₂MoS₂/Al₂O₃ catalysts with different precursors

Catalyst	CO conversion	CH ₄ %	C2-4 Olefin%	C2-4 Paraffin%	MeOH%	C2+ Alcohol%	C5+ HC%	CO ₂ %
15K15M(S)	28.1%	32.2%	0.1%	14.2%	10.1%	0.4%	3.2%	40.0%
15K15M	21.3%	18.9%	10.7%	15.9%	13.2%	1.9%	6.3%	33.2%
15K15M(H)	10.6%	23.6%	3.2%	2.7%	16.8%	1.5%	20.1%	33.6%

III-2-2 Distribution of sulphur containing products

The gaseous sulphur compounds in the reactor outlet were analyzed by the GC with PFPD detector. Several different sulphur compounds were detected: hydrogen disulphide, carbonyl sulphide, methanethiol, ethanethiol and dimethyl sulphide. The concentration of these compounds is presented in Figure 6-16. The composition of sulphur compounds depends on the potassium precursor. First of all, similar to previous catalytic tests, the total sulphur concentration in gas outlet reactor was always higher than the H₂S concentration in the reactor inlet (13.3 ppmv). This indicates a loss of sulphur from the catalyst during the reaction. The loss was more noticeable with the catalysts promoted with KOH promoter.

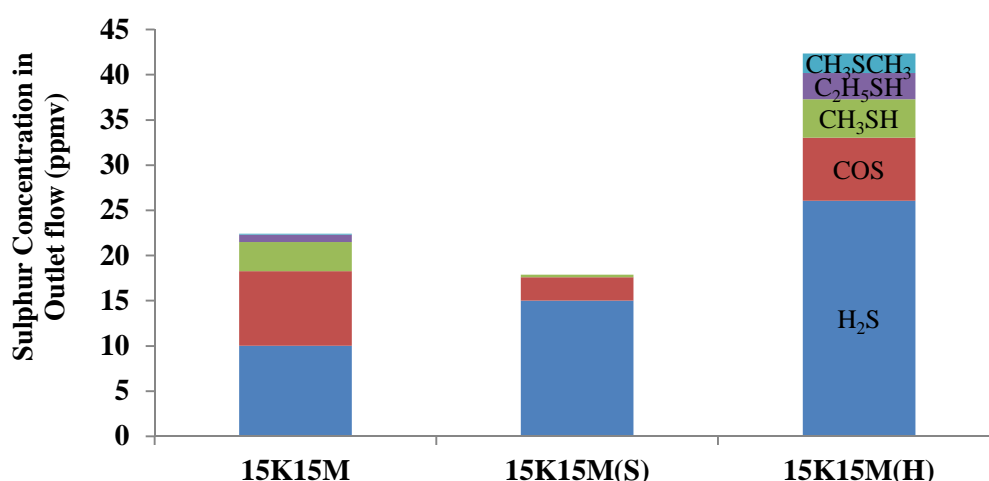


Figure 6-16: Concentration of different sulphur compounds in the reactor outlet on 15%K15%Mo/Al₂O₃ catalysts with different potassium precursor.

The composition of different sulphur compounds also varies as a function of potassium precursor. On 15K15M(S) catalyst, H₂S was the major sulphur product probably because of its lower conversion on the catalysts with some amounts of COS and very few CH₃SH. On MoS₂/Al₂O₃ catalyst promoted with K₂CO₃, more CH₃SH and C₂H₅SH/CH₃SCH₃ were produced. The concentrations of C₂H₅SH and CH₃SCH₃ were significantly higher on 15K15M(H) catalyst. Previous chapters of this thesis suggest that production of mercaptans on potassium promoted catalysts from H₂S containing syngas may coincide with the noticeable selectivity to alcohols and long-chain hydrocarbons. This may suggest some similarity in the mechanisms of the formation of mercaptans, hydrocarbons and alcohols on MoS₂ catalysts. The 15K15M(H) catalyst showed the highest selectivity to long-chain mercaptans (C₂H₅SH) compared to 15K15M(S) and 15K15M catalysts. It could be related to higher capacity of the catalyst promoted with KOH to produce long-chain hydrocarbons

III-3 Discussion

Depending of the potassium promoter, different phases have been observed on the catalyst. Those phases are summarized in Table 6-9.

Table 6-9: Species on catalysts surface of calcined and sulphided Mo/Al₂O₃ catalysts with different potassium precursors (according to XRD and XPS results)

Catalysts	After Calcination			After Sulphidation		
	Mo oxide	K-Mo Oxides	K-Mo-Al mixed phases	Mo sulphides *	K-Mo sulphides	Mo oxysulphides **
15K15M	MoO ₃	K ₂ MoO ₄ K ₂ Mo ₄ O ₆	Al ₂ (MoO ₄) ₃ KAl(MoO ₄) ₂	MoS ₂ (69.7%)	K ₂ MoS ₄ KMoS ₂	High (13.2%)
15K15M(S)	MoO ₃	K ₂ Mo ₄ O ₆	Al ₂ (MoO ₄) ₃ KAl(MoO ₄) ₂	MoS ₂ (73.8%)	-	low (8.2%)
15K15M(H)	MoO ₃	K ₂ MoO ₄	Al ₂ (MoO ₄) ₃ KAl(MoO ₄) ₂	MoS ₂ (78.6%)	K ₂ MoS ₄ KMoS ₂	very high (21.4%)

*: The quantity of MoS₂ was determined by XPS. This phase could be presented by Mo⁴⁺ specie.

** : The quantity of Mo oxysulphides was decided by XPS. This phase could be presented by Mo⁵⁺ phase.

The promotion of alumina supported molybdenum sulphide catalysts using different potassium precursors significantly affects their catalytic performance. Different basicity of precursors K₂SO₄, K₂CO₃ and KOH could be the principal responsible for these effects. CO₂-TPD results suggest that basicity of catalysts depends on the used precursor. The catalytic activity decreases with the increase in basicity, while C₅₊ selectivity increases. Our results indicate however that a moderate basicity could be favorable for light olefin production. Lower catalyst basicity favours production of methane and light paraffins (K₂SO₄ promoted MoS₂/Al₂O₃ catalyst). Too strong basicity was also harmful because it would lead to more alcohol and heavy hydrocarbon production (KOH promoted MoS₂/Al₂O₃ catalyst).

XPS gave more information about Mo and S species in the catalysts. With different K precursors, the same Mo and S species can be found: Mo⁴⁺, Mo⁵⁺, Mo⁶⁺; S²⁻, S₂²⁻, SO₄²⁻. The ratio of these species also depends on the potassium precursor. On KOH promoted MoS₂/Al₂O₃ catalyst, higher alcohol selectivity coincides with a very low ratio of Mo⁶⁺ [6]. The K₂CO₃ promoted MoS₂/Al₂O₃ catalyst showed the highest light olefin selectivity. This catalyst showed a lowest fraction of Mo⁴⁺ species. It is known that Mo⁴⁺ species can be associated to MoS₂ [41]. The MoS₂ phase can be responsible for methane production [8], and is rather favourable for hydrogenation [42]. In agreement with the report of Colley et al [43], high hydrogenation ability could be harmful for the light olefin selectivity because of secondary hydrogenation. Thus, lower fraction of MoS₂ could be favorable for light olefin selectivity.

TEM provided interesting information on molybdenum dispersion in the promoted MoS₂/Al₂O₃ catalysts. Correlations could be observed between catalytic performance of CO hydrogenation and MoS₂ particle size distribution. Jiang et al [44] reported that the CO conversion was higher on Co_MoS₂ based catalysts, with a smaller MoS₂ slab length. We found that 15K15M(S) was the most active catalyst however it showed the smallest slab length. The slab length in 15K15M(H) was shorter than 15K15M, while the CO conversion was lower on 15K15M(H). The highest olefins selectivity was observed on 15K15M which had higher number of stacking layer and smaller slab length.

IV Conclusion

In this Chapter, different alkali metals (Na, K, and Cs) and different precursors for potassium promoter (K₂CO₃, KOH and K₂SO₄) were employed to modify the catalytic performance. The best results in terms of light olefin productivity were observed with potassium carbonate. The catalyst basicity and crystallite size of mixed K-Mo sulphides are important parameters affecting olefin productivity. Moderate basicity could be favourable for producing light olefins. Large molybdenum supplied particles result in higher yield of light olefins.

Reference

- [1] K. Klier, J. Santiesteban, J. Nunan. Preprints Symposia. 22 (1987) 190
- [2] J. Spivey, A. Egbebi. Chem. Soc. Rev. 36 (2007) 1514
- [3] J. Iranmahboob, H. Toghiani, D. Hill. Appl. Catal. A: General. 247 (2003) 207
- [4] N. Koizumi et al. Catalysis Today 89 (2004) 465
- [5] J. Zhang, Y. Wang, L. Chang, Appl. Catal. A. 126 (1995) 205.
- [6] H. Woo, T. Park, Y. Kim, I. Nam, J. Lee, J. Chung. Stud. in Surf. Sci. and Catal. 75 (1993) 2749
- [7] T. Tatsumi, A. Muramatsu, H. Tominaga, J. Catal. 101 (1986) 553
- [8] D. Ferrari, G. Budroni, L. Bisson, N. Rane, B. Dickie, J. Kang, S. Rozeveld. Appl. Catal. A: General. 462–463 (2013) 302
- [9] D. Li, C. Yang, W. Li, Y. Sun, B. Zhong. Top. Catal. 32 (2005) 233
- [10] J. Iranmahboob, D. Hill. Catal. Lett. 78 (2002) 49
- [11] N. Kinkade. Tantalum-containing catalyst useful for producing alcohols from synthesis gas. U.S. Patent No. 4,994,498, February 1991.
- [12] V. Subramani, S. Gangwal. Energy & Fuels. 22 (2008) 814
- [13] S. DeCanio, M. Cataloo, E. DeCanio, D. Storm. J. Catal. 119 (1989) 256–260
- [14] Th. Weber, J. Muijsers, J. van Wolput, C. Verhagen, and J. Niemantsverdriet. J. Phys. Chem. 1996 (100) 14144
- [15] T. Patterson, J. Carver, D. Leyden, D. Hercules. J. Phys. Chem. 80 (1976) 1700
- [16] J. Iranmahboob, S. Gardner, H. Toghiani, D. Hill. Journal of Colloid and Interface Science 270 (2004) 123–126
- [17] J. Ramirez, L. Cedenio, G. Busca. J. Catal. 184 (1999) 59–67
- [18] S. Andersson, R. Howe. J. Phys. Chem. 93 (1989) 4913
- [19] L. Benois, D. Gonbeau, G. Pfister-Guillouzo, E. Schmidt, G. Meunier, A. Levasseur. Thin Solid Films 258 (1995) 110
- [20] A. Muller, R. Joster, W. Jaegermann. Inorg. Chim. Acta. 41 (1980) 259
- [21] L. Benois, D. Gonbeau, G. Pfister-Guillouzo, E. Schmidt, G. Meunier, A. Levasseur. Surf. Interface Anal. 22 (1994) 206
- [22] G. Seifert, J. Finster, H. Mueller. Chem. Phys. Lett. 75 (1980) 373
- [23] G.L. Schrader and C.P. Cheng. J. Catal. 80 (1983) 369
- [24] E. Zdansky, M. Ohno, N. Martensson. J. Electron Spectrosc. Relat. Phenom. 67 (1994) 141
- [25] H. Toulhouat, S. Kasztelan, in: M.J. Phillips, M. Ternan (Eds.), Proceedings, 9th International Congress on Catalysis, Calgary, 1988, vol.1, Chem. Institute of Canada, Ottawa. (1988) 152
- [26] W. Lai, L. Pang, J. Zheng, J. Li, Z. Wu, X. Yi, W. Fang, L. Jia. Fuel Processing Technology. 110 (2013) 8
- [27] R. Cordero, A. Agudo. Appl. Catal. A: General. 202 (2000) 23
- [28] H. Ramakrishna Matte, A. Gomathi, A. K. Manna, D. J. Late, R. Datta, S. K. Pati, and C. N. R. Rao. Angew. Chem. Int. Ed. 49 (2010) 4059–4062
- [29] A. Chen, Q. Wang, Q. Li, Y. Hao, W. Fang, Y. Yang. J. Mol. Catal. A: Chemical. 283 (2008) 69
- [30] O. Gutiérrez, C. Kaufmann, A. Hrabar, Y. Zhu, J. Lercher. J. Catal. 280 (2011) 264
- [31] A. Muramatsu, T. Tatsumi, H. Tominaga. J. Phys. Chem. 96 (1992) 1334
- [32] T. Ishihara, K. Harada, K. Eguchi, H. Arai. J. Catal. 136 (1992) 161
- [33] N. Koizumi, G.Z. Bian, K. Murai, T. Ozaki and M. Yamada. J. Mol. Catal. A: Chem. 207 (2004) 173
- [34] H. Xiao, D. Li, W. Li, Y. Sun. Fuel Processing Technology. 91 (2010) 383
- [35] E. Lowenthal, S. Schwarz, H.C. Foley. Catal. Today. 51 (1999) 187
- [36] G.Z. Bian, Y. Fu, Y. Ma. Appl. Catal. A: General. 170 (1998) 255

- [37] M. Jiang, B. Wang, J. Lv, H. Wang, Z. Li, X. Ma, S. Qin, Q. Sun. *Appl. Catal. A: General*. 466 (2013) 224
- [38] E. Hensen, P. Kooyman, Y. van der Meer, A. van der Kraan, V. de Beer, J. van Veen, R. van Santen. *J. Catal.* 199 (2001) 224
- [39] K. Suzuki, M. Soma, T. Onishi, K. Tamaru. *J. Electron Spectrosc. Relate. Phenom.* 5 (1974) 351
- [40] X. Yu, F. Liu, Z. Wang, Y. Chen. *J. Electron Spectrosc. Relat. Phenom.* 50 (1990) 159
- [41] J. Iranmahboob, D. Hill, H. Toghiani. *Appl. Surf. Sci.* 185 (2001) 72-78
- [42] H. Woo, I. Nam, J. Lee, J. Chung, K. Lee, Y. Kim. *J. Catal.* 138 (1992) 525
- [43] S. Colley, R. Copperthwaite, G. Hutchings, G. Foulds, N. Coville. *Appl. Catal. A: General*. 84 (1992) 1
- [44] M. Jiang, B. Wang, Y. Yao, Z. Li, X. Ma, S. Qin, Q. Sun. *Catal. Sci. Technol.* 3 (2013) 2793

General Conclusion

General Conclusion

Development of novel routes for the efficient utilization of non-petroleum resources including biomass and coal to produce chemicals and ultraclean liquid fuels has attracted much attention because of environmental concerns and depletion of petroleum resources. This thesis addresses the effect of sulphur on FT synthesis on supported cobalt and molybdenum catalysts. The research work was realized in the context of valorisation of biomass and coal. The syngas feed from gasification of biomass and coal always contains sulphur compounds [1]. Hydrogen disulphide is one of the most important impurities in biosyngas.

In FT process, Co based catalysts present a high catalytic activity, especially with noble metal promotion. In this thesis we find that the presence of H_2S , even at quite low concentration, leads to obvious deactivation of alumina supported Co and Pt-Co catalysts. The catalytic activity and C_{5+} hydrocarbon productivity on both catalysts decreased dramatically. The XPS results showed the presence of Co-S species ($CoSO_4$) in the catalysts exposed to sulphur containing syngas. H_2S could block the active site of cobalt based catalysts and cause the deactivation.

Thus, the conventional catalysts for FT synthesis readily deactivate in the presence of sulphur in syngas. It is a necessity to find an active catalyst in FT synthesis with sulphur resistance. Our attention focused on the MoS_2 based catalyst [2]. The catalytic tests showed that supported MoS_2 catalysts presented a stable catalytic activity in FT synthesis with syngas feed mixing with H_2S . On unpromoted MoS_2 catalysts, methane was the main product. The supported MoS_2 catalysts promoted with alkali ions produce light olefins, alcohols and heavy hydrocarbons. The catalytic performance was a function of the promoter and support.

The CO hydrogenation with K promoted catalyst was more significant than that of Cs or Na promoted catalysts. The highest C₂-C₄ olefin selectivity was observed on the catalyst promoted with K, while C₅₊ hydrocarbons was the main product on Cs promoted catalyst. Sodium promoted catalyst produce mostly light paraffins. We studied K promoted catalyst, using different potassium promoters: K₂CO₃, K₂SO₄ and KOH. For the catalysts synthesized with different precursors for potassium promoter (K₂CO₃, KOH and K₂SO₄), the best results in terms of light olefin productivity were observed with potassium carbonate. The catalyst promoted with potassium sulphate produced mostly light paraffins, while the catalysts promoted with KOH showed higher C₅₊ selectivity.

The structure and performance of MoS₂ based catalysts were also affected by γ -alumina or carbon nanotube (CNT) supports. The alumina supported potassium promoted MoS₂ catalysts showed higher activity in CO hydrogenation which could be attributed to a higher Mo sulphidation degree. The promoter affects the basicity and influences reaction rates and selectivity in FT synthesis in the MoS₂ supported catalysts. Potassium carbonate was added in catalysts at different content. On alumina support, the light olefin yield attained a maximum at K/Mo ratio of 2.5. On CNT support, the light olefin yield attained a maximum at K/Mo ratio of 0.5.

The results obtained with different promoters and with MoS₂ catalysts supported by γ -alumina or carbon nanotube (CNT) suggest that the catalytic performance is influenced by the presence of different molybdenum phases, sizes of molybdenum sulphide nanoparticles and catalyst basicity.

Two kinds of active sites, Mo sulphides and K-Mo mixed sulphides were detected on surface of K-MoS₂ catalysts. The MoS₂ phase can be responsible for methane production, and is rather favourable for hydrogenation [3]. Active sites for the synthesis of light olefins and oxygenates are probably contained in K-Mo mixed phases.

The catalysts with lower concentration of basic sites produce mostly methane and carbon dioxide. A moderate basicity seems to be favourable for producing light olefins. Higher catalyst basicity results in higher selectivity to C₅₊ hydrocarbons but is unfavourable for producing light olefins.

Layer stacking and slab length of MoS₂ particle can be detected by TEM. The relation between MoS₂ particle size and light olefin productivity is presented in Figure 7-1. Strong interaction between alkali metal and Mo leads to a high slab length of MoS₂. Productivity of light olefin became higher with larger MoS₂ particle, especially high MoS₂ number layer. The small MoS₂ particles that favoured the hydrogenation on catalysts [4,5], these particles were believed to be more selective for production of methane and light paraffins. High hydrogenation ability could be harmful for the light olefin production.

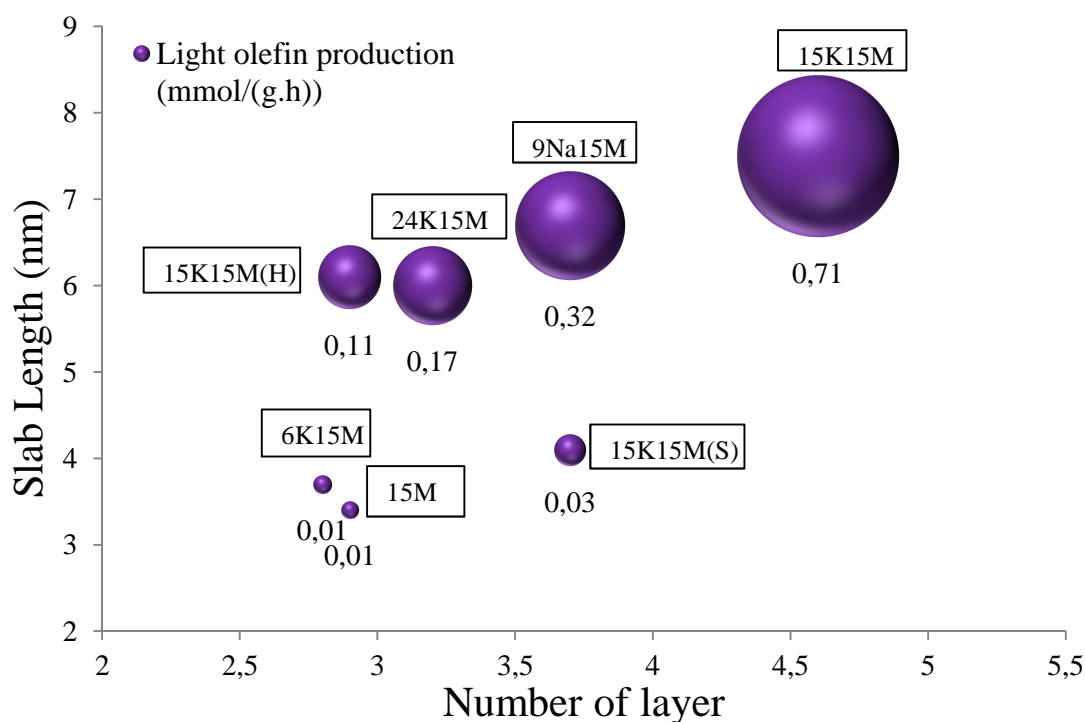


Figure 7-1: Production of C₂-C₄ olefins as a function of MoS₂ particle size (measured by TEM) on MoS₂/Al₂O₃ catalysts.

The reaction condition also affected the catalytic performance. Lower reaction pressure could improve the light olefin selectivity but inhibit the catalytic activity. Lower H₂/CO ratio in syngas feed should improve the productivity of light olefin. The highest light olefin

selectivity could reach 16.6% at $T = 360^{\circ}\text{C}$, $P = 20$ bar, $\text{H}_2/\text{CO} = 1$, $\text{GHSV} = 2100 \text{ h}^{-1}$, with a CO conversion of 20%, with the presence of 15%K15%Mo/ Al_2O_3 catalyst.

Perspectives

From our knowledge, application of MoS_2 based catalysts for synthesis of light olefin has not been studied. This thesis could be considered as a new development in FT procedure on MoS_2 based catalysts. In order to continue improving the olefin productivity, some perspectives are summarized below:

1. More different reaction conditions should be involved in order to modify the catalytic performance. The different condition could be different temperature, pressure, H_2/CO ratio, etc.
2. Synthesis method other than impregnation can be considered, for example the thermal decomposition method. Interaction between molybdenum and promoters can affect the catalytic performance. The synthesis method could modify this interaction.
3. The activation step is important for MoS_2 catalysts. In this work we always used the H_2S gas to sulphide the catalysts. However, some other sulphur compounds can be also used to active the Mo based catalysts. These different activation methods may help us obtain a better yield of products in FTS.
4. We can used several new techniques to detect the active site of promoted molybdenum disulphide catalysts, such as SSITKA (steady-state isotopic transient kinetic analysis) and in-situ IR technique. In future work the FT reaction on MoS_2 based catalysts can be researched by the density function theory modelling. This should be interesting to understand the mechanism of FTS on MoS_2 based catalysts.

Reference

- [1] P.Mathieu, R. Dubuisson. *Energy Conv. Mana.*43 (2002) 1291
- [2] K. Smith, R. Herman, K. Klier, *Chem. Eng. Sci.* 45 (1990) 2639
- [3] H. Woo, I. Nam, J. Lee, J. Chung, K. Lee, Y. Kim. *J. Catal.* 138 (1992) 525
- [4] E. Hensen, P. Kooyman, Y. van der Meer, A. van der Kraan, V. de Beer, J. van Veen, R. van Santen. *J. Catal.* 199 (2001) 224
- [5] Y. Sakashita, Y. Araki, H. Shimada. *Appl. Catal. A: General.* 215 (2001) 101

